University of South Bohemia in České Budějovice

Faculty of Science

Excited States of Carotenoids and Their Roles in Light Harvesting Systems

Ph.D. Thesis

Gürkan KEŞAN

Supervisor: **prof. RNDr. Tomáš Polívka, Ph.D.**

Faculty of Science, University of South Bohemia, České Budějovice,

Czech Republic

Co-Supervisor: **assoc. prof. Cemal Parlak, Ph.D.**

Faculty of Science, Ege University, İzmir,

Turkey

České Budějovice 2016

Annotation

Carotenoids are an extensive group of natural pigments employed by a majority of organisms on earth. They are present in most organisms, including humans, but can be synthesized only by plants and microorganisms. They perform two major roles in photosynthesis, often in partnership with the more prevalent chlorophylls (Chls) / bacteriochlorophylls (BChls): light-harvesting and photoprotection. Carotenoids absorb radiation in a spectral region inaccessible to Chls and BChls and transfer the absorbed energy to (B)Chls which, in turn, funnel it into the photosynthetic reaction center (RC). It is determined that the structures and dynamics of excited states of carotenoids found in photosynthetic proteins provide an explanation of their roles as light-harvesting and photoprotective agents. The conjugation length and the type of carotenoids play a big part in understanding the energy transfer from carotenoids to Chls and BChls, because excited-state properties of carotenoids are affected by number of conjugated C=C bonds and their structures. An accurate description of these states is, therefore, the crucial first step in explaining carotenoid photochemistry and understanding the interactions between carotenoids and other molecules in photobiological processes. The research in this thesis, femtosecond ultrafast transient absorption spectroscopy was used to study the light-harvesting function of carotenoids both in solvent and protein environment. The findings were supported with computational methods. Based on spectroscopic indications, the light-harvesting function of carotenoids has a bearing on their structures, and specific light-harvesting strategies are explicitly dependent with the structure of the light-harvesting complexes.

Declaration [in Czech]

Prohlašuji, že svoji disertační práci jsem vypracoval samostatně pouze s použitím pramenů a literatury uvedených v seznamu citované literatury.

Prohlašuji, že v souladu s § 47b zákona č. 111/1998 Sb. v platném znění souhlasím se zveřejněním své disertační práce, a to v úpravě vzniklé vypuštěním vyznačených částí archivovaných Přírodovědeckou fakultou elektronickou cestou ve veřejně přístupné části databáze STAG provozované Jihočeskou univerzitou v Českých Budějovicích na jejích internetových stránkách, a to se zachováním mého autorského práva k odevzdanému textu této kvalifikační práce. Souhlasím dále s tím, aby toutéž elektronickou cestou byly v souladu s uvedeným ustanovením zákona č. 111/1998 Sb. zveřejněny posudky školitele a oponentů práce i záznam o průběhu a výsledku obhajoby kvalifikační práce. Rovněž souhlasím s porovnáním textu mé kvalifikační práce s databází kvalifikačních prací Theses.cz provozovanou Národním registrem vysokoškolských kvalifikačních prací a systémem na odhalování plagiátů.

České Budějovice, 22. listopadu 2016　　　　　……………………

Gürkan Keşan

iv

Financial support

The reaserch presented in this thesis was supported by grants from the Czech Science Foundations (P202/09/1330, P205/11/1164, P501/12/G055).

Acknowledgements

Firstly, I would like to express my sincere gratitude to my advisor **Tomáš Polívka** for the continuous support of my Ph.D. study and related research, for his patience, motivation, and immense knowledge. His guidance helped me in all the time of research and writing of this thesis. I could not have imagined having a better advisor and mentor for my Ph.D. study. Thank you so much!

Besides my advisor, I would like to thank my co-supervisor, **Cemal Parlak**. I have been extremely lucky to have a person who cared so much about my life and scientific carrier from my master degree. Thank you so much!

I must express my gratitude to my colleagues: *V. Šlouf, M. Durchan, M. Fuciman, V. Kuznetsova, R. G. West, V. Šebelík, H. Staleva Musto, D. Bína* and *R. Litvín* for the discussions on the projects and for all the fun we have had in the last five years. Thank you all so much!

I want to give special thanks to *V. Šlouf* and *M. Durchan* who help me to solve my all issues in Czech Republic. Further, I will never forget the memorable days with your families. Thank you so much for all your help!

My friends, who provided a much needed form of escape from my studies, *Vašek, Valja, Ivan, Robert, Saurabh, Vasilina, Alex, Zoltan, Dhiraj, Katya, Tomáš, Denys* and *Babak* also deserve thanks for making more enjoyable life in Budweis.

I would like to thanks my colleagues in Turkey: *Ö. Alver, M. Bilge, M. Tursun, M. Fatih Kaya, E. Güneş, Ö. Bağlayan* and also *A. Engin Çalık*.

Last but not the least, I would like to thank *my big family* and *my fiancée* for their supports in all my life. I love all of you, thanks a lot! Also, I have a special thanks to *Yusuf Ertürk* who is not with us anymore. I will never forget you and the days we spent together…

Dedicated to my family and Yusuf Ertürk...

Aileme ve Yusuf Ertürk'e ithafen...

List of papers and author's contribution

Included in the thesis

PAPER 1. Milan Durchan, Marcel Fuciman, Václav Šlouf, **Gürkan Keşan**, Tomáš Polívka, Effect of polarity and aggregation on excited-state dynamics of 8'-apo-β-carotenal, *J. Phys. Chem A*, **2012**, 116: 12330-12338. (IF=2.7)

GK participated the experimental work and data analysis.

PAPER 2. Marcel Fuciman, Milan Durchan, Václav Šlouf, **Gürkan Keşan**, Tomáš Polívka, Excited-state dynamics of astaxanthin aggregates, *Chem. Phys. Lett.,* **2013**, 568–569: 21–25. (IF=1.9)

GK participated in the experimental work and data analysis.

PAPER 3. Marcel Fuciman, **Gürkan Keşan**, Amy M. La Fountain, Harry A. Frank, and Tomáš Polívka, Tuning the Spectroscopic Properties of Aryl Carotenoids by Slight Changes in Structure, *J. Phys. Chem. B,* **2015**, 119(4): 1457–1467. (IF=3.3)

GK carried out the computational work and took part in writing and revision of the manuscript.

PAPER 4. Gürkan Keşan, Milan Durchan, Josef Tichý, Babak Minofar, Valentyna Kuznetsova, Marcel Fuciman, Václav Šlouf, Cemal Parlak, Tomáš Polívka, Different response of carbonyl carotenoids to solvent proticity helps to estimate structure of unknown carotenoid from Chromera velia, *J. Phys. Chem. B,* **2015**, 119 (39): 12653–12663. (IF=3.3)

GK conducted a vast majority of the experiments, computational work, data analysis, and took part in writing and revision of the manuscript.

PAPER 5. Robert West, **Gürkan Keşan**, Eliška Trsková, Roman Sobotka, Radek Kaňa, Marcel Fuciman, Tomáš Polívka, Spectroscopic properties of the triple bond carotenoid alloxanthin, *Chem. Phys. Lett.,* **2016**, 653: 167–172. (IF=1.9)

GK carried out the computational work and took part in writing and revision of the manuscript.

PAPER 6. Milan Durchan, **Gürkan Keşan**, Václav Šlouf, Marcel Fuciman, Hristina Staleva, Josef Tichý, Radek Litvín, David Bína, František Vácha, Tomáš Polívka, Highly efficient energy transfers from a carbonyl carotenoid to chlorophyll a in the main light harvesting complex of *Chromera velia*, *Biochimica et Biophysica Acta (BBA)*, **2014**, 1837: 1748–1755. (IF=5.35)

GK participated in performing the experiments, and analysed the data.

PAPER 7. Gürkan Keşan, Radek Litvín, David Bína, Milan Durchan, Václav Šlouf, Tomáš Polívka, Efficient light-harvesting using non-carbonyl carotenoids: Energy transfer dynamics in the VCP complex from *Nannochloropsis oceanica*, *Biochimica et Biophysica Acta (BBA),* **2016**, 1857: 370–379. (IF=5.35)

GK *conducted a vast majority of the experiments, computational work, data analysis and took part in writing and revision of the manuscript.*

Other related papers of GK

1. **Gürkan Keşan**, Özge Bağlayan, Cemal Parlak, Özgür Alver, Mustafa Şenyel, FT-IR and Raman spectroscopic and quantum chemical investigations of some metal halide complexes of 1-phenylpiperazine, *Spectrochimica Acta A*, **2012**, 88: 144-155. (IF=2.35)

2. **Gürkan Keşan**, Mehmet Fatih Kaya, Metin Bilge, Özgür Alver, Cemal Parlak, DFT, FT-IR and Raman investigations of 1-pyrrolidino-1-cyclopentene, *Spectrochimica Acta A,* **2013**, 101: 22-30. (IF=2.35)

3. Mehmet Fatih Kaya, Cemal Parlak, **Gürkan Keşan,** Özgür Alver and Mahir Tursun, Vibrational spectroscopic investigation of 1-pyrrolidino-1-cyclohexene: A comparative density functional study, *Spectrochimica Acta A*, **2013**,113: 1-9. (IF=2.35)

4. Mahir Tursun, **Gürkan Keşan**, Cemal Parlak and Mustafa Şenyel, Vibrational spectroscopic investigation and conformational analysis of 1-heptylamine: A comparative density functional study, *Spectrochimica Acta A*, **2013**, 114: 668-680. (IF=2.35)

5. **Gürkan Keşan**, Cemal Parlak, Infrared and Raman spectra, conformational stability and vibrational assignment of 1-formylpiperazine, *Spectrochimica Acta A,* **2014**, 118: 1113-1120. (IF=2.35)

6. Chandraju Sadolalu Chidan Kumar, Cemal Parlak, Hoong-Kun Fun, Mahir Tursun, **Gürkan Keşan**, Siddegowda Chandraju, Ching Kheng Quah, Experimental and theoretical FT-IR, Raman and XRD study of 2-acetyl-5-chlorothiophene, *Spectrochimica Acta A,* **2014,** 127: 67-73. (IF=2.35)

7. Nesrin Emir, Metin Bilge, Mahir Tursun, **Gürkan Keşan** and Cemal Parlak, A joint theoretical and experimental study of 1-acetylpiperazine: conformational stability, infrared and Raman spectra, *Spectrochimica Acta A,* **2014**, 127: 388-395. (IF=2.35)

8. C. Parlak, C.S.C. Kumar, H.K. Fun, **G. Keşan**, L. Rhyman, P. Ramasami, S. Chandraju, C.K. Quah, 4-Chloro-3-fluorobenzaldehyde: Experimental (XRD, FT-IR and Raman) and DFT studies, *J. Fluorine Chem.,* **2014**, 164: 7-15. (IF=1.9)

9. C.S.C. Kumar, C. Parlak, M. Tursun, H.K. Fun, L. Rhyman, P. Ramasami, **G. Keşan,** S. Chandraju, C.K. Quah, 3-Iodobenzaldehyde: combined XRD, FT-IR, Raman and DFT studies, *Spectrochimica Acta A,* **2015**, 145 90-97. (IF=2.35)

10. K. Gör, M. Tursun, **G. Keşan,** G. S. Kürkçüoğlu, L. Rhyman, C. Parlak, P. Ramasami, O. Z. Yeşilel, Orhan Büyükgüngör, Novel cyanide-bridged heterometallic two-dimensional complex of 3-methylpyridazine: synthesis, crystallographical, vibrational, thermal and DFT studies, J. *Inorg. Organomet. Polym.,* **2015**, 25: 1205-1217. (IF=1.2)

11. Assia Sid, Amel Messai, Cemal Parlak, Nadide Kazancı, Dominique Luneau, **Gürkan Keşan**, Lydia Rhyman, Ibrahim A. Alswaidan, Ponnadurai Ramasami, 1-Formyl-3-phenyl-5-(4-isopropylphenyl)-2-pyrazoline: Synthesis characterization, antimicrobial activity and DFT studies, *J. Mol. Structure*, **2016**, 1121: 46-53. (IF=1.6)

**CONTENTS**

Chapter 1. INTRODUCTION

1.1   OVERVIEW

In this thesis, spectroscopic properties of light-harvesting pigments, mainly carotenoids, in photosynthetic apparatus are presented. Chapter 1 describes the general concept of photosynthesis, cholorophylls as the main pigments, structural and spectroscopic behavior of carotenoids, and finally, energy transfer processes among the pigments. In the last part of the introduction, computational methods used for characterization of structural/spectroscopic properties of carotenoids are presented. In Chapter 2, the experimental methods are introduced. Ultrafast pump-prope spectroscopy is used as the main experimental method. Chapter 3 contains all results in the form of published papers. Last chapter, Chapter 4, includes a summary and the conclusion of the papers presented in Chapter 3.

1.2   PHOTOSYNTHESIS

Life on Earth relies on solar energy. Photosynthesis is an energy storage process on Earth: for without it neither plants nor animals (including humans) could survive. In this process, energy of sunlight is captured by a photosynthetic organism and stored as chemical energy. There are two major types of photosynthesis which are based on different mechanisms: chlorophyll-based and rhodopsin-based photosynthesis. Chlorophyll-based photosynthesis, the process which will be discussed in this thesis, can be further divided into oxygenic and anoxygenic photosynthesis in terms of whether oxygen is generated during the photosynthetic process. While plants, algae, and cyanobacteria utilize oxygenic photosynthesis[1],[2] to exploit the solar energy, photosynthetic bacteria use the simpler anoxygenic photosynthesis[1],[2]. An illustration of the general process in oxygenic chlorophyll-based photosynthesis is given in Figure 1.2.1. The whole process consists of two stages: light-dependent reactions and dark reactions. In the first stage, solar energy is absorbed and utilized to create ATP and NADPH. Then, these products are used in the second stage, called the Calvin cycle, to produce carbohydrates by assimilation of carbon dioxide.

Figure 1.2.1 shows the process.

$$\text{Light energy} + 2\,H_2O + CO_2 \longrightarrow H_2O + O_2 + (CH_2O)_n$$
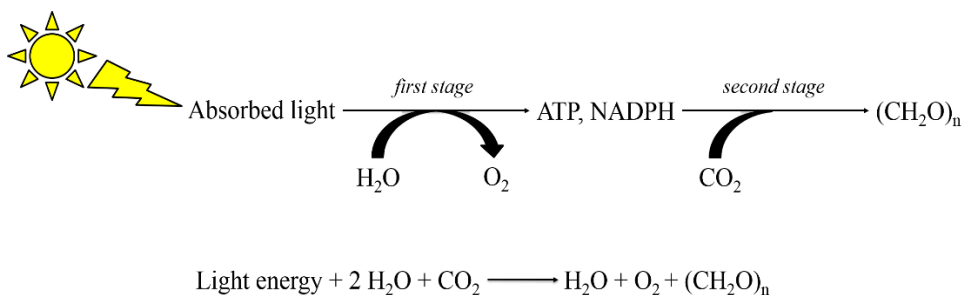
**Figure 1.2.1** Process of oxygenic chlorophyll-based photosynthesis.

Light-dependent reactions of photosynthesis are carried out in photosynthetic membranes. In plants and algae, these membranes are organized into organelles called chloroplasts. In cyanobacteria and bacteria, which are prokaryotic cells without complex internal organelles, an internal membrane system plays the role of the photosynthetic membrane. These membranes incorporate pigment-protein complexes which are responsible for the light-driven reactions during photosynthesis. These complexes are clusters of pigments associated with proteins which act as a scaffolding. Two types of such pigment-protein complexes relevant to the earliest phases of light-dependent reactions are light-harvesting complexes (LHC) and reaction centers (RC). The LHCs absorb light and this harvested energy is consequently transferred to the RCs[2]-[4]. In the reaction center occurs the charge separation, which is the first step towards conversion of light energy into chemical energy [1]-[3].

LHCs include antenna pigments which are responsible to absorb certain wavelengths of light such as chlorophylls (Chls) / bacteriochlorophylls (BChls), carotenoids, and phycobilins. Chls (present in photosynthetic eukaryotes) and BChls (found exclusively in photosynthetic bacteria) are both the main pigments in LHCs, and BChls absorb light of a longer wavelength than chlorophyll. Carotenoids and phycobilins (occuring in cyanobacteria) are especially efficient at absorbing wavelengths that are not well absorbed by Chls and BChls. They are responsible for funneling the absorbed energy to Chls or BChls. Thus, they are called accessory pigments in LHCs. Since this thesis is mainly about LHCs pigments of Chl-based photosynthesis, properties of Chls and carotenoids and their interactions in LHCs will be introduced in more detail.

1.3   CHLOROPHYLLS

Chlorophylls (Chls), substituted cyclic tetrapyrroles, are the main pigments to absorb energy from the sun in the visible region of spectrum. Although several types of Chls have been discovered in photosynthetic eukaryotes, Chl *a* is the most common pigment in antenna complexes. Other types of Chls, typically Chl *b* and Chl *c*, are often found as accessory pigments in a number of antenna complexes. Both Chl *a* and Chl *b* have a chlorin ring which is derived from a porphyrin ring; the four nitrogen atoms of the ring are coordinated to a central magnesium ion and include a phytol chain is connected by an ester linkage. By contrast to those, Chl *c* has a porphyrin ring and lacks the phytol chain. Their chemical structures are given in Figure 1.3.1.

All Chls share common features in their absorption spectra, the Soret and Q spectral bands. While the Soret band is in the blue part of absorption spectrum, peaking for various Chls in the 430-470 nm spectral range, Q bands split into the lowest energy Q_y band (620-700 nm) and a higher energy Q_x band (550-630 nm) that often overlaps with higher vibrational bands of the Q_y band. Having conjugated π electron system in the rings, these bands are due to π-π* transitions. The Q_y band is a basic HOMO – LUMO transition, representing a transition from the ground state to the first excited state, while the Soret band corresponds to a transition to higher excited state. The actual maxima of these spectral bands are affected by structural differences among different types of chlorophylls.
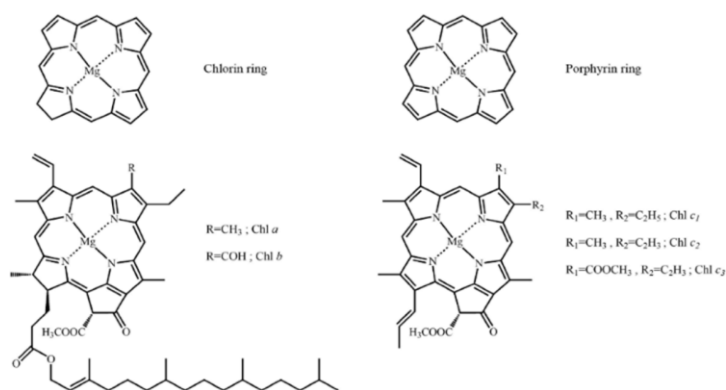
Figure 1.3.1 Molecular structures of Chl *a, b* and *c*.

(top) Macrocycles of different types of Chls. (bottom) The chemical structures of different Chls.

1.4   CAROTENOIDS

Carotenoids are an extensive group of natural pigments occurring in essentially all groups of organisms including bacteria, fungi, algae, green plants, animals, and humans. They have multiple functions in nature. In photosynthetic organisms, they perform two major roles: light harvesting and photoprotection. As light-harvesting pigments, they absorb radiation in the visible spectral region not accessible by Chls and transfer the absorbed energy to Chls [1]-[4]. As photoprotective agents, they quench singlet oxygen and both singlet and triplet states of Chls, preventing various reactive oxygen species (ROS) from formation and accumulation [2]-[6]. Moreover, in non-photosynthetic organisms, they have antioxidative and anti-cancer function[7]. This thesis focuses on carotenoid spectroscopic properties related to their light-harvesting function.

To understand the spectroscopic properties of carotenoids and underlying molecular mechanisms of energy transfer from carotenoids to Chls, it is important to know the molecular structures of carotenoids. The structures of some carotenoids, which are discussed in detail within this thesis, are shown in Figure 1.4.1. Carotenoids can be formally divided into two subgroups: carotenes and xanthophylls. While carotenes (lycopene, β-carotene, isorenieratene, renierapurpurin) are purely hydrocarbons, xanthophylls always have at least one oxygen atom in their structure: violaxanthin, fucoxanthin, isofucoxanthin, peridinin, vaucheriaxanthin and 8'-apo-β-carotenal. A common structural feature of all carotenoids is a conjugated π-electron system (*chromophore*), which consists of a chain of carbon atoms with alternating single (C–C) and double (C=C) bonds, and is responsible for their electronic properties. The number of conjugated C=C bonds (N) is usually denoted as the carotenoid conjugation length.

Most of the carotenoids are insoluble in water, which is the consequence of the non-polar nature of their structure. Only a few water-soluble carotenoids can be found in nature. These carotenoids have hydrophilic group(s) in their structure. Among them only crocin (isolated from crocus flowers and giving the typical color to saffron) Figure 1.4.1 exhibits appreciable water-solubility. In addition to natural carotenoids, there are some synthetic carotenoids with increased solubility in water such as astalysine (Figure 1.4.1).

Some carotenoids have a conjugated C=O group in their chromophore and are therefore called "carbonyl carotenoids" (Figure 1.4.1). While 8'-apo-β-carotenal,

fucoxanthin, and isofucoxanthin have the C=O group directly attached to the linear conjugated backbone, peridinin has a lactone ring, placing the C=O group aside from the main conjugation. Moreover, some carotenoids have more than one conjugated C=O group in their structure, and these two C=O groups are always positioned symmetrically in respect to the rest of conjugation: astaxanthin, astalysine and crocin. The positional effect of C=O groups in those carotenoids will be discussed in more detail in further sections.
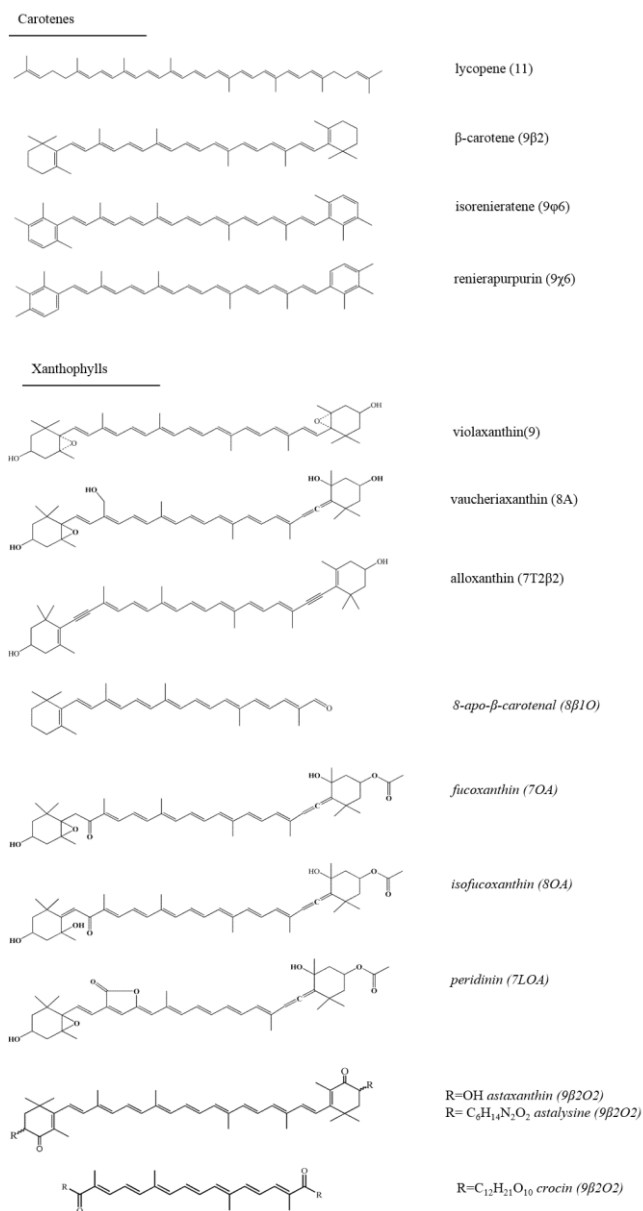
Figure 1.4.1 Molecular structures of carotenoids, mainly discussed in this thesis.
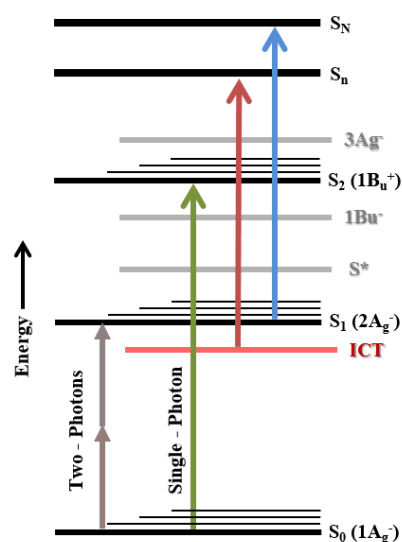
In the parenthesis: number of C=C bonds in chromophore, terminal ring type to which the conjugation is extended, number of C=C bonds at the terminal rings, O: conjugated carbonyl group, L: lactone ring, A: allene group, T: triple bond. Carbonyl carotenoids have their names shown in italic.

1.4.1 Electronic properties of carotenoids

To describe excited states of carotenoids, it often helps to use the terminology and knowledge gathered from numerous studies of their cousins, polyenes, which also have a linear conjugated π-electron system consisting of alternating C–C and C=C bonds. The major difference between polyenes and carotenoids lies in various functional groups attached to the conjugated backbone. In terms of geometry of polyenes, carotenoids belong to the C_{2h} symmetry point group. Then, the electronic states of polyenes can be described by four irreducible representations: A_g, A_u, B_g, B_u. Here 'A' and 'B' refer to symmetric and antisymmetric representations with respect to the 180º rotation operation (C_2), while 'u' and 'g' refer to symmetric and antisymmetric representations with respect to the inversion operation (i.e. combination of C_2 and $σ_h$ operations). In addition to the symmetry notations, the state labels for polyenes usually carry '+' and '-' superscripts, which denote the pseudoparity character introduced by Pariser[8]. The order of the states of the same symmetry is labelled by a number in front of the symmetry symbol, and the singlet (triplet) character is denoted by the superscript number. Thus, for example, symbol $3^1A_g^-$ denotes the third singlet excited state with A_g^- symmetry.

The scheme of the low-lying singlet excited states of carotenoids in the C_{2h} symmetry group is shown in Figure 1.4.2. Following the general notation used in literature, we denote the ground state as S_0, the lowest excited state is S_1, and the strongly absorbing in the blue-green region is the S_2 state. According to symmetry rules described above, the S_0 is labeled as the $1^1A_g^-$ ground state wavefunction, which is symmetric with respect to the C_2 group, where i and $σ_h$ operations with a negative pseudoparity sign. The S_1 state of carotenoids /polyenes has the same symmetry elements as S_0 state; it is, therefore, labelled $2^1A_g^-$. Because of this, the lowest single excitation is optically inaccessible (dark) via one-photon processes.

Figure 1.4.2 Low-lying singlet states of carotenoids in the C_{2h} symmetry point.

However, due to complementary selection rules between one- and two-photon

absorption, a two-photon absorption process is allowed for this transition. The S_2 state is denoted as $1^1B_u^+$. The $S_0 - S_2$ transition is allowed via single photon absorption in the blue-green region because symmetry labels of these two states are different. This simplified three-level scheme is valid for carotenoids/polyenes with N>3. Otherwise, the B_u state lies below the A_g state [9],[10]. This three-state model is useful for a basic description of excited state dynamics of carotenoids for N=7-9. It turns out that carotenoids with longer conjugation lengths (N>10) have other dark states within S_1-S_2 energy gap [11],[12]. These additional dark states shown in Figure 1.4.2, denoted as $1B_u^-$ and S*, are supposedly involved in relaxation pathways between S_2 and S_1 state [13],[14]. Additionally, for most carotenoids with N$\approx$13, one more dark state, $3A_g^-$, is predicted to lie above the S_2 state[15].

Carbonyl carotenoids are a group of carotenoids with specific spectroscopic properties. Since they have C=O group in their *chromophore,* another dark state with a charge-transfer character, an intramolecular charge transfer (ICT) state, exists in their excited-state manifold (Figure 1.4.2) The spectroscopic markers of this additional dark state are: i) an ICT band in their transient absorption spectra that is more pronounced in polar-environment[16][17][18]; ii) S_1 lifetime shortening[17][19] iii) a weak stimulated emission in the near-IR spectral region[17].

Hereafter, two groups of carotenoids will be recognized in this thesis based on the presence (*carbonyl carotenoids*) or absence (*non-carbonyl carotenoids*) of the conjugated C=O group. The dynamics of excited states of these two groups will be discussed in the following sections.

1.4.2   The S_2 State

As mentioned in the previous section, the $S_0 - S_2$ transition is strongly one-photon allowed. This transition usually exhibits three well-resolved vibrational bands [12] resulting from combinations of two symmetric vibrational modes (C=C and C–C stretching). The typical energy gap between the vibrational bands is ~1350 cm^{-1} as a result of mixing the C–C and C=C stretches with frequencies of ~1150 and ~1600 cm^{-1}, respectively. The absorption spectra of violaxanthin, a non-carbonyl carotenoid, in non-polar and polar solvent are shown in Figure 1.4.3A as an example. The resolution of vibrational bands of non-carbonyl carotenoids is not affected by solvent polarity (Figure 1.4.3A), but it is affected by the carotenoid structure. Due to a broader distribution of conformers, less resolved vibrational bands are typically observed for non-carbonyl carotenoids with conjugation extended to various end groups [PAPER 3].

Comparison of absorption spectra of violaxanthin and β-carotene shown in Figure 1.4.3B demonstrates this effect. Moreover, one of our findings regarding spectroscopic properties of aryl carotenoids is that the resolution of these bands is independent on the type of terminal ring (PAPER 3/Figure 3.3.2).

Another important conclusion taken from Figure 1.4.3B is that the S_2 state of β-carotene has lower energy than violaxanthin as evidenced by the ~10 nm red-shift of β-carotene absorption spectrum. The red shift thus shows that there is a relation between the S_2 state energy and structure of carotenoids (Table 1.4.1) [12]. This relation can be explained by molecular orbital theory of linear polyenes and/or by the "electron-in-a-box" model[20]-[22]. In terms of molecular orbital theory, the 0-0 energy (the S_2 state energy) can be described by basic properties of a HOMO – LUMO transition. Increasing the number of π electrons in conjugation system of carotenoids leads to a decrease of the energy gap between HOMO (π) and LUMO (π*) orbitals. In the free electron model, the π orbitals in conjugated system of carotenoids act as a box for the electrons. Then, according to the fundamental principles of quantum mechanics, energy of an electron in a box is inversely proportional to the square of the box length. Thus, the energy must decrease with increasing the conjugation length. Both models thus explain why the red-shift of the S_0-S_2 transition occurs with increasing the conjugation length of carotenoids.
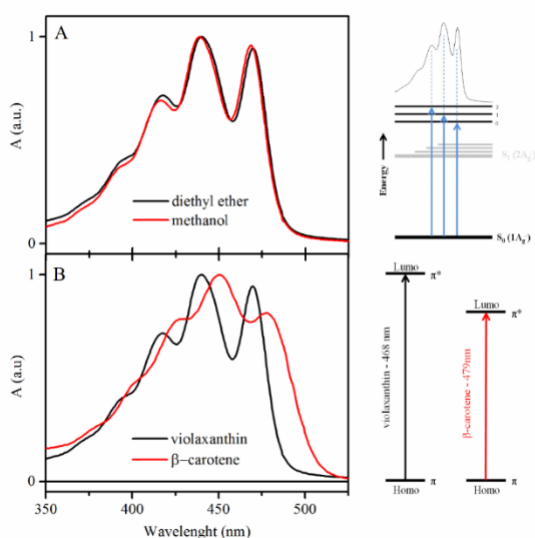
Figure 1.4.3 Absorption spectra of violaxanthin and β-carotene.

A violaxanthin in non-polar and polar solvent, diethyl ether and methanol, respectively. **B** comparison of absorption spectra of violaxanthin and β-carotene in a non-polar solvent.
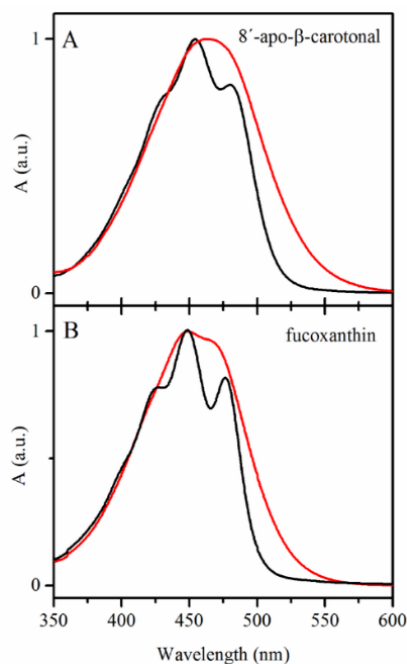
Figure 1.4.4 Absorbance spectra of carbonyl carotenoids.

A 8'-apo-β-carotenal and **B** fucoxanthin in non-polar (n-hexane, black) and polar solvent (methanol, red).

In contrast to non-carbonyl carotenoids, the S_0-S_2 transition of carbonyl carotenoids is affected by solvent polarity [12],[23],[PAPER 1],[PAPER 4]. Solvent effects on the S_0-S_2 transition of carbonyl carotenoids are demonstrated in Figure 1.4.4. 8'-apo-β-carotenal [PAPER 1] and fucoxanthin[PAPER 4] are chosen as examples of carbonyl carotenoids. Good resolution of vibrational bands of the S_0-S_2 transition is preserved in a non-polar solvent, but changing to polar solvent leads to significant loss of the resolution of vibrational bands due to increasing conformational disorder [12], [PAPER 1]. The disappearance of pronounced vibrational bands is also observed for other carbonyl carotenoids [17],[24],[25]. Additionally, an asymmetric broadening of the S_0-S_2 transition towards lower energies is also often detected in absorption spectra of carbonyl carotenoids in polar solvents [12],[23]. The S_2 state energies of carbonyl carotenoids are given in Table 1.4.1.
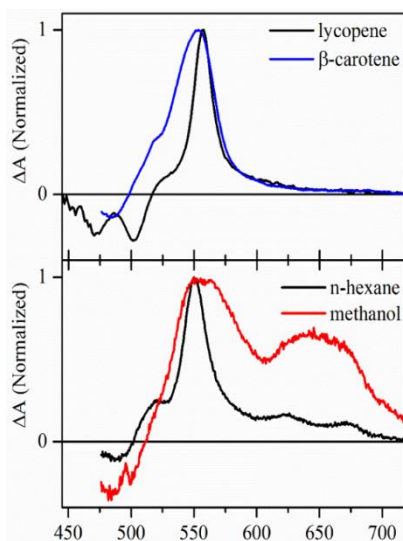
Since the S_1 state is invisible in absorption spectra of carotenoids, other methods, based on investigation of transient species populated by the decay of the initially-excited S_2 state, must be applied to investigate of spectroscopic behavior of this dark state. After a carotenoid is excited into the S_2 state, it will first decay to the S_1 state and then to the ground state. The first, S_2-S_1 internal conversion takes place on the scale of hundreds of femtoseconds, typically 100-300 fs for non-carbonyl carotenoids[12]. The question of the precise mechanism of the S_2-S_1 internal conversion is still a subject of a considerable debate because calculations suggest there are additional states within the S_1-S_2 gap[11]-[15] which may facilitate this internal conversion. For carbonyl carotenoids the depopulation of the S_2 state can be even shorter than 100 femtoseconds (<60 fs for peridinin in methanol) due to their quite narrow S_2-S_1 energy gap[23].

1.4.3 The S_1 state

Because the S_0-S_1 transition is forbidden, gaining information about the S_1 state is a more complicated task. To have the state populated, the carotenoid must be excited into its S_2 state. Afterwards, through the process of internal conversion, the electron population arrives at the S_1 state. Thus, several techniques have been employed to gain information about this state. In brief, these methods are fluorescence[26],[27], resonance Raman[28]-[30], two-photon[31]-[34], and pump-probe spectroscopy, the last being presented in more detail in the methods section of this thesis. All these methods have their advantages and disadvantages in terms of both S_1 state energy and lifetime determination; but, the last method has been largely used to gain information about S_1 lifetime and spectra. In this method, carotenoid is excited to the lowest vibrational band of the S_2 state by femtosecond excitation pulse and then relaxes to the S_1 state through the S_2-S_1 internal conversion (~50-200 fs) [12],[Chapter 3]. Already in the S_1 state the vibrational cooling takes place on the sub-picosecond timescale[4],[12],[PAPER 3]. Consequently, upon application of the probe pulse some photons with different energies are absorbed from the relaxed S_1 state. The time evolution of this characteristic band (S_1-S_N, see Figure 1.4.2), called excited-state absorption (ESA), bears information regarding the relaxation dynamics of the S_1 state. The bandwidth and position of the S_1-S_N band contain information about carotenoid structure. The width of the S_1-S_N band for linear carotenoids is narrower than that of carotenoids which are influenced by conformational disorder such as in β-carotene (Figure 1.4.5A). For carbonyl carotenoids, this effect (Figure 1.4.5B) is intensified in solvents with higher polarity due to hydrogen bonding between the C=O group and the solvent [19],[25],[PAPER 1],[PAPER 4]. The decay of the S_1-S_N band provides information about the S_1 lifetime. It is well-known there is a linear relationship between the conjugation length and the S_1 lifetime for linear carotenoids: the S_1 lifetime gets shorter with increasing conjugation length[12],[35]. Thus, for carotenoids of more complicated structures it is useful to introduce a concept of *effective conjugation length (N_{eff})*. The S_1 lifetime from the measurement may then be used to determine N_{eff} due to their mutual linear dependence. N_{eff}, then, is a measure of how the conjugation extended to terminal rings affects the total conjugation length of a carotenoid. This effect is discussed in more detail in the research section (Chapter 3/PAPER 3).

The spectroscopic properties of excited states of carbonyl carotenoids are more complicated than that of non-carbonyl carotenoids because of their strong polarity-dependent behavior (Figure 1.4.5). For this type of carotenoid, the ICT-S_n transition, which is red shifted from the S_1-S_N transition, is observed in their transient absorption spectra[16],[25]. The magnitude of this signal increases with increasing solvent polarity [19],[23],[24],[PAPER 4] provided that the conjugated C=O group is asymmetrically positioned. For a symmetrically positioned C=O group, as in astaxanthin, astalysine, or crocin, no polarity effect is observed in solution[36],[37]. Additionally, it was found that for peridinin analogs the position of lactone ring on the conjugated chain influences a magnitude of the ICT band [38]. Moreover, the S_1-lifetime shortening correlates with the magnitude of ICT signal [19],[PAPER 4], most probably due to ICT coupling to the S_1 state.

Figure 1.4.5 Transient absorption spectra of lycopene, β-carotene, and 8'-apo-β-carotenal

A lycopene (blue line) and β-carotene (black line) in n-hexane. **B** 8'-apo-β-carotenal in n-hexane (black line) and methanol (red line).

Despite extensive experimental and computational efforts, the relation between the ICT and the S_1 state is still a controversial topic. Three models have been suggested. In the first model the ICT state is strongly coupled with the S_1 state (S_1/ICT). There are thus two minima in the potential energy surface from which the population decays with the same time constant to the ground state[16],[25],[33],[39]. In the second model the ICT state is essentially the S_1 state (S_1=ICT) in a molecule with a different conformation/configuration [40],[41],[PAPER 1]. In our paper (see the Chapter 3/PAPER 1) on 8'-apo-β-carotenal, we proposed that the S_1-S_3 transition, forbidden in C_{2h} symmetry, becomes allowed in the polar solvent where for some sub-ensemble of molecules this symmetry is broken. Thus, the S_1 state itself yields some ICT character, and the S_1-S_3 transition is considered as the ICT-S_n transition [PAPER 1]. In the last model the ICT state is created via solvent-induced S_1 and S_2 state mixing ((S_1+S_2)/ICT) [42].

Table 1.4.1 Energies of the S_0-S_2, S_1-S_N and ICT-S_n transitions. S_1/ICT and S_1 lifetimes.

Carotenoids	Solvents	S_0-S_2 [a]	S_1-S_N	ICT-S_n	τ_{S1} [b]	References
non-carbonyl						
lycopene	n-hexane	19 930	17 953		4	[PAPER 3]
β-carotene	n-hexane	20 870	18 149		8.2	[PAPER 3]
isorenieratene	n-hexane	20 850	17 889		12	[PAPER 3]
renierapurpurin	n-hexane	19 930	17 212		6.7	[PAPER 3]
violaxanthin	methanol	21 368	19 455		26	[PAPER 7]
vaucheriaxanthin	methanol	21 277	19 455		29	[PAPER 7]
alloxanthin	methanol	20 877	18 248		19	[PAPER 5]
carbonyl						
8'-apo-β-carotenal						
	n-hexane	20 747	18 182	16 051 14 925	26	[PAPER 1] [43]
	methanol	21 692	18 018	15 385	8	[PAPER 1] [43][44]
	acetonitrile	21 834	18 149	15 314	8	[44][45]
fucoxanthin						
	n-hexane	21 008	19 305	16 949 15 504	63	[16][23]
	methanol	22 321	19 048	16 667 15 625	21	[PAPER 4] [16][32][46][47]
	acetonitrile	22 422	19 120	16 667 15 625	31	[PAPER 4] [16][23]
peridinin						
	n-hexane	20 576	19 608	15 152	166	[16][17][19] [23][24][25] [48][49]
	methanol	21 052	19 400	16 900	10	[16][17][19] [24][25][48]
	acetonitrile	20 620	19 610	16 950	8	[19][23][25] [48][49]
isofucoxanthin-like						
	n-hexane	20 161	18 018	16 000 – 14 286	42	[PAPER 4]
	methanol	~20 202	17 699		11	[PAPER 4]
	acetonitrile				4	[PAPER 4]

[a] Energies for 0-0 transitions are given for all carotenoids apart from carotenal and peridinin (0-1 transitions in these two cases). All values are given in cm^{-1}. [b] The S_1 lifetimes for non-carbonyl carotenoids are taken from our experiments. The S_1/ICT lifetimes, except for isofucoxanthin-like, represent mean values obtained from various experiments

Even though all asymmetrically positioned carbonyl carotenoids exhibit typical polarity-dependent behavior, as discussed above, their response to solvent proticity (ability of the solvent to make hydrogen bonds with solute) are different. The effect of solvent proticity on spectroscopic properties of on carbonyl carotenoids is also a subject of this thesis (Chapter 3/PAPER 4). It is hypothesized that carbonyl carotenoids can be divided into three groups with respect to different response to solvent proticity. The first group contains apo-carotenals which have almost the same S_1/ICT lifetime in both protic (methanol) and aprotic (acetonitrile) solvent. The second group includes fucoxanthin, which has shorter lifetimes in methanol than in acetonitrile. The last group involves peridinin, its analogues, and a structurally unknown carbonyl carotenoid related to isofucoxanthin which all have shorter lifetime in aprotic acetonitrile (Table 1.4.1).

1.5 ENERGY TRANSFER MECHANISMS IN LIGHT-HARVESTING COMPLEXES

Harvested energy is transferred as excitation energy first among pigments within the same complex and then to other LHCs until it reaches the reaction center. In order to achieve energy transfer, the energy of the donor states must be higher than energy of the acceptor states. Thus, the pathway of transferred energy can be depicted as an energetically 'downhill' model (Figure 1.5.1). The energy transfer processes are significantly dependent on the interaction between donor and acceptor. In this sense, the mutual orientation of the donor and acceptor, including their distance, play a crucial role. Theoretically, the energy transfer rate given in Eq. 1.5.1. In this equation, the coupling term, V, represents the Coulomb dipole-dipole interaction between donor and acceptor (Eq. 1.5.2), and J is spectral overlap between donor fluorescence and acceptor absorption bands (Eq. 1.5.3). This energy transfer mechanism was first described by Theodor Förster, now known as the Förster theory, to estimate energy transfer rate between donor and acceptor. He showed that the larger spectral overlap gives the higher rate of transferred energy. In the dipole-dipole approximation, combination of Eq. 1.5.1 and Eq. 1.5.2, one can see that the scale of energy transfer rate exhibits inverse sixth power dependence on donor-acceptor separation. It is important to mention that this approximation is valid only when donor and acceptor distance is larger than their molecular size. Otherwise, the theory usually fails to reproduce experimental data.

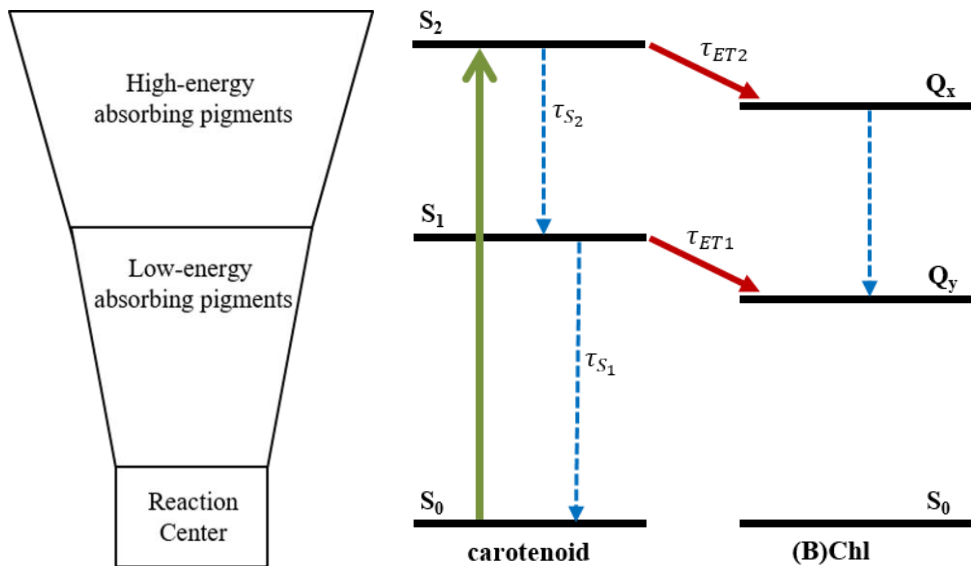$$\kappa_{ET} = \frac{1}{\hbar^2 c} V^2 J$$

Eq. 1.5.1

V: Coupling term, J: Spectral overlap

$$V = \frac{1}{4\pi\varepsilon_0} \frac{\kappa |\overrightarrow{\mu_D}||\overrightarrow{\mu_A}|}{R_{AD}^3}$$

Eq. 1.5.2

D: Donor, A: Acceptor, R_{AD}: Distance between D and A, $\overrightarrow{\mu_D}$ and $\overrightarrow{\mu_A}$: transition dipole moments, $\kappa = \hat{\mu}_D . \hat{\mu}_A - 3(\hat{\mu}_D . \hat{R}_{AD})(\hat{\mu}_A . \hat{R}_{AD})$: the orientation factor.

$$J = \int F_D(\lambda) \, \varepsilon_A(\lambda) \, \lambda^4 \, d\lambda$$

Eq. 1.5.3

$F_D(\lambda)$: normalized area of donor emission, $\varepsilon_A(\lambda)$: the extinction coefficient of acceptor absorption

Figure 1.5.1 Downhill energy transfer model between pigments and antennas.

Figure 1.5.2 Scheme of energy transfer pathways between carotenoids and (B)Chl.

Although chlorophylls are the primary pigments in an antenna system, carotenoids assist them to absorb light at wavelengths that are not accessible to chlorophylls. In carotenoid-to-Chl energy transfer, both S_1 and S_2 states may act as energy donors, while the Q_y and Q_x states of Chls are energy acceptors [1]-[3],[22] (Figure 1.5.2). In order to achieve energy transfer the transfer rate must compete with the

state's intrinsic lifetime [50]. In this sense, carotenoid structure and their spectroscopic properties, which determine the energies and intrinsic lifetimes as a donor, obtain a critical role. S_2-mediated energy transfer of carotenoids in LHCs can be calculated by the Förster mechanism because of proper donor acceptor distance and large dipole moment of S_2 state. Morever, S_1-mediated energy transfer cannot be explained by the Förster mechanism due to a virtually zero dipole moment of this state. Thus, it is necessary to compute higher orders of Coulombic interaction, which influences directly the quantum mechanical nature of the energy-transfer mechanism between donor and acceptor states[1]. To deal with these problems, the transition density cube (TDC) method was developed by Krueger et al.[51], using discrete charge and the Coulombic interaction between all pair, is determined. In other words, instead of dipole-dipole interactions, the multipole transition interaction between the transition densities of the donor and acceptor states are used for a three-dimensional grid of finite-sized volume cells[1],[51].

1.6   COMPUTATIONAL METHODS

In addition to experimental investigations of carotenoids, computational methods were used in this thesis to gain more information about their spectroscopic properties. Thus, in this section, a general description of computational methods will be given, followed by their application to compute some excited-state properties of carotenoids.

The computational methods applied to biological systems assist with understanding macroscopic world of the laboratory. In the widest sense, there are two main computational methods: molecular dynamics (MM) and electronic structure theory (QM). The first one is mostly governed by the laws of classical physics. This method is based on the basis of Newton's equation of motion. Energy of the system is described by applying of integration with a function of the atomic coordinates (called force field). Since this method is based on interaction among nuclei in the system, it is useful for very large systems like proteins, DNA, membranes, and complexes.

The second method uses rules of quantum physics which express explicitly that the energy and other related properties of the system could be obtained from solving the Schrödinger equation which is based on wave characteristics of particles. Because this method is computationally very demanding, application of this method for biological systems is rather limited. However, a combination of these two

methods, which is called QM/MM, is largely used to obtain specific information about the excited states of an interesting part of the greater system. In this approach, QM calculations are used for the site of interest, and the behavior of rest of the system is calculated by MM methods[52],[53],[54]. Hereafter, we will bring out the foundation of quantum mechanical calculations of the molecular system called the many-body system. The general expression of Schrödinger equation for such a system is given in Eq. 1.6.1. Since $\hat{H}$ itself is not dependent on time, this equation is called the time-independent Schrodinger equation.

$$\hat{H}\,\Psi(\vec{r},\vec{R},t) = E\Psi(\vec{r},\vec{R},t)$$
$$\left(\hat{T}_e(\vec{r}) + \hat{T}_N(\vec{R}) + V_{ee}(\vec{r}) + V_{NN}(\vec{R}) + V_{eN}(\vec{r},\vec{R})\right)\Psi(\vec{r},\vec{R}) = E\,\Psi(\vec{r},\vec{R})$$

Eq. 1.6.1

where $\hat{H}$: the total energy operator (Hamiltonian) , E : total energy, Ψ :the wavefunction of the system, $\hat{T}_e$: kinetic energy operator for electrons, $\hat{T}_N$: kinetic energy operator for nuclei, V_{ee} : electron-electron repulsion, V_{NN} : nuclei-nuclei repulsion, V_{eN} : electron-nuclei attraction, $\vec{r}$: coordinate of electrons and $\vec{R}$: coordinate of the nuclei.

The Hamiltonian includes all electrons and nuclei and also interactions among them. Furthermore, the wavefunction depends on the positions of the particles and time, even in the case for time-independent Hamiltonian. However, the analytic solution of Schrödinger equation is impossible for many-electron, and some approximations are needed. The basic approximation helping to solve the Schrödinger equation is the Born-Oppenheimer approximation. Since electrons are much lighter and move much faster than nuclei, the kinetic energy of nuclei can be neglected and nucleus-nucleus repulsion can be thought as constant in electronic Schrödinger equation (Eq. 1.6.2). Hence, the general method is called Electronic Structure Theory. In calculating properties of molecules, useful approximations employ linear combinations of atomic orbitals (MO-LCAO). The molecular orbitals are found as linear combinations of atomic orbitals known as basis functions, which represent mathematical description of atomic orbitals in which electron functions have finite probability. Thus, the *basis sets* are important for each electron in molecular systems.

Another approximation is related to single-electron motion in the molecular system. In this approximation, each electron moves in an 'averaged field' created by other electrons in the many-electrons system (self-consistent field), and total wavefunction is then obtained as a product of one-electron functions using a single Slater determinant. This method is known as the Hartree-Fock (HF) theory [20],[21],[55]. All approximations mentioned above then lead to the following equation

$$\underbrace{\hat{H}\,\Psi(\vec{r},\vec{R}) = E_{total}\Psi(\vec{r},\vec{R})}_{\textit{Schrodinger equation}} \quad \Rightarrow \quad \underbrace{\hat{H}_{elec}\Psi(\vec{r}) = E_{elec}\Psi(\vec{r})}_{\textit{Electronic part of the equation}}$$ Eq. 1.6.2

$$\hat{H}_{elec} = \hat{T}_e(\vec{r}) + V_{eN}(\vec{r},\vec{R}) + V_{ee}(\vec{r})$$

Due to inadequate treatment of electron-electron repulsion between the motions of electrons in the many-electron systems, HF does not cover electron correlations. Thus, the energies obtained in the HF level of theory are higher than the true energies of the system. To deal with this problem, electron correlation methods, such as Configuration Interaction (CI), Coupled Cluster (CC), or Møller-Plesset (MP) Perturbation Theory have been developed. All these methods are based on giving more space to electrons by a larger basis set and use more Slater determinants for the many-electron systems.

The methods discussed above are called wavefunction-based methods in electronic structure theory. Another method commonly used to solve properties of many-electron systems is Density Functional Theory (DFT)[56]. Unlike wavefunction methods related with coordinate of the particles, DFT is based on the changes in density which is proved in Hohenberg-Kohn theorem[57]. The key point of this method is that electron-electron interaction is defined as consisting of two components, exchange and correlation, which are modeled by a general function of electron density (ρ). The exchange term is arising from the antisymmetric properties of the wavefunction, and the correlation is related to the motion of the individual electrons. Consequently, electronic energy, as a function of electron density of the many-electron system, is identified as

$$E_{elec}(\rho) = E_T(\rho) + E_V(\rho) + E_J(\rho) + E_{XC}(\rho)$$ Eq. 1.6.3

$E_T(\rho)$: kinetic energy of electrons, $E_V(\rho)$: potential energy term (including nuclear-electron attraction and electron-electron repulsion term), $E_J(\rho)$: electron-electron repulsion, and $E_{XC}(\rho)$: exchange-corelation term for electron-electron interaction.

According to the chosen exchange correlation functions, DFT has various levels of theory. These can be divided into three groups called *Local density functionals*, which includes local electron spin densities; *Gradient-Corrected functionals*, involving local spin gradient as well as their local densities; and Hybrid functions, which are defined by linear combinations of Hartree-Fock, local and gradient-corrected exchange functionals, and local and/or gradient corrected correlation functional. Widely-used exchange-correlation functions are listed in Table 1.6.1.

**Table 1.6.1**. Exchange-correlation functionals in DFT methods.

DFT Methods	Exchange functional	Correlation functional
Local Density functions	Slater (S)	Vosvo, Wilk, Nunair (VWN)
Gradient-corrected Functions	Becke (B)	Lee, Yang, Parr (LYP) Perdew 86 (P86) Perdew-Wang 91 (PW91)
Hybrid functions	Becke's three parameters (B3)	Lee, Yang, Parr (LYP) Perdew-Wang 91 (PW91)

After briefly discussing the general concept of electronic structural methods, we can turn to computational studies on carotenoids. Due to the inclusion of electron correlation, DFT methods give more suitable results for π-electron system. The B3LYP exchange-correlation functional in combination with a middle-sized basis set like 6-31G(d)[58] or triple-ξ-quality (TZVP)[59] is widely-used to investigate ground state structure and vibrational spectroscopic properties of carotenoids[30],[60]-[65]. The ground state structure including conformation and intramolecular interaction of carotenoids are important to investigate how many π-electrons are involved in the conjugation [PAPER 3],[PAPER 5].

The overall electron contributions to the ground state of carotenoids influence also excited state properties of carotenoids. Thus, ground state conformational analysis is crucial for further excited state calculations. Excited state calculations of carotenoids are computationally more demanding and time consuming. Since molecular orbitals are optimized by HF theory, which is the easiest way to perform these calculations, the CI method is favorable for excited state calculations of carotenoids. The CI single (CIS) method is used to create excited state geometries for carbonyl carotenoids, especially in solution[18],[38]. Also, Multi Reference CI (MRCI) in combination with DFT gives more accurate results for excited state configurations[66] and provide correct order of excited state energy levels by putting the calculated S_1 state below the S_2 state[67]. Another approach used to calculate excited state properties of carotenoids exploits time dependency of the external potential. This method, known as time dependent DFT (TD-DFT), provides substantially better results than CI for excited state energies. Alternatively, the Tamm-Dancoff approximation is added to TD-DFT, which is mainly a minor code modification of TD-DFT developed to use only virtual-occupied orbitals, resulting in TD-DFT/TDA method[68],[69]. Since this method is based on TDDFT, it gives proper state ordering according to energy (E (S_1) < E (S_2)), especially if used in combination with gradient-corrected functionals and the TZVP basis set, and provides double

excitation configurations in terms of molecular orbitals ((HOMO, HOMO) – (LUMO, LUMO)) for the S_1 state and a single HOMO – LUMO transition for the S_2 state[PAPER 3],[PAPER 4],[PAPER 5]. While the range-separated version of B3LYP utilizes CAM-B3LYP[70] functionals which reasonably reproduce the S_2 state energies, they cannot reproduce the S_1 energy as they usually place the S_1 state above the S_2 state.

In order to support our experimental results obtained for non-carbonyl carotenoids given in Chapter 3/PAPER 3 and PAPER 5, the transition energies of those carotenoids were calculated using TD-DFT/TDA method with BLYP functional (S_0-S_1 transitions) and with CAM-B3LYP functional (S_0-S_2 transitions) in combination with TZVP. Although the calculated state energies are higher than experimentally observed, these methods are useful to compare properties of carotenoids with different structures. In the Chapter 3/PAPER 4, only S_0-S_2 transitions are calculated for carbonyl carotenoids because the molecular orbital transition provided by the TD-DFT/TDA method is mixed for carbonyl carotenoids with the higher transition orbitals for the S_1 state; thus, one cannot observed the true ordering of the states. The calculated transition values are presented in Table 1.6.2.
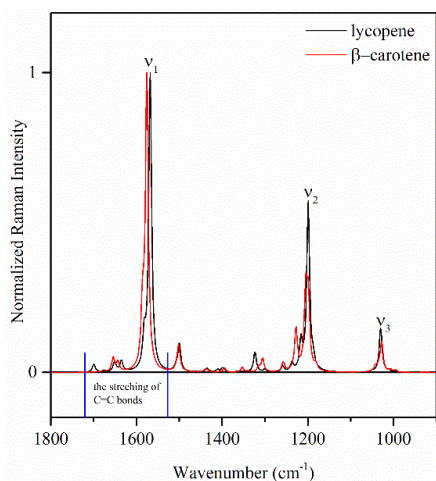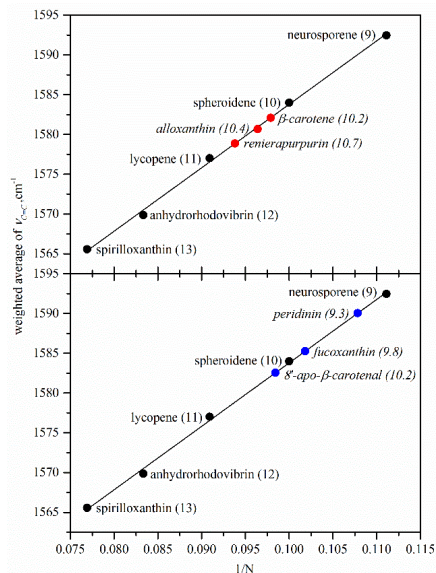

Figure 1.6.1 Calculated Raman spectra of lycopene and β-carotene.

A spectroscopic method providing information about ground state conformation/structure of carotenoids is Raman spectroscopy. When the frequency of light inducing the Raman effect matches an electronic transition, the method known as resonance Raman (RR) spectroscopy, which is favorable for π-electron and complex systems[28],[71]-[73]. Carotenoids have four main characteristic peaks in their Raman or RR spectra. These bands mainly arise from the stretching of C=C bonds (ν_1), C-C bonds stretching with C-C bending modes of conjugated chain (ν_2), rocking vibrational motion of methyl groups which are attached to the conjugation length (ν_3), and coupling with C=C torsional modes and C-H vibrational wagging motion (ν_4). Calculated Raman spectra of lycopene and β-carotene are given in Figure 1.6.1 to show these bands.

Since this thesis does not address the Raman spectra of carotenoids, the details will not be discussed. However, since the stretching frequency of C=C bond ($\nu_{c=c}$) is sensitive to conjugation length of carotenoids [64],[65], this band is related to the conjugation length, effective conjugation length (Figure 1.6.1), and the electronic properties of carotenoids. Thus, here we will focus on this peak which is calculated using B3LYP with the 6-31G(d,p) basis set for linear carotenoids. The conjugation of non-carbonyl carotenoids, which extends to their terminal rings, and carbonyl carotenoids are given in Table 1.6.2 and Figure 1.6.2. The aim of these calculations is to estimate N_{eff} of non-linear carotenoids based on their ground state $\nu_{c=c}$ frequencies. The weighted mean of $\nu_{c=c}$ frequencies is used in order to include all C=C stretching Raman bands. Figure 1.6.2 shows that the $\nu_{c=c}$ frequencies of linear carotenoids from

Figure 1.6.2 Dependence of calculated Raman C=C stretching band on conjugation length.

(top) non-carbonyl carotenoids, (bottom) carbonyl carotenoids. The corresponding effective conjugation lengths are given in parentheses.

N=9 to 13 can be fitted by a linear function. Using this function, one can obtained N_{eff} for non-linear and carbonyl carotenoids (Table 1.6.2). The advantage of using Raman spectra for excited state geometry calculation, as discussed in detail above, is that it may provide a way to investigate the spectroscopic properties of carbonyl carotenoids, especially for their response to solvent proticity.

Table 1.6.2. Calculated Raman C=C stretching bands[b] and transition energies[c] of carotenoids.

| Carotenoids [a]	$v_{C=C}$	$S_0 \rightarrow S_2$	$S_0 \rightarrow S_1$
linear			
neurosporene	1592.46	25 930 *24 580*	17 456
spheroidene	1583.98	23 409 *24 020*	16 241
lycopene	1577.00	21 324 *23 105*	15 172
anhydrorhodovibrin	1569.86	19 980 *22 578*	14 252
spirilloxanthin	1565.58	18 982 *22 145*	13 487
non-linear			
β-carotene	1582.09	23 580 *21 980*	15 310
renierapurpurin	1578.87	20 280 *21 320*	14 530
alloxanthin	1580.66	21 551 *22 271*	16 077
carbonyl			
8'-apo-β-carotenal	1582.54	- *24 385*	-
fucoxanthin	1585.25	- *25 062*	-
peridinin	1590.03	- *24 278*	-

[a] Non-carbonyl carotenoids are listed as linear and non-linear in terms of their end groups. [b] The weighted Raman C=C stretching bands are calculated using B3LYP/6-31G (d,p). [c] Calculations of energies were carried out using TDA BLYP/TZVP and TDA Cam-B3LYP/TZVP (results shown in italics).

Chapter 2. EXPERIMENTAL METHODS

2.1   OVERVIEW

Spectroscopic methods are widely used to detect and determine molecular structures as well as obtain information about dynamics and energetics of molecular systems. Various types of spectroscopic techniques are also used to study properties of photosynthetic light-harvesting systems and their pigments, aiming to obtain details about excited-state properties (energies, lifetimes, and transition probabilities) of individual pigments as well as information about interaction between pigments in light-harvesting systems. Each spectroscopic method is based on interaction of radiation with matter though the spectral range, given in Figure 2.1.1, varies for different methods. Experiments in this thesis involve exclusively absorption spectroscopy techniques in the VIS-NIR spectral region. When a photon is absorbed by a molecule, transitions from lower-energy states to higher-energy states occur according to the energy of the absorbed photon. This part of the thesis briefly introduces the steady-state and transient absorption spectroscopies used in experiments described in this thesis. Using the first method, steady-state spectroscopy, one can get direct information about the absorbing state energy and steady-state molecular properties such as conformation, aggregation, etc., of light-harvesting systems and the pigments which exist in the systems. The second method, transient absorption spectroscopy, provides information about excited-state dynamics.
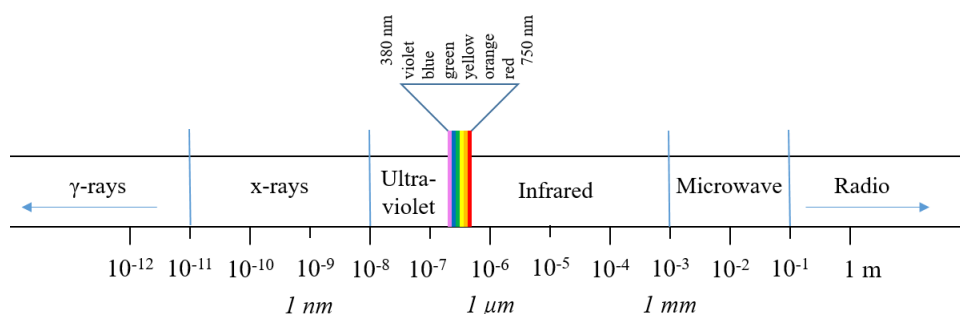
Figure 2.1.1 Electromagnetic spectrum.

2.2 STEADY-STATE ABSORPTION SPECTROSCOPY

The measurement of absorption spectra is a basic aspect of optical spectroscopy. The absorption spectrum shows the fraction of incident light absorbed by the sample over a range of frequencies. When the beam interacts with the sample, the intensity of light decreases at certain wavelengths due to absorption of photons of certain energy by molecules in the sample. When the beam passes through the sample, absorbance is a logarithm of the ratio between light intensity before (I_b) and after (I_a) the sample Eq. 2.2.1. Moreover, it is directly related to the concentration and path length of the sample. This relation among absorbance, concentration and path length is described by the Lambert-Beer Law (Eq. 2.2.1). An absorption spectrum is plotted against the wavelength. The position and intensity of the spectral bands in the absorption spectrum provide crucial information such as the energy of the absorbing states and the corresponding transition dipole moments related by the integrated absorption coefficient (Eq. 2.2.2). From the shape of absorption bands further important information about the studied sample, such as conformational disorder or vibrational structure of individual transitions, can be inferred.

$$A = log\frac{I_b}{I_a} = \varepsilon \, c \, l$$

Eq. 2.2.1

A: absorbance, I_b: light intensity before sample, I_a: light intensity after sample ε: molar extinction coefficient, c: molar concentration, l:path length

$$\mathcal{A} = \frac{\pi v_{fi} N_A |\mu_{fi}|^2}{3\varepsilon_0 \hbar c}$$

Eq. 2.2.2

$\mathcal{A}$: integrated absorption coefficient, N_A: Avagadro's constant, v_{fi}: transition frequency between initial and final states, μ: transition dipol moment.

From a technical point of view, there are different types of steady-state absorbance spectrometers. In this thesis, two types of measurements were used to obtain absorption spectra of the samples: single and double-beam spectrometers. The first one is the simplest application of a spectrophotometer which measures the absorbance at a specified wavelength. The scheme of the single-beam spectrophotometer in our lab is given in Figure 2.2.1 (upper). Here, there are two sources. These two sources are optically combined and share a common axis with the
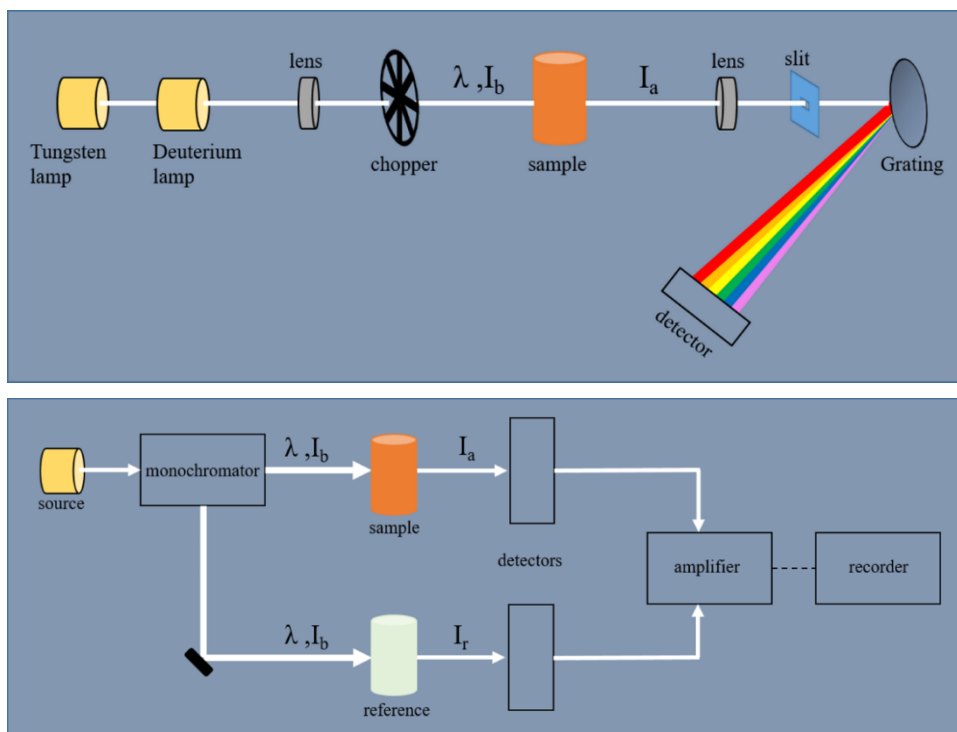
Figure 2.2.1 Steady-State spectrometers: Single-beam (top) and Double-beam (bottom).

source lens. While the first source, the tungsten lamp, is for the visible and near-infrared spectral regions, the second one, the deuterium lamp, provides the ultraviolet wavelength range of the spectrum. The combined single beam passes through firstly the chopper then through the sample to the spectrograph lens and slit. In the spectrograph, light is dispersed onto a diode array by a holographic grating which allows simultaneous access to all wavelength information. In a double-beam spectrometer Figure 2.2.1 (lower), the beam from the light source is split in the sample and reference beams that are measured simultaneously and the signal from the reference is subtracted from the sample signal. In the double-beam spectrometer the sample absorbance is recorded at multiple wavelengths via monochromator inserted before the sample. Since high energy throughput due to non-splitting of source beam results in high sensitivity of detection in the single-beam. On the other hand, the intensity of the light source can change the baseline and sample measuring due to, for example, thermal instability. This effect will not happen in double-beam

spectrometers since the ratio of them remain same even though both reference and signal beam are changed spontaneously.

2.3   TRANSIENT ABSORBTION SPECTROSCOPY

Many biological and chemical processes occur on time scales extending up to seconds or even longer, but the most elementary photophysical processes, such as excited-state relaxation, energy and electron transfer or isomerization typically occur on a sub-nanosecond time scales. This ultrafast timescale (femtoseconds to nanoseconds) is the time regime explored in this thesis. Thus, a spectroscopic technique with sufficient temporal resolution to follow ultrafast processes is required. Femtosecond transient absorption (pump-probe) spectroscopy has become a widely-used and useful technique to fulfill this task. In this technique, a laser beam consisting of short, typically <100 fs pulses, is split into two beams, usually denoted as the pump and probe. These two beams are sent through different optical paths and then directed to a sample with a defined time delay between the pump and probe pulses (Figure 2.3.1). While a fraction of the sample is promoted to an electronically excited state by means of pump beam, the probe beam is used to probe the state of the sample at certain time after excitation. The resulting spectra are measured using broadband detection combined with white-light continuum probing at a range of delay times to provide transient absorption spectra for a range of wavelengths as the system evolves. The absorption change (ΔA) is the difference of the ratios of the reference and probe signals at a given wavelength, measured for the excited fraction of the sample (with pump) and for the non-excited fraction of the sample (without pump). The equation is given in Eq. 2.3.1, and a basic illustration of the pump-probe technique is shown in Figure 2.3.1.
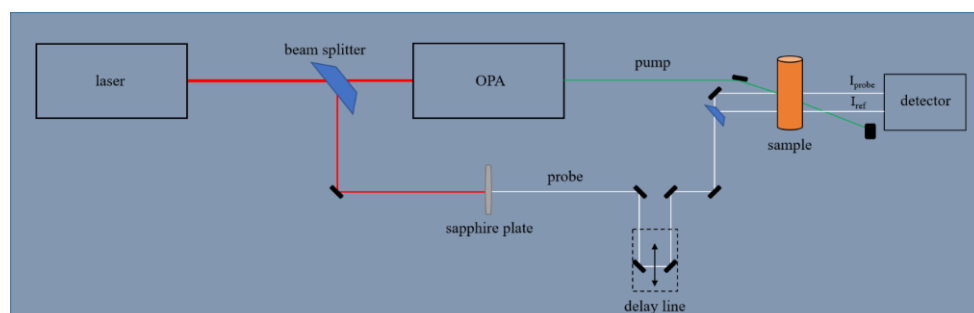
Figure 2.3.1 Basic scheme of the pump-probe technique.

$$\Delta A(\Delta t, \lambda) = A_{\substack{with \\ pump}} - A_{\substack{without \\ pump}} = log\left[\frac{I_{ref}}{I_{probe}}\right]_{\substack{with \\ pump}} - log\left[\frac{I_{ref}}{I_{probe}}\right]_{\substack{without \\ pump}} \qquad \text{Eq. 2.3.1}$$

A: absorbance I_{ref}: Intensity of reference beam, I_{prope}: intensity of probe beam, Δt: time delay between pump and probe and λ is probe wavelength.

ΔA(t) contains information about dynamical processes that occur in the studied system, such as relaxation, excited-state energy migration, electron and/or proton transfer processes, isomerization, etc. The ΔA spectrum consists of three basic signal types: ground-state bleaching, stimulated emission and excited-state absorption.

Ground state bleaching: Probability of absorption process depends on the number of molecules in the ground state. When the sample is excited with pump pulse, some molecules are promoted to an excited state, and the number of molecules in the ground state decreases in comparison with a non-excited sample. As a result, ground state absorption as detected by the probe pulse for the excited sample is less than for the non-excited one ($A_{\substack{with \\ pump}} < A_{\substack{without \\ pump}}$), and negative signal appears in ΔA spectra in the spectral region of ground state absorption of the sample.

S*imulated emission*: when the probe photon with an appropriate energy triggers molecules in the excited state, it can induce return of the molecule to the ground state by emitting a photon. This process is known as stimulated emission and occurs only for optically allowed transitions. Since the induced photon is emitted in the same direction as the probe photon, the light intensity at the detector will increase due to stimulated emission process, again leading to a negative signal in transient absorption spectrum. The stimulated emission signal is typically red shifted with respect to the ground state bleaching observed in ΔA spectra.

Excited state absorption: Excited sample can absorb photons which have different energy then those absorbed when the sample is in the ground state. These extra absorbed photons compared with the non-excited sample cause positive signal in ΔA spectra ($A_{\substack{with \\ pump}} > A_{\substack{without \\ pump}}$).

2.3.1   Technical details

A basic scheme of the transient absorption setup used in this thesis is shown in Figure 2.3.2. The pulses are derived from a commercial Ti-sapphire regenerative
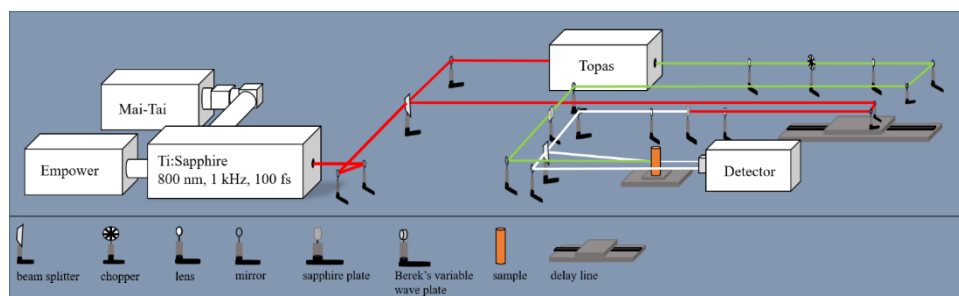
Figure 2.3.2 Basic scheme of the transient absorption setup from our lab.

amplifier seeded with the oscillator and pumped with the Q-switched diode-pumped Nd-YLF pulsed laser operating at 1 kHz repetition rate. The produced pulses are split by a beam splitter, 90% transmitted and 10% reflected. The transmitted beam, the pump, is sent through an optical parametric amplifier (OPA) tunable to a broad range of the pump wavelengths (240 – 2500 nm). A chopper in the pump beam is used to block every second pulse, allowing to alternate measurements with and without pump pulse (Eq. 2.3.1), thereby reducing background effects. After the chopper, the pump pulse is focused to the sample in order to excite the sample, then it is blocked. The reflected beam, the probe, is sent to a computer-controlled delay line. Then, the beam is focused to a sapphire plate to generate a white light continuum (WLC) for probing covering the VIS and NIR spectral region for a range of 430-1000 nm. The WLC is split into probe and reference beams. The reference beam is sent directly to the spectrograph without passing through the sample, while the probe beam goes to the sample (Figure 2.3.2). Before the probe beam hits the sample, reflective optics, spherical and an off-axis parabolic mirrors are used to direct and focus the probe beam to the sample. Reflective optics are used to minimize chirp, which is a time-dependent frequency distribution (the red light moves faster than blue light when passing through a material). The probe beam is focused to the sample in such a way that it overlaps spatially with the pump beam. The diameter of the probe beam at the sample is ~3 times smaller than the pump beam to assure probing of all excite molecules in the sample. For all experiments described in this thesis, the mutual polarization of the pump and probe beams is set at the 54.7° (magic angle), which prevents occurrence of polarization and photoselection effects. The polarization is set by means of a Berek variable wave plate placed in the pump beam. Finally, probe and reference beams are directed to the slit of a spectrograph, in which they are dispersed using optical grating onto a pair of 1024-element diode-arrays.

References

[1]   T. Mirkovic, E.E. Ostroumov, J.M. Anna, R. van Grondelle, Govindjee, G.D. Scholes **(2016)** Light Absorption and Energy Transfer in the Antenna Complexes of Photosynthetic Organisms. *Chem. Rev. **Article ASAP.*** doi:10.1021/acs.chemrev.6b00002.

[2]   G.D. Scholes, G.R. Fleming, A. Olaya-Castro, R. van Grondelle **(2011)** Lessons from nature about solar light harvesting. *Nat. Chem. 3, 763–774.* doi:10.1038/nchem.1145.

[3]   R. Croce, H. van Amerongen **(2014)** Natural strategies for photosynthetic light harvesting, *Nat. Chem. Biol. 10, 492–501.* doi:10.1038/nchembio.1555.

[4]   H. Hashimoto, Y. Sugai, C. Uragami, A.T. Gardiner, R.J. Cogdell **(2015)** Natural and artificial light-harvesting systems utilizing the functions of carotenoids. *J. Photochem. Photobiol. C: Photochem. Rev. 25, 46–70.* doi:10.1016/j.jphotochemrev.2015.07.004.

[5]   H. Staleva, J. Komenda, M.K. Shukla, V. Šlouf, R. Kaňa, T. Polívka, R. Sobotka **(2015)** Mechanism of photoprotection in the cyanobacterial ancestor of plant antenna proteins. *Nat. Chem. Biol. 11, 287–291.* doi:10.1038/nchembio.1755.

[6]   L. Dall'Osto, M. Bressan, R. Bassi **(2015)** Biogenesis of light harvesting proteins *Biochim. Biophys. Acta. 1847, 861–871.* doi:10.1016/j.bbabio.2015.02.009.

[7]   T. Tanaka, M. Shnimizu, H. Moriwaki **(2012)** Cancer Chemoprevention by Carotenoids. *Molecules 17, 3202–3242.* doi:10.3390/molecules17033202.

[8]   R. Pariser **(1956)** Electronic Spectrum and Structure of Azulene. *J. Chem. Phys. 25, 1112.* doi:10.1063/1.1743159.

[9]   B.S. Hudson, B.E. Kohler, K. Schulten **(1982)** Linear Polyene Electronic Structures and Potential Surfaces. *Exited States 6, 1–95.*

[10]   P.T. and K. Schulten **(1979)** Correlation effects in the spectra of polyacenes, *Jcp. 67, 5414.* doi:10.1063/1.437452.

[11]   T. Polívka, V. Sundström **(2009)** Dark excited states of carotenoids: Consensus and controversy. *Chem. Phys. Lett. 477, 1–11.* doi:10.1016/j.cplett.2009.06.011.

[12]   T. Polívka, V. Sundström **(2004)** Ultrafast dynamics of carotenoid excited states-from solution to natural and artificial systems. *Chem. Rev. 104, 2021–2071.* doi:10.1021/cr020674n.

[13]   C.C. Gradinaru, J.T. Kennis, E. Papagiannakis, I.H. van Stokkum, R.J. Cogdell, G.R. Fleming, R. a Niederman, R. van Grondelle **(2001)** An unusual pathway of excitation energy deactivation in carotenoids: singlet-to-triplet conversion on an ultrafast timescale in a photosynthetic antenna. *Proc. Natl. Acad. Sci. 98, 2364–2369.* doi:10.1073/pnas.051501298.

[14]   Y. Koyama, F.S. Rondonuwu, R. Fujii, Y. Watanabe **(2004)** Light-Harvesting Function of Carotenoids in Photo-synthesis: The Roles of the Newly Found $1^1B_u^-$ State. *Biopolymers. 74, 2–18.* doi:10.1002/bip.20034.

[15]   P. Tavan, K. Schulten **(1987)** Electronic excitations in finite and infinite polyenes, *Phys. Rev. B. 36, 4337–4358.* doi:10.1103/PhysRevB.36.4337.

[16]   H. A. Frank, J. A. Bautista, J. Josue, Z. Pendon, R.G. Hiller, F.P. Sharples, D. Gosztola, M.R. Wasielewski **(2000)** Effect of the Solvent Environment on the Spectroscopic Properties and Dynamics of the Lowest Excited States of Carotenoids, *J. Phys. Chem. B. 104, 4569–4577.* doi:10.1021/jp000079u.

[17]   D. Zigmantas, T. Polfvka, R.G. Killer, A. Yartsev, V. Sundstrom **(2001)** Spectroscopic and dynamic properties of the peridinin lowest singlet excited states. *J. Phys. Chem. A. 105, 10296–10306.* doi:10.1021/jp010022n.

[18]   N.L. Wagner, J.A. Greco, M.M. Enriquez, H.A. Frank, R.R. Birge **(2013)** The nature of the intramolecular charge transfer state in Peridinin. *Biophys. J. 104, 1314–1325.* doi:10.1016/j.bpj.2013.01.045.

[19]   J. A. Bautista, R.E. Connors, B.B. Raju, R.G. Hiller, F.P. Sharples, D. Gosztola, M.R. Wasielewski, H. A. Frank **(1999)** Excited State Properties of Peridinin: Observation of a Solvent Dependence of the Lowest Excited Singlet State Lifetime and Spectral Behavior Unique among Carotenoids, *J. Phys. Chem. B. 103, 8751–8758.* doi:10.1021/jp9916135.

[20]   F.L. Pilar **(1990)** Elementary quantum chemistry, *2nd ed., United State of America.*

[21]   P. Atkins, R. Friedman **(2005)** Molecular quantum mechanics, *4th ed., Oxford University, New York.*

[22]   R.E. Blankkenship **(2002)** Molecular mechanisms of photosynthesis, *Blackwell Science, UK.*

[23]   D. Zigmantas, R.G. Hiller, F.P. Sharples, H.A. Frank, V. Sundström, T. Polívka **(2004)** Effect of a conjugated carbonyl group on the photophysical

properties of carotenoids. *Phys. Chem. Chem. Phys. 6, 3009-3016.* doi:10.1039/b315786e.

[24]   D.M. Niedzwiedzki, N. Chatterjee, M.M. Enriquez, T. Kajikawa, S. Hasegawa, S. Katsumura, H.A. Frank **(2009)** Spectroscopic investigation of peridinin analogues having different-electron conjugated chain lengths: Exploring the nature of the intramolecular charge transfer state, *J. Phys. Chem. B. 113, 13604–13612.* doi:10.1021/jp903923r.

[25]   D. Zigmantas, R.G. Hiller, A. Yartsev, V. Sundstro **(2003)** Dynamics of Excited States of the Carotenoid Peridinin in Polar Solvents: Dependence on Excitation Wavelength , Viscosity , and Temperature. *J. Phys. Chem. B. 107, 5339–5348.* doi:10.1021/jp0272318.

[26]   V. Chynwat, H.A. Frank **(1995)** The application of the energy gap law to the S_1 energies and dynamics of carotenoids. *Chem. Phys. 194, 237–244.* doi:10.1016/0301-0104(95)00017-I.

[27]   R. Fujii, T. Ishikawa, Y. Koyama, M. Taguchi, Y. Isobe, H. Nagae, Y. Watanabe **(2011)** Fluorescence Spectroscopy of All-trans-anhydrorhodovibrin and Spirilloxanthin: Detection of the $^1B_u^-$ Fluorescence. *J. Phys. Chem. A, 105, 5348–5355.* doi:10.1021/JP010150B.

[28]   B. Robert **(2009)** Resonance Raman spectroscopy. *Photosynth. Res. 101, 147–155.* doi:10.1007/s11120-009-9440-4.

[29]   T. Sashima, Y. Koyama, T. Yamada, H. Hashimoto **(2000)** The $1B_u^+$, $1B_u^-$, and $2A_g^-$ energies of crystalline lycopene, β-carotene, and mini-9- β-carotene as determined by resonance-Raman excitation profiles: Dependence of the $1B_u^-$ state energy on the conjugation length. *J. Phys. Chem. B. 104 5011–5019.* Doi: 10.1021/jp994185b.

[30]   J.M. Boereboom, M.C. Van Hemert, J. Neugebauer **(2011)** The resonance raman spectra of spheroidene revisited with a first-principles approach. *Chem. Phys. Chem. 12, 3157–3169.* doi:10.1002/cphc.201100545.

[31]   S. Shima, R.P. Ilagan, N. Gillespie, B.J. Sommer, R.G. Hiller, F.P. Sharples, H.A. Frank, R.R. Birge **(2003)** Two-photon and fluorescence spectroscopy and the effect of environment on the photochemical properties of peridinin in solution and in the peridinin-chlorophyll-protein from amphidinium carterae, *J. Phys. Chem. A. 107, 8052–8066.* doi:10.1021/jp022648z.

[32]   D. Kosumi, T. Kusumoto, R. Fujii, M. Sugisaki, Y. Iinuma, N. Oka, Y. Takaesu, T. Taira, M. Iha, H.A. Frank, H. Hashimoto **(2009)** One- and two-photon pump-probe optical spectroscopic measurements reveal the S_1 and

intramolecular charge transfer states are distinct in fucoxanthin. *Chem. Phys. Lett. 483, 95–100.* doi:10.1016/j.cplett.2009.10.077.

[33] P.A. Linden, J. Zimmermann, T. Brixner, N.E. Holt, H.M. Vaswani, R.G. Hiller, G.R. Fleming **(2004)** Transient Absorption Study of Peridinin and Peridinin−Chlorophyll a Protein after Two-Photon Excitation. *J. Phys. Chem. B. 108, 10340–10345.* doi:10.1021/jp031331b.

[34] P.J. Walla, P.A Linden, C.P. Hsu, G.D. Scholes, G.R. Fleming **(2000)** Femtosecond dynamics of the forbidden carotenoid S_1 state in light-harvesting complexes of purple bacteria observed after two-photon excitation. *Proc. Natl. Acad. Sci. 97,10808–10813.*
doi:10.1073/pnas.190230097.

[35] R. Fujii, T. Inaba, Y. Watanabe, Y. Koyama, J.-P. Zhang **(2003)** Two different pathways of internal conversion in carotenoids depending on the length of the conjugated chain. *Chem. Phys. Lett. 369, 165-172.*
doi:10.1016/S0009-2614(02)01999-1.

[36] R.P. Ilagan, R.L. Christensen, T.W. Chapp, G.N. Gibson, T. Pascher, T. Polívka, H.A. Frank **(2005)** Femtosecond time-resolved absorption spectroscopy of astaxanthin in solution and in α-crustacyanin. *J. Phys. Chem. A. 109, 3120–3127.* doi:10.1021/jp0444161.

[37] P. Chábera, M. Fuciman, K. Razi Naqvi, T. Polívka **(2010)** Ultrafast dynamics of hydrophilic carbonyl carotenoids - Relation between structure and excited-state properties in polar solvents. *Chem. Phys. 373, 56–64.*
doi:10.1016/j.chemphys.2010.01.007.

[38] M.M. Enriquez, S. Hananoki, S. Hasegawa, T. Kajikawa, S. Katsumura, N.L. Wagner, R.R. Birge, H.A. Frank **(2012)** Effect of molecular symmetry on the spectra and dynamics of the intramolecular charge transfer (ICT) state of peridinin. *J. Phys. Chem. B. 116, 10748–10756.* doi:10.1021/jp305804q.

[39] T. Polívka, I.H.M. Van Stokkum, D. Zigmantas, R. Van Grondelle, V. Sundström, R.G. Hiller **(2006)** Energy transfer in the major intrinsic light-harvesting complex from Amphidinium carterae. *Biochemistry. 45 8516–8526.* doi:10.1021/bi060265b.

[40] S. Shima, R.P. Ilagan, N. Gillespie, B.J. Sommer, R.G. Hiller, F.P. Sharples, H.A. Frank, R.R. Birge **(2003)** Two-Photon and Fluorescence Spectroscopy and the Effect of Environment on the Photochemical Properties of Peridinin in Solution and in the Peridinin-Chlorophyll-Protein from Amphidinium carterae. *J. Phys. Chem. A, 107, 8052–8066.* doi:10.1021/JP022648Z.

[41] A. Dreuw, M. Head-Gordon **(2004)** Failure of time-dependent density functional theory for long-range charge-transfer excited states: The zincbacteriochlorin-bacterlochlorin and bacteriochlorophyll-spheroidene complexes. *J. Am. Chem. Soc. 126, 4007–4016.* doi:10.1021/ja039556n.

[42] M.M. Enriquez, M. Fuciman, A.M. Lafountain, N.L. Wagner, R. Robert, H.A. Frank **(2011)** The Intramolecular Charge Transfer State in Carbonyl-Containing Polyenes and Carotenoids. *J. Phys. Chem. B. 114, 12416–12426.* doi:10.1021/jp106113h.

[43] F. Ehlers, D.A. Wild, T. Lenzer, Kawon Oum **(2007)** Investigation of the S_1/ICT $\rightarrow S_0$ Internal Conversion Lifetime of 4'-apo-β-caroten-4'-al and 8'-apo-β-caroten-8'-al: Dependence on Conjugation Length and Solvent Polarity. *J. Phys. Chem. A. 111, 2257–2265.* doi:10.1021/JP0676888.

[44] M. Kopczynski, F. Ehlers, T. Lenzer, K. Oum **(2007)** Evidence for an Intramolecular Charge Transfer State in 12'-Apo-β-caroten-12'-al and 8'-Apo-β-caroten-8'-al: Influence of Solvent Polarity and Temperature. *J. Phys. Chem. A. 111,5370–5381.* doi:10.1021/JP0672252.

[45] Z. He, D. Gosztola, Y. Deng, G. Gao, M.R. Wasielewski, L.D. Kispert **(2000)** Effect of Terminal Groups, Polyene Chain Length, and Solvent on the First Excited Singlet States of Carotenoids. *J. Phys. Chem. B, 104, 6668–6673.* doi:10.1021/JP0008344.

[46] D. Kosumi, T. Kajikawa, S. Okumura, M. Sugisaki, K. Sakaguchi, S. Katsumura, H. Hashimoto **(2014)** Elucidation and Control of an Intramolecular Charge Transfer Property of Fucoxanthin by a Modification of Its Polyene Chain Length. *J. Phys. Chem. Lett. 5, 792–797.* doi: 10.1021/jz5000287

[47] D. Kosumi, R. Fujii, M. Sugisaki, N. Oka, M. Iha, H. Hashimoto **(2004)** Characterization of the intramolecular transfer state of marine carotenoid fucoxanthin by femtosecond pump-probe spectroscopy. *Photosynth. Res. 121, 61–68.* doi:10.1007/s11120-014-9995-6.

[48] N.M. Magdaong, D.M. Niedzwiedzki, J.A. Greco, H. Liu, K. Yano, T. Kajikawa, K. Sakaguchi, S. Katsumura, R.R. Birge, H.A. Frank **(2014)** Excited state properties of a short π-electron conjugated peridinin analogue, *Chem. Phys. Lett. 593, 132–139.* doi:10.1016/j.cplett.2014.01.002.

[49]   D.M. Niedzwiedzki, T. Kajikawa, K. Aoki, S. Katsumura, H.A. Frank **(2013)** Excited states energies and dynamics of peridinin analogues and the nature of the intramolecular charge transfer state in carbonyl-containing carotenoids, *J. Phys. Chem. B. 117, 6874–6887.* doi:10.1021/jp400038k.

[50]   T. Polívka, H.A. Frank **(2010)** Molecular Factors Controlling Photosynthetic Light Harvesting by Carotenoids. *Acc. Chem. Res. 43 1125–1134.* doi:10.1021/ar100030m.

[51]   B.P. Krueger, G.D. Scholes, G.R. Fleming **(1998)** Calculation of Couplings and Energy-Transfer Pathways between the Pigments of LH2 by the ab Initio Transition Density Cube Method. *J. Phys. Chem. B, 102, 5378–5386.* doi:10.1021/JP9811171.

[52]   H.P. Lamichhane, G. Hastings **(2011)** Calculated vibrational properties of pigments in protein binding sites. *Proc. Natl. Acad. Sci. 108, 10526–10531.* doi:10.1073/pnas.1104046108.

[53]   M. Di Valentin, C.E. Tait, E. Salvadori, L. Orian, A. Polimeno, D. Carbonera **(2014)** Evidence for water-mediated triplet-triplet energy transfer in the photoprotective site of the peridinin-chlorophyll a-protein. *Biochim. Biophys. Acta - Bioenerg. 1837, 85–97.* doi:10.1016/j.bbabio.2013.07.005.

[54]   T. Vreven, K.S. Byun, I. Komáromi, S. Dapprich, J.A. Montgomery, K. Morokuma, M.J. Frisch **(2006)** Combining Quantum Mechanics Methods with Molecular Mechanics Methods in ONIOM. *J. Chem. Theory Comput. 2, 815–826.* doi:10.1021/ct050289g.

[55]   J.B. Foresman, Æ. Frisch **(1996)** Exploring chemistry with electronic structure methods, 2nd ed., USA.

[56]   W. Kohn, L.J. Sham **(1965)** Self-consistent equations including exchange and correlation effects. *Phys. Rev. 140.* doi:10.1103/PhysRev.140.A1133.

[57]   P. Hohenberg, W. Kohn **(1964)** Inhomogeneous Electron Gas. *Phys. Rev. 136, B864–B871.* doi:10.1103/PhysRev.136.B864.

[58]   A.D. Becke **(1993)** Density-functional thermochemistry. III. The role of exact exchange. *J. Chem. Phys. 98, 5648.* doi:10.1063/1.464913.

[59]   A. Schäfer, C. Huber, R. Ahlrichs **(1994)** Fully optimized contracted Gaussian basis sets of triple zeta valence quality for atoms Li to Kr. *J. Chem. Phys. 100, 5829.* doi:10.1063/1.467146.

[60] H.M. Vaswani, C.P. Hsu, M. Head-Gordon, G.R. Fleming **(2003)** Quantum Chemical Evidence For An Intramolecular Charge-Transfer State In The Carotenoid Peridinin Of Peridinin-Chlorophyll-Protein, *J. Phys. Chem. B. 107, 7940–7946.* doi:10.1021/Jp030086T.

[61] K. V. Berezin, V. V. Nechaev **(2005)** Calculation of the IR spectrum and the molecular structure of β-carotene. *J. Appl. Spectrosc. 72, 164–171.* doi:10.1007/s10812-005-0049-x.

[62] J.P. Ceron-Carrasco, A. Bastida, J. Zuniga, A. Requena, B. Miguel **(2009)** Density Functional Theory Study of the Stability and Vibrational Spectra of the β-Carotene Isomers. *J. Phys. Chem A. 113, 9899–9907.* doi: 10.1021/jp9037446

[63] W. Liu, Z. Wang, Z. Zheng, L. Jiang, Y. Yang, L. Zhao, W. Su **(2012)** Density functional theoretical analysis of the molecular structural effects on raman spectra of β-carotene and lycopene. *Chinese J. Chem. 30, 2573–2580.* doi:10.1002/cjoc.201200661.

[64] M. Macernis, J. Sulskus, S. Malickaja, B. Robert, L. Valkunas **(2014)** Resonance Raman Spectra and Electronic Transitions in Carotenoids: A Density Functional Theory Study. *J. Phys. Chem. A, 118, 1817−1825.* doi: 10.1021/jp406449c

[65] M. Macernis, D. Galzerano, J. Sulskus, E. Kish, Y.-H. Kim, S. Koo, L. Valkunas, B. Robert **(2015)** Resonance Raman Spectra of Carotenoid Molecules: Influence of Methyl Substitutions. *J. Phys. Chem. A. 119, 56–66.* doi:10.1021/jp510426m.

[66] S. Grimme, M. Waletzke **(1999)** A combination of Kohn–Sham density functional theory and multi-reference configuration interaction methods, *J. Chem. Phys. 111, 5645.* doi:10.1063/1.479866.

[67] C.M. Marian, N. Gilka **(2008)** Performance of the Density Functional Theory/Multireference Configuration Interaction Method on Electronic Excitation of Extended π-Systems, *J. Chem. Theory Comput. 4, 1501–1515.* doi:10.1021/ct8001738.

[68] A. Dreuw, M. Head-Gordon **(2005)** Single-reference ab initio methods for the calculation of excited states of large molecules. *Chem. Rev. 105, 4009–4037.* doi:10.1021/cr0505627.

[69] S. Hirata, M. Head-Gordon **(1999)** Time-dependent density functional theory within the Tamm–Dancoff approximation. *Chem. Phys. Lett. 314, 291–299.* doi:10.1016/S0009-2614(99)01149-5.

[70]   T. Yanai, D.P. Tew, N.C. Handy **(2004)** A new hybrid exchange-correlation functional using the Coulomb-attenuating method (CAM-B3LYP). *Chem. Phys. Lett. 393, 51–57.* doi:10.1016/j.cplett.2004.06.011.

[71]   J.C. Merlin **(1985)** Resonance Raman spectroscopy of carotenoids and carotenoid-containing systems. *Pure Appl. Chem. 57, 785–792.* doi:10.1351/pac198557050785.

[72]   A.M. Dokter, M.C. Van Hemert, C.M. In't Velt, K. Van der Hoef, J. Lugtenburg, H.A. Frank, E.J.J. Groenen **(2002)** Resonance Raman spectrum of all-trans-spheroidene. DFT analysis and isotope labeling. *J. Phys. Chem. A. 106, 9463–9469.* doi:10.1021/jp026164e.

[73]   T.S. and, Y. Koyama, T.Y. and, H. Hashimoto **(2000)** The $1B_u^+$, $1B_u^-$, and $2A_g^-$ Energies of Crystalline Lycopene, β-Carotene, and Mini-9-β-carotene as Determined by Resonance-Raman Excitation Profiles: Dependence of the $1B_u^-$ State Energy on the Conjugation Length. *J. Phys. Chem. B. 104, 5011–5019.* doi:10.1021/JP994185B.

Chapter 3. RESEARCH SECTION

This part of the thesis includes publications which are listed on page viii. These publications have been re-formatted based on the thesis style.

3.1 PAPER 1

Effect of Polarity and Aggregation on Excited-State Dynamics of 8'-Apo-β-Carotenal

Milan Durchan, Marcel Fuciman, Václav Šlouf, **Gürkan Keşan**, Tomáš Polívka,

3.1.1 Abstract

Excited-state properties of the carbonyl carotenoid monomeric and aggregated 8'-apo-β-carotenal were studied by means of femtosecond transient absorption spectroscopy. For 8'-apo-β-carotenal monomers, the polarity-dependent behavior characteristic of carotenoids with conjugated carbonyl group was observed. While in n-hexane the S_1 lifetime of 8'-apo-β-carotenal is 25 ps, it is shortened to 8 ps in methanol. This shortening is accompanied by appearance of new spectral bands in transient absorption spectrum. Based on analysis of the transient absorption spectra of monomeric 8'-apo-β-carotenal in n-hexane and methanol we propose that the polarity-induced spectral bands are due to the $S_1(A_g^-)$–$S_3(A_g^+)$ transition, which is enhanced upon breaking the symmetry of the molecule. This symmetry breaking is caused by the conjugated carbonyl group; it is much stronger in polar solvents where the S_1 state gains significant charge-transfer character. Upon addition of water to methanol solution of 8'-apo-β-carotenal we observed formation of aggregates characterized either by blue-shifted (H-aggregate) or red-shifted (J-aggregate) absorption spectrum. Both aggregate types exhibit excited-state dynamics significantly different from those of monomeric 8'-apo-β-carotenal. Lifetime of the relaxed S_1 state is 20 and 40 ps for the H- and J-aggregates, respectively. In contrast to monomeric 8'-apo-β-carotenal, aggregation promotes formation of triplet state, most likely by homofission occurring between tightly-packed molecules within the aggregate.

3.1.2 Introduction

Carotenoids are natural pigments that have been a subject of a number of photochemical and photophysical studies because of their rich excited-state dynamics involving dark excited states [P1.1]. The complex photophysics of carotenoids is directly related to their vital roles in photosynthesis where they act as both light-harvesting and photoprotective pigments [P1.2], [P1.3]. Carotenoids with conjugated carbonyl group have attracted a lot of attention in recent years, because they add another dimension to the rich photophysics of carotenoids as their excited-state properties depend on polarity of the environment [P1.4], [P1.5]. It was also demonstrated that this polarity-dependent behavior is advantageous for a large group of photosynthetic organisms which employ light-harvesting strategy relying on specific excited-state properties of carbonyl carotenoids [P1.2], [P1.6]. In artificial systems, utilizing carbonyl carotenoids attached to a molecule mimicking chlorophyll allows

to tune energy transfer efficiency by solvent polarity [P1.7].

Excited-state properties carotenoids are traditionally described in a three state model: the ground state S_0 (of A_g^- symmetry in the C_{2h} point group), the S_1 state forbidden for transition from the ground state because it has the same A_g^- symmetry as the ground state, and the strongly absorbing S_2 (B_u^+) state. Yet, it must be noted that there is growing evidence that inclusion of more dark excited states is likely necessary to explain all experimental data [P1.8]-[P1.10]. In the three-state model, a carotenoid excited into the S_2 state decays within a few hundred femtoseconds to the S_1 state whose lifetime depends on conjugation length of the carotenoid (N) [P1.1]. For non-carbonyl carotenoids this relaxation scheme is independent of solvent polarity. However, carbonyl carotenoids exhibit polarity-dependent excited-state dynamics that are explained as due to an intramolecular charge transfer (ICT) state that likely couples to the S_1 state [P1.4], [P1.5].

The dependence of spectroscopic properties on polarity was first discovered in the carotenoid peridinin [P1.11], and subsequently demonstrated for a number of carbonyl carotenoids that occurs in photosynthetic systems [P1.4], [P1.5]. Recently, the polarity-dependent behavior was reported also in a synthetic model carotenoid, 8'-apo-β-carotenal (Figure 3.1.1). Knowledge of spectroscopic properties of this carotenoid and their dependence on environment is important also because of frequent use of its analogue, 8'-apo-β-carotenoic acid, in various molecular systems aiming to exploit solar energy. It was used as a TiO_2 sensitizer and both electron-donating [P1.12], [P1.14] and photoprotective [P1.15] functions were reported.

In a series of papers, group of Oum and Lenzer measured lifetime of the lowest excited state of 8'-apo-β-carotenal in a number of solvents and showed that while in nonpolar solvents the lifetime is ~25 ps, it is shortened to ~8.5 ps in polar solvents [P1.16]-[P1.18]. This polarity-induced shortening of the S_1 lifetime is assigned to its coupling to the ICT state, resulting in a state usually denoted as S_1/ICT. The magnitude of the lifetime shortening depends on conjugation length; it is much larger for a shorter analogue, 12'-apo-β-carotenal, whose lifetime is ~200 ps in n-hexane and ~8 ps in methanol [P1.17]-[P1.20], but no shortening was reported for 4'-apo-β-carotenal which has the conjugation length longer by two C=C bonds compared to 8'-apo-β-carotenal [P1.16].

The polarity-dependent lifetime of carbonyl carotenoids is accompanied by another characteristic marker, the ICT band in transient absorption spectrum. All carotenoids have the typical S_1-S_n transition in the visible spectral region [P1.15], but

carbonyl carotenoids in polar solvents usually have additional transition, presumably due to a transition from the ICT state, which is always red-shifted from the S_1-S_n band. The ICT state also exhibits weak stimulated emission in the near-IR [P1.4],[P1.5], and kinetics of 8'-apo-β-carotenal in methanol demonstrated that this stimulated emission occurs also for 8'-apo-β-carotenal [P1.17][P1.15]. However, full transient absorption spectrum showing the intensity of the ICT-like transition in the visible region, which is a measure of magnitude of the polarity-induced effects, have not been reported so far. For the shorter 12'-apo-β-carotenal in methanol the transient absorption spectra revealed strong ICT-like transition [P1.19], [P1.20].

Besides the polarity-dependent behavior of carbonyl carotenoids another phenomenon that leads to significant changes in spectroscopic properties of carotenoids is aggregation. It is known for a couple of decades that carotenoids, when dissolved in hydrated solvents, exhibit large changes in absorption spectra [P1.21]-[P1.24]. Significant shifts of absorption maximum, whose magnitude and direction depends on organization of carotenoid molecules within the aggregate, are caused by excitonic interaction of the molecules within the aggregate as demonstrated by both experimental[P1.25]-[P1.30] and theoretical [P1.31], [P1.32] studies. Traditionally, carotenoid aggregates are denoted as either 'card-pack' H-aggregates with blue-shifted absorption maximum, or 'head-to-tail' J-aggregates whose maximum is red-shifted from the

Figure 3.1.1 Normalized absorption spectra of 8'-apo-β-carotenal in n-hexane (black) and methanol (red). Molecular structure of 8'-apo-β-carotenal is also shown.

absorption maximum of a monomer [P1.23]. We will keep this notation throughout the paper though recent calculations going beyond the dipole-dipole approximation showed that essentially all absorption spectra of carotenoid aggregates can be

explained in terms of H-type interactions with different coupling strengths and orientation of the molecules within the aggregate [P1.30]-[P1.32].

Despite number of studies aiming to explain changes in absorption spectra of carotenoid aggregates, very little is known about how aggregation affects the excited-state dynamics. Billsten et al. reported changes in excited state dynamics taking place upon aggregation of the non-carbonyl carotenoid zeaxanthin [P1.27]; the S_1 state exhibited multiexponential decay with components both shorter and longer than the S_1 lifetime of monomeric zeaxanthin. Wang and Tauber demonstrated aggregation-induced changes in the same carotenoid by picosecond time-resolved Raman spectroscopy, and identified ultrafast triplet formation via singlet-singlet homofission [P1.28],[P1.29].

Because of potential use of 8'-apo-β-carotenal in systems requiring depositing carotenoid on a thin film, a process that also induces aggregation of carotenoids [P1.12], [P1.15], [P1.33], [P1.34], it is of interest to study effects of aggregation on excited-state dynamics of this carotenoid. Moreover, hydrated solvents inducing aggregation exposes 8'-apo-β-carotenal to extremely polar environment that may lead to enhancement of polarity-induced effects as it was demonstrated for a series of hydrophilic carotenoids that remain monomeric even in water [P1.35]. Yet, effect of aggregation on the ICT-like transition has not been studied so far. Thus, here we first measure full transient absorption spectra of monomeric 8'-apo-β-carotenal in polar and nonpolar solvents to characterize the ICT-like transition. Then, aggregated 8'-apo-β-carotenal is examined by femtosecond transient absorption spectroscopy, revealing significant aggregation-induced changes in excited-state dynamics of 8'-apo-β-carotenal.

3.1.3 Materials and Methods

8′-apo-β-carotenal was purchased from Sigma and stored at -80°C in dark. Prior to transient absorption measurements, 8′-apo-β-carotenal was dissolved in spectroscopic grade methanol or n-hexane (Fluka) to yield optical density of 0.5/mm at absorption maximum. To prepare 8′-apo-β-carotenal aggregates, we first prepared saturated methanol solution of 8′-apo-β-carotenal. Then, the stock solution was further diluted by methanol and water was added to the diluted 8′-apo-β-carotenal methanol solution. H-aggregates were formed in methanol/water ratio of 1:9, while 1:1 ratio was necessary to generate J-aggregates. The concentration of the diluted solution was set to yield final concentration of about 100 M for both J- and H-

aggregates.

Transient absorption spectra were measured with a femtosecond spectrometer employing a Ti: sapphire laser system (Intregra-i, Quantronix) as a primary source of femtosecond pulses. It consists of an Er-fiber oscillator and Ti: sapphire amplifier producing ~130 fs pulses at a repetition rate of 1 kHz. Central wavelength of the output pulses is 795 nm. The amplified pulses were divided by a 10/90 beam-splitter into two paths. Most of the light was used to seed an optical parametric amplifier (TOPAS, Light Conversion) to generate excitation pulses. A fraction of light was focused to a 2-mm sapphire plate to produce a white-light single filament continuum that was used as a broadband probe. Mutual orientation of the excitation and probe beams polarization was set to the magic angle (54.7°) by means of Berek polarization rotator placed into the excitation beam. A 2-mm path length quartz cuvette was used for all transient absorption measurements. To prevent sample degradation, a micro-magnetic stirrer was used to continuously mix the sample during the measurements. Time-resolved absorption changes were measured in a broad spectral range from 470 to 750 nm by detecting the white light dispersed in a spectrograph by a double-diode array. Excitation pulses were set at 435 nm (H-aggregates), 490 nm (monomers), and 557 nm (J-aggregates). Using neutral-density filters, the intensity of excitation was kept at ~10^{14} photons pulse^{-1} cm^{-2}. Femtosecond transient absorption data collected by diode array detectors were fitted globally. To visualize the excited state dynamics, we assume that the excited states evolves according to a sequential, irreversible scheme, in which the extracted time constants correspond to lifetimes of the individual excited-state species in the sequential scheme. The spectral profile of each species is called evolution-associated difference spectrum (EADS).

3.1.4   Results

We first present results on monomeric 8'-apo-β-carotenal in polar and nonpolar solvents. Absorption spectra of 8'-apo-β-carotenal in the nonpolar n-hexane and polar methanol are shown in Figure 3.1.1. Change of solvent polarity induced effects typical for carotenoids with conjugated carbonyl group; the characteristic vibrational structure of the S_0-S_2 transition, which have well-resolved peaks at 482, 455 and 432 nm, is lost in methanol where a broad S_0-S_2 transition lacking any hints of vibrational band is observed. This effect is caused by interaction of the conjugated carbonyl group with polar solvent that causes increase of conformational disorder, leading to the observed loss of vibrational structure. Interaction involving the

conjugated carbonyl group also leads to the increase of absorption in the red part of absorption spectrum, which is most likely related to hydrogen bonding to the carbonyl oxygen [P1.36].

Transient absorption spectra of 8'-apo-β-carotenal are depicted in Figure 3.1.2. In both solvents, 8'-apo-β-carotenal was excited at 490 nm, a wavelength that excites the low-energy part of the S_0-S_2 transition, thereby avoiding interference of the initial dynamics with relaxation in the vibrational manifold of the S_2 state. In n-hexane, the transient absorption spectrum has narrow excited-state absorption band at 550 nm, which is clearly due to S_1-S_n transition of 8'-apo-β-carotenal. At high energy side of the S_1-S_n band there is a distinct peak at 520 nm that was observed in many other carotenoids; it is usually denoted as the S* signal [P1.37] whose origin is still a matter of debate [P1.38]. However, in contrast to linear non-carbonyl carotenoids whose transient absorption spectra have a single narrow S_1-S_n band [P1.39], transient absorption spectrum of 8'-apo-β-carotenal in n-hexane has additional bands at 620 and 640 nm. In fact, the transient absorption spectrum of 8'-apo-β-carotenal in n-hexane is, except the position of the S_1-S_n band, remarkably similar to that of its shorter relative, 12'-apo- β –carotenal [P1.19]. This suggests that the low energy bands in transient absorption spectrum of 8'-apo-β-carotenal in n-hexane may be due to the carbonyl group. Then, the low energy bands that are likely forbidden in nearly ideally symmetric non-carbonyl linear carotenoids become allowed because the conjugated carbonyl group introduces asymmetry into the conjugated system.

Significant changes in transient absorption spectrum are observed when 8'-apo-β-carotenal is dissolved in methanol. Direct comparison of spectra in n-hexane and methanol in Figure 3.1.2. shows that upon keeping the bleaching magnitude comparable in both solvents, the intensity of the S_1-S_n
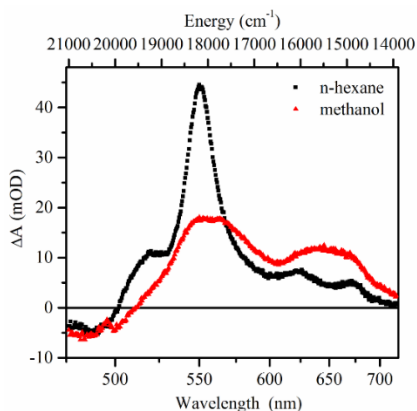
Figure 3.1.2 Transient absorption spectra of 8-apo-β-carotenal in n-hexane (black) and methanol (red) measured at 3 ps after excitation at 490 nm.

band and the S* signal decreases while magnitude the low energy bands above 600 nm, associated in carbonyl carotenoids with the ICT state, increases with solvent
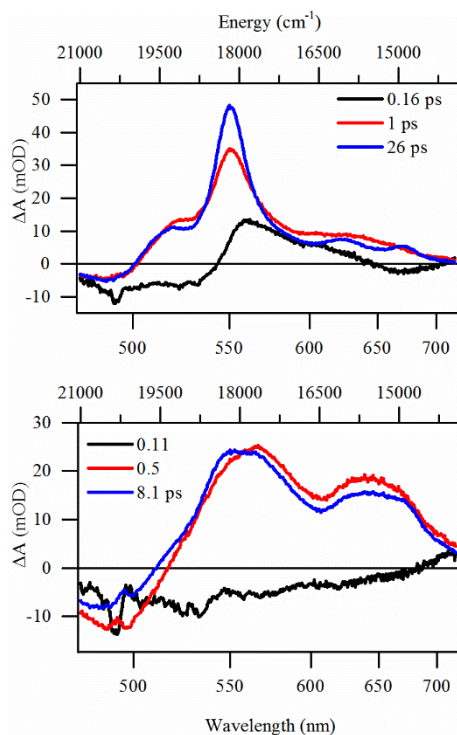
polarity. Similar effect was reported earlier for 12'-apo- β -carotenal [P1.19], except the increase of intensity of the ICT band is much larger than observed here for 8'-apo-β-carotenal, confirming that polarity-induced effect on transient absorption spectrum increases in carotenoids with shorter conjugation [P1.17], [P1.40] . It must be noted, however, that although intensities of the S_1-like and ICT-like transitions vary significantly with solvent polarity, their energies remain nearly constant as it is evidenced by deconvolution of the transient absorption spectra into Gaussian bands (Figure 3.1.9).
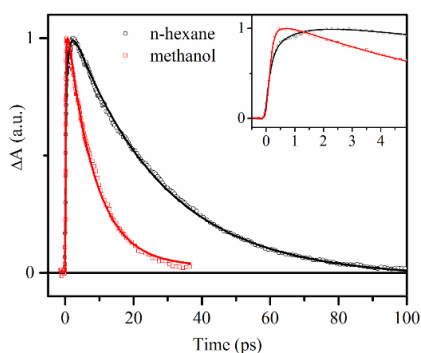
Figure 3.1.3 Kinetics measured at 550 nm for 8-apo-β-carotenal in n-hexane (black) and methanol (red). Kinetics are normalized to maximum. Solid lines are fits resulting from global fitting. The inset shows magnification of the first few ps. Excitation at 490 nm.

It is well known that besides the changes in transient absorption spectra of carbonyl carotenoids, the polarity also affects the lifetime of the S_1/ICT state. This effect was reported earlier also for 8'-apo-β–carotenal [P1.16], [P1.17] .Here it is demonstrated in Figure 3.1.3 showing kinetics of 8'-apo-β-carotenal taken at

Figure 3.1.4 EADS obtained from global fitting the transient absorption data measured for 8'-apo-β-carotenal in n-hexane (top) and methanol (bottom).

550 nm in both solvents. But while earlier data relied on single-wavelength fitting, here we report the whole spectro-temporal datasets that allows for global fitting the data. This approach provides deeper insight into the excited- state dynamics as it is evidenced in Figure 3.1.4 that shows global fitting results. The change in S_1/ICT lifetime is obvious from comparison of the blue EADS, which in both solvents

correspond to the S_1/ICT state decaying to the ground state. It has a lifetime of 26 ps in n-hexane and 8 ps in methanol. These values agree with the single-wavelength data reported earlier that ranged from 21-25 ps in n-hexane and 7.6-8.7 ps in methanol [P1.16], [P1.17] . Although the change of the S_1/ICT lifetime is the major polarity-dependent feature observed in global fitting results shown in Figure 3.1.4., the initial dynamics of 8'-apo-β-carotenal also depends slightly on polarity. The S_2 lifetime, characterized by the decay of the initial EADS (black) is faster in methanol (110 fs) than in n-hexane (160 fs). The second EADS (red) is associated with a hot S_1/ICT state that in n-hexane decays in 1 ps to generate relaxed S_1/ICT state. The corresponding process is markedly faster in methanol (0.5 ps, see also inset of Figure 3.1.3.)

Having explored the excited-state properties of 8'-apo-β-carotenal in n-hexane and methanol, we now turn to 8'-apo-β-carotenal aggregates. Absorption spectra of 8'-apo-β-carotenal in methanol/water mixture are in Figure 3.1.5 compared with that of monomeric 8'-apo-β-carotenal. At methanol/water ratio of 1:9 the absorption spectrum is blue-shifted compared to the monomeric 8'-apo-β-carotenal signaling formation of H-aggregates with absorption maximum around 430 nm. At methanol/water ratio of 1:1 the absorption spectrum contains a red-shifted band at ~550 nm due to J-aggregates. It must be noted however, that both samples contain bands attributable to both blue-shifted H-aggregates and red-shifted J-aggregates, and change of
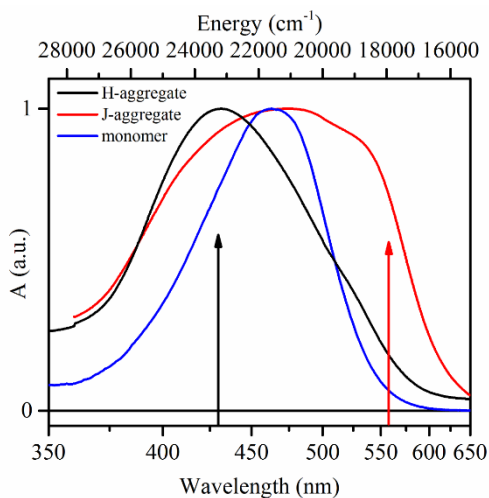
Figure 3.1.5 Absorption spectra of 8'-apo-β-carotenal in hydrated methanol. Arrows denote excitation wavelengths used to excite H-aggregates (435 nm, MeOH/water, 1:9) and J-aggregates (557 nm, MeOH/water, 1:1)

methanol/water ratio shifts the equilibrium either toward H- or J-aggregates. This is in contrast with aggregates of zeaxanthin [P1.27]-[P1.30] or astaxanthin [P1.25],[P1.26] that usually form well-defined J- or H-aggregates. The coexistence of H- and J- aggregates of 8'-apo-β-carotenal is most likely due to presence of the carbonyl group that

introduces asymmetry to the molecule preventing formation of ideal J- or H-type assemblies. Thus, to allow for separating excited-state dynamics of J- and H-aggregates, we have chosen two excitation wavelengths (indicated in Figure 3.1.5); 435 nm that excites preferentially H-aggregates, and 557 nm, which is close to the red-shoulder associated with J-aggregates.
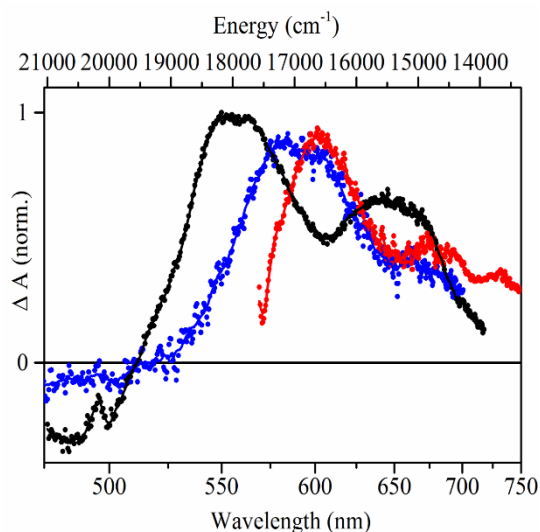
Figure 3.1.6 Transient absorption spectra of 8'-apo-β-carotenal aggregates measured at 3 ps after excitation. H-aggregates were excited at 435 nm (blue), J-aggregates were excited at 557 nm (red). Transient absorption spectrum of monomeric 8'-apo-β-carotenal dissolved in methanol excited at 490 nm is shown for comparison (black). All spectra are normalized to maximum. The solid lines are results of data smoothing using Savitzky-Golay method.

Transient absorption spectra of H- and J-aggregates compared with that of monomer are shown in Figure 3.1.6. Both aggregates exhibit a S_1-like transition that is red-shifted compared to that of monomeric 8'-apo-β-carotenal. Transient absorption spectrum of the H-aggregate is dominated by a broad band with a double-peak with maxima at 580 and 600 nm. There is only weak and flat negative signal below 550 nm demonstrating that molecules excited at 435 nm are indeed H-aggregates indicating that the sample denoted as H-aggregate does not contain significant fraction of monomers. If monomers were present, they would be certainly excited at 435 nm resulting in bleaching signal below 500 nm. For J-aggregate, strong scattering of the 557 nm excitation prevents to record data at wavelengths shorter than 570 nm. It has a single S_1-S_n peak located at ~600 nm that is accompanied by two weak bands at 680 and 730 nm. Comparison of transient absorption spectra of monomer and both aggregates taken at 3 ps also show that the red-shifted ICT-like bands are suppressed in aggregates formed in water/methanol mixtures.

The changes of excited-state properties occurring upon aggregation are further demonstrated by kinetics measured at the maxima of the S_1-S_n transitions

depicted in Figure 3.1.7. While monomeric 8'-apo-β-carotenal in methanol decays with 8 ps time constant (see also Figure 3.1.3 and Figure 3.1.4), decays of both J- and H-aggregates are clearly multiexponential, containing components both faster and slower than monomer (see below global fitting results). This agrees with previous results on zeaxanthin aggregates [P1.27], though in contrast to zeaxanthin J- and H-aggregates of 8'-apo-β-carotenal exhibit comparable dynamics of the S_1 state.

Global fitting results presented in Figure 3.1.8 provide quantitative information about dynamics of 8'-apo-β-carotenal aggregates. For H-aggregate excited at 435 nm, the initial excited state (black EADS) does not contain much bleaching below 550 nm again confirming absence of monomers excited at 435 nm. The initial spectrum decays in 100 fs to produce EADS (red) that is dominated by the S_1-S_n transition at ~610 nm. Further dynamics occurs with a time constant of 640 fs and produces a slight blue-shift of the S_1-S_n band to 585 nm accompanied by a loss of intensity of the red part of the S_1-S_n band while intensity increases at the blue edge of the S_1-S_n transition. This dynamics is characteristic of S_1 state relaxation [P1.41], thus the blue EADS in Figure 3.1.8 is assigned to the relaxed S_1 state of the H-aggregate, which decays in 20 ps thus more than twice longer than in monomer. Moreover, in

Figure 3.1.7. Kinetics of 8'-apo-β-carotenal aggregates measured at 610 nm compared with kinetics monitoring the S_1 decay of monomer in methanol measured at 550 nm. Kinetics are normalized to maximum; solid lines are fits resulting from global fitting. Excitation at 435 nm (H-aggregate), 490 nm (monomer), and 557 nm (J-aggregate).

contrast to monomer, the S_1 state of the aggregate does not fully decay to the ground state. Instead, a weak excited-state absorption band centered at 565 nm does not decay within the time window of the experiment (1 ns) indicating that triplet state of 8'-apo-β-carotenal is generated in the aggregate.

Global fitting of data obtained after exciting the J-aggregate at 557 nm results in EADS comparable in shape to those of H-aggregate, but the underlying dynamics is more complicated. The initial excited state contains pronounced negative signal below 620 nm confirming that the red-most absorbing J-aggregates are excited at 557

nm. The first EADS decays in 130 fs to form red EADS that has the S_1-S_n transition at 610 nm, but it is accompanied by intensive red-shifted bands at ~680 nm and 730 nm. The red bands disappear during the subsequent dynamics characterized by a time constant of 320 fs and typical S_1-like EADS peaking at 605 nm is formed. Contrary to H-aggregates, global fitting of J-aggregates requires one more time constant, 2.7 ps, which characterizes further blue shift of the S_1-S_n transition. The resulting EADS (green spectrum in Figure 3.1.8b) has the S_1-S_n band centered at 600 nm. As for the H-aggregate, there is only weak signal in the ICT spectral region. The S_1 state of the J-aggregate decays in 40 ps, and presence of a small non-decaying signal again indicates formation of the triplet state.

3.1.5 Discussion

Monomeric 8'-apo-β-carotenal

Polarity-induced changes of absorption spectra of monomeric 8'-apo-β-carotenal were in detail discussed elsewhere [P1.16]-[P1.18]. Upon going from nonpolar hexane to polar methanol, there is increased absorption at the red tail of absorption spectrum that also loses the characteristic three-peak vibrational structure due to increased conformational disorder in polar solvent. Both these effects are typical of essentially all carotenoids with conjugated carbonyl group studied so far [P1.4], [P1.5], [P1.16]-[P1.20], [P1.35], [P1.40].

Transient absorption spectrum of monomeric 8'-apo-β-carotenal in n-hexane (Figure 3.1.2) is comparable to S_1 spectra of other carotenoids, except the additional bands in the red part of the spectrum. Deconvolution of the transient absorption spectrum into Gaussian bands shown in Figure 3.1.9 reveals that in addition to the characteristic sharp S_1-S_n band, spectrum of monomeric 8'-apo-β-carotenal in n-hexane contains three additional bands at lower energy. Closer inspection shows that these bands are separated by 1200-1400 cm^{-1} thus it is likely that these three bands correspond to a vibrational progression of a single transition. Following the interpretation of these bands in the shorter relative of 8'-apo-β-carotenal, 12'-apo-β-carotenal [P1.19], we assign these bands to an $S_1(A_g^-) - S_3(A_g^+)$ transition. The S_3 state is known as the final state of the "cis-peak" usually observed in ground state absorption spectra of cis-carotenoids [P1.42], [P1.43], because deviation from the C_{2h} symmetry of cis-carotenoids renders the S_0-S_3 transition partially allowed. Similarly, we propose that the S_1-S_3 transition is forbidden in symmetric linear carotenoids, while in carotenoids with some deviation from C_{2h} symmetry caused by the

conjugated carbonyl group, this transition becomes allowed. Contrary to cis-carotenoids however, there is no cis-peak in the ground state absorption spectra of 8'-apo-β-carotenal Figure 3.1.10, indicating that the S_0-S_3 transition remains forbidden. This observation supports the hypothesis that the symmetry breaking in carbonyl carotenoids is significantly enhanced in the S_1 state, making the S_1-S_3 transition more allowed than the S_0-S_3 transition.

Since we have assigned the red-shifted bands in the transient absorption spectrum of monomeric 8'-apo-β-carotenal in n-hexane to the S_1-S_3 transition, we may ask a question what is the origin of the ICT-like transition that appears when 8'-apo-β-carotenal is dissolved in polar methanol (Figure 3.1.2). Comparison of the underlying individual bands in transient absorption spectra of 8'-apo-β-carotenal in n-hexane and methanol Figure 3.1.9 suggests an explanation. In fact, the polarity-induced change does not require introducing any new bands. Instead, we may interpret the observed change as a decrease of intensity of the S_1-S_n transition at 550 nm and increase of intensity of the bands which we assigned to the S_1-S_3 transition.

Such an assignment would imply that both the 'S$_1$-like' and 'ICT-like' bands originate from the same state, S_1, which would resolve the long-standing puzzle as to why these two bands always decay with the same time constant [P1.4], [P1.5]. Although some results indicate that kinetics

Figure 3.1.8 EADS obtained from global fitting the transient absorption data measured for 8'-apo-β-carotenal aggregates. (top) H-aggregates were excited at 435 nm, (bottom) J-aggregates were excited at 557 nm. Note different scales at horizontal axis in top and bottom panels.

taken at the maxima of the S_1 and ICT bands are not identical [P1.44], these differences are very small. In all experiments reported so far, both bands decay with nearly the

same time constant regardless the solvent polarity, and this decay matches the recovery of the ground state. This situation led to the concept of a coupled S_1/ICT state that consists of 'S$_1$-like' and 'ICT-like' potential minima that both decay with the same time constant to the ground state [P1.36]. An alternative explanation that we propose here for 8'-apo-β-carotenal is that polarity alters the intensity of separate electronic transitions originating from the S_1 state.

It is known that an asymmetrically positioned carbonyl group makes the 'ICT-like' band of carbonyl carotenoids in polar solvents more intense [P1.45][P1.47]. Thus, we can assume that the asymmetry in electron distribution caused by the carbonyl group in the excited state is enhanced in polar solvents. Consequently, the 'standard' S_1-S_n transition, which is strongly allowed in C_{2h} symmetry, will become less allowed upon introduction of asymmetry. On the other hand, the S_1-S_3 transition, which is forbidden in C_{2h} symmetry, will gain intensity upon symmetry breaking. Consequently, it is the S_1 state itself that yield some ICT character in polar solvents.

Thus, we can explain the transient absorption spectral features observed in 8'-apo-β-carotenal by assuming that the transitions observed in both polar and nonpolar solvents are the same, and result from the S_1-S_n and S_1-S_3 transitions whose intensities are altered by solvent polarity. In the same manner, the appearance of the red-shifted stimulated emission of 8'-apo-β-carotenal [P1.17] or other carbonyl carotenoids [P1.5], [P1.36] in polar solvents is due to enhancing the allowedness of the S_1-S_0 transition. We must note however that both stimulated emission and the ICT-like (S_1-A_g^+) bands of some carbonyl carotenoids exhibit a pronounced rise that is also dependent on solvent polarity [P1.36], [P1.46]. As it was shown recently, the formation of the asymmetric state with charge transfer character is a dynamical process [P1.45], [P1.47]. Therefore, we may define the ICT state of 8'-apo-β-carotenal as the S_1 (A_g^-) state with admixed S_2 (B_u^+) character [P1.45], [P1.47] that results in an increase in the asymmetry of the electron distribution of the excited state. The polarity-dependent rise time observed in kinetics recorded at maximum of the ICT band in some carbonyl carotenoids thus can be considered as a 'stabilization of asymmetry' of the molecule, which may be viewed as a solvation process that stabilizes charge distribution over the carotenoid, in this case 8'-apo-β-carotenal. Following the relaxation from the S_2 state, the S_1 state is not ideally solvated thus distribution of charges over the molecule is different than that realized after solvation. If the electron distribution prior to solvation is slightly less asymmetric than the electron distribution after solvation, the solvation process also increases the magnitude of the S_1-S_3 transition, because the

asymmetry in electron distribution is directly proportional to the magnitude of the S_1-S_3 transition. Such arrangement explains the appearance of the slow rise component of the ICT-like band in polar solvents.

Recent reports that ICT-like bands of another carbonyl carotenoids, fucoxanthin, can be 'switched off' by changing excitation wavelength either in one-photon [P1.44] or two-photon [P1.48] excitation experiment could be within our hypothesis explained by excitation of different subsets of molecules, each having S_1 state with different degree of ICT character and/or mixing. The same argument can be applied to reconcile our hypothesis with the pump-dump-probe experiments on peridinin in methanol, which demonstrated that dump pulse centered at 800 nm can selectively affect the ICT-like band [P1.49]. These results were interpreted in terms of the S_1 and ICT states of peridinin being separate, though coupled entities. Yet, the selective dumping can be also achieved if the dump pulse interacts with a subset of peridinin molecules having stronger charge transfer character of the S_1 state. We would also like to mention that our hypothesis cannot explain why the S_1 lifetime is significantly shorter in polar solvent. This phenomenon is characteristic of a number of carbonyl carotenoids [P1.4], [P1.5], [P1.16] and remains unexplained. Since the S_1 energy is not affected by solvent polarity, alterations in electron distribution and the S_1/S_2 mixing induced by polarity must somehow affect the S_1-S_0 coupling via the C=C stretching mode that determines the S_1 lifetime [P1.50]. Therefore, spectroscopic methods directly probing the vibrational frequencies or coupling of vibrational modes to the phonon bath, such as femtosecond Raman spectroscopy [P1.51], [P1.52], or photon echo [P1.53], [P1.54], hold promise to reveal the mechanism responsible for the shortening of the S_1 lifetime in polar solvents.

8'-apo-β-carotenal aggregates

Aggregation of 8'-apo-β-carotenal occurs upon addition of water to the methanol solution of the monomeric carotenoid. Absorption spectra of 8'-apo-β-carotenal aggregates exhibit features typical of carotenoid aggregates. Depending on water/methanol ratio either H- or J-aggregates are formed, confirming earlier reports on zeaxanthin [P1.27], [P1.30] and astaxanthin aggregates [P1.25], [P1.26], [P1.55]. In contrast to zeaxanthin or astaxanthin, aggregation induced shifts of 8'-apo-β-carotenal absorption spectrum are smaller. Maximum of the H-aggregate is at 430 nm, resulting in aggregation-induced blue shift of ~2000 cm^{-1}, thus much less than for zeaxanthin, astaxanthin or lycopene that all exhibit blue-shift of more than 3000 cm^{-1} [P1.24], [P1.25], [P1.27], [P1.30]. For J-aggregate, the J-band peaks around 535 nm. Aggregation-induced

red shift from the absorption maximum of a monomer is thus larger, ~2800 cm^{-1}, a value comparable to that reported for J-aggregates of carotenoids zeaxanthin or lutein [P1.27], [P1.30], [P1.31]. It should be noted that these values cannot be directly translated into interaction strength, because part of the shift is caused by non-resonant dispersion interactions [P1.30]. These results suggest that structure of 8'-apo-β-carotenal prevents formation of tightly packed aggregates with strong intermolecular interaction as it is for nearly planar and symmetric carotenoids such as zeaxanthin and lycopene. On the other hand, the asymmetric structure of 8'-apo-β-carotenal apparently does not hinder formation of assemblies consisting of molecules that are shifted (head-to-tail arrangement) and/or twisted (helical structures) in respect to each other – structures leading to the J-type absorption spectrum [P1.30]-[P1.32].

Absorption spectra of 8'-apo-β-carotenal aggregates are also much broader than those of other carotenoids, suggesting that broader distribution of sizes and assemblies occur in 8'-apo-β-carotenal aggregates. This fact complicates interpretation of excited-state dynamics, because excitation pulse inevitably excites aggregates of different sizes. Yet, transient absorption spectra of aggregates taken at 3 ps after excitation (Figure 3.1.6) do not differ significantly from transient absorption spectrum of the monomer, except the S_1-S_n transitions of aggregates are red shifted. This reflects the known fact that the carotenoid S_1 state, having negligible dipole moment, is rather insensitive to aggregation; the observed red-shift is rather due to aggregation-induced changes in energy of the final S_n state.

Transient absorption spectra shown in Figure 3.1.6 also reveal that even though water/methanol mixture is more polar than pure methanol, the ICT-like bands at 3 ps are much weaker in aggregates. In fact, as demonstrated in Supporting Information (Figure 3.1.11), transient absorption spectrum of J-aggregate is somewhat similar to that of 8'-apo-β-carotenal monomer in n-hexane. This seemingly contradictive result can be readily explained, because not all molecules in the aggregates are exposed to water. Recent transmission electron microscopy data of zeaxanthin J-aggregates show that they form tubes more than 2 m long with diameter ~500 nm [P1.30]. A lot of molecules are therefore buried deep inside the aggregate with their C=O groups protected from the polar environment. Interior of the aggregate is thus rather nonpolar, resulting in transient absorption spectrum comparable to that of monomer in n-hexane. The same explanation likely holds also for H-aggregates though they should be somewhat smaller than J-aggregates [P1.30].

The nonpolar environment inside the aggregates may also partly explain the

changes in the excited-state dynamics. Global fitting shown in Figure 3.1.8 revealed a multiexponential decay of the S_1 state of aggregates, but the longest lifetime associated with the S_1 state of aggregated 8'-apo-β-carotenal, 20 ps for H-aggregate and 40 ps for J-aggregate, is significantly longer than 8 ps measured for monomer in methanol (Figure 3.1.7); instead, it is closer to the 26 ps measured for monomer in n-hexane (Figure 3.1.4a). It is thus tempting to argue that the long S_1 lifetime corresponds to the molecules buried inside the aggregate, an environment that somewhat mimics the nonpolar solvent. But the situation is more complicated, because comparable prolongation of the S_1 lifetime, to ~20 ps in H-aggregate and to ~30 ps in J-aggregate, was reported for zeaxanthin [P1.27] that has the monomeric S_1 lifetime of 9 ps regardless the solvent polarity [P1.56].

For zeaxanthin aggregates, the longer S_1 lifetime was explained as due to changes in vibrational coupling through the C=C stretching mode, which facilitates the S_1-S_0 internal conversion [P1.50]. This proposal is supported by recent time-resolved Raman measurements of zeaxanthin aggregates. Frequency of the ground state C=C stretching mode is affected by aggregation only moderately; the frequency is down-shifted from 1525 cm⁻¹ in monomer to 1516 cm⁻¹ in J-aggregate [P1.28]. The C=C stretching mode in the S_1 state that is up-shifted to 1700-1800 cm⁻¹ due to strong coupling to the S_0 state in monomeric carotenoids [P1.50] has not been detected in aggregates at all [P1.28]. This clearly implies that aggregation of carotenoids somehow diminish the S_1-S_0 coupling through the C=C stretching mode, resulting in longer S_1 lifetimes of aggregates.

Besides the long S_1 lifetime described in the previous paragraph the global fitting revealed a few faster time components. The fastest component of 100-130 fs is close to limits of our time resolution and obviously corresponds to relaxation from the S_2 state to the S_1 state. The blue EADS with 2.7 ps lifetime revealed in J-aggregate has a shape very similar to that of the 40 ps EADS assigned to the S_1 lifetime, except the S_1-S_n maximum is slightly red-shifted. This likely reflects the inhomogeneity of the aggregate, which is probably larger than for H-aggregate. Then the 2.7 ps process is due to trapping of the excitations in S_1 states of carotenoids with lowest S_1 energies.

Most intriguing is the subpicosecond time component, which yields 640 fs in H-aggregates and 320 fs in J-aggregates. Especially in J-aggregates, the spectrum of this component contains spectral bands reminiscent of the ICT-like transitions in monomeric 8'-apo-β-carotenal, except the bands are more intense. Moreover, the 320 fs component has the largest amplitude in the spectral region associated with these

bands, while it is rather weak within the S_1-S_n band (Figure 3.1.8b). It is thus possible that this spectrum reflects a subpopulation of molecules in the J-aggregate that are presumably in contact with water that amplifies the polarity-induced effects observed for monomer in methanol.

Significant polarity effect of water was demonstrated in a set of water-soluble hydrophilic carbonyl carotenoids, which have two symmetrically positioned carbonyl groups [P1.35]. Since it is known that the polarity effect is much stronger when there is a single asymmetric carbonyl group [P1.45], we may assume that combination of the asymmetric carbonyl of 8'-apo-β-carotenal in water/methanol mixture may significantly enhance the polarity effect. Thus, we suggest that the red EADS in Figure 3.1.8b is due to a fraction of molecules in J-aggregate that are in direct contact with solvent, leading to enhancement of ICT character of the S_1 state, resulting in intense ICT-like transitions and S_1 lifetime of 320 fs. Although this lifetime is much shorter than S_1 lifetime of 8'-apo-β-carotenal in methanol (8 ps), we note that a comparable dramatic shortening was reported for another carbonyl carotenoid, hydroxyechinenone whose S_1 lifetime is under specific conditions induced by binding to the Orange Carotenoid Protein shortened from 6 ps in methanol to 0.6-0.9 ps in protein [P1.57], [P1.58]. The 640 fs EADS obtained from global fitting the H-aggregate is likely of similar origin though the ICT-like band is much less pronounced than for J-aggregate.

3.1.6   Conclusions

In this work we propose an alternative explanation of the origin of the ICT bands observed in transient absorption spectra of 8'-apo-β-carotenal in methanol. Contrary to the widely accepted notion of the coupled S_1/ICT state, we propose that both S_1-like and ICT-like transitions occurs from a single state, the lowest singlet excited state, S_1, of 8'-apo-β-carotenal, whose charge transfer character depends on solvent polarity. This conclusion is in agreement with recent quantum chemical calculations on peridinin [P1.47]. With increasing the solvent polarity, the charge transfer character of the S_1 state also increases, resulting in asymmetry of electron distribution. This relaxes the symmetry rules and makes the S_1-S_3 (A_g^--A_g^+) transition, which is forbidden in the ideal C_{2h} symmetry, partially allowed. The ICT-like band is thus due to the S_1-S_3 transition that becomes allowed due to the symmetry breaking in polar solvents.

Aggregation of 8'-apo-β-carotenal is induced by adding water into methanol

solution. Depending on water content, either blue-shifted H-aggregates or red-shifted J-aggregates are formed. Both types of aggregates exhibit significantly different excited state dynamics. Even though the methanol/water mixture is significantly polar, aggregates do not exhibit characteristic ICT-like bands, most likely due to large assemblies of molecules in which most of the molecules are protected from solvent. Contrary to monomers, both types of aggregates exhibit ultrafast formation of triplet states via singlet homofission.

3.1.7 Acknowledgment

3.1.8 References

[P1.1] Polívka, T.; Sundström, V. *Chem. Rev.* 2004, *104*, 2021–2071.

[P1.2] Polívka, T.; Frank, H. A. *Acc. Chem. Res.* 2010, *43*, 1125–1134.

[P1.3] Scholes, G.D.; Fleming, G.R.; Olaya-Castro, A.; van Grondelle, R. *Nature Chemistry* 2011, *3*, 764–774.

[P1.4] Frank, H.A.; Bautista, J.A.; Josue, J.; Pendon, Z.; Hiller, R.G.; Sharples, F.P.; Gosztola, D.; Wasielewski, M.R. *J. Phys. Chem. B* 2000, *104*, 4569–4577.

[P1.5] Zigmantas, D.; Hiller, R.G.; Sharples, F.P.; Frank, H.A.; Sundström, V.; Polívka, T. *Phys. Chem. Chem. Phys.* 2004, *6*, 3009–3016.

[P1.6] Polívka, T.; Hiller, R.G.; Frank, H.A. *Arch. Biochem. Biophys.* 2007, *458*, 111–120.

[P1.7] Polívka, T.; Pellnor, M.; Melo, E.; Pascher, T.; Sundström, V.; Osuka, A.; Naqvi, K.R. *J. Phys. Chem. C*, 2007, *111*, 467–476.

[P1.8] Ostroumov, E.; Müller, M.G.; Marian, C.M.; Kleinschmidt, M.; Holzwarth, A.R. *Phys. Rev. Lett.* 2009, *103*, 108302.

[P1.9] Maiuri, M.; Polli, D.; Brida, D.; Luer, L.; LaFountain, A.M.; Fuciman, M.; Cogdell, R.J.; Frank, H.A.; Cerullo, G. *Phys. Chem. Chem. Phys.* 2012, *14*, 6312–6319

[P1.10] Marek, M.S.; Buckup, T.; Motzkus, M. *J. Phys. Chem. B* 2011, *115*, 8328–8337

[P1.11] Bautista, J.A.; Hiller, R.G.; Sharples, F.P.; Gosztola, D.; Wasielewski, M.; Frank, H.A. *J. Phys. Chem. A*, 1999, *103*, 2267–2273.

[P1.12] Gao, F.G.; Bard, A.J.; Kispert, L.D. *J. Photochem. Photobiol. A* 2000, *130*, 49–56

[P1.13] Pan, J.; Benkö, G.; Xu, Y.H.; Pascher, T.; Sun, L.C.; Sundström, V.; Polívka, T. *J. Am. Chem. Soc.* 2002, *124*, 13949–13957.

[P1.14] Xiang, J.F.; Rondonuwu, F.S.; Kakitani, Y.; Fujii, R.; Watanabe, Y.; Koyama, Y.; Nagae, H.; Yamano, Y.; Ito, M. *J. Phys. Chem. B* 2005, *109*, 17066–17077.

[P1.15] Pan, J.X.; Xu, Y.H.; Sun, L.C.; Sundström, V.; Polívka, T. *J. Am. Chem. Soc.* 2004, *126*, 3066–3067.

[P1.16] Ehlers, F.; Wild, D.A.; Lenzer T.; Oum, K. *J. Phys. Chem. A* 2007, *111*, 2257–2265.

[P1.17] Kopczynski, M.; Ehlers, F.; Lenzer, T.; Oum, K. *J. Phys. Chem. A* 2007, *111*, 5370–5381.

[P1.18] Ehlers, F.; Lenzer, T.; Oum, K. *J. Phys. Chem, B* 2008, *112*, 16690–16700.

[P1.19] Polívka, T.; Kaligotla, S.; Chábera, P.; Frank, H.A. *Phys. Chem. Chem. Phys.* 2011, *13*, 10787−10796.

[P1.20] Oum, K.; Lohse, P.W.; Ehlers, F.; Scholz, M.; Kopczynski, M.; Lenzer, T. *Angew. Chem. Int. Ed.* 2010, *49*, 2230–2232.

[P1.21] Buchwald, M.; Jencks, W.P. *Biochemistry* 1968, *7*, 834–843.

[P1.22] Ruban, A.V.; Horton, P.; Young, A.J. *J. Photochem. Photobiol. B* 1993, *21*, 229–234.

[P1.23] Simonyi, M.; Bikadi, Z.; Zsila, F.; Deli, J. *Chirality*, 2003, *15*, 680–698.

[P1.24] Polívka, T. In *Carotenoids: Physical, Chemical, and Biological Functions and Properties*; Landrum, J.T., Ed.; CRC Press, 2010, p.137–157.

[P1.25] Mori, Y.; Yamano, K.; Hashimoto, H. *Chem. Phys. Lett.* 1996, *254*, 84–88.

[P1.26] Köpsel, C.; Möltgen, H.; Schuch, H.; Auweter, H.; Kleinermanns, K.; Martin, H.-D.; Bettermann, H. *J. Mol. Struct.* 2005, *750*, 109–115.

[P1.27] Billsten, H.H.; Sundström, V.; Polívka, T. *J. Phys. Chem. A* 2005, *109*, 1521–1529.

[P1.28] Wang, C.; Tauber, M.J. *J. Am. Chem. Soc.* 2010, *132*, 13988–13991.

[P1.29] Wang, C.; Schlamadinger, D.E.; Desai, V.; Tauber, M.J. *Chem. Phys. Chem.* 2011, *12*, 2891–2894.

[P1.30] Wang, C.; Berg, C.J.; Hsu, C.C.; Merrill, B.A.; Tauber, M.J. *J. Phys. Chem. B* 2012, *116*, 10617−10630.

[P1.31] Spano, F.C. *J. Am. Chem. Soc.* 2009, *131*, 4267–4278.

[P1.32] Olsina, J.; Durchan, M.; Minofar, B.; Polívka, T.; Mančal, T. http://arxiv.org/abs/1208.4958.

[P1.33] Zsila, F.; Bikadi, Z.; Keresztes, Z.; Deli, J.; Simonyi, M. *J. Phys. Chem. B* 2001, *105*, 9413–9421.

[P1.34] Ray, K.; Misra, T.N. *J. Photochem. Photobiol. A*, 1997, *107*, 201–205.

[P1.35] Chábera, P.; Fuciman, M.; Naqvi, K.R.; Polívka, T. *Chem. Phys.* 2010, *373*, 56–64.

[P1.36] Zigmantas, D.; Hiller, R.G.; Yartsev, A.; Sundström, V.; Polívka, T. *J. Phys. Chem. B*, 2003, *107*, 5339–5348.

[P1.37] Gradinaru, C.C.; Kennis, J.T.M.; Papagiannakis, E.; van Stokkum, I.H.M.; Cogdell, R.J.; Fleming, G.R.; Niederman, R.A.; van Grondelle, R. *Proc. Natl. Acad. Sci. U.S.A.* 2001, *98*, 2364–2369.

[P1.38] Polívka T.; Sundström, V. *Chem. Phys. Lett.*, 2009, *477*, 1–11.

[P1.39] Niedzwiedzki, D.; Koscielecki, J.F.; Cong, H.; Sullivan, J.O.; Gibson, G.N.; Birge, R.R.; Frank, H.A. *J. Phys. Chem. B* 2007, *111*, 5984–5998.

[P1.40] Niedzwiedzki, D.M.; Chatterjee, N.; Enriquez, M.M.; Kajikawa, T.; Hasegawa, S.; Katsumura, S.; Frank, H.A. *J. Phys. Chem. B* 2009, *113*, 13604–13612.

[P1.41] de Weerd, F.L.; van Stokkum, I.H.M.; van Grondelle, R. *Chem. Phys. Lett.* 2002, *354*, 38–43.

[P1.42] Koyama, Y.; Fujii, R. In *The Photochemistry of Carotenoids*; Frank, H.A.; Young, A.J.; Britton, G.; Cogdell, R.J. Eds.; Kluwer Academic Publishers, Dordrecht, 1999, p. 161–188.

[P1.43] Niedzwiedzki, D.M.; Sandberg, D.J.; Cong, H., Sandberg, M.N.; Gibson, G.N.; Birge, R.R.; Frank, H.A. *Chem. Phys.* 2009, *357*, 4–16.

[P1.44] Kosumi, D.; Kusumoto, T.; Fujii, R.; Sugisaki, M.; Iinuma, Y.; Oka, N.; Takaesu, Y.; Taira, T.; Iha, M.; Frank, H.A. et al. *Phys. Chem. Chem. Phys.* 2011, *13*, 10762–10770.

[P1.45] Enriquez, M.M.; Fuciman, M.; LaFountain, A.M.; Wagner, N.L.; Birge, R.R.; Frank, H.A. *J. Phys. Chem. B* 2010, *114*, 12416–12426.

[P1.46] Zigmantas, D.; Polívka, T.; Hiller, R.G.; Yartsev A.; Sundström, V. *J. Phys. Chem. A* 2001, *105*, 10296–10306.

[P1.47] Enriquez, M.M.; Hananoki, S.; Hasegawa, S.; Kajikawa, T.; Katsumura, S.; Wagner, N.L.; Birge, R.R.; Frank, H.A. *J. Phys. Chem. B* 2012, *116*, 10748−10756.

[P1.48] Kosumi, D.; Kusumoto, T.; Fujii, R.; Sugisaki, M.; Iinuma, Y.; Oka, N.; Takaesu, Y.; Taira, T.; Iha, M.; Frank, H.A. et al. *J. Lum.* 2011, *131*, 515–518.

[P1.49] Papagiannakis, E.; Larsen, D.S.; van Stokkum, I.H.M.; Vengris, M.; Hiller, R.G.; van Grondelle, R. *Biochemistry* 2004, *43*, 15303–15309.

[P1.50] Nagae, H.; Kuki, M.; Zhang, J.P.; Sashima, T.; Mukai, Y.; Koyama, Y. *J. Phys. Chem. A* 2000, 104, 4155–4166.

[P1.51] Shim, S.; Mathies, R.A. *J. Phys. Chem. B* 2008, *112*, 4826–4832.

[P1.52] Kloz, M.; van Grondelle, R.; Kennis, J.T.M. *Phys. Chem. Chem. Phys.* 2011, *13*, 18123–18133.

[P1.53] Sugisaki, M.; Yanagi, K.; Cogdell, R.J.; Hashimoto, H. *Phys. Rev. B* 2007, *75*, 155110.

[P1.54] Christensson, N.; Polívka, T.; Yartsev, A.; Pullerits, T. *Phys. Rev. B* 2009, *79*, 245118.

[P1.55] Giovannetti, R.; Alibabaei, L.; Pucciarelli, F. *Spectrochimica Acta Part A- Molecular and Biomolecular Spectroscopy* 2009, *73*, 157–162.

[P1.56] Billsten, H.H.; Zigmantas, D.; Sundström, V.; Polívka, T. *Chem. Phys. Lett.* 2002, *355*, 465–470.

[P1.57] Polívka, T.; Kerfeld, C.A.; Pascher, T.; Sundström, V. Biochemistry 2005, 44, 3994–4003.

[P1.58] Berera, R.; van Stokkum, I.H.M.; Gwizdala, M.; Wilson, A.; Kirilovsky, D.; van Grondelle, R. *J. Phys. Chem. B* 2012, *116*, 2568–2574.

3.1.9 Supporting information
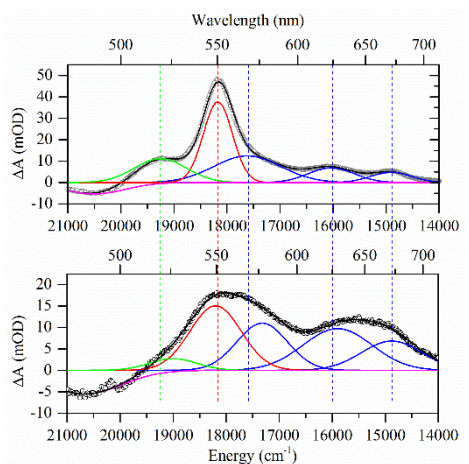
Figure 3.1.9 Deconvolution of transient absorption spectra of 8'-apo-β-carotenal in n-hexane (top) and methanol (bottom) into Gaussian bands. Transient absorption spectra were measured 3 ps after excitation at 490 nm. The spectral band shown in red correspond to the 'standard' S_1-S_n ($2A_g^-$ to nB_u^+) transition, while the bands shown in blue represent vibrational progression of the S_1-S_3 transition that gains intensity in polar solvents. Yet, these bands are observed even in the nonpolar n-hexane due to the asymmetry of 8'-apo-β-carotenal induced by the conjugated carbonyl group. The green spectral band is due to the S* signal whose origin is still a matter of debate.
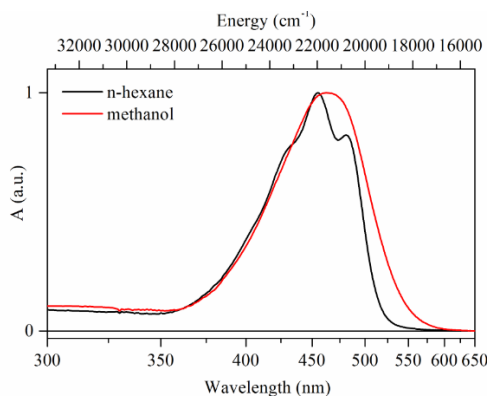
Figure 3.1.10 Absorption spectra of 8'-apo-β-carotenal in n-hexane and methanol measured down to 300 nm. They show that no cis-peak is observed either in n-hexane or methanol, because for a cis-carotenoid with comparable conjugation length the cis-peak should occur in the spectral region 330-350 nm.[1]
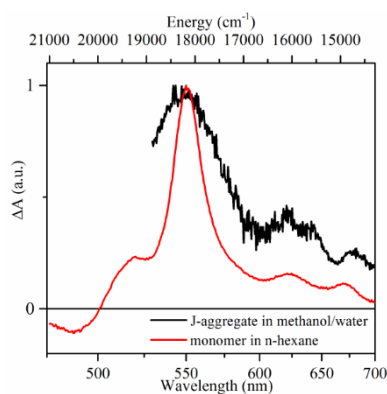
Figure 3.1.11 Comparison of EADS corresponding to the relaxed S_1 state of monomeric 8'-apo-β-carotenal in n-hexane and J-aggregate in 50/50 water/methanol mixture. Transient absorption spectrum of J-aggregate is blue-shifted to match the S_1-S_n maximum of the transient absorption spectrum measured for the monomeric 8'-apo-β-carotenal.

3.2   PAPER 2

Excited State Dynamics of Astaxanthin Aggregates

Marcel Fuciman, Milan Durchan, Václav Šlouf, **Gürkan Keşan**, Tomáš Polívka,

3.2.1 Abstract

Astaxanthin forms three types of aggregates in hydrated dimethyl sulfoxide (DMSO). In DMSO/water ratio of 1:1, a red-shifted J-aggregate with maximum at 570 nm is generated, while a ratio of 1:9 produces blue-shifted H-aggregates with peaks at 386 nm (H1) and 460 nm (H2). Monomeric astaxanthin in DMSO has an S_1 lifetime of 5.3 ps, but a long-lived (33 ps) S* signal was also identified. Aggregation changes the S_1 lifetimes to 17 ps (H1), 30 ps (H2), and 14 ps (J1). Triplet state of astaxanthin, most likely generated via singlet homofission, was observed in H1 and H2 aggregates.

3.2.2 Introduction

Carotenoids are a group of natural pigments that play a number of important roles in biological systems. They are important for light-harvesting and photoprotection in photosynthesis [P2.1], [P2.2]; they are also widespread natural colorants and serve as antioxidants scavenging various radicals and deleterious singlet oxygen in essentially all living organisms [P2.3]. Carotenoids also attract a lot of attention due to their rich photophysics [P2.4], [P2.5]. Excited-state manifold of carotenoids contains a number of 'dark' excited states involved in excited-state dynamics. Based on a number of studies of monomeric carotenoids it is now a well-established fact that the strongly absorbing transition from the ground state is not the lowest energy transition in carotenoids. Instead, at least one dark singlet state, denoted as the S_1 state, lies below the absorbing state which is accordingly denoted as S_2 state [P2.4].

Carotenoids are, with a few rare exceptions [P2.6], hydrophobic molecules which readily aggregate in hydrated solvents [P2.7], [P2.8]. Two types of carotenoid aggregates can be distinguished according to their absorption spectra. The first type is associated with a large blue shift of the absorption spectrum. These aggregates are usually denoted as H-aggregates, in which the conjugated chains are closely packed and oriented parallel to each other. The second aggregation type (J-aggregate) is characterized by a red-shift of absorption band. They were traditionally attributed to a head-to-tail organization of conjugated chains [P2.7], but recent calculations suggest that they may also result from weakly-interacting H-type aggregates that form helical structures [P2.9]. Regardless the organization, J-aggregates form a loose association of carotenoid molecules [P2.7]-[P2.9]. Besides changes in absorption spectra, carotenoid

aggregates also exhibit significant changes in circular dichroism (CD) [P2.7]-[P2.9]. Further changes, albeit smaller, were also observed in Raman spectra [P2.8], [P2.10].

While the excited-state dynamics of monomeric carotenoids were studied to great details [P2.4], [P2.5], much less is known about excited-state dynamics of carotenoid aggregates. Time-resolved data for carotenoid aggregates are so far available only for zeaxanthin whose aggregates were studied by means of femtosecond transient absorption [P2.11], [P2.12] and picosecond Raman spectroscopy [P2.10], [P2.13], and synthetic 8'-apo-β-carotenal [P2.14]. For both carotenoids, significant aggregation-induced changes in excited-state dynamics were reported. Although the S_1 state energies are not much affected by aggregation, in most cases their lifetimes are altered significantly in aggregates, suggesting changes in S_1-S_0 vibronic coupling [P2.11], [P2.12], [P2.14]. Yet, some J-aggregates may have S_1 lifetimes close to those reported for monomers [P2.11], [P2.12]. Moreover, aggregation facilitates ultrafast formation of a triplet state, most likely via singlet fission [P2.10], [P2.13] that may prove important for the future design of devices aiming for conversion of solar energy [P2.15].

Aggregation-induced shifts of absorption spectrum may also play a role in tuning the colour of crustaceans [P2.16] or birds [P2.17], for which carotenoids were identified as natural colorants. Carotenoid astaxanthin, which is the subject of this study, is known as the colorant of the lobster carapace where it is the only pigment of the carotenoprotein crustacyanin [P2.16]. Upon binding to crustacyanin, absorption spectrum of astaxanthin undergoes a large red shift whose origin is still a matter of debate and excitonic interaction due to aggregation has been also suggested to contribute to the red shift [P2.18]. Aggregates of astaxanthin were so far studied only by steady-state spectroscopies that described formation of both H- and J-type aggregates in various hydrated solvents [P2.19]-[P2.23]. Here we employ transient absorption spectroscopy to reveal aggregation-induced changes of excited-state dynamics of astaxanthin.

3.2.3   Materials and Methods

Astaxanthin (Figure 3.2.1) was purchased from Sigma Aldrich. Dimethyl sulfoxide (DMSO, Fluka), of analytical grade was used for preparation of samples that is in detail described below. Transient absorption spectra were measured with a femtosecond spectrometer described in detail elsewhere [P2.6]. The pulses from Ti:sapphire amplifier (795 nm, 1.9 mJ/pulse, 1 kHz) were used to pump an optical parametric amplifier to generate excitation pulses, while a fraction of light was

focused to a 2-mm sapphire plate to produce a white-light continuum used as a broadband probe. Mutual polarization of the excitation and probe beams was set to the magic angle (54.7°). A 2-mm path length quartz cuvette was used for all transient absorption measurements. To prevent sample degradation, a micro-magnetic stirrer was used to continuously mix the sample during the measurements. The intensity of excitation was kept at $\sim 10^{14}$ photons pulse^{-1} cm^{-2}. Femtosecond transient absorption data collected by diode array detectors were fitted globally. To visualize the excited state dynamics, we assume a sequential, irreversible scheme of excited-state evolution. The extracted time constants correspond to lifetimes of the individual excited-state species in the sequential scheme. The spectral profile of each species is called evolution-associated difference spectrum (EADS) [P2.24].

3.2.4 Results and Discussion

Steady-state absorption spectra

An absorption spectrum of monomeric astaxanthin in pure DMSO is shown, along with spectra of astaxanthin aggregates in hydrated DMSO, in Figure 3.2.1. The
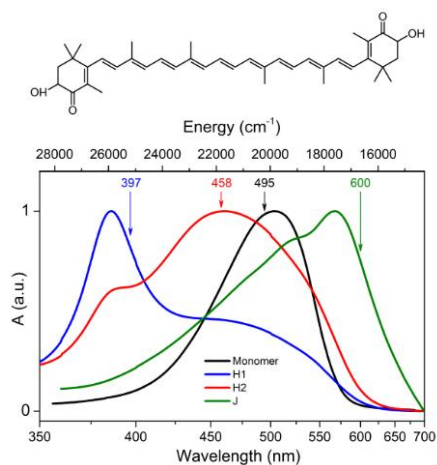
Figure 3.2.1 Normalized absorption spectra of astaxanthin monomer in DMSO (black), H1-aggregate (blue), H2-aggregate (red) and J-aggregate (green) in hydrated DMSO. DMSO:water ratio is 1:9 for H1 and H2 aggregates, and 1:1 for J-aggregate. Molecular structure of astaxanthin is also shown.

absorption spectrum of the monomer has a maximum at 504 nm and does not exhibit any vibrational structure. Due to dispersion interactions, the maximum of the S_0-S_2 transition of astaxanthin in DMSO is significantly red-shifted compared to the absorption spectra measured in methanol or acetone that peak around 476 nm [P2.19]-[P2.22]. A comparable S_0-S_2 maximum, 506 nm, was reported for astaxanthin in the nonpolar but highly polarizable CS_2 [P2.25].

The choice of DMSO allowed to readily control formation of astaxanthin aggregates, because this solvent facilitates formation of both H- and J-aggregates [P2.23]. The H-aggregate was prepared by mixing 100 μL of 1.7 mM astaxanthin in

DMSO with 900 μL of water to yield 170 μM of astaxanthin in DMSO/water ratio of 10/90. Absorption spectrum is dominated by a narrow peak with maximum at 386 nm, which is accompanied by a broad band extending from 400 to 550 nm (Figure 3.2.1). Based on recent modelling of absorption spectra of astaxanthin aggregates [P2.23], we assign the narrow peak to an H-aggregate consisting of a large number of astaxanthin molecules, while the broad band is due to smaller aggregates including the astaxanthin dimer [P2.23]. Hereafter, we will denote these two types of H-aggregates as H1 and H2 aggregates. The fraction of H2 aggregates in the sample is enhanced when 950 μL of 1:18 DMSO/water was mixed with 50 μL of 3.4mM astaxanthin in DMSO. The H1 and H2 aggregate solutions are both 1 mL in total volume, and contain 170 μM astaxanthin in 10/90 mixture of DMSO/water. Under this preparation conditions the absorption spectrum is dominated by the H2 absorption band peaking at 460 nm, while the H1 absorption is visible only as a weak shoulder at 386 nm (Figure 3.2.1). The J aggregate is formed by mixing of 500 μL of 0.34 mM astaxanthin in DMSO with 500 μL of water. The resultant 1 mL solution of J aggregate is 170 μM astaxanthin in 50/50 DMSO/water mixture. Absorption spectrum of J-aggregates is red-shifted in respect to monomer. The reddest band, corresponding to the 0-0 band of the S_0-S_2 transition of the aggregate, peaks at 570 nm. Prior to experiments, the samples were left for 12 hours in dark at room temperature to stabilize. All aggregates prepared as described above had optical density of ~0.3 in a 2-mm cuvette at absorption maximum.

If we compare maxima of absorption bands of astaxanthin aggregates with those reported earlier, it is obvious that while dispersion interaction significantly affects the absorption maximum of the monomer, it has only marginal effect on absorption maxima of the aggregates. H-aggregate of astaxanthin prepared in hydrated methanol peaks at 388 nm [P2.22], thus essentially at the same wavelength as we observed in hydrated DMSO even though absorption spectrum of astaxanthin monomer in DMSO is red-shifted by nearly 30 nm. The same is observed for J-aggregates; the 0-0 band was reported at 560 nm [P2.20] and 562 nm [P2.21] in hydrated acetone, and around 570 nm in hydrated methanol [P2.22] and DMSO (Figure 3.2.1). The absence of solvent polarizability-related red-shift in aggregates is caused by the size of the aggregates; the aggregates are large, thus majority of molecules is buried inside the aggregate thus it is not exposed to solvent, resulting in observed absence of the solvent-dependent shift of absorption spectrum.

The magnitude of the aggregation-induced shift of absorption maximum is directly related to the strength of the excitonic interaction between molecules forming the aggregate [P2.9], [P2.23], [P2.26]. For the H1 aggregate the displacement is extremely large, but we have to take into account the dispersion interaction that is diminished in 10/90 DMSO/water mixture. Thus, to estimate the strength of the interaction, we make use of results reported for hydrophilic analogue of astaxanthin, astalysine, which remains monomeric even in water and has absorption maximum in water at 480 nm (~20800 cm^{-1}) [P2.6]. Then, the magnitude of the aggregation-induced shift in the H1 aggregate is estimated to ~5000 cm^{-1}. It must be noted, however, that the displacement should be calculated from the 0-0 transition of the monomer [P2.8]. Absorption spectrum of astaxanthin does not exhibit vibrational structure in any solvent [P2.20], [P2.22], [P2.25], [P2.27], but it is known that essentially all carotenoids have the absorption maximum at the 0-1 vibrational band [P2.28]. The energy of the 0-0 band of astaxanthin monomer therefore should be approximately 1300 cm^{-1} below the absorption maximum [P2.4]. Taking this into account, we obtain the displacement >6000 cm^{-1}, which is comparable only to H-aggregate of the linear carotenoid lycopene [P2.29]. Values reported for strongly-interacting H-aggregates of other carotenoids are usually in the 4000-5000 cm^{-1} range [P2.7]-[P2.11].

For the H2 aggregate the same analysis yields shift of the absorption maximum of ~2500 cm^{-1}, indicating different organization of the molecules within the H2 aggregate. Based on our recent theoretical analysis [P2.23], H2 aggregate is likely much smaller than the strongly-interacting H1 aggregate. J-aggregate of astaxanthin peaks at 570 nm, which is ~2200 cm^{-1} below the absorption maximum (the 0-1 vibrational band) of astaxanthin monomer in DMSO. Since J-aggregate occurs at 50/50 DMSO/water ratio, the influence of dispersion interactions may be slightly different than for H-aggregates, but since J-aggregates form very large assemblies [P2.8] only negligible fraction of molecules may interact with DMSO. Thus, if we use the position of the 0-0 band of the S_0-S_2 transition of the hydrophilic astaxanthin (astalysine) in water, we obtain an upper limit of the shift of the absorption spectrum, ~2000 cm^{-1}.

The shape of absorption spectrum of the J-aggregate helps to understand the organization of the molecules within the aggregate. It was recently demonstrated that most of the absorption spectra of carotenoid aggregates can be explained in terms of H-type interaction (with positive excitonic coupling, J). While the blue-shifted absorption spectrum is due to strongly-interacting card-pack assemblies, weakly-

interacting H-aggregates assembled into helical structures give a red-shifted absorption spectrum [P2.9]. For these helical structures, however, the lowest energy band is always weaker than the absorption maximum [P2.9]. Here, the lowest energy band is the strongest (Figure 3.2.1), suggesting the astaxanthin forms a 'true' J-aggregate characterized by head-to-tail organization with $J < 0$ [P2.9], [P2.23].

It is interesting to discuss the role of the primary solvent, because the situation when the 0-0 band of the J-aggregate is the strongest occurs only for astaxanthin in hydrated DMSO presented here. Previous reports discussing astaxanthin aggregates in hydrated methanol [P2.22] or acetone [P2.20], [P2.21] always have the 0-0 band weaker than the absorption maximum. This underscores the role of the primary solvent in formation of carotenoid aggregates. Solvent dependence is observed also for H-aggregates. Absorption maximum of astaxanthin H-aggregates prepared in hydrated acetone varies from 405 nm [P2.20] to 450 nm [P2.21], indicating that acetone facilitates formation of the H2 aggregates while the strongly-interacting H1 aggregates of astaxanthin are preferentially generated in polar solvents such as methanol or DMSO.

Excited-state dynamics

Transient absorption spectrum of monomeric astaxanthin in DMSO measured at 2 ps after excitation of the S_2 state at 495 nm is shown in Figure 3.2.2a. It has the typical S_1-S_n band that in DMSO peaks at 640 nm. Global fitting reveals that the spectrum associated with the S_1 state (green EADS in Figure 3.2.3a) decays with a time constant of 5.3 ps, in agreement with the astaxanthin S_1 lifetimes reported in other organic solvents that vary from 4.3 to 5.6 ps [P2.25], [P2.27], [P2.30]. The two faster processes, associated with depopulation of the initially excited S_2 state (140 fs, black EADS in Figure 3.2.3a) and vibrational relaxation in the S_1 state (340 fs, red EADS in Figure 3.2.3a), also concur with those reported earlier. It must be noted, however, that although the 340 fs process has in the 550-750 nm region typical features associated with vibrational relaxation, it also exhibits a rise in the bleaching region, which is inconsistent with this assignment. The origin of the rise could be due for example to excited-state absorption band overlapping with bleaching, but the precise origin remains unknown. Similar component was found also for astaxanthin in CS_2 [P2.25].
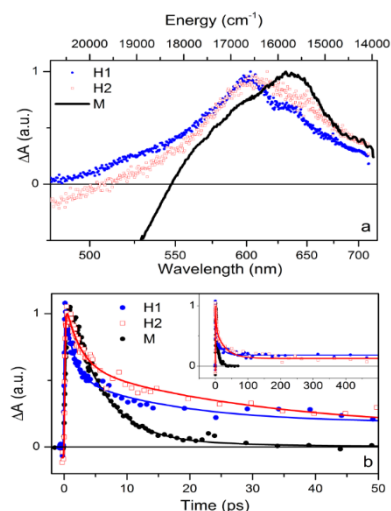
Figure 3.2.2 (a) Transient absorption spectra measured at 2 ps after excitation, and (b) kinetics measured at maxima of the S_1-S_n bands for astaxanthin monomer (M, black line) and H1 (full symbols) and H2 (open symbols) aggregates. Excitation wavelengths were 390 nm (H1), 458 nm (H2) and 495 nm (M). All data are normalized to maximum. Solid lines in (b) are fits obtained from global fitting.
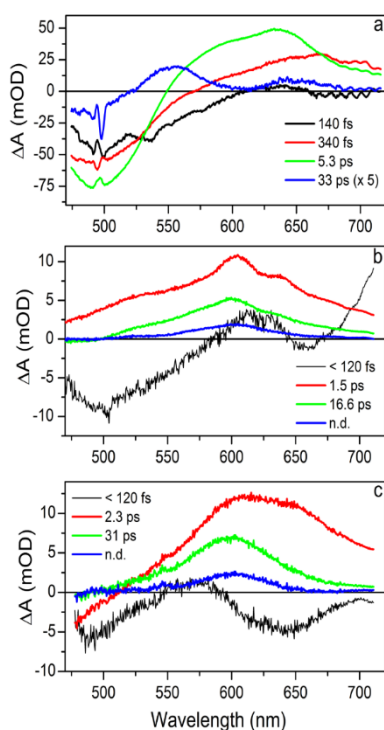
Figure 3.2.3 EADS obtained from global fitting the transient absorption data measured for astaxanthin monomer (a), H1 (b), and H2 (c) aggregates. Note that the 33 ps EADS of monomeric astaxanthin is multiplied by 5 to allow comparison with other spectra.

The global fitting also revealed an additional, weak component characterized by a time constant of 33 ps (blue EADS in Figure 3.2.3a) that is reminiscent of the S* signal observed for other carotenoids [P2.5], [P2.31]-[P2.34]. The component is weak, but normalized kinetics measured at the S_1-S_n and S* maxima clearly reveal the presence of a slow decay in the S* region (Supporting Information). It should be noted that this component was not observed for astaxanthin in CS_2, methanol or acetonitrile [P2.25], but it was identified for the hydrophilic analogue of astaxanthin, astalysine, in both 2-propanol and water [P2.6]. Yet, in these two solvents, the lifetime of the S* signal is about 7 ps, thus significantly faster than 33 ps observed here. If the S* signal is due to a twisted S_1 conformation as proposed earlier [P2.34], the long S* lifetime observed here may be related to high viscosity of DMSO. The S* decay corresponds to

relaxation back to the ground state while restoring the original, non-twisted conformation, a process that should be longer in a high viscosity solvent.

Figure 3.2.2a also shows transient absorption spectra of H1 and H2 aggregates taken at 2 ps after excitation at 397 nm (H1) and 458 nm (H2). Both spectra differ markedly from that of astaxanthin monomer. The S_1-S_n maximum is at 600 nm for both H1 and H2 aggregates, but both H1 and H2 aggregates lack the negative signal above 500 nm. This indicates that no monomers are excited at the selected excitation wavelengths, because any excited monomer would exhibit a strong bleaching signal around 500 nm (see the magnitude of bleaching for monomer in Figure 3.2.2a). This is especially important for the H2 aggregate, because it shows that the sample contains only a negligible fraction of monomers as these would be excited at 458 nm. On the other hand, absence of any negative signal in H2 aggregate indicates that the sample is highly inhomogeneous; the molecules absorbing above 500 nm are not excited at 458 nm, which means that the bandwidth of H2 absorption spectrum is not due to vibrational bands associated with the same molecule but it is rather in homogeneously broadened due to a distribution of aggregates of different sizes.

Comparison of transient absorption spectra of H1 and H2 aggregates also demonstrates that although steady-state absorption spectra of these two aggregates are markedly different, only a small difference occurs in transient absorption spectra. This is because the transient absorption spectrum monitors the S_1 state, which has negligible dipole moment and is therefore only marginally affected by excitonic interaction. The shift of the H-aggregate transient absorption spectrum in respect to that of monomer is caused mainly by the aggregation-induced changes of the final S_n state [P2.11].

The aggregation however affects the S_1 lifetime (Figure 3.2.2b). Both H1 and H2 aggregates exhibit multiexponential S_1 decay reported also for aggregated zeaxanthin [P2.11], [P2.12] and 8'-apo-β-carotenal [P2.14]. In astaxanthin, the fast component associated with annihilation [P2.11] yields 1.5 ps for H1 and 2.3 ps for H2 (Figure 3.2.3). The slightly shorter lifetime in H1 reflects tighter packing of molecules within H1 aggregate. Global fitting reveals that EADS associated with the 1.5 and 2.3 ps components are broad and relax to narrower spectra associated with the relaxed S_1 state (Figure 3.2.3).The EADS of the relaxed S_1 state peaks at 600 nm and has a lifetime of 30 ps for H2 and 17 ps for H1. The prolongation of the S_1 lifetime in aggregate is likely related to a change in S_1-S_0 coupling via the C=C stretching mode

that is known to facilitate the S_1-S_0 internal conversion [P2.35]. Recent picosecond Raman experiments on zeaxanthin revealed that the up-shifted frequency of the C=C stretching mode in the S_1 state, which is characteristic of monomeric carotenoids [P2.35], is nearly absent in aggregates. This change is likely the reason for the longer S_1 lifetime of the aggregate.

Moreover, in contrast to monomer, in both H1 and H2 aggregates the S_1 relaxation produces a signal that does not decay on the time scale of our experiment
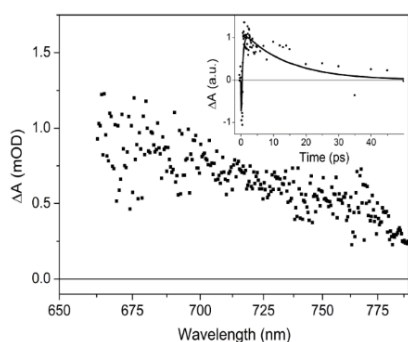
Figure 3.2.4 Transient absorption spectra of J-aggregate measured at 2 ps after excitation at 600 nm. Inset shows data (symbols) and fit (solid line) for kinetic measured at 680 nm.

(Figure 3.2.3 and inset of Figure 3.2.2). The residual spectrum has maximum at 600 nm that is close to the triplet band of astaxanthin [P2.36]. Thus, we assign the residual spectrum to the astaxanthin triplet that was generated exclusively in astaxanthin aggregates. Tight packing of molecules within the aggregate promotes the singlet homofission between the neighboring molecules. Our data does not allow identifying the parent state for the singlet homofission. A possible candidate is the S_1 state that has significant doubly-excited character and can be viewed as two coupled triplet states delocalized over the π-conjugation resulting in a singlet state [P2.37]. Then, the S_1 state can break down to two triplets localized at individual molecules in the aggregate [P2.15]. But since the carotenoid S_2 state was also proposed to be the parent state [P2.12], [P2.38], we cannot reliably determine the parent state for singlet homofission in astaxanthin aggregates.

Contrary to H1 and H2 aggregates, transient absorption spectra of J-aggregate are complicated to measure due to scattering caused by the size of J-aggregates. Also, J-aggregates usually have low stability [P2.11], [P2.12] thus only a few traces could be measured resulting in poor S/N ratio. The long-wavelength part of transient absorption spectrum of the J-aggregate excited at 600 nm is depicted in Figure 3.2.4. It shows that signal associated with the S_1-S_n transition is rather featureless and extends up to 800 nm. The S_1 lifetime is 14 ps (Figure 3.2.4, inset), thus shorter than for H aggregates, again underscoring the effect of intermolecular interaction on lifetime of the carotenoids in aggregate. The S_1 lifetimes of J-aggregates are always longer than the corresponding monomeric S_1 lifetimes: 14 ps in J-aggregate vs. 5 ps

in monomer in astaxanthin, 30 ps vs. 9 ps in zeaxanthin [P2.11], and 40 ps vs. 25 ps in 8'-apo-β-carotenal [P2.14], though it must be noted that for 8'-apo-β-carotenal the monomeric S_1 lifetime depends on solvent polarity [P2.14]. Also, the long S_1 lifetime was not observed in the weakly-interacting J1 aggregate of zeaxanthin [P2.12].

3.2.5   Acknowledgments

3.2.6   References

[P2.1]   G. D. Scholes, G. R. Fleming, A. Olaya-Castro, R. van Grondelle, Nature Chemistry 3 (2011) 764.

[P2.2]   T. Polívka, H. A. Frank, Acc. Chem. Res. 43 (2010) 1125.

[P2.3]   R. Edge, D. J McGarvey, T. G. Truscott, J. Photochem. Photobiol. B 41 (1997) 189.

[P2.4]   T. Polívka, V. Sundström, Chem. Rev. 104 (2004) 2021.

[P2.5]   T. Polívka, V. Sundström, Chem. Phys. Lett. 477 (2009) 1.

[P2.6]   P. Chábera, M. Fuciman, K.R.Naqvi, T. Polívka, Chem. Phys. 373 (2010) 56.

[P2.7]   M. Simonyi, Z. Bikadi, F. Zsila, J. Deli, Chirality 15 (2003) 680.

[P2.8]   C. Wang, C. J. Berg, C. C. Hsu, B. A. Merrill, M. J. Tauber, J. Phys. Chem. B 116 (2012) 10617.

[P2.9]   F. C. Spano, J. Am. Chem. Soc. 131 (2009) 4267.

[P2.10] C. Wang, M. J. Tauber, J. Am. Chem. Soc. 132 (2010) 13988.

[P2.11] H. H. Billsten, V. Sundström, T. Polívka, J. Phys. Chem. A 109 (2005) 1521.

[P2.12] C. Wang, M. Angelella, C. H. Kuo, M. J. Tauber, Proc. of SPIE, 8459 (2012) 845905.

[P2.13] C. Wang, D. E. Schlamadinger, V. Desai, M. J. Tauber, Chem. Phys. Chem. 12 (2011) 2891.

[P2.14] M. Durchan, M. Fuciman, V. Šlouf, G. Kesan, T. Polívka, J. Phys. Chem. A, in press. DOI: 10.1021/jp310140k.

[P2.15] M. B. Smith, J. Michl, Chem. Rev. 110 (2010) 6891.

[P2.16] M. Cianci, P. J. Rizkallah, A. Olczak, J. Raftery, N. E. Chayen, P. F. Zagalsky, J. R. Helliwell, Proc. Natl. Acad. Sci. U.S.A. 99 (2002) 9795.

[P2.17] K. J. McGraw, In: Bird coloration, Vol.1, p. 177. Harvard University Press, 2006.

[P2.18] A. A. C. van Wijk, A. Spaans, N. Uzunbajakava, C. Otto, H. J. M. de Groot, J. Lugtenburg, F. Buda, J. Am. Chem. Soc. 127 (2005) 1438.

[P2.19] M. Buchwald, W. P. Jencks, Biochemistry 7 (1968) 834.

[P2.20] Y. Mori, K. Yamano, H. Hashimoto, Chem. Phys. Lett.254 (1996) 84.

[P2.21] C. Köpsel, H. Möltgen, H. Schuch, H. Auweter, K. Kleinermanns, H.-D. Martin, H. Bettermann, J. Mol. Struct. 750 (2005) 109.

[P2.22] R. Giovannetti, L. Alibabaei, F. Pucciarelli, Spectrochim. Acta A 73 (2009) 157.

[P2.23] J. Olšina, M. Durchan, B. Minofar, T. Polívka, T. Mančal, http://arxiv.org/abs/1208.4958.

[P2.24] I. H. M. van Stokkum, D. S. Larsen, R. van Grondelle, Biochim. Biophys. Acta 1657 (2004) 82.

[P2.25] R. P. Ilagan, R. L. Christensen, T. W. Chapp, G. N. Gibson, T. Pascher, T. Polívka, H. A. Frank, J. Phys. Chem. A 109 (2005) 3120.

[P2.26] H. van Amerongen, L. Valkunas, R. van Grondelle, Photosynthetic excitons, World Scientific, 2000.

[P2.27] N. Christensson, T. Polívka, A. Yartsev, T. Pullerits, Phys. Rev. B 79 (2009) 245118.

[P2.28] G. Britton, S. Liaaen-Jensen, H.P. Pfander, Carotenoids Handbook, Birkhäuser Basel, 2004.

[P2.29] L. X. Wang, Z. L. Du, R. X. Li, D. C. Wu, Dyes and Pigments, 65 (2005) 15.

[P2.30] M. Kopczynski, T. Lenzer, K. Oum, J. Seehusen, M. T. Seidel, V. G. Ushakov, Phys. Chem. Chem. Phys. 7 (2005) 2793.

[P2.31] C. C. Gradinaru, J. T. M. Kennis, E. Papagiannakis, I. H. M. van Stokkum, R. J. Cogdell, G. R. Fleming, R. A. Niederman, R. van Grondelle, Proc. Natl. Acad. Sci. U.S.A.98 (2001) 2364.

[P2.32] P. Chábera, M. Fuciman, P. Hříbek, T. Polívka, Phys. Chem. Chem. Phys. 11 (2009) 8795.

[P2.33] T. Lenzer, F. Ehlers, M. Scholz, R. Oswald, K. Oum, Phys. Chem. Chem. Phys. 12 (2010) 8832.

[P2.34] D. Niedzwiedzki, J. F. Koscielecki, H. Cong, J. O. Sullivan, G. N. Gibson, R. R. Birge, H. A. Frank, J. Phys. Chem. B 111 (2007) 5984.

[P2.35] H. Nagae, M. Kuki, J. P. Zhang, T. Sashima, Y. Mukai, Y. Koyama, J. Phys. Chem. A 104 (2000) 4155.

[P2.36] B. R. Nielsen, K. Jorgensen, L. H. Skibsted, J. Photochem. Photobiol. A 112 (1998) 127.

[P2.37] P. Tavan, K. Schulten, Phys. Rev. B 36 (1987) 4337.

[P2.38] E. Jailaubekov, M. Vengris, S.H. Song, T. Kusumoto, H. Hashimoto, D.S. Larsen, J. Phys. Chem. A 115 (2011) 3905–3916.

3.2.7 Supporting information
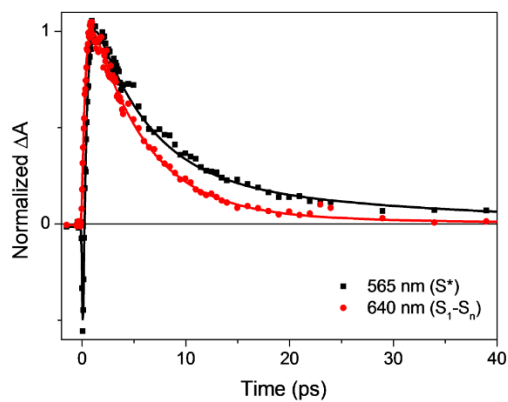
Figure 3.2.5 Kinetics measured at maximum of the S_1-S_n band at 640 nm and at the maximum of the S* signal at 565 nm. The kinetic taken at the S* signal exhibits an additional slower component (33 ps). The sharp negative signal observed in the 565 nm kinetic is due to stimulated emission from the S_2 state.

3.3 PAPER 3

Tuning the Spectroscopic Properties of Aryl Carotenoids by Slight Changes in Structure

Marcel Fuciman, **Gürkan Keşan**, Amy M. LaFountain, Harry A. Frank, Tomáš Polívka,

3.3.1 Abstract

Two carotenoids with aryl rings were studied by femtosecond transient absorption spectroscopy and theoretical computational methods, and the results were compared with those obtained from their non-aryl counterpart, β-carotene. Although isorenieratene has more conjugated C=C bonds than β-carotene, its effective conjugation length, N_{eff}, is shorter than of β-carotene. This is evidenced by a longer S_1 lifetime and higher S_1 energy of isorenieratene compared to the values for β-carotene. On the other hand, although isorenieratene and renierapurpurin have the same π-electron conjugated chain structure, N_{eff} is different for these two carotenoids. The S_1 lifetime of renierapurpurin is shorter than that of isorenieratene, indicating a longer N_{eff} for renierapurpurin. This conclusion is also consistent with a lower S_1 energy of renierapurpurin compared to the other carotenoids. Density functional theory (DFT) was used to calculate equilibrium geometries of ground and excited states of all studied carotenoids. The terminal ring torsion in the ground state of isorenieratene (41°) is very close to that of β-carotene (45°), but equilibration of the bond lengths within the aryl rings indicates that each aryl ring forms its own conjugated system. This results in partial detachment of the aryl rings from the overall conjugation making N_{eff} of isorenieratene shorter than that of β-carotene. The different position of the methyl group at the aryl ring of renierapurpurin diminishes the aryl ring torsion to ~20°. This planarization results in a longer N_{eff} than that of isorenieratene, rationalizing the observed differences in spectroscopic properties.
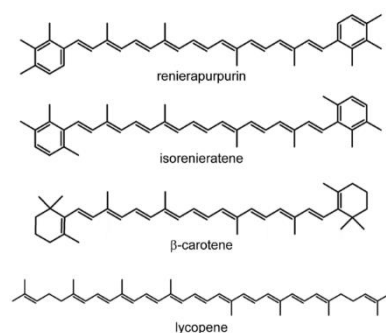
3.3.2 Introduction

The excited states of carotenoids have exceedingly complex excited-state dynamics, the elucidation of which is key to understanding the various functions the molecules perform in many biological systems. These functions include light-harvesting, [P3.1]-[P3.3] photoprotection [P3.2]-[P3.4], scavenging deleterious active oxygenic radicals [P3.5] and providing coloration in plants and animals [P3.6].

Many of the spectroscopic properties of carotenoids can be explained using a three-state model consisting of the ground state (S_0), and two excited states denoted S_1 and S_2. It is now well established that the $S_0 \rightarrow S_1$ transition is forbidden for carotenoids because the S_0 and S_1 states have the same symmetry in the idealized C_{2h} point group [P3.7], [P3.8]. The characteristic visible coloration of carotenoids is due the $S_0 \rightarrow S_2$ transition that gives rise to strong absorption in the blue-green spectral region. Thus, excitation of a carotenoid into the S_2 state results in fast (<200 fs) internal

conversion to the S_1 state whose lifetime is between a few picoseconds and hundreds of picoseconds depending on the molecule [P3.8]. Although these two excited states provide a framework from which to explain the basic photophysics of carotenoids, there is significant evidence that other 'dark' states may exist in the vicinity of the S_1 and S_2 states that may affect the network of relaxation pathways in the molecules [P3.9]-[P3.12].

The excited state energies and lifetimes of carotenoids are determined primarily by the number of conjugated C=C bonds (N). The dependence of these factors on N is straightforward for linear carotenoids such as neurosporene (N=9), spheroidene (N=10) and lycopene (N=11, Figure 3.3.1) whose conjugated backbone consists of a linear chain of π-electron conjugated C=C bonds. For this type of carotenoid, knowledge of the S_1 and S_2 excited state energies, and the S_1 lifetime of an arbitrary linear carotenoid in a specific solvent, allows a reasonably good prediction of these values for another member of this group. However, such a prediction is not possible for the S_2 lifetime because it has a complicated dependence on N possibly due to the presence of other dark state(s) in the vicinity of S_1 and S_2 that may affect the mechanism of S_2 depopulation [P3.13].

A large number of important naturally-occurring carotenoids do not have linear conjugated chains. For example, β-carotene (Figure 3.3.1) has π-electron conjugation that extends into two terminal β-rings, and this affects the spectroscopic properties of the molecule. A comparison of β-carotene and lycopene, which both have N=11, [P3.14] shows that β-carotene, which has terminal rings, behaves as if its conjugation length were shorter than that of lycopene, which is an open-chain carotenoid (Figure 3.3.1): The S_2 state of β-carotene is higher, and its S_1 lifetime is longer than that of lycopene. However, a systematic

Figure 3.3.1 Structures of the carotenoids used in this study. Renierapurpurin has two χ-rings, isorenieratene has two φ-rings, and β-carotene has two β-rings.

analysis of the behavior of linear conjugated carotenoids and polyenes led to the empirical observation that the S_1 lifetime, S_2 energy and the Raman frequency of the C=C stretch in the ground state, have a well-defined dependence on $1/N$ [P3.15]-[P3.20]. Therefore, knowing the value of one of these parameters for *any* carotenoid, and

comparing the value to that of a linear carotenoid, allows one to obtain an effective value of N, denoted N_{eff}, which can even be a non-integer number for that specific carotenoid [P3.18]-[P3.21]. The notion of effective conjugation length can also be extended to carotenoids having one or more conjugated keto (C=O) groups, although due to the complex effect of polar solvents on the dynamics and spectroscopic properties of this type of carotenoid, a meaningful comparison of this type is possible only for the molecules dissolved in non-polar solvents [P3.21], [P3.22].

Substantial theoretical and experimental investigations have described the properties of linear carotenoids [P3.8], [P3.10], [P3.15], [P3.17], those having terminal β-rings (such as β-carotene or zeaxanthin) [P3.12]-[P3.14], [P3.23], and carotenoids with conjugated C=O groups [P3.21], [P3.25]. However, much less is known about excited state properties of aryl carotenoids which contain one or two aromatic rings, denoted φ- or χ- depending on the positions of attached methyl groups (Figure 3.3.1). These substituents add further C=C bonds to the conjugated backbone. Aryl carotenoids are important constituents of light-harvesting systems of green sulfur bacteria, chlorosomes [P3.26] and synthetic analogues have been used in artificial antenna systems [P3.27], [P3.28]. Previous studies suggested that the aryl carotenoids, isorenieratene (Figure 3.3.1) and dihydroxyisorenieratene both of which have two φ- rings, exhibit spectroscopic properties comparable to those of β-carotene which has two β-rings, even though both isorenieratene and dihydroxyisorenieratene have four additional conjugated C=C bonds compared to β-carotene [P3.29], [P3.30]. This suggestion was confirmed by a study that compared the aryl carotenoids chlorobactene (one φ- ring), β-isorenieratene (one φ-ring and one β-ring) and isorenieratene (two φ-rings, Figure 3.3.1) with their non-aryl counterparts, β-carotene (one β-ring) and β-carotene (two β-rings) [P3.31]. The results showed that isorenieratene has a nearly identical absorption spectrum to β-carotene, but the S_1 lifetime of isorenieratene was found to be 12 ps, which is longer than the ~9 ps value reported for β-carotene. This suggests, counterintuitively, that N_{eff} for isorenieratene is shorter than for β-carotene [P3.31]. The same trend was observed comparing β-carotene, which has one β-ring, to chlorobactene which has two additional C=C bonds in one aryl φ-ring. Despite this, chlorobactene has a longer S_1 lifetime than γ-carotene. This effect is unique. There are number of cases for which adding a C=C bond to the conjugated system increases N_{eff} by a positive value less than one; e.g. in comparing the spectroscopic properties of β-carotene with those of lutein which has one β- and one ε-ring [P3.32]. Only for aryl carotenoids does the addition of C=C bonds to the conjugated system *decrease N_{eff}*.

The origin of this effect has been hypothesized to be due to torsion of the aryl ring that would effectively isolate it from the linear portion of the π-electron conjugated chain resulting in the overall conjugation length becoming shorter [P3.31]. To test this hypothesis, the present work compares the photophysical properties of two aryl carotenoids, isorenieratene and renierapurpurin, to those of β-carotene (Figure 3.3.1). Isorenieratene is an important constituent of the chlorosomes of green sulfur bacteria and renierapurpurin is a rare carotenoid that can be isolated from the sea sponge, *Reniera japonica* [P3.33]. Renierapurpurin is also found in certain cyanobacteria where it is an intermediate in the biosynthetic pathway that converts β-carotene to synechoxanthin [P3.34]. Although isorenieratene and renierapurpurin have identical π-electron conjugated systems, they differ in the position of methyl groups on the aryl rings (Figure 3.3.1). It is shown here that this difference in methyl group position affects the torsional angle of the aryl ring with respect to the plane of the central linear conjugated chain. Thus, a comparison of isorenieratene and renierapurpurin elucidates the role of the torsional angle of the terminal ring on the spectroscopic properties and excited state dynamics of carotenoids.

3.3.3   Materials and Methods

Sample preparation

Renierapurpurin was isolated from cells of *Synechococcus* sp. strain PCC 7002 (cruH mutant) which were obtained as a gift from Prof. Donald Bryant and Dr. Gaozhong Shen. Whole cells were ruptured by passage through a French press (SLM Aminco) at 1000 psi. Alternatively, a probe-type sonicator may be used [P3.34]. The sample was then centrifuged for 5 min at 3000 x g and 4ºC in a Sorvall RC-5B centrifuge in order to remove cellular debris. Pigments were extracted by the addition of an equal amount of 7:2 (v/v) acetone and methanol to the supernatant from the centrifugation, followed by partitioning using an equal amount of methyl tert-butyl ether (MTBE). The pigment contained in the MTBE solution was then dried under nitrogen gas, redissolved in methanol/acetonitrile/water (21:16.5:62.5 v/v/v), and filtered using a Millex 0.2 μm syringe driven filter. The sample was then injected into a Waters 600 HPLC system equipped with a Waters NovaPak C18 column (4μm, 3.9 mm x 300 mm) and purified using the mobile phase protocol described by Graham and Bryant [P3.34]. β-carotene and lycopene were purchased from Carotenature; isorenieratene was isolated and purified as described in [P3.31]. Prior to the experiments, all carotenoids were re-purified by HPLC and then dissolved in hexane, cyclohexane or benzene (all

solvents from Sigma Aldrich, Spectroscopic grade) to obtain a solution having an optical density between 0.4 and 0.5 at the laser excitation wavelength in a 2 mm cuvette.

Spectroscopy

All of the spectroscopy was performed on samples at room temperature. Steady-state absorption spectroscopy was carried out using a Varian Cary 50 UV-visible spectrophotometer. Femtosecond transient pump-probe absorption experiments were done using a Helios transient absorption spectrometer (Ultrafast Systems, LCC), coupled to a femtosecond laser system described in detail previously.[35] The system is based on a Ti:sapphire amplifier with pulse stretcher and compressor (Spitfire-50 fs, Spectra-Physics) pumped at a 1 kHz repetition rate by an Q-switched Nd:YLF laser (Evolution 15, Coherent), and seeded by pulses from a mode-locked Ti:sapphire oscillator (Tsunami, Spectra-Physics) pumped by a diode-pumped $Nd:YVO_4$ CW visible laser (Millenia V, Spectra Physics). Output pulses with a central wavelength of 800 nm, energy of 600 µJ/pulse, ~50 fs duration, and a 1 kHz repetition rate were split into two beams by a beamsplitter. Ninety per cent of the signal was sent to optical parametric amplifier (OPA-800C, Spectra-Physics) to generate the pump beam. The remaining 10% was used for generation of probe pulses. A white light continuum probe spanning 450 – 800 nm in, and slightly beyond, the visible region, and 850 – 1450 nm in the near infra-red (NIR) region was generated by a 3 mm sapphire (YAP) plate. A charge-coupled detector with a 2048-pixel array (S2000, Ocean Optics) was used as a detector in the visible range. In the NIR, a 512 InGaAs pixel array (SU-LDV, Sensors Unlimited) was used. The pump and probe beams were overlapped at the sample at the magic-angle (54.7°) polarization. The signals were averaged over 5 seconds. The samples were excited by the pump beam tuned between 490 and 520 nm which excited the 0-0 band of the S_2 state of the carotenoid. The energy of the pump beam was 1 µJ/pulse in a spot size of 1 mm diameter. This corresponds to an intensity of $~3.0 \times 10^{14}$ photons/cm^{2}pulse. The samples were mixed continuously using a magnetic micro-stirrer to prevent photo-degradation. The integrity of the samples was checked by taking steady-state absorption spectra before and after every experiment.

Calculations

The geometries of the electronic ground states of β-carotene, isorenieratene and renierapurpurin were optimized with standard ground-state density functional theory (DFT) [P3.36] using the Becke3-Lee-Yang-Parr (B3LYP) [P3.37] and Becke-Lee-Yang-Parr (BLYP) [P3.38], [P3.39] exchange-correlation functional in combination with the triple-ζ-quality (TZVP) basis set [P3.40]. This basis set has polarization function and is thus larger than the commonly used 6-31g(d) basis set, making it more suitable for calculations of structure geometry. The equilibrium geometries of the excited states were determined by means of time-dependent density functional theory within the Tamm-Dancoff approximation (TD-DFT/TDA) [P3.41] using the BLYP and hybrid exchange–correlation functional (Cam-B3LYP) [P3.42] with the TZVP basis set. After the optimization for both the ground state and excited states, vibrational frequencies were calculated in order to confirm the convergence minima on the potential energy surface. No imaginary frequencies were observed. In contrast to Cam-B3LYP, BLYP functional provides the correct energy ordering for the two lowest excited states of carotenoids [P3.43], [P3.44]. Thus, this level of theory has been chosen as the standard for both ground state and relaxed excited state geometries. All calculations were carried out using a gas phase approximation, and very loose symmetry constraints were used to maintain C_i symmetry. All calculations were performed with Gaussian09 package [P3.45], while Gauss View 5.0.8 [P3.46] was used for visualization of the structures.

3.3.4 Results

Absorption spectra of lycopene, isorenieratene, renierapurpurin and β-carotene in *n*-hexane are shown in Figure 3.3.2. All of the spectra exhibit typical $S_0 \rightarrow S_2$ absorption lineshapes for carotenoids with the max of the transition corresponding to the 0-1 vibronic band. For β-carotene, isorenieratene and renierapurpurin, which have π-electron conjugation extended into terminal aryl rings, the vibrational structure is less resolved than for the linear carotenoid, lycopene (Figure 3.3.2a). It is clear from a comparison of the absorption spectra of β-carotene, isorenieratene and renierapurpurin that the resolution of the vibronic bands is essentially independent of the type of terminal ring. The 0-0 band is readily identified for the carotenoids and the position of the 0-0 band allows categorization of the molecules into two groups. The first group consists of β-carotene and isorenieratene which despite having different terminal rings (β and φ, respectively) and
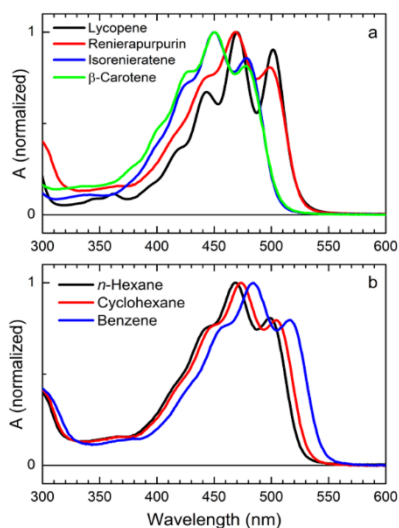
Figure 3.3.2 (a) Absorption spectra of lycopene, renierapurpurin, isorenieratene and β-carotene in *n*-hexane. (b) Solvent dependence of the absorption spectrum of renierapurpurin.

consequently, a different number of conjugated C=C bonds, their absorption spectra are nearly identical (Figure 3.3.2a) with the 0-0 band of the $S_0 \rightarrow S_2$ transition at 20,830 cm^{-1} (480 nm). The second group contains renierapurpurin and lycopene. Renierapurpurin, with its aromatic χ-rings, has the same number of conjugated C=C bonds as isorenieratene (Figure 3.3.1), but has a 0-0 band significantly red-shifted to 19,920 cm^{-1} (502 nm) which is the same as that of lycopene, a linear carotenoid having *N*=11. The absorption spectra of the carotenoids were also recorded in cyclohexane and benzene. The solvent dependence of the absorption spectrum of renierapurpurin is shown in Figure 3.3.2b. Except for a shift due to the different polarizability of the solvents, no changes in the spectral profile of the $S_0 \rightarrow S_2$ transition were detected. This is in agreement with results obtained previously for β-carotene and isorenieratene [P3.31]. The energies of the 0-0 bands of the absorption spectra of the carotenoids dissolved in *n*-hexane, benzene and cyclohexane are summarized in Table 3.3.1.

Time-resolved transient absorption measurements were carried out in both the visible (440-740 nm) and NIR (880-1410 nm) spectral regions to examine the excited state dynamics of the molecules. Whereas the visible spectral region covers the ground state bleaching and characteristic $S_1 \rightarrow S_n$ excited-state absorption of carotenoids [P3.8], the spectral region above 1000 nm captures the $S_1 \rightarrow S_2$ transition that allows a determination of the S_1 energy of carotenoids [P3.47].

Table 3.3.1 Energies of the S_2 and S_1 states, $S_1 \rightarrow S_n$ transient absorption maxima and bandwidths (fwhm), and S_1 state lifetimes (τ_{S1}).[a] The linear π-electron chain length and the number and type of terminal rings is given in parentheses under the carotenoid name.

Carotenoids	solvent	S_0-S_2 (0-0)		S_1	S_1-S_n max	S_1-S_n fwhm	τ_{S1}
		nm	cm^{-1}	cm^{-1}	nm	cm^{-1}	ps
renierapurpurin	*n*-hexane	502	19 930	13190	581	800	6.7
(9+2χ)	benzene	520	19 240	13060	603	880	7.0
	cyclohexane	508	19 700	13180	587	780	6.4
isorenieratene	*n*-hexane	480	20 850	14030	559	1550	12.0
(9+2φ)	benzene	494	20 220	14000	579	1640	13.5
	cyclohexane	485	20 850	13990	567	1610	13.0
β-carotene	*n*-hexane	479	20 870	n.m.	551[b]	1280[b]	8.2[b]
(9+2β)	benzene	495	20 210	n.m.	564[b]	1530[b]	9.4[b]
	cyclohexane	485	20 610	13700	561	1320	9.3
lycopene	*n*-hexane	502	19 930	12540	557	590	4.0
(11)	benzene	519	19 250	12400	578	680	4.5
	cyclohexane	508	19 690	12460	564	570	4.0

a) n.m.- not measured
b) data from Ref. 31

Transient absorption spectra in the visible spectral region recorded at 2 ps after excitation into the 0-0 band of the $S_0 \rightarrow S_2$ transition for all carotenoids in *n*-hexane are shown in Figure 3.3.3a. At this time delay, the relaxation processes associated with S_2-S_1 internal conversion (100-200 fs) [P3.48] and vibrational cooling in the S_1 state (300-800 fs) [P3.14], [P3.17], [P3.49] are mostly finished. Therefore, the transient absorption spectra are dominated by an $S_1 \rightarrow S_n$ transition from the relaxed S_1 state.

The transient absorption data reveal that the energies of the $S_1 \rightarrow S_n$ transitions do not follow the same trend as the $S_0 \rightarrow S_2$ transitions. The transient absorption lineshapes of β-carotene and isorenieratene are similar, but the $S_1 \rightarrow S_n$ transition maximum of isorenieratene (559 nm) is red-shifted compared to that of β-carotene (551 nm). This stands in contrast to the essentially identical energies of their $S_0 \rightarrow S_2$ transitions (Figure 3.3.2 and Table 3.3.1). Also, the $S_1 \rightarrow S_n$ band of lycopene at 557 nm is close to that of β-carotene and isorenieratene, in striking contrast to the energy of its $S_0 \rightarrow S_2$ transition, which is >20 nm red-shifted from that of these two other molecules (Table 3.3.1). The $S_1 \rightarrow S_n$ band of renierapurpurin is significantly red-shifted compared to the three other carotenoids, and peaks at 581 nm. Note that in the ground state bleaching region between 450 and 525 nm, the lowest energy band of lycopene at ~500 nm matches that of renierapurpurin, whereas the $S_1 \rightarrow S_n$ maxima

of these two carotenoids are markedly different. This further confirms the distinct behavior of the $S_0 \rightarrow S_2$ and $S_1 \rightarrow S_n$ transitions of lycopene and renierapurpurin.

The bandwidth of the $S_1 \rightarrow S_n$ transition provides information about conformational disorder of carotenoids in the S_1 state. It is well-known that extension of the π-electron conjugation into the terminal rings broadens the width of the $S_1 \rightarrow S_n$ transition compared to that seen for linear carotenoids [P3.8]. This effect is caused by the presence of an ensemble distribution of angles by which the terminal rings are twisted which then results in a distribution of effective conjugation lengths of the carotenoid. The magnitude of the twisting determines the extent to which the C=C bond(s) in the terminal ring contributes to the overall conjugation. The broader $S_1 \rightarrow S_n$ transition of isorenieratene (fwhm 1550 cm^{-1} in n-hexane) compared to β-carotene (1280 cm^{-1}) indicates a larger degree of conformational disorder induced by the φ-ring of isorenieratene. Yet, renierapurpurin whose χ-ring is very similar to the ϕ-ring of isorenieratene, has a markedly narrower $S_1 \rightarrow S_n$ band than isorenieratene, suggesting less conformational disorder in the S_1 state than for isorenieratene and β-carotene. In fact, the $S_1 \rightarrow S_n$ bandwidth of renierapurpurin (~800 cm^{-1}) is approaching that of the linear carotenoid, lycopene (590 cm^{-1}). The dependence of the bandwidth on carotenoid structure is independent of solvent (Table 3.3.1), although the bandwidths are broadest in benzene for all carotenoids.

Figure 3.3.3 Transient absorption data measured for the carotenoids in n-hexane. (a) Transient absorption spectra taken 2 ps (1.5 ps for lycopene) after excitation into the 0-0 band of the S_2 state. (b) Kinetic traces taken at the maxima of the S_1-S_n ESA bands. Solid lines represent the fits obtained from a global fitting analysis. Inset shows the rising part of the kinetics. All data are normalized to the maximum intensity. Excitation wavelengths were 500 nm (lycopene and renierapurpurin), 486 nm (isorenieratene), and 478 nm (β-carotene).

The properties of the S_1 state of the carotenoids are further revealed by comparing their S_1 lifetimes obtained from the kinetics recorded at the maxima of the
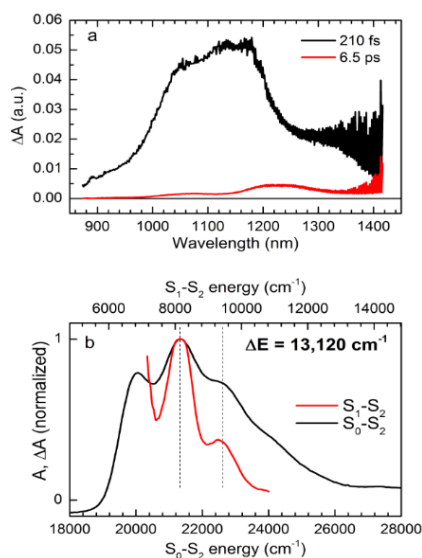
$S_1 \rightarrow S_n$ bands (Figure 3.3.3b). The S_1 lifetimes of β-carotene (~9 ps) and lycopene (~4 ps) have been measured a number of times in various solvents [P3.14], [P3.15], [P3.32]. The S_1 lifetime of the aryl carotenoid isorenieratene was measured previously to be ~12 ps [P3.29], [P3.31]. As mentioned above, this value is longer than that of β-carotene even though isorenieratene has four extra conjugated C=C bonds in its terminal rings compared to β-carotene. The S_1 lifetime of renierapurpurin was measured for the first time here, and was found to be 6.7 ps. The fact that it is significantly different from the other molecules further underscores the key role of the terminal rings in governing the excited-state dynamics of these carotenoids. Even though the ϕ-rings of isorenieratene and the χ-rings of renierapurpurin contain the same number of conjugated C=C bonds, the S_1 lifetime of these two carotenoids is markedly different.

Deeper insight into excited-state dynamics is provided by global analysis of the transient absorption data. For all datasets recorded in the visible region three decay components were required for a successful fit based on an irreversible sequential fitting model [P3.50]. The resulting Evolution Associated Difference Spectra (EADS) are depicted in Figure 3.3.4 for β-carotene, isorenieratene and renierapurpurin in *n*-hexane. For these three carotenoids, the overall pattern of excited-state dynamics is the same. The first EADS corresponds to the excited S_2 state which decays in 100-200 fs. While the S_2 lifetimes of β-carotene (125 fs) and isorenieratene (130 fs) correspond to the typical S_2 carotenoid lifetimes reported previously for these or similar carotenoids [P3.13], [P3.48], the S_2 lifetime of 200 fs for renierapurpurin is unusually long. Such a long S_2 lifetime has been reported only for shorter carotenoids such as neurosporene having N=9 [P3.13], [P3.17]. Therefore, the 200 fs S_2 lifetime of renierapurpurin which has 15 total conjugated C=C bonds is rather surprising. The second EADS also has a subpicosecond lifetime and a lineshape characteristic of a vibrationally hot, unrelaxed S_1 state [P3.14], [P3.17], [P3.49]. The values of 660 fs, 735 fs and 980 fs for β-carotene, renierapurpurin and isorenieratene, respectively are within the range of the values reported for a number of other carotenoids [P3.14], [P3.17], [P3.32], [P3.49]. The final EADS is due to the vibrationally relaxed S_1 state which decays back to the ground state with a time constant corresponding to the S_1 lifetime. The values are 8.2 ps for β-carotene, 12 ps for isorenieratene and 6.7 ps for renierapurpurin (Table 3.3.1). The global fitting analysis was also carried out on datasets recorded for the carotenoids dissolved in benzene and cyclohexane. All of the S_1 lifetime data are summarized in Table 3.3.1.
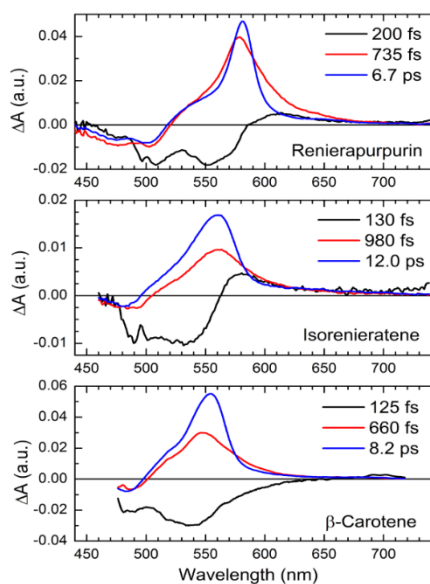
Figure 3.3.4 Global fitting results shown as EADS of renierapurpurin (top), isorenieratene (middle) and β-carotene (bottom) in *n*-hexane.

Figure 3.3.5 (a) EADS extracted from global fitting the NIR data of renierapurpurin dissolved in *n*-hexane. (b) The 6.5 ps EADS from panel *a* (red) shifted in energy to coincide with the steady-state absorption spectrum of renierapurpurin from Fig. 2 (black) plotted on a wavenumber scale. The magnitude of the shift in energy that brings the spectra into coincidence determined the S_1 energy of renierapurpurin is 13,120 cm^{-1}.

The transient absorption spectra were also measured in the NIR region where the $S_1 \rightarrow S_2$ transition of carotenoids can be detected [P3.47]. Data measured in the spectral region between 900 and 1400 nm were fitted globally to test whether the S_2 and S_1 lifetimes obtained from the NIR region match those extracted from the datasets recorded in the VIS range. EADS obtained from fits to the NIR spectra for renierapurpurin recorded in *n*-hexane are shown in Figure 3.3.5a. Two decay components were sufficient to fit the data. The initial EADS has a shape characteristic of an $S_2 \rightarrow S_N$ transition [P3.51] and has a lifetime of 210 fs which matches the 200 fs S_2 lifetime of renierapurpurin obtained from the global fit to the VIS dataset recorded in the same solvent (Figure 3.3.4). The second EADS has much weaker amplitude and a lifetime of 6.5 ps, which is also consistent with the 6.7 ps S_1 lifetime of renierapurpurin in *n*-hexane identified from the decay of the $S_1 \rightarrow S_n$ transition in the VIS region (Figure 3.3.4). Magnification of this EADS (Figure 3.3.5b) allows the assignment of two peaks at 8170 cm^{-1} (1224 nm) and 9400 cm^{-1} (1064 nm). The 1230

cm^{-1} energy separation between these two peaks indicates that they correspond to two vibrational bands of the S_2 state. Thus, the second EADS is assigned to the $S_1 \rightarrow S_2$ transition.

The energy of the S_1 state can be obtained by subtraction of the energy of the $S_1 \rightarrow S_2$ transition from that of the $S_0 \rightarrow S_2$ transition, but to do this properly the vibrational bands of the $S_1 \rightarrow S_2$ spectrum must be assigned correctly [P3.47], [P3.52], [P3.53]. The analysis is facilitated by simply shifting the transient $S_1 \rightarrow S_2$ spectrum on an energy scale until it comes into coincidence with the $S_0 \rightarrow S_2$ steady state absorption spectrum (Figure 3.3.5b). The energy shift required to align the two spectra will correspond to the S_1 energy. Aligning the NIR vibronic feature at 8170 cm^{-1} band with the 0-1 vibronic band of the steady-state $S_0 \rightarrow S_2$ absorption transition leads to an S_1 energy of $13,200 \pm 100$ cm^{-1} where the margin of error is determined by the uncertainty in the band positions. Alternatively, aligning the 8170 cm^{-1} feature with the 0-0 band of the steady-state $S_0 \rightarrow S_2$ absorption transition would push the S_1 energy below 12,000 cm^{-1}, which is unrealistically low for a carotenoid having a relatively long 6.5 ps S_1 lifetime [P3.8]. Therefore, it is concluded that the most pronounced vibrational band in the $S_1 \rightarrow S_2$ spectrum corresponds to the 0-1 vibronic transition and that the S_1 energy of renierapurpurin is determined to be $13,200 \pm 100$ cm^{-1}. A similar analysis was carried out for isorenieratene, β-carotene and lycopene in the various solvents, and the resulting S_1 state energies are summarized in Table 3.3.1. The values in cyclohexane for β-carotene (13,700 cm^{-1}) and isorenieratene (13,990 cm^{-1}) are significantly higher than for renierapurpurin (13,180 cm^{-1}), which matches the trend in the S_1 lifetimes which increase in the order renierapurpurin < β-carotene < isorenieratene (Table 3.3.1). As a control, data were also recorded for the linear carotenoid, lycopene which was determined to have an S_1 lifetime of ~4 ps consistent with previous measurements [P3.14], [P3.15]. As expected based on this relatively fast lifetime, the S_1 energy of ~12,500 cm^{-1} in the three solvents determined from the spectral analysis, is lower than for the three other carotenoids which have terminal rings. This value for the S_1 energy also matches that reported previously from the $S_1 \rightarrow S_2$ transient spectrum of lycopene recorded over a broader spectral region [P3.54]. This validates the present assignment of the 0-1 vibronic bands in the $S_1 \rightarrow S_2$ spectra of the aryl carotenoids investigated here.

3.3.5   Discussion

The results summarized in Table 3.3.1 show a clear correlation between the S_1 lifetime and the S_1 energy of all the carotenoids examined in this work. The S_1 lifetime decreases in line with a decrease of S_1 energy, a trend expected on the basis of the energy gap law that was shown to be applicable for non-carbonyl carotenoids [P3.55]. However, in contrast to the behavior of a series of linear carotenoids [P3.15], [P3.17], or a series of carotenoids having identical terminal rings, the properties of the S_1 state for the aryl carotenoids examined here cannot be correlated with their number of conjugated C=C bonds. This is supported by the following observations made in the present investigation:

First, increasing the number of conjugated C=C bonds by four in going from β-carotene to isorenieratene (Figure 3.3.1) increases both the S_1 lifetime (from ~9 ps to ~13 ps) and the S_1 energy (from 13,700 cm^{-1} to ~14,000 cm^{-1}). For linear carotenoids, such a change in N would lead to a pronounced decrease of both of these parameters; e.g. the 23 ps S_1 lifetime of neurosporene (N=9) drops to 1.4 ps for spirilloxanthin (N=13) [P3.17], and the S_1 energy decreases from 15,300 cm^{-1} for neurosporene [P3.56] to 11,500 cm^{-1} for spirilloxanthin [P3.57]. Thus, it is surprising that for the β-carotene/isorenieratene pair, an *increase* in N leads to a *decrease* in N_{eff}.

Second, even though the isorenieratene/renierapurpurin pair has the same value of N, they exhibit markedly different spectral properties. This is not surprising for carotenoids having the same value of N but different structures, because it is well-known that extending the π-electron conjugation into the terminal rings decreases N_{eff} [P3.8]. However, the isorenieratene/renierapurpurin pair has an identical number of double bonds and differs only in the position of two symmetric methyl groups on the two terminal rings (Figure 3.3.1). In renierapurpurin there are methyl groups on the rings at carbon positions C1, C2 and C3 (and C1', C2' and C3'), whereas in isorenieratene the methyl groups are at carbon positions C1, C2 and C5 (and C1', C2' and C5'). A cursory examination of these two structures suggests that no significant changes in spectroscopic properties should be expected. Yet, renierapurpurin has nearly half the S_1 lifetime as isorenieratene, and its S_1 energy is lower by almost 1000 cm^{-1} compared to isorenieratene (Table 3.3.1). Thus, despite nearly identical structures, it can be concluded that N_{eff} of renierapurpurin is longer than that of isorenieratene.

The present results indicate that terminal aryl rings have the capacity to significantly tune the spectroscopic properties of carotenoids. To reveal the origin of this effect, quantum mechanical calculations were carried out to determine the relaxed geometries and transition energies of the carotenoids. Relaxed ground state geometries of β-carotene, isorenieratene and renierapurpurin, calculated using the BLYP/TZVP level of theory, are shown in Figure 3.3.6. Bond lengths corresponding to these relaxed structures in the ground state are depicted in Figure 3.3.7a. The bond lengths exhibit a
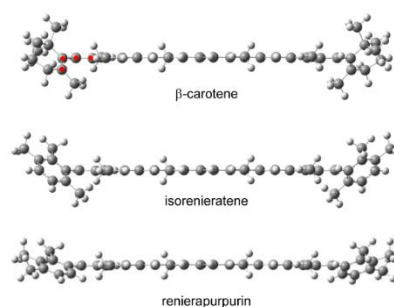
Figure 3.3.6. Relaxed ground state geometries of β-carotene, isorenieratene and renierapurpurin. The dihedral angle, formed by the four carbon atoms denoted by red dots in β-carotene structure, defines the torsion of the terminal ring with respect to the central part of the conjugation.

characteristic alternating pattern demonstrating that in the ground state, the single and double bond character is retained [P3.44], [P3.58]. This alternating pattern is very similar for all three carotenoids in the central part of the conjugation, but clear differences occur in the terminal rings.

Whereas the carbon-carbon bonds at positions C5-C6, C5'-C6' in the terminal rings of β-carotene have clear double bond character, these same bond lengths are noticeably extended for both isorenieratene and renierapurpurin (Figure 3.3.7). Also, compared to β-carotene the carbon-carbon bonds in the terminal rings of isorenieratene and renierapurpurin have approximately the same length, which is somewhere between the single (~1.45 Å) and double (~1.38 Å) bond lengths. This means that while the C5-C6 and C5'-C6' double bonds in the β-rings of β-carotene contribute significantly to the overall conjugation length of that carotenoid, the double bonds in the φ- and χ-rings of aryl carotenoids are quantifiably different. Thus, although the equilibration of the bond lengths within the aryl rings indicates that each aryl ring forms its own conjugated system, the conjugation of aryl rings is substantially different from the conjugation of the central part of molecule. This results in a partial detachment of the terminal rings from the overall conjugation in aryl ring-containing carotenoids. The equilibration of the bond lengths at the aryl rings is also observed for the equilibrium geometries of the molecules in the S_1 and
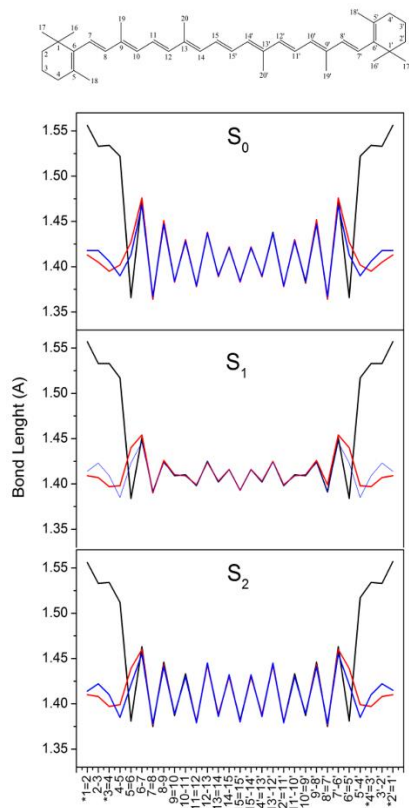
Figure 3.3.7. Comparison of the bond lengths in the ground state (top), S_1 state (middle) and S_2 state (bottom) geometries of β-carotene (black), isorenieratene (red) and renierapurpurin (blue). The bond lengths were extracted from relaxed geometries of each state obtained by DFT calculations using the BLYP functional and TZVP basis set in the gas phase. The double bonds marked by an asterisk are single bonds in β-carotene. The β-carotene structure with bond numbering is also shown.

S_2 states (Figure 3.3.7b,c), although the S_1 equilibrium geometry leads to bond length equilibration of the conjugated chain especially in the middle part of the molecule. These findings are in agreement with previous calculations of bond lengths for zeaxanthin [P3.44].

The detachment of the aryl rings is also evidenced by a calculation of the π-electron distributions in the molecules which indicates that the electron density associated with the carbon-carbon bonds in the aromatic rings does not change significantly in going from the HOMO to the LUMO, in contrast to a substantial change that appears along the conjugated polyene (Supporting Information Table 3.3.3). The fact that aryl rings exhibit very little single-double bond alternation among the carbon-carbon bonds is a major reason why adding four double bonds to the conjugation system of a carotenoid can result in a smaller N_{eff} as is the case for isorenieratene compared to β-carotene. However, it cannot explain why isorenieratene and renierapurpurin have different spectroscopic properties. To understand the key difference between these carotenoids requires examining the dihedral angles formed by carbons C5-C6-C7-C8 and C5'-C6'-C7'-C8'. These angles define the torsion of the terminal rings with respect to the plane of the central π-electron conjugated system (Figure 3.3.6). It is known that this torsional angle is in the range of 44°-48° for carotenoids having terminal rings with a methyl group at the C5 (or C5') position. β-carotene [P3.59], zeaxanthin [P3.44], and astaxanthin [P3.60] fit into this category where the torsional twist of the terminal

ring is caused by repulsion between the methyl group and the hydrogen atoms near the ends of the conjugated chain [P3.61].

In the present work, the dihedral angles were calculated for the ground state using the BLYP/TZVP level of theory. The results are shown in Table 3.3.2 and reveal a dihedral angle of 45.1° for β-carotene, which is in the range obtained previously using the B3LYP/6-31g method [P3.59]. The aryl ring of isorenieratene, which retains a methyl group at the C5 (and C5') position(s), decreases the ring torsion slightly and yields a dihedral angle of 40.9°. For renierapurpurin, which has a methyl group at position C3 (and C3') instead of at position C5 (and C5') for isorenieratene (Figure 3.3.1), the repulsion between the methyl group and hydrogens along the main conjugated chain is no longer present. This leads to a significant degree of planarization of the molecule resulting in a dihedral angle of 20.3°. Thus, the difference in dihedral angles of isorenieratene and renierapurpurin is the reason for the red shift of absorption spectrum and shorter S_1 lifetime of renierapurpurin. The planarization of renierapurpurin molecule promotes extension of the conjugation into the ring, in contrast to isorenieratene where the ring is significantly detached. This planarization of renierapurpurin leads to a lowering of the energies of both the S_2 and S_1 states, a red-shift in the spectral profiles associated with these states compared to isorenieratene, and a shortening of the S_1 lifetime. Thus, the dihedral angle of the aryl ring is the key factor in determining whether the additional double bonds contribute to the overall conjugated π-electron system. Closer inspection of the bond lengths illustrated in Figure 3.3.7 indicates that the broken pattern of alternating bond lengths is less pronounced for the χ-rings of renierapurpurin compared to the φ-rings of isorenieratene, which apparently contributes to the partial conjugation of the bonds within the χ-rings of renierapurpurin.

To examine whether these experimental observations can be reproduced in calculations, both $S_0 \rightarrow S_2$ and $S_0 \rightarrow S_1$ transition energies have been computed. Here, different levels of theory must be used because, while the Cam-B3LYP and B3LYP functionals reasonably reproduce the S_2 energies, it gives the wrong excited state ordering resulting in the forbidden S_1 state being placed above the S_2 state [P3.44]. Thus, the TDA Cam-B3LYP/TZVP approach was used to calculate the S_2 energies, but BLYP functional, which is known to give the proper state ordering, was used to calculate S_1 energies. The results, shown in Table 3.3.2, demonstrate that calculated vertical transition energies of the $S_0 \rightarrow S_2$ transition, which correspond to the 0-1 vibrational band of the $S_0 \rightarrow S_2$ transition are 21,980 cm^{-1}, 21,790 cm^{-1} and 21,320 cm^{-1}

for β-carotene, isorenieratene and renierapurpurin, respectively. Thus, the calculations do not reproduce the ~950 cm^{-1} red-shift observed experimentally for isorenieratene and renierapurpurin (Figure 3.3.2). The calculations also predict a slight blue-shift of the S$_2$ energy of isorenieratene compared to β-carotene, which is also not observed experimentally. Yet, the similarity of the S$_2$ energies of β-carotene and isorenieratene which have different N, and the large difference between the S$_2$ energies of isorenieratene and renierapurpurin, which have the same N, is reproduced in the calculations. Using the BLYP functional to calculate S$_0 \rightarrow$ S$_2$ transition energies (values in italics in Table 3.3.2) places the S$_2$ energy of β-carotene far above that of isorenieratene, confirming that this method cannot reproduce experimental data.

Table 3.3.2. Calculated dihedral angles (C5-C6-C7-C8) and vertical excitation energies[a]

	Dihedral angle (degrees)			Transition energy (cm^{-1})	
	S$_0$	S$_1$	S$_2$	S$_0$-S$_2$	S$_0$-S$_1$
β-carotene	45.1	29.1	36.9	23 580 (4.764)	15 310 (0.000)
			42.4	*21 980 (5.028)*	
isorenieratene	40.9	28.7	32.6	21 500 (5.714)	15 360 (0.000)
			37.2	*21 790 (5.310)*	
renierapurpurin	20.3	0.8	2.5	20 280 (6.156)	14 530 (0.000)
			14.2	*21 320 (5.460)*	

a) Calculations were carried out using either the BLYP/TZVP (ground state) or TDA BLYP/TZVP (excited states) level of theory. Calculations involving the S$_2$ state were also carried out by TDA Cam-B3LYP/TZVP (results shown in italics). Oscillator strengths of the transitions are shown in parentheses.

The S$_1$ energies calculated at the TDA BLYP/TZVP level of theory are also shown in Table 3.3.2. The calculated vertical energies of the S$_0 \rightarrow$ S$_1$ transition yields 15,310 cm^{-1} for β-carotene, 15,360 cm^{-1} for isorenieratene and 14,530 cm^{-1} for renierapurpurin. These calculated values are clearly too low, because it is known that for the S$_0 \rightarrow$ S$_1$ transition, the maximum should correspond to the 0-2 vibrational band [P3.61]. Thus, the calculated vertical energies should be about 2600 cm^{-1} higher than the 0-0 energies obtained from experiment (see Table 3.3.1), which is clearly not the case. Yet, the trend in the shifts of the S$_1$ energy for the three carotenoids is well-reproduced in calculations. The highest energy of the vertical S$_0 \rightarrow$ S$_1$ transition is found at 15,360 cm^{-1} for isorenieratene, agreeing well with the experiment, even though the calculated 50 cm^{-1} blue shift from β-carotene is much less than the experimental value of ~300 cm^{-1} (Table 3.3.1). The lowest S$_1$ energy calculated is 14,530 cm^{-1} for renierapurpurin, and in this case even the calculated 830 cm^{-1} red-shift compared to isorenieratene matches that obtained from experiment.

Thus, a combination of experimental data and quantum chemical calculations shows that the shift of methyl group from carbon positions C5 (and C5') on a φ-ring to C3 (and C3') on a χ-ring induces significant changes in spectroscopic properties many of which are accounted for by planarization of the χ-ring. Because no carotenoid having a φ-ring has been analyzed by time-resolved spectroscopy or quantum chemical calculations so far, it is worth mentioning further properties specific to renierapurpurin. First, using the TDA Cam-B3LYP/TZVP and TDA BLYP/TZVP the geometries of the S_2 state of all three carotenoids have been optimized. Although there are no significant changes in bond order compared to the ground state (Figure 3.3.7b), the calculated dihedral angles in the relaxed S_2 state differ from those in the ground state (Table 3.3.2). For β-carotene and isorenieratene, the ring torsion decreases in the S_2 state by 5-9°, depending on the chosen level of theory. Renierapurpurin exhibits a much larger change and TDA BLYP/TZVP predicts the dihedral angle in the S_2 state to be only 2.5° suggesting that the relaxed geometry of the S_2 state makes this molecule nearly planar. This would require a twist of the χ-ring of about 20° upon relaxation in the S_2 state, which is much larger than for β-carotene and isorenieratene. Since such twist would take some time, relaxation of the S_2 geometry after excitation of the S_2 state could be the reason for the relatively long (200 fs) S_2 lifetime obtained here from both VIS (Figure 3.3.4) and NIR (Figure 3.3.5) data. Further planarization of the molecule is predicted for all three carotenoids in the relaxed S_1 state (Table 3.3.2).

The transient absorption spectra in Figure 3.3.3 reveal another feature specific to renierapurpurin. The $S_1 \rightarrow S_n$ band of this carotenoid is markedly narrower than the $S_1 \rightarrow S_n$ bands of β-carotene and isorenieratene; its width being even close to that of the linear carotenoid lycopene. The bandwidth of the $S_1 \rightarrow S_n$ transition conveys information regarding conformational disorder in the S_1 state, which for carotenoids with conjugation extended into the terminal rings usually corresponds to an ensemble distribution of dihedral angles. Thus, the narrow $S_1 \rightarrow S_n$ band of renierapurpurin suggests that the dihedral angles of renierapurpurin in the S_1 state are restricted to a rather narrow distribution, making the width of the $S_1 \rightarrow S_n$ band comparable to that of a linear carotenoid. This is logical because the methyl group at position C3 (and C3') on the χ-ring of renierapurpurin would not interact with the atoms on the central chain, which could lead to linear carotenoid-like behavior. Interestingly, however, a bandshape narrowing is not observed in the ground state absorption spectrum (Figure 3.3.2), meaning that the conformation disorder in the

ground state is about the same for renierapurpurin as for β-carotene and isorenieratene, and the reduction in conformational disorder exists only when renierapurpurin is in the S_1 state.

A direct comparison of the spectroscopic properties of isorenieratene and renierapurpurin has provided a unique opportunity to study the effect of torsional twisting of the terminal rings of carotenoids that contain conjugated C=C bonds. A difference in methyl group position on the φ- and χ-rings results in different dihedral angles that cause changes in spectroscopic properties. The measured S_1 lifetimes allow a calculation of N_{eff} of the carotenoids. A comparison of the S_1 lifetimes of the present molecules with those reported for linear carotenoids is shown in Figure 3.3.8. It is clear that when the S_1 lifetimes of linear carotenoids are plotted on a logarithmic scale vs. $1/N$, they can be fitted by a linear function. Placing the S_1 lifetimes of the carotenoids studied here on this graph results in N_{eff} values of 9.6 for isorenieratene, 10 for β-carotene, and 10.4 for renierapurpurin. Thus, the change in dihedral angle of the terminal aryl ring in

Figure 3.3.8 Dependence of the S_1 lifetimes on conjugation length. Black symbols denotes the S_1 lifetimes of linear carotenoids in *n*-hexane (data taken from Ref. [P3.20]) plotted against $1/N$. The solid line is a linear fit to the S_1 lifetimes of linear carotenoids. Red circles show the S_1 lifetimes of β-carotene, isorenieratene and renierapurpurin. Placing these lifetimes on the black line allows a determination of the effective conjugation length, N_{eff}, of these carotenoids. Each point is labeled by a corresponding S_1 lifetime and N (or N_{eff}).

the ground state from ~40° to ~20° in going from isorenieratene to renierapurpurin increases the effective conjugation by nearly one unit. While this twist can be achieved in solution only by change in the carotenoid structure as it has been demonstrated here, for protein-bound carotenoids, much larger twists can be achieved depending on the design of the carotenoid binding pocket. Examples of protein binding resulting in tuning the spectroscopic properties of carotenoids are found in the orange-carotenoid protein (OCP) and in xanthorhodopsin where either an increase (for OCP) [P3.62] or a decrease (for xanthorhodopsin) [P3.63] of N_{eff} is achieved by twisting the terminal ring of the carotenoid in the binding site. The results presented here suggest that aryl carotenoids offer a significant potential for tuning their

spectroscopic and kinetic properties, which may provide an evolutionary advantage to the organisms in which they accumulate.

3.3.6   Acknowledgement

3.3.7   References

[P3.1]   Polívka, T.; Frank, H. A. Molecular Factors Controlling Photosynthetic Light-Harvesting by Carotenoids. *Acc. Chem. Res.* 2010, *43*, 1125–1134.

[P3.2]   Croce, R.; van Amerongen, H. Natural strategies for photosynthetic light harvesting. *Nat. Chem. Biol.* 2014, *10*, 492-501.

[P3.3]   Scholes, G.D.; Fleming, G.R.; Olaya-Castro, A.; van Grondelle, R. Lessons from nature about solar light harvesting. *Nat. Chem.* 2011, *3*, 764–774.

[P3.4]   Jahns, P.; Holzwarth, A. R. The role of the xanthophyll cycle and of lutein in photoprotection of photosystem II. *Biochim. Biophys. Acta* 2012, *1817*, 182-193.

[P3.5]   Edge, R.; Truscott, T. G. Carotenoid radicals and the interaction of carotenoids with active oxygen species. In *The Photochemisry of Carotenoids*; Frank, H. A; Young, A. J; Britton, G.; Cogdell, R. J.; Eds. Kluwer Academic Publishers, Dordrecht 2004, p. 223-234.

[P3.6]   McGraw, K. J. 2006 Mechanics of carotenoid-based coloration. In Bird coloration volume 1: mechanisms and measurements (eds G. E. Hill & K. J. McGraw), pp. 177–242. Cambridge, MA: Harvard University Press.

[P3.7]   Tavan, P.; Schulten, K. Electronic excitations in finite and infinite polyenes. *Phys. Rev. B* 1987, *36*, 4337-4358.

[P3.8]   Polívka, T.; Sundström, V. Ultrafast dynamics of carotenoid excited states. From solution to natural and artificial systems. *Chem. Rev.* 2004, *104*, 2021–2071.

[P3.9]   Polívka T.; Sundström, V. Dark excited states of carotenoids: Consensus and controversy. *Chem. Phys. Lett.*, 2009, *477*, 1–11.

[P3.10] Maiuri, M.; Polli, D.; Brida, D.; Luer, L.; LaFountain, A.M.; Fuciman, M.; Cogdell, R.J.; Frank, H.A.; Cerullo, G. Solvent-dependent activation of intermediate excited states in the energy relaxation pathways of spheroidene. *Phys. Chem. Chem. Phys.* 2012, *14*, 6312–6319.

[P3.11] Buckup, T.; Motzkus, M. Multidimensional Time-Resolved Spectroscopy of Vibrational Coherence in Biopolyenes. *Annu. Rev. Phys. Chem.* 2014, *65*, 39-57.

[P3.12] Jailaubekov, A. E.; Vengris, M.; Song, S. H.; Kusumoto, T.; Hashimoto, H.; Larsen, D. S. Deconstructing the Excited-State Dynamics of beta-Carotene in Solution. *J. Phys. Chem. A* 2011, *115*, 3905-3916.

[P3.13] Kosumi, D.; Fujiwara, M.; Fujii, R.; Cogdell, R. J.; Hashimoto, H.; Yoshizawa, M. The dependence of the ultrafast relaxation kinetics of the S_2 and S_1 states in β-carotene homologs and lycopene on conjugation length studied by femtosecond time-resolved absorption and Kerr-gate fluorescence spectroscopies. *J. Chem. Phys.* 2009, *130*, 214506.

[P3.14] Billsten, H. H.; Zigmantas, D.; Sundström, V.; Polívka, T. Dynamics of vibrational relaxation in the S_1 state of carotenoids having 11 conjugated C=C bonds. *Chem. Phys. Lett.* 2002, *355*, 465-470.

[P3.15] Koyama, Y.; Rondonuwu, F. S; Fujii, R.; Watanabe, Y. Light-harvesting function of carotenoids in photosynthesis: The roles of the newly found $1B_u^-$ state. *Biopolymers* 2004, *74*, 2-18.

[P3.16] Frank, H. A.; Cua, A.; Chynwat, V.; Young, A.; Gosztola, D.; Wasielewski, M. R. Photophysics of the Carotenoids Associated with the Xanthophyll Cycle in Photosynthesis. *Photosynth. Res.* 1994, *41*, 389-395.

[P3.17] Niedzwiedzki, D.; Koscielecki, J. F.; Cong, H.; Sullivan, J. O.; Gibson, G. N.; Birge, R. R.; Frank, H. A. Ultrafast dynamics and excited state spectra of open-chain carotenoids at room and low temperatures. *J. Phys. Chem. B* 2007, *111*, 5984- 5998.

[P3.18] Mendes-Pinto, M. M.; Sansiaume, E.; Hashimoto, H.; Pascal, A. A.; Gall, A.; Robert, B. Electronic Absorption and Ground State Structure of Carotenoid Molecules. *J. Phys. Chem. B* 2013, *117*, 11015–11021.

[P3.19] Christensen, R. L.; Enriquez, M. M.; Wagner, N. L.; Peacock-Villada, A. Y.; Scriban, C.; Schrock, R. R.; Polívka, T.; Frank, H. A.; Birge, R. R. Energetics and dynamics of the low-lying electronic states of constrained polyenes: Implications for infinite polyenes. *J. Phys. Chem. A* 2013, *117*, 1449-1465.

[P3.20] Fujii, R.; Inaba, T.; Watanabe, Y.; Koyama, Y.; Zhang, J.P. Two different pathways of internal conversion in carotenoids depending on the length of the conjugated chain. *Chem. Phys. Lett.* 2003, *369*, 165-172.

[P3.21] Chábera, P.; Fuciman, M.; Hříbek, P.; Polívka, T. Effect of carotenoid structure on excited state dynamics of carbonyl carotenoids. *Phys. Chem. Chem. Phys.* 2009, *11*, 8795-8803.

[P3.22] Niedzwiedzki, D. M.; Kajikawa, T.; Aoki, K.; Katsumura, S.; Frank, H. A. Excited States Energies and Dynamics of Peridinin Analogues and the Nature

of the Intramolecular Charge Transfer State in Carbonyl-Containing Carotenoids. *J. Phys. Chem. B* 2013, *117*, 6874-6887.

[P3.23] Kleinschmidt, M.; Marian, C. M.; Waletzke, M.; Grimme, S. Parallel multireference configuration interaction calculations on mini-β-carotenes and β-carotene. *J. Chem. Phys.* 2009, *130*, 044708.

[P3.24] Kosumi, D.; Kusumoto, T.; Fujii, R.; Sugisaki, M.; Iinuma, Y.; Oka, N.; Takaesu, Y.; Taira, T.; Iha, M.; Frank, H. A.; Hashimoto, H. Ultrafast excited state dynamics of fucoxanthin: excitation energy dependent intramolecular charge transfer dynamics. *Phys. Chem. Chem. Phys.* 2001, *13*, 10762-10770.

[P3.25] Zigmantas, D.; Hiller, R.G.; Sharples, F.P.; Frank, H.A.; Sundström, V.; Polívka, T. Effect of conjugated carbonyl group on photophysical properties of carotenoids. *Phys. Chem. Chem. Phys.* 2004, *6*, 3009–3016.

[P3.26] Frigaard, N. U.; Bryant, D. A. Chlorosomes: Antenna Organelles in Photosynthetic Green Bacteria. In *Complex Intracellular Structures in Prokaryotes*, Shively, J. M., Ed.; Springer, 2010, p. 79-114.

[P3.27] Gould, S. L.; Kodis, G.; Liddell, P. A.; Palacios, R. E.; Brune, A.; Gust, D.; Moore, T. A.; Moore, A. L. Artificial photosynthetic reaction centers with carotenoid antennas. *Tetrahedron* 2006, *62*, 2074- 2096.

[P3.28] Kloz, M.; Pillai, S.; Kodis, G.; Gust, D.; Moore, T. A.; Moore, A. L.; van Grondelle, R.; Kennis, J. T. M. Carotenoid Photoprotection in Artificial Photosynthetic Antennas. *J. Am. Chem. Soc.* 2011, *133*, 7007- 7015.

[P3.29] Pšenčík, J.; Ma, Y.-Z.; Arellano, J. B.; Garcia-Gil, L. J.; Holzwarth, A. R. Gillbro, T. Excitation energy transfer in chlorosomes of *Chlorobium phaeobacteroides* strain CL1401: the role of carotenoids. *Photosynth. Res.* 2002, *71*, 5-18.

[P3.30] Marian, C. M.; Kock, C. M.; Hundsdorfer, C.; Martin, H.-D.; Stahl, W.; Ostroumov, E.; Muller, M. G.; Holzwarth, A. R. Spectroscopic properties of phenolic and quinoid carotenoids: a combined theoretical and experimental study. *Photochem. Photobiol. Sci.* 2009, *8*, 270-278.

[P3.31] Fuciman, M.; Chábera, P.; Župčanová, A.; Hříbek, P.; Arellano, J. B.; Vácha, F.; Pšenčík, J.; Polívka, T. Excited state properties of aryl carotenoids. *Phys. Chem. Chem. Phys.* 2010, *12*, 3112-3120.

[P3.32] Niedzwiedzki, D. M.; Sullivan, J. O.; Polívka, T.; Birge, R. R.; Frank, H. A. Femtosecond time-resolved transient absorption spectroscopy of xanthophylls. *J. Phys. Chem. B* 2006, *110*, 22872-22885.

[P3.33] Yamaguchi, M. On Carotenoids of a Sponge *Reniera japonica*. *Bull. Chem. Soc. Jap.* 1957, *30*, 111-114.

[P3.34] Graham, J. E.; Bryant, D. A. The Biosynthetic Pathway for Synechoxanthin, an Aromatic Carotenoid Synthesized by the Euryhaline, Unicellular Cyanobacterium *Synechococcus sp*. Strain PCC 7002 *J. Bacteriol.* 2008, *190*, 7966–7974.

[P3.35] Ilagan, R. P.; Christensen, R. L.; Chapp, T. W.; Gibson, G. N.; Pascher, T.; Polívka, T.; Frank, H. A. Femtosecond time-resolved absorption

spectroscopy of astaxanthin in solution and in alpha-crustacyanin. *J. Phys. Chem. A* 2005, *109*, 3120-3127.

[P3.36] Kohn, W.; Sham, L. J. Self-Consistent Equations Including Exchange and Correlation Effects. *Phys. Rev.* 1965, *140*, A1133–A1138.

[P3.37] Becke, A. D. Density-Functional Thermochemistry. III. The Role of Exact Exchange. *J. Chem. Phys.* 1993, *98*, 5648–5652.

[P3.38] Becke, A. D. Density-Functional Exchange-Energy Approximation with Correct Asymptotic Behavior. *Phys. Rev. A* 1988, *38*, 3098–3100.

[P3.39] Lee, C.; Yang, W.; G. Parr, R. Development of the Colle-Salvetti Corelation-Energy Formula into a Functional of the Electron Density. *Phys. Rev. B* 1988, *37*, 785.

[P3.40] Schaefer, A.; Huber, C.; Ahlrichs, R. Fully Optimized Contracted Gaussian-Basis Sets of Triple Zeta Valence Quality for Atoms Li to Kr. *J. Chem. Phys.* 1994, *100*, 5829–5853.

[P3.41] Hirata, S.; Head-gordon, M. Time-Dependent Density Functional Theory within the Tamm–Dancoff Approximation. 1999, *314*, 291–299.

[P3.42] Yanai, T.; Tew, D. P.; Handy, N. C. A New Hybrid Exchange–correlation Functional Using the Coulomb-Attenuating Method (CAM-B3LYP). *Chem. Phys. Lett.* 2004, *393*, 51–57.

[P3.43] Hsu, C.; Hirata, S.; Head-gordon, M. Excitation Energies from Time-Dependent Density Functional Theory for Linear Polyene Oligomers : Butadiene to Decapentaene. 2001, *105*, 451–458.

[P3.44] Dreuw, A. Influence of Geometry Relaxation on the Energies of the S_1 and S_2 States of Violaxanthin, Zeaxanthin, and Lutein. *J. Phys. Chem. A* 2006, *110*, 4592–4599.

[P3.45] Frisch, M. J.; Trucks, G. W.; Schlegel, H. B.; Scuseria, G. E.; Robb, M. A.; Cheeseman, J. R.; Scalmani, G.; Barone, V.; Mennucci, B.; Petersson, G. A.; et al. Gaussian, 09W, Gaussian Inc., Wallingford CT, 2009.

[P3.46] Dennington, T.A.; Keith, J. M. M. GaussView, 5.0.8, Gaussian Inc., Wallingford CT, 2008.

[P3.47] Polívka, T.; Herek, J. L.; Zigmantas, D.; Åkerlund, H. E.; Sundström, V. Direct Observation of the (Forbidden) S_1 State in Carotenoids. *Proc. Natl. Acad. Sci. U.S.A.* 1999, *96*, 4914-4917.

[P3.48] Macpherson, A. N.; Gillbro, T. Solvent dependence of the ultrafast S_2-S_1 internal conversion rate of □-carotene *J. Phys. Chem. A* 1998, *102*, 5049-5058.

[P3.49] de Weerd, F. L.; van Stokkum, I. H. M.; van Grondelle, R. Subpicosecond dynamics in the excited state absorption of all-trans-β-carotene. *Chem. Phys. Lett.* 2002, *354*, 38-43.

[P3.50] van Stokkum, I. H. M.; Larsen, D. S.; van Grondelle, R. Global and target analysis of time-resolved spectra. *Biochim. Biophys. Acta* 2004, *1657*, 82-104.

[P3.51] Zhang, J. P.; Skibsted, L. H.; Fujii, R.; Koyama, Y. Transient absorption from the $^1B_u^+$ state of all-trans-□-carotene newly identified in the near-infrared region. *Photochem. Photobiol.* 2001, *73*, 219-222.

[P3.52] Polívka, T.; Zigmantas, D.; Frank, H. A.; Bautista, J. A.; Herek, J. L.; Koyama, Y.; Fujii, R.; Sundström, V. Near-infrared time-resolved study of the S_1 state dynamics of the carotenoid spheroidene. *J. Phys. Chem. B* 2001, *105*, 1072-1080.

[P3.53] Enriquez, M. M.; LaFountain, A. M.; Budarz, J.; Fuciman, M.; Gibson, G. N.; Frank, H. A. Direct determination of the excited state energies of the xanthophylls diadinoxanthin and diatoxanthin from *Phaeodactylum tricornutum*. *Chem. Phys. Lett.* 2010, *493*, 353-357.

[P3.54] Billsten, H. H.; Herek, J. L.; Garcia-Asua, G.; Hashoj, L.; Polívka, T.; Hunter, C. N.; Sundström, V. Dynamics of energy transfer from lycopene to bacteriochlorophyll in genetically-modified LH2 complexes of *Rhodobacter sphaeroides*. *Biochemistry* 2002, *41*, 4127-4136.

[P3.55] Chynwat, V.; Frank, H. A. The Application of the Energy-Gap Law to the S_1 Energies and Dynamics of Carotenoids. *Chem. Phys.* 1996, *194*, 237-244.

[P3.56] Fujii, R.; Onaka, K.; Kuki, M.; Koyama, Y.; Watanabe, Y. The $^2A_g^-$ energies of all-trans-neurosporene and spheroidene as determined by fluorescence spectroscopy. *Chem. Phys. Lett.* 1998, *288*, 847-853.

[P3.57] Papagiannakis, E.; van Stokkum, I. H. M.; van Grondelle, R.; Niederman, R. A.; Zigmantas, D.; Sundström, V.; Polívka, T. Near-infrared transient absorption study of the excited state dynamics of the carotenoid spirilloxanthin in solution and in the LH1 complex of *Rhodospirillum rubrum*. *J. Phys. Chem. B* 2003, *107*, 11216-11223.

[P3.58] Lukeš, V.; Christensson, N.; Milota, F.; Kauffmann, H. F.; Hauer, J. Electronic ground state conformers of β-carotene and their role in ultrafast spectroscopy. *Chem. Phys. Lett.* 2011, *506*, 122-127.

[P3.59] Requena, A.; Ceron-Carrasco, J. P.; Bastida, A.; Zuniga, J.; Miguel, B. Density functional theory study of the structure and vibrational spectra of beta-carotene, capsanthin, and capsorubin. *J. Phys. Chem. A* 2008, *112*, 48-15-4825.

[P3.60] Young, A. J.; Phillip, D. M.; Hashimoto, H. Ring-to-chain conformation may be a determining factor in the ability of xanthophylls to bind to the bulk light-harvesting complex of plants. *J. Mol. Struct.* 2002, *642*, 137-145.

[P3.61] Christensen, R. L.; Goyette, M.; Gallagher, L.; Duncan, J.; DeCoster, B.; Lugtenburg, J.; Jansen, F. J.; van der Hoef, I. S_1 and S_2 states of apo- and diapocarotenes. *J. Phys. Chem. A* 1999, *103*, 2399-2407.

[P3.62] Polívka, T.; Kerfeld, C. A.; Pascher, T.; Sundström, V. Spectroscopic properties of the carotenoid 3'-hydroxyechinenone in the orange carotenoid protein from the cyanobacterium *Arthrospira maxima*. *Biochemistry* 2005, *44*, 3994-4003.

[P3.63] Polívka, T.; Balashov, S. P.; Chábera, P.; Imasheva, E. S.; Yartsev, A.; Sundström, V.; Lanyi, J. K. Femtosecond carotenoid to retinal energy transfer in xanthorhodopsin. *Biophys. J.* 2009, *96*, 2268–2277.

3.3.8 Supporting Information

Table 3.3.3. Attachment/detachment electron densities for HOMO-LUMO transitions of β-carotene, isorenieratene and renierapurpurin calculated at the BLYP/TZVP level of theory.
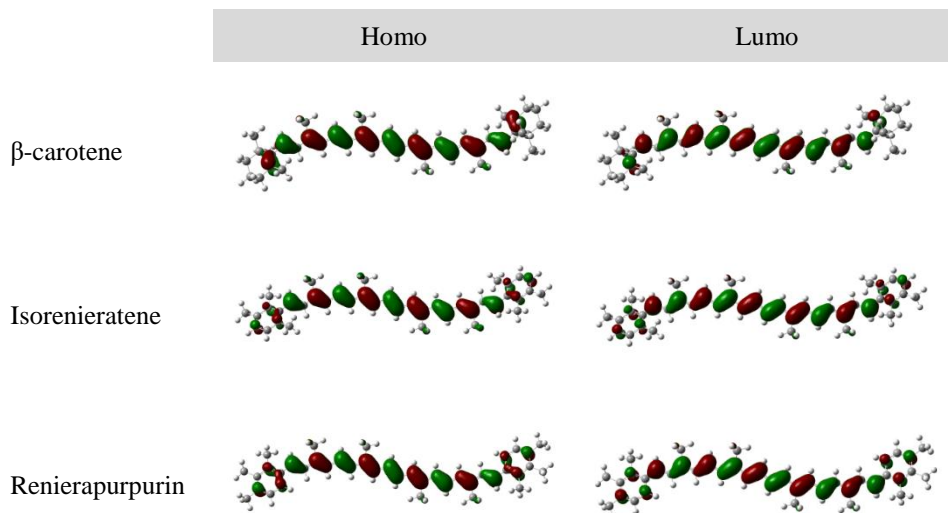
3.4 PAPER 4

Different Response of Carbonyl Carotenoids to Solvent Proticity helps to Estimate Structure of Unknown Carotenoid from *Chromera velia*

Gürkan Keşan, Milan Durchan, Josef Tichý, Babak Minofar, Valentyna Kuznetsova, Marcel Fuciman, Václav Šlouf, Cemal Parlak, Tomáš Polívka,

3.4.1 Abstract

In order to estimate the possible structure of the unknown carbonyl carotenoid related to isofucoxanthin from *Chromera velia* denoted as isofucoxanthin-like carotenoid (Ifx-l), we employed steady-state and ultrafast time-resolved spectroscopic techniques to investigate spectroscopic properties of Ifx-l in various solvents. The results were compared with those measured for related carotenoids with known structure, fucoxanthin (Fx) and isofucoxanthin (Ifx). The experimental data were complemented by quantum chemistry calculations and molecular modelling. The data show that Ifx-l must have longer effective conjugation length than Ifx. Yet, the magnitude of polarity-dependent changes in Ifx-l is larger than for Ifx, suggesting significant differences in structure of these two carotenoids. The most interesting spectroscopic feature of Ifx-l is its response to solvent proticity. The transient absorption data shows that (1) the magnitude of the ICT-like band of Ifx-l in acetonitrile is larger than in methanol, and (2) the S_1/ICT lifetime of Ifx-l in acetonitrile, 4 ps, is markedly shorter than in methanol (10 ps). This is opposite behavior than for Fx and Ifx whose S_1/ICT lifetimes are always shorter in protic solvent methanol (20 and 13 ps) than in aprotic acetonitrile (30 and 17 ps). Comparison with other carbonyl carotenoids reported earlier showed that proticity response of Ifx-l is consistent with presence of a conjugated lactone ring. Combining the experimental data and quantum chemistry calculations, we estimated a possible structure of Ifx-l.

3.4.2 Introduction

Photophysics of carotenoids received much attention during the past few decades. These molecules are essential constituents of many biological systems where they play a number of significant roles ranging from light-harvesting and photoprotection in photosynthetic organism [P4.1]-[P4.4] to radical and singlet oxygen scavenging [P4.5], [P4.6] in nearly all living organisms. Most of the carotenoid actions in living systems are triggered by light; thus, knowledge of excited-state processes is a key prerequisite to describe their actions on molecular level. Numerous studies of carotenoid photophysics revealed a complex network of excited state pathways involving also dark excited states [P4.7], [P4.8]. Basic photophysical properties of carotenoids may be described in a simplified three-level scheme consisting of the ground state (S_0), the lowest excited state S_1 which is a dark state since the S_0-S_1 transition is forbidden by symmetry rules, and the strongly absorbing S_2 state through

which the carotenoids acquire their typical color [P4.7]. Energies and lifetimes of the S_1 and S_2 excited states depend on number of conjugated C=C bonds (*N*) [P4.7], [P4.9], [P4.10]. Both S_1 and S_2 states are involved in photophysical processes such as light-harvesting [P4.1], [P4.7], photoprotection [P4.11], [P4.12], or radical formation [P4.13] in photosynthetic systems.

Though this simple three-level scheme is useful for basic description of excited-state dynamics of carotenoids, it is known that it cannot provide a full description of the light-triggered processes as other dark excited states exist within the S_2-S_1 energy gap [P4.8], [P4.14], [P4.15]. Whether these additional dark states affect the excited-state dynamics depends on carotenoid structure. There is now solid experimental evidence that for carotenoids with *N*>10 additional states, usually denoted as Bu- state and the S* state, are involved in relaxation pathways following the excitation of the S_2 state [P4.14]-[P4.16].

Another dark excited state with a charge transfer character, an intramolecular charge transfer (ICT) state exists in an excited-state manifold of a specific family of carotenoids, the carbonyl carotenoids. These carotenoids have in their structure one or more keto (C=O) groups that are in conjugation with the main C=C conjugated chain. Since the seminal paper describing excite-state dynamics of a member of this carotenoid family, the carotenoid peridinin [P4.17], it is known that carbonyl carotenoids exhibit polarity-dependent spectroscopic properties. New band(s) induced by the ICT state appear in their transient absorption spectra and their S_1 lifetime, most likely due to a coupling to the ICT state, has a polarity-dependent lifetime. During the last decade, a number of carbonyl carotenoids were studied by time-resolved spectroscopy. Studies of carbonyl carotenoids with one [P4.17]-[P4.23], two [P4.24]-[P4.26] and, even four [P4.27] conjugated C=O groups showed that magnitude of the polarity-dependent behavior depends on carotenoid structure. First, asymmetrically positioned conjugated C=O group greatly enhances the polarity dependence [P4.25]. Second, the shorter the carbonyl carotenoid, the larger the polarity-dependent effect [P4.20], [P4.28]-[P4.30]. Thus, for short carotenoids with asymmetrical conjugated C=O group such as peridinin, the S_1 lifetime changes over nearly two orders of magnitude when switching from nonpolar to polar solvent, while for long carotenoids with symmetrically positioned C=O groups such as astaxanthin essentially no polarity effect is observed.
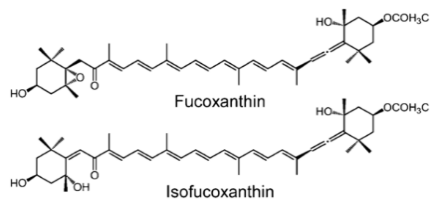
Figure 3.4.1 Molecular structures of fucoxanthin and isofucoxanthin.

Recently, a lot of attention was devoted to studies of excited-state dynamics of the carbonyl carotenoid fucoxanthin (Figure 3.4.1). It is the most abundant carotenoid on Earth and is commonly found in photosynthetic marine algae where it serves as efficient light-harvesting pigment [P4.31]. Fucoxanthin (Fx) has 7 conjugated C=C bonds terminated by one conjugated C=O group at one side and an allene group at other side. This configuration results in a rather short conjugation length with asymmetrically positioned C=O group, making it a good candidate to study polarity-dependent effects. Indeed, the Fx S_1 lifetime decreases from 60 ps in nonpolar solvent *n*-hexane to about 20 ps in polar solvent methanol. In addition, the spectral band attributable to the ICT state appears in transient absorption spectra in methanol [P4.18], [P4.21], [P4.28], [P4.32]. A series of studies from Hashimoto's group characterized this carotenoid in great detail, showing that 1) the excited-state dynamics is also excitation-wavelength dependent due to large conformational disorder in the ground state in polar solvents [P4.21], [P4.32], [P4.33]; 2) shortening of the conjugated chain of Fx enhances the polarity-dependent behavior [P4.28]; 3) an allene group mildly enhances the ICT character of the lowest excited state [P4.34]; 4) the ICT state is possible to excite directly via two-photon excitation [P4.32].

While Fx and even its analogs with varying conjugation lengths [P4.28] were studied in great detail by time-resolved spectroscopy, there are close relatives of this highly-abundant carotenoid that were not studied at all. One such relative is isofucoxanthin (Figure 3.4.1) which has one extra conjugated C=C bond in the conjugated system. In contrast to Fx, isofucoxanthin (Ifx) has never been identified as a photosynthetic pigment, but it is known as a metabolite of Fx [P4.35]. Ifx was isolated from seaweeds [P4.36] or from egg yolk [P4.37], though presence of Ifx was hypothesized to be an isolation artifact formed from Fx during the isolation [P4.38]. Recently, however, pigment analysis of a newly discovered photosynthetic organism, *Chromera velia*, showed that major carotenoid in this organism is a so-far unidentified pigment related to Ifx [P4.39]. Electrospray mass spectrometry in combination with chemical analysis demonstrated that composition ($C_{42}H_{58}O_6$) and chemical properties of the unknown carotenoid resembled those of Ifx. Yet the absorption spectrum in methanol is red-shifted from that of Ifx, indicating longer conjugation length [P4.39].

This unknown carotenoid was denoted as isofucoxanthin-like (Ifx-l) carotenoid and its basic spectroscopic characterization showed the typical polarity-dependent behavior of carbonyl carotenoids [P4.40]. It is the major carotenoid in Chromera light harvesting (CLH) protein [P4.41]. The unknown carotenoid transfers energy to Chl-a with nearly 100% efficiency but, in contrast to other light-harvesting complexes with carbonyl carotenoids, optimization of carotenoid-to-chlorophyll energy transfer is achieved in CLH by decreasing the charge transfer character of the S_1/ICT state of Ifx-l upon binding to protein [P4.40]. Here, to explore the spectroscopic properties of Ifx-l in detail, we measured transient absorption spectroscopy data on Ifx-l in a number of solvents with different polarity and compared the data with Fx and Ifx. Combination of spectroscopic data with quantum chemical calculations and classical molecular dynamics (MD) simulations allowed to discern specific spectroscopic properties of Ifx-1 and to estimate possible structure of this unknown carotenoid.

3.4.3 Materials and Methods

Sample preparation. Ifx was prepared by treatment of Fx by KOH in methanol according to Ref. [P4.35]. Fx (0.2 mg, 0.3 μmol, Sigma-Aldrich) was dissolved in 0.05% KOH in methanol (250 μl), molar ratio KOH: Fx = 11. After 40 min in dark at room temperature, ether (ca. 700 μl) and water (ca. 1000 μl) were added. The ether phase was washed with saturated aq. NaCl solution (ca. 1000 μl) and water (3 x 1000 μl) and dried. Dried sample was resolved in 100% methanol and the mixture of products was separated by high-performance liquid chromatography (HPLC) on a reverse phase. Ifx-l was isolated from *Chromera velia*. Frozen cells of *Chromera velia* were used as a source of Ifx-l. The cells were resuspended with methanol, homogenized in glass homogenizer and broken by 10 cycle circulation in an EmulsiFlex-C5 High Pressure cell disrupter (Avestin Inc., Canada) at a pressure of 100-150 MPa, while keeping the apparatus refrigerated on ice in the dark. Insoluble material was removed by centrifugation for 6 min at 6000×g. The methanol extract was then dried. Prepared cell extracts were dissolved in 100% methanol and the mixture was separated by HPLC on a reverse phase column as described in Ref. [P4.41].

The final separation of carotenoids from mixtures was carried on HPLC system consisting of Pump Controller Delta 600 and a PDA 2996 detector (Waters, USA), a reverse phase SunfireTM C8 column (4.6 x 250 mm, 5 µm, silica-based, end-

capped, Waters, USA). For the separation on reverse phase a ternary solvent system was used (0-1 min 40% A, 60% B, 11-13 min 100% B, 14 min 100% C; where the solvent A was 50% methanol, 25% acetonitrile and 25% water, B was 100% methanol, C was 80% methanol and 20% *n*-hexane). Flow rate was 1 or 2 ml.min−1. All pigment samples were dried in the dark in glass desiccator under vacuum made by a membrane vacuum pump and stored at -20 °C for later use.

*Spectroscopy***.** Steady-state absorption spectra of the samples were measured by Jasco V-530 spectrophotometer. A femtosecond spectrometer employing an amplified Ti:sapphire laser system as the source of femtosecond pulses (1 kHz, 110 fs, 800 nm) was used for transient absorption measurements. The 800 nm femtosecond pulses were divided into two beams by a beam splitter. Most of the output intensity was used to generate pump pulse to excite sample. Excitation pulses were further modified by an optical parametric amplifier (TOPAS, Light Conversion) to excite the lowest vibrational band of the S_0-S_2 transition. The rest of the split beam was focused to a 2 mm sapphire plate to generate a broadband (450-750 nm) white-light probe pulses. Time-resolved absorption changes were measured in a broad spectral range by detecting the dispersed white light by a double-diode array, the time delay between excitation and probe pulses was introduced by a computer controlled delay line. For each time delay, about 300 spectra were collected and averaged. The full spectro-temporal data set consisted typically of 150-200 time points. Mutual polarization of the excitation and probe beams was set to the magic angle (54.7°). For all measurements, a 2 mm path length quartz cuvette was used. The sample was mixed by a micro stirrer to prevent degradation of the sample during the measurements. To keep the excitation intensity at ∼1014 photons pulse^{-1} cm^{-2}, a neutral-density filter was used. All measurements were carried out at room temperature.

The collected data were fitted globally using the software DAFit (Pascher Instruments, Lund, Sweden). To visualize the excited-state dynamics, we assume that the excited states evolves according to a sequential, irreversible scheme, in which the extracted time constants correspond to lifetimes of the individual excited-state species in the sequential scheme. The spectral profile of each species is called evolution-associated difference spectrum (EADS).

*Computational details***.** The geometries of the ground states of carotenoids were optimized with standard ground-state density functional theory (DFT) [P4.42] using the Becke3−Lee−Yang−Parr (B3LYP) [P4.43] with the 6-31G(d,p) basis set. Vertical transition energies were calculated by means of time-dependent density

functional theory within the Tamm−Dancoff approximation (TD-DFT/TDA) [P4.44] using the hybrid exchange−correlation functional (Cam-B3LYP) [P4.45] with the TZVP [P4.46] basis set which is larger than the commonly used 6-31G(d,p) basis set. Calculations were carried out in the gas phase. All quantum chemical computations were performed by Gaussian09 software package [P4.47], while Gauss View 5.0.8 was used for visualization of the structures. Classical molecular dynamics (MD) simulations were performed with general AMBER force field (GAFF) [P4.48] with Gromacs package [P4.49].

3.4.4   Results

Absorption spectra of Fx, Ifx and Ifx-l are compared in nonpolar and polar solvent in Figure 3.4.2a and Figure 3.4.2b. Diethyl ether was used as a nonpolar solvent due to very low solubility of Ifx in nonpolar solvents. Diethyl ether was the least polar solvent in which we could reach concentrations required for experiments. The vibronic structure of the S_0-S_2 transition is visible in both solvents, though in polar acetonitrile the resolution of vibrational bands is diminished. The preserved vibronic structure even in the polar solvent allows to readily read the energy of the S_2 state, which is given by the 0-0 band of the S_0-S_2 transition. In diethyl ether, the S_2 energies of Fx and Ifx are essentially identical, with the 0-0 band peaking at 470 nm. The 0-0 band of Ifx-l is shifted to ~495 nm, indicating longer conjugation length in comparison with Fx and Ifx. In the polar solvent acetonitrile there is slight difference between absorption maxima of Fx and Ifx. While the 0-0 band of Fx remains unchanged (470 nm) when switching from diethyl ether to acetonitrile, for Ifx the 0-0 band in polar acetonitrile is red-shifted to 473 nm. Structure of vibrational bands of Ifx-l is nearly gone in acetonitrile, but it is still possible to determine the position of the 0-0 band at ~495 nm. Thus, no significant shift of the S_2 energy is observed for Ifx-l upon change of solvent polarity.
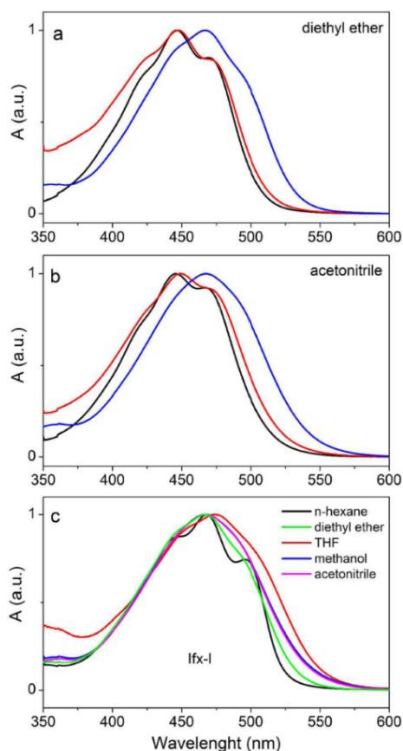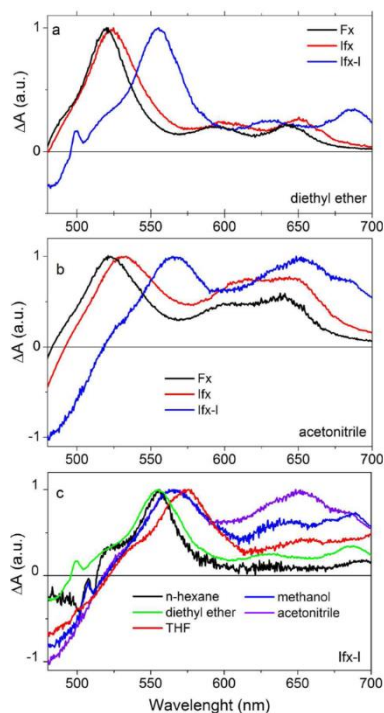
Figure 3.4.2 Normalized absorption spectra of Fx, Ifx and Ifx-l. (a) Comparison of absorption spectra of Fx (black), Ifx (red) and Ifx-l (blue) in the non-polar solvent diethyl ether. (b) Comparison of absorption spectra of Fx (black), Ifx (red) and Ifx-l (blue) in the polar solvent acetonitrile. (c) Absorption spectra of Ifx-l in various solvents.

To study the influence of solvent polarity on spectroscopic properties of Ifx-l in more detail, the carotenoid was dissolved in various other solvents and absorption spectra of these samples are shown Figure 3.4.2c. Ifx-l exhibits typical polarity-dependent behavior known for a number of other carbonyl carotenoids. Vibrational structure diminishes with increasing polarity and characteristic asymmetric broadening towards longer wavelengths is observed. The S_2 energy remains essentially untouched by solvent polarity, though the vibrational bands broaden with increasing polarity, resulting in the characteristic decrease of resolution of vibrational bands in polar solvents. In tetrahydrofuran (THF), we observe ~7 nm red-shift of the whole absorption spectrum due to high polarizability of THF. In contrast to other carbonyl carotenoids such as peridinin or astaxanthin whose absorption spectra in polar solvents are completely featureless [P4.18], [P4.19], [P4.26], Ifx-l retains certain resolution of vibrational bands even in the most polar solvents. The observed polarity-dependent behavior is a clear indicator that Ifx-l must contain a conjugated carbonyl group.

Transient absorption spectra of all samples are shown in Figure 3.4.3. The differences among the three carotenoids and their response to solvent polarity observed in steady-state absorption (Figure 3.4.2) are further enhanced in transient absorption. The transient absorption spectra were recorded in the visible spectral region, 480-700 nm, where the characteristic features of the S_1/ICT state of carbonyl carotenoids can be monitored. The most prominent feature in all transient spectra is the excited-state absorption band peaking in the 520-560 nm region. This band is attributed to an S_1-S_n transition [P4.7] and is most pronounced in nonpolar solvents. The bands in the 600-700 nm region are much more sensitive to polarity, and they are usually attributed to an ICT-S_n transition [P4.7], [P4.18], [P4.19]. Since the precise nature of the lowest excited state of carbonyl carotenoids remains unknown and a few hypotheses were proposed [P4.32], [P4.50], [P4.51], these two bands are often denoted as S_1-like and ICT-like due to the similarity of the former to the standard S_1-S_n transition of non-carbonyl carotenoids and polarity-dependent

Figure 3.4.3 Transient absorption spectra of Fx, Ifx and Ifx-l measured 1 ps after excitation at 480 nm (Fx and Ifx) or 510 nm (Ifx-l). Transient absorption spectra of Fx, Ifx, and Ifx-l in diethyl ether (a), and in acetonitrile (b), and transient absorption spectra of Ifx-l in various solvents (c).

behavior of the latter. While the absorption spectra of Fx and Ifx are nearly identical in diethyl ether (Figure 3.4.2a), their transient absorption spectra depicted in Figure 3.4.3a are distinct. The S_1-S_n transition of Fx peaks at 520 nm while it is red-shifted to 525 nm for Ifx. Moreover, the S_1-Sn band of Ifx is slightly broader indicating larger conformation disorder in the S_1/ICT state for Ifx. The small red-shift and broadening is also manifested in the two clearly-pronounced ICT bands which peak at 594 and 643 nm (Fx) and at 600 and 650 nm (Ifx). As for absorption spectra, Ifx-l exhibits significant red shift compared to Fx and Ifx; its S_1-S_n band has maximum at 555 nm, the ICT bands have their maxima at 630 and 686 nm.
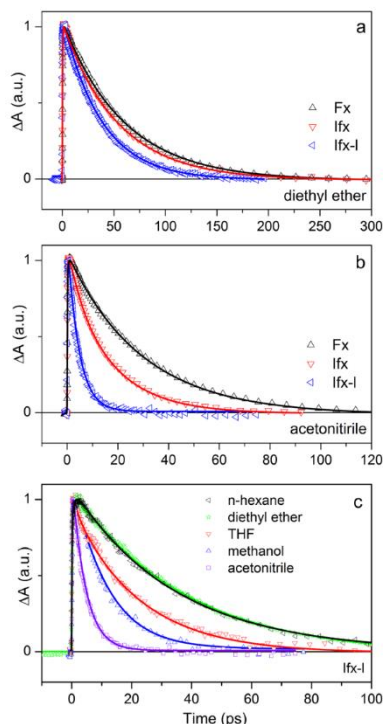
Figure 3.4.4 Kinetics recorded at the S_1-like maxima of the transient absorption spectra of Fx, Ifx, and Ifx-l. Comparison of kinetics for different carotenoids in diethyl ether (a), acetonitrile (b) and comparison of Ifx-l kinetics in various solvents (c). All kinetics are normalized to maximum, excitation wavelengths were 480 nm (Fx and Ifx) or 510 nm (Ifx-l). Solid lines are fits.

In the polar acetonitrile (Figure 3.4.3b), the S_1-S_n bands of all three carotenoids are broadened and slightly shifted to longer wavelengths with maxima located at 523 nm (Fx), 531 nm (Ifx), and 564 nm (Ifx-l). Increasing polarity led to an increase of the ratio of amplitudes of the S_1-like and ICT-like bands. While in diethyl ether the S_1-like bands dominated the transient spectrum, switching to acetonitrile made the intensities of the ICT-like bands comparable to the S_1-S_n bands. It is known that the ICT-to-S_1 intensity ratio monitors the degree of the charge transfer character of the S_1/ICT state. For the carbonyl carotenoids with the most pronounced polarity dependence this ratio can be even larger than one [P4.18]-[P4.20], [P4.29]. Thus, transient absorption spectra shown in Figure 3.4.3b would indicate that the S_1/ICT state exhibits increased charge transfer character according to Fx < Ifx < Ifx-l. For Ifx-l in acetonitrile, the ICT-like band has the same intensity as the S_1-like band, suggesting strong polarity-dependent behavior. This is a rather surprising observation, because it is known that for carbonyl carotenoids with similar structure the degree of charge transfer character of the

S_1/ICT state increases with shortening the conjugation length [P4.28], [P4.29], [P4.30]. Here, Ifx-l, which must have a longer conjugation length than Fx and Ifx as evidenced by both absorption and transient absorption spectra, exhibits stronger charge transfer character of the S_1/ICT state.

Figure 3.4.3c compares transient absorption spectra of Ifx-l in a few solvents with different polarity. It is obvious that three polarity-dependent effects can be traced in the figure. First, the S_1-S_n band broadens with increasing polarity, mirroring the polarity effects on the S_0-S_2 transition (Figure 3.4.2c). Second, the maximum of the

S_1-S_n band shifts to longer wavelengths. This results from comparison of S_1-S_n peaks in *n*-hexane and methanol (or acetonitrile) which have comparable polarizability. The peak is shifted from 555 nm (*n*-hexane and diethyl ether) to 565 nm (methanol and acetonitrile). In THF, which has moderate polarity, the S_1-S_n band is shifted even further to 575 nm, but this shift is induced by large polarizability of THF. Third, the magnitude of the ICT bands increases with polarity. While in *n*-hexane no ICT bands are observed, in acetonitrile they have intensity compared to the S_1-like transition. Interestingly, there is a significant increase of ICT band intensity when going from methanol to acetonitrile. Although acetonitrile has slightly larger polarity than methanol (Table 3.4.1), only mild differences in transient absorption spectra measured in these two solvents were observed for other carbonyl carotenoids such as peridinin or apo-carotenals [P4.17], [P4.18], [P4.20].

Table 3.4.1. S_1/ICT Lifetimes of Ifx-l in Various Solvents.

Solvent	Polarity P(ε)[a]	S_1/ICT lifetime (ps)
n-hexane	0.229	42
diethyl ether	0.526	37
tetrahydrofuran	0.687	22
2-propanol	0.852	19
acetone	0.868	9
methanol	0.913	11
acetonitrile	0.921	4

a) polarity factor calculated from dielectric constant as $P(\varepsilon) = (\varepsilon-1)/(\varepsilon+2)$

The increased degree of charge transfer character of the S_1/ICT state is usually accompanied by changes in the S_1/ICT lifetime. Figure 3.4.4 shows kinetics measured at the S_1-Sn maxima of all three carotenoids in various solvents. Since the S_1-like and ICT bands in most cases decay with the same time constant [P4.18], [P4.19], [P4.21], [P4.29], the kinetics measured at the maximum of the S_1-like band monitors dynamics of the S_1/ICT state, as further evidenced by global fitting (see below). In the nonpolar diethyl ether, the lifetimes of Fx, Ifx and Ifx-l are 60, 53 and 37 ps, respectively. The shortening of the S_1 lifetime in the nonpolar solvent reflects the change of effective conjugation length of the carotenoids, further confirming that while one additional C=C bond of Ifx compared to Fx does not affect much the effective conjugation, Ifx-l must have markedly longer effective conjugation length. As for the magnitude
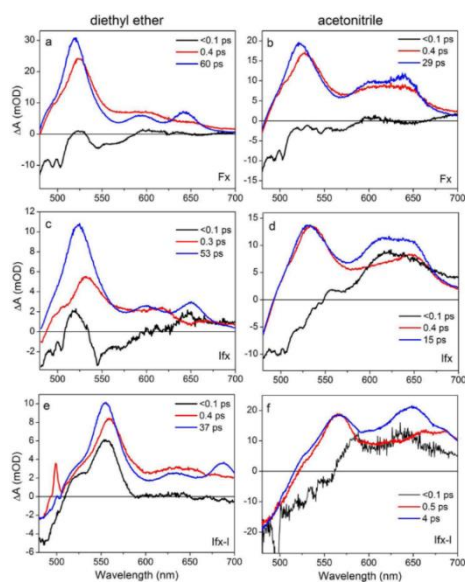
Figure 3.4.5 EADS obtained from global fitting the transient absorption data measured for Fx, Ifx, and Ifx-l in diethyl ether (a, c and e) and in acetonitrile (b, d and f).

of the ICT bands in transient absorption spectra, the polarity effect on the S_1/ICT lifetime increases in a series Fx < Ifx < Ifx-l. In acetonitrile, the S_1/ICT lifetime is shortened to 29 ps (Fx), 17 ps (Ifx), and even to 4 ps for Ifx-l. Thus, for Ifx-l the S_1/ICT lifetime is shortened by one order of magnitude when going from diethyl ether to acetonitrile, further underscoring the large polarity effect on excited-state properties of this carotenoid. Global analysis shown in Figure 3.4.5 demonstrates that the S_1/ICT lifetimes are the same in the spectral regions associated with S_1-like and ICT-bands. Also, a subpicosecond time component of 0.3-0.5 ps is detected in all datasets. In diethyl ether the spectral shape of this component corresponds to a hot S_1 state and, therefore, reflects vibrational cooling in the S_1 state [P4.52], [P4.53]. In polar solvent it rather reflects stabilization of the ICT state as it is pronounced only in the ICT-like band. Figure 3.4.4c demonstrates the dependence of the S_1/ICT lifetime of Ifx-l on polarity. There is almost no change in the S_1/ICT lifetime between *n*-hexane and diethyl ether, which may justify using the diethyl ether as a nonpolar solvent. With further increase of solvent polarity the S_1/ICT lifetime of Ifx-l decreases to 22 ps in THF, to 11 ps in methanol, and further to 4 ps in acetonitrile. The S_1/ICT lifetimes in various solvents are summarized in Table 3.4.1.

The most surprising observation is the large difference between the S_1/ICT lifetimes of Ifx-l in methanol and acetonitrile. Since earlier studies reported also different S_1/ICT lifetimes of Fx, yielding 18-23 ps in methanol [P4.18], [P4.21], [P4.28], [P4.32], [P4.33] and 30-35 ps in acetonitrile [P4.18], [P4.19], we have compared dynamics of all three carotenoids in these two polar solvents. The results are shown in Figure 3.4.6. Indeed, data confirm the different S_1/ICT lifetimes of Fx in polar, but aprotic, acetonitrile and in both polar and protic methanol. The decay of the S_1/ICT state is markedly slower in acetonitrile, at 29 ps as compared to 19 ps in methanol. Interestingly, this change

in the S_1/ICT lifetime is not mirrored in transient absorption spectra measured in methanol and acetonitrile; they are nearly identical. For Ifx, a carotenoid which has not been studied by time-resolved spectroscopy so far, the trend is the same though the difference is smaller than for Fx; the S_1/ICT lifetime is 13 ps in methanol and 17 ps in acetonitrile. Transient absorption spectra have a comparable shape in both solvents, but the spectrum of Ifx in methanol is slightly red-shifted. Finally, for Ifx-l the S_1/ICT lifetime exhibits opposite dependence on solvent proticity, as it is markedly shorter in aprotic acetonitrile (4 ps) than in protic methanol (11 ps). The different response of Ifx-l in these two
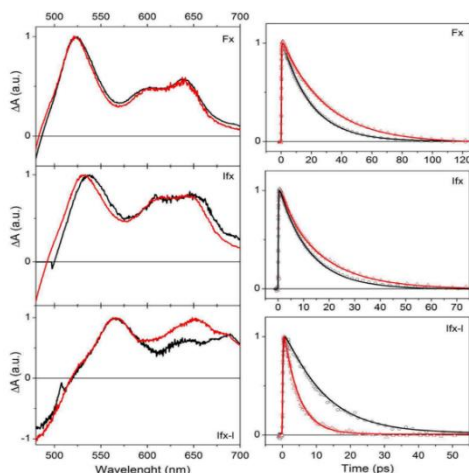
Figure 3.4.6 Comparison of transient absorption spectra at 1 ps (left column) and kinetics measured at the maximum of the S_1-like transition (right column) for Fx, Ifx and Ifx-l in methanol (black) and acetonitrile (red). All data are normalized to maximum. Solid lines are fits. Excitation wavelength were 480 nm (Fx and Ifx) or 510 nm (Ifx-l).
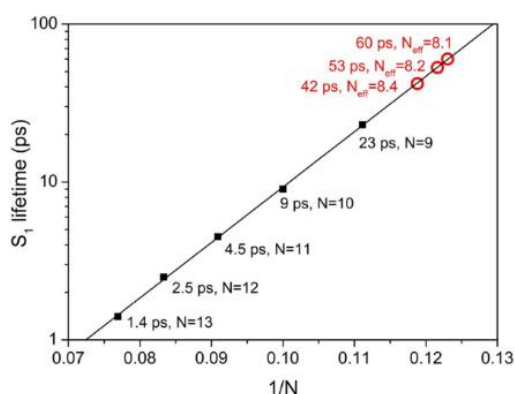
solvents is underscored by changes in transient absorption spectra. These results show that a solvent's ability to form hydrogen bonds is crucial for determining the excited state properties of Ifx-l in polar solvents. This is further demonstrated by measurements of the S_1/ICT lifetime of Ifx-l in 2-propanol and acetone (Table 3.4.1) resulting in lifetimes of 19 and 9 ps, respectively. Thus, even though polarity of methanol is larger than that of acetone, the S_1/ICT lifetime of Ifx-l in acetone (9 ps) is shorter than in methanol (11 ps). Clearly, protic alcohols make the S_1/ICT lifetime longer than aprotic solvents with comparable polarity.

3.4.5 Discussion

Transient absorption data confirms the prediction reported by Moore et al. [P4.39] that Ifx-l must have longer conjugation length than Ifx. Both position of the S_1-S_n band and lifetime of the S_1/ICT state indicate a conjugation length markedly longer than that of Ifx. On the basis of comparison with other carotenoids we may estimate the effective conjugation length, *N*eff [P4.54], [P4.55]. For carotenoids containing conjugated carbonyl group, the S_2 energy extracted from absorption spectrum is not suitable for determining *N*eff, because carbonyl carotenoids have usually lower S_2

energy than their non-carbonyl counterparts, and this effect is independent of solvent polarity [P4.19]. Instead, the S_1/ICT lifetime in nonpolar solvent is better parameter to estimate *Neff* as the behavior of the S_1/ICT state of carbonyl carotenoids in nonpolar solvents is comparable to that of the S_1 state of non-carbonyl carotenoids [P4.18], [P4.19].

A comparison of the S_1/ICT lifetimes of Fx, Ifx, and Ifx-l in diethyl ether with known S_1 lifetimes of linear carotenoids is shown in Figure 3.4.7. It is clear that when the S_1 lifetimes of linear carotenoids are plotted on a logarithmic scale vs. $1/N$, they can be fitted by a linear function. Placing the S_1/ICT lifetimes in nopolar solvents of the carotenoids studied here on this graph results in *N*eff values of 8.5 for Ifx-l, 8.2 for Ifx, and 8.1 for Fx. *N*eff values suggest that extension of the conjugated system of Fx by one extra C=C bond located beyond the conjugated C=O group (Ifx, see Figure 3.4.1) leaves *Neff* almost unaffected. This is in line with observation of the essentially identical S_2 energies of Fx and Ifx (Figure 3.4.2) as well as with the mild difference in energy of the S_1-S_n transition in diethyl ether for these two carotenoids shown in Figure 3.4.3. In contrast, there must be structural feature in Ifx-l that extends *Neff*. Even though our estimation gives the prolongation of *Neff* by

Figure 3.4.7 Dependence of the S_1 lifetimes on conjugation length. Black symbols denote the S_1 lifetimes of linear carotenoids in *n*-hexane plotted against $1/N$. The solid line is a linear fit to the S_1 lifetimes of linear carotenoids. Red circles show the S_1/ICT lifetimes of fucoxanthin, and isofucoxanthin-like carotenoid in a non-polar solvent. Placing these lifetimes on the black line allows to determine the effective conjugation length, N_{eff}, of these carotenoids. Each point is labeled by a corresponding S_1 (or S_1/ICT) lifetime and N (or N_{eff}).

about ~0.5 when going from Fx to Ifx-l, for carotenoids with *Neff* < 10 such seemingly small changes in effective conjugation markedly affect the spectroscopic properties.

All three carotenoids exhibit typical polarity-dependent behavior characteristic of carbonyl carotenoids. Their S_1/ICT lifetimes become shorter in polar solvents and ICT-bands in the 600-700 nm spectral region gain intensity with increasing polarity. The magnitude of the polarity-induced effect is, however, different. The S_1/ICT lifetime of Ifx-l in polar acetonitrile is 4 ps, being the shortest

S_1/ICT lifetime in solution reported so far. For most carbonyl carotenoids studied so far, the S_1/ICT lifetime in the most polar solvents converges to values of 8-10 ps [P4.20], [P4.29], independent of their S_1/ICT lifetimes in nonpolar solvent. Moreover, the polarity-induced effects usually diminishes with increase of conjugation length. This is especially obvious when comparing a set of carbonyl carotenoids with identical structure but different conjugation lengths, such as β-apo-carotenals [P4.20], peridinin [P4.29], [P4.30] or Fx [P4.28] analogs. The magnitude of the ICT-like band, which reflects the degree of a charge transfer character of the S_1/ICT state [P4.18], [P4.19], [P4.28]-[P4.30], always increases with decrease of conjugation length for carbonyl carotenoids in solution.

Here, although Ifx-l has the longest conjugation of the carotenoids reported here, it exhibits largest magnitude of the polarity-induced effects. The S_1/ICT lifetime shortens from 40 ps in *n*-hexane to 4 ps in acetonitrile (Figure 3.4.4c), and the magnitude of the ICT-like band is also the largest (Figure 3.4.3b). Even in absorption spectra, the loss of vibrational structure of the S_0-S_2 transition in polar solvents, which is another characteristic polarity-induced effect, is most pronounced for Ifx-l (Figure 3.4.2). This implies that Ifx-l cannot be a longer version of Ifx. To achieve enhanced response to polarity, Ifx-l must have different structure of the conjugated chain than Fx and Ifx. Since the polarity-dependent behavior is driven by the conjugated carbonyl group, the expected differences in structure most likely involve the conjugated carbonyl group.

Qualitative difference between Ifx-l and Ifx (Fx) is further underscored by different response of Ifx-l to solvent proticity. For Fx and Ifx the hydrogen-bonding solvent methanol produces the S_1/ICT lifetime that is shorter than in aprotic solvent acetonitrile, but Ifx-l exhibits opposite response to proticity (Figure 3.4.6). The S_1/ICT lifetimes in protic methanol and aprotic acetonitrile reported in literature for various carbonyl carotenoids are summarized in Table 3.4.2. According to data in Table 3.4.2, we can divide carbonyl carotenoids into three groups. The first group contains apo-carotenals, for which the conjugated carbonyl group terminates the conjugated system, do not exhibit any effect of solvent proticity; the S_1/ICT lifetimes are the same in methanol and acetonitrile regardless the conjugation length. In the second group are Fx, Ifx and uriolide acetate. These carotenoids have their S_1/ICT lifetimes shorter in methanol than in acetonitrile. Moreover, the difference between the S_1/ICT lifetime in protic and aprotic solvent increases with decrease of conjugation length. The carbonyl group of the carotenoids from the second group is

also at the end of the conjugated system, but it is positioned in s-cis configuration in respect to the main conjugation (see Figure 3.4.9, Supporting Information for structure of uriolide acetate). For Ifx, the conjugated C=O group is not truly at the end of the conjugated system (see Figure 3.4.1), but the extra C=C bond beyond the carbonyl group has minimal effect on spectroscopic properties. The third group involves peridinins and Ifx-l. Only these carotenoids have the S_1/ICT lifetime shorter in aprotic acetonitrile. In this group, the difference between the S_1/ICT lifetime in protic and aprotic solvent increases with increasing effective conjugation. The characteristic structural feature in peridinins is presence of a lactone ring through which the carbonyl group is attached asymmetrically to the main conjugated backbone (Figure 3.4.9 Supporting Information). It must be noted that uriolide acetate, which exhibits opposite response to solvent proticity, has also a lactone ring, but attached in a way that places the carbonyl group at the end of the conjugated system (Figure 3.4.9, Supporting Information). Thus, only if the conjugated carbonyl group at the lactone ring does not terminate the conjugated system, we observe behavior typical for the third group.

Thus, it is tempting to conclude that Ifx-l contains a lactone ring positioned in a way comparable to that of peridinin. In fact, C39-peridinin (C39P), explored in detail by Niedzwiedzki et al. [P4.29], [P4.30], [P4.56], exhibits spectroscopic properties closest to those reported here for Ifx-l. The S_1/ICT lifetimes of C39P are 40, 10 and 6 ps in n-hexane, methanol and acetonitrile, respectively, while for Ifx-l these values yield 40, 11 and 4 ps. Moreover, the S_2 energies in n-hexane, ~20,000 cm-1 (C39P) and 20,200 cm^{-1} (Ifx-l), underscore the spectroscopic similarity of C39P and Ifx-l. Then, naturally, a question arises: could the unknown carotenoid in *Chromera velia* actually be the C39P? The answer is no for the reasons given below.

First, there is a difference in maxima of the S_1-S_n bands in n-hexane that peak at 540 nm (C39P) and 555 nm (Ifx-l). Second, the detailed mass spectroscopy studies carried out by Moore et al. [P4.39] rules out C39P as a candidate for Ifx-l. The major differences between C39P and Ifx-l are the following. 1) The molecular mass of Ifx-l is 658.42167, corresponding to a composition of $C_{42}H_{58}O_6$ while composition of C39P is $C_{41}H_{52}O_7$; 2) Ifx-l does not contain an epoxy group. On the other hand, it is known that the part of the molecule containing the allene group and the terminal ring attached to the allene is the same for Fx, Ifx, Ifx-l, and C39P [P4.39].

Table 3.4.2 Lifetimes of S_1/ICT States (in picoseconds) for Various Carbonyl Carotenoids in *n*-hexane, methanol and acetonitrile.[a]

carotenoid	*n*-hexane	methanol	acetonitrile	Reference
12′-apo-β-carotenoic acid	200	58	56	[P4.23]
12'-apo-β-carotenal	200	7	8	[P4.20]
8'-apo-β-carotenal	25	8	8	[P4.20], [P4.51]
uriolide acetate	70	26	46	[P4.18]
fucoxanthin	60	20	30	[P4.18][P4.19][P4.21]
isofucoxanthin	53	13	17	*This work*
C35-peridinin	> 1000	12	11	[P4.29][P4.30]
peridinin	160	10	8	[P4.17][P4.18][P4.19] [P4.29] [P4.30]
C39-peridinin	40	10	6	[P4.29][P4.30]
isofucoxanthin-like	37	11	4	*This work*

a) The S_1/ICT lifetimes of peridinin, fucoxanthin, 12'-apo-β-carotenal and 8'-apo-β-carotenal represent mean values obtained from various experiments.

It is, however, obvious that Ifx-l should share certain structural features with C39P due to their common specific response to solvent proticity. To evaluate the effect of solvent on local structure of Fx, Ifx, and C39P, molecular dynamics (MD) simulations have been performed. MD simulations of all three carotenoids in methanol and acetonitrile showed that in all cases the carbonyl group is solvated though in the case of methanol long-lived hydrogen bonds appear between the carotenoid C=O group and OH groups of methanol. In order to understand this effect further, we performed *ab initio* DFT calculations with B3LYP/CC-PVDZ level of theory to calculate the interaction energies of C39P-acetonitrile and Fx-acetonitrile complexes (Figure 3.4.8, Supporting Information). Calculated interaction energies are -2.75 kcal/mol for Fx complex and -3.02 kcal/mol for C39P complex. The stability of complexes is achieved through dispersion interaction and non-standard hydrogen bonding [P4.57]. Such hydrogen bonds were also reported in solutions of acetonitrile with benzene, acetone and dimethylsulphoxide [P4.58]. Thus, even though the aprotic acetonitrile cannot make standard hydrogen bonds with C=O group, DFT calculations proved the existence of non-standard hydrogen bonds in acetonitrile. The lifetime and strength of hydrogen bonding between solvent and C=O group can be further influenced by intramolecular interactions. MD simulations showed that in the structure of Ifx there is a potential for intramolecular hydrogen bond between the OH

group attached to carbon C1 and the C=O group, which may make the hydrogen bonding between the C=O group and solvent molecules less frequent.
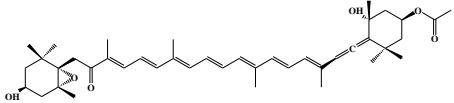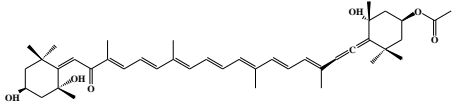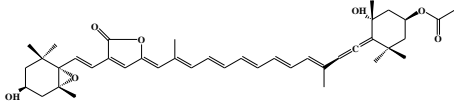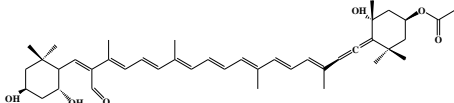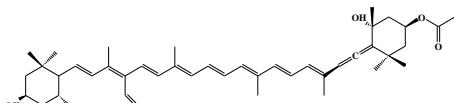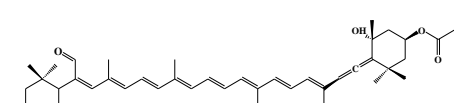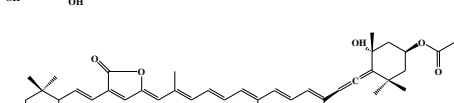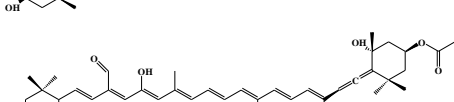
Thus, both experimental data and calculations indicate that the different response of carbonyl carotenoids to solvent proticity is related to presence of a lactone ring. Only carbonyl carotenoids with a lactone ring whose C=O group does not terminate the conjugated system have the S_1/ICT lifetime shorter in acetonitrile than in methanol. DFT calculations indicate that this could be related to stronger non-standard hydrogen bonds formed between acetonitrile and C=O group located at the lactone ring. Moreover, intramolecular hydrogen bonding may play its role by diminishing formation of hydrogen bonds with methanol as it is in case of Ifx.

We have used this knowledge to construct a series of hypothetical structures denoted as Models 1-5 (Table 3.4.3). For these molecules, quantum chemical calculations were used to compute the S_2 energy to find out whether it matches the S_2 energy of C39P and Ifx-l. The calculations provide energies of vertical S_0-S_2 transition in vacuum so they do not reproduce the experimental values, but they can monitor shifts of the S_2 energy induced by changes in structure. To test this, we have calculated the S_2 energies of Fx, Ifx and C39P. The calculations fairly reproduce the nearly identical S_2 energies of Fx and Ifx, confirming that position of the one extra C=C group of Ifx does not significantly prolong the effective conjugation length. The calculated S_2 energy of C39P is down-shifted by 1180 cm^{-1} from that of Ifx, which reasonably matches the measured ~900 cm^{-1}.

The Models 1 and 2 are just slight modifications of Ifx structure, which is taken as the basis for the structure of Ifx-l [P4.39]. Model 1 retains the possibility of intramolecular hydrogen bond identified in Ifx, but the calculations show that neither Model 1 nor Model 2 downshift the S_2 energy thus cannot be taken as a possible structure of Ifx-l. Model 3, which puts the conjugated carbonyl group at the end of the conjugated system induces the desirable shift of the S_2 energy. Yet, placing the carbonyl group at the end of the conjugation should produce different response to proticity than observed for Ifx-l as evidenced by data in Table 3.4.3. Model 4 introduces the lactone ring into the structure and this feature induces the correct shift

Table 3.4.3. Molecular structures of fucoxanthin, isofucoxanthin and C39P together with five modelled structures and their calculated S_0-S_2 energies.

molecular structure	name chemical formula	S_0-S_2	
		nm	cm^{-1}
	Fucoxanthin $C_{42}H_{58}O_6$	399	25 062
	Isofucoxanthin $C_{42}H_{58}O_6$	402	24 875
	C_{39} Peridinin $C_{41}H_{52}O_7$	422	23 696
	Model 1 $C_{42}H_{58}O_6$	397	25 188
	Model 2 $C_{42}H_{58}O_6$	396	25 252
	Model 3 $C_{42}H_{58}O_6$	416[a] 413[b]	24 038 24 213
	Model 4 $C_{42}H_{56}O_6$	424	23 585
	Model 5 $C_{42}H_{58}O_6$	423	23 641

[a] cis conformation. [b] trans conformation.

of the S_2 energy. However, the structure with lactone ring has an incorrect composition of $C_{42}H_{56}O_6$, so further modifications are needed. Opening the lactone ring (Model 5) then gives the correct S_2 energy and correct chemical formula. Attaching the conjugated carbonyl group via one of the methyls is known to generate large polarity-induced effects as evidenced by report on bacteriorubixanthinal [P4.59];

thus, even the structure with opened lactone ring is expected to likely lead to spectroscopic behavior observed here for Ifx-l.

The different response to solvent proticity of Fx, Ifx, and Ifx-l is another interesting feature of carbonyl carotenoids which has not been addressed earlier although the different S_1/ICT lifetimes in methanol and acetonitrile were reported earlier for Fx [P4.18], [P4.19], [P4.28]. The experimental and theoretical results presented here helped to estimate structure of the unknown carotenoid from CLH complexes of *Chromera velia*. The specific response of Ifx-l to solvent proticity, the S_1/ICT lifetime being markedly shorter in polar aprotic solvent than in a protic one, and comparison of data with spectroscopic properties of known carotenoid structures reported earlier showed that a 'hybrid' structure somewhere between Ifx and C39P should be expected for Ifx-l. Final structure elucidation will require detailed NMR or X-ray diffraction studies. So far, the amount of purified Ifx-l was not enough to obtain reliable NMR data, preventing us from determining final structure of Ifx-l.

3.4.6 Acknowledgment

3.4.7 References

[P4.1]   Polívka, T.; Frank, H. A. Molecular Factors Controlling Photosynthetic Light-Harvesting by Carotenoids. *Acc. Chem. Res.* 2010, *43*, 1125–1134.

[P4.2]   Croce, R.; van Amerongen, H. Natural Strategies for Photosynthetic Light Harvesting. *Nat. Chem. Biol.* 2014, *10*, 492-501.

[P4.3]   Ruban, A.V.; Johnson, M. P.; Duffy, C. D. P. The Photoprotective Molecular Switch in the Photosystem II Antenna, *Biochim. Biophys. Acta* 2012, *1817*, 167-181.

[P4.4]   Jahns, P.; Holzwarth, A. R. The Role of the Xanthophyll Cycle and of Lutein in Photoprotection of Photosystem II. *Biochim. Biophys. Acta* 2012, *1817*, 182-193.

[P4.5]   Stahl, W.; Sies, H. Antioxidant Activity of Carotenoids. *Molecular Aspects of Medicine* 2003, *24*, 345-351.

[P4.6]   Edge, R.; Truscott, T. G. Carotenoid Radicals and the Interaction of Carotenoids with Active Oxygen Species. In *The Photochemisry of*

Carotenoids; Frank, H. A; Young, A. J; Britton, G.; Cogdell, R. J.; Eds. Kluwer Academic Publishers, Dordrecht 1999, p. 223-234.

[P4.7]   Polívka, T.; Sundström, V. Ultrafast Dynamics of Carotenoid Excited States. From Solution to Natural and Artificial Systems. *Chem. Rev.* 2004, *104*, 2021–2071.

[P4.8]   Polívka T.; Sundström, V. Dark Excited States of Carotenoids: Consensus and Controversy. *Chem. Phys. Lett.*, 2009, *477*, 1–11.

[P4.9]   Christensen, R. L.; Enriquez, M. M.; Wagner, N. L.; Peacock-Villada, A. Y.; Scriban, C.; Schrock, R. R.; Polívka, T.; Frank, H. A.; Birge, R. R. Energetics and Dynamics of the Low-Lying Electronic States of Constrained Polyenes: Implications for Infinite Polyenes. *J. Phys. Chem. A* 2013, *117*, 1449-1465

[P4.10] Christensen, R. L. The Electronic States of Carotenoids. In *The Photochemistry of Carotenoids*; Frank, H. A., Young, A. J., Britton, G., Cogdell, R. J., Eds.; Kluwer Academic Publishers: Dordrecht, The Netherlands, 1999; Vol. 8, pp 137−159.

[P4.11] Ruban, A. V.; Berera, R.; Ilioaia, C.; van Stokkum, I. H. M.; Kennis, J. T. M.; Pascal, A. A.; van Amerongen, H.; Robert, B.; Horton, P.; van Grondelle, R. Identification of a Mechanism of Photoprotective Energy Dissipation in Higher Plants. *Nature* 2007, *450*, 575-578.

[P4.12] Staleva, H.; Komenda, J.; Shukla, M. K.; Šlouf, V.; Kaňa, R.; Polívka, T.; Sobotka, R. Mechanism of Photoprotection in the Cyanobacterial Ancestor of Plant Antenna Proteins. *Nat. Chem. Biol.* 2015, *11*, 287-291.

[P4.13] Polívka,T.; Pullerits,T.; Frank,H.A.; Cogdell,R.J.; Sundström,V. Ultrafast Formation of a Carotenoid Radical in LH2 Antenna Complexes of Purple Bacteria. *J. Phys. Chem. B* 2004, *108*, 15398- 15407.

[P4.14] Maiuri, M.; Polli, D.; Brida, D.; Luer, L.; LaFountain, A.M.; Fuciman, M.; Cogdell, R.J.; Frank, H.A.; Cerullo, G. Solvent-Dependent Activation of Intermediate Excited States in the Energy Relaxation Pathways of Spheroidene. *Phys. Chem. Chem. Phys.* 2012, *14*, 6312–6319.

[P4.15] Buckup, T.; Motzkus, M. Multidimensional Time-Resolved Spectroscopy of Vibrational Coherence in Biopolyenes. *Annu. Rev. Phys. Chem.* 2014, *65*, 39-57.

[P4.16] Balevičius, V.; Pour, A. G.; Savolainen, J.; Lincoln, C. N.; Lukeš, V.; Riedle, E.; Valkunas, L.; Abramavicius, D.; Hauer, J. Vibronic Energy Relaxation Approach Highlighting Deactivation Pathways in Carotenoids. *Phys. Chem. Chem. Phys.* 2015, *17*, 19491-19499.

[P4.17] Bautista, J. A.; Connors, R. E.; Raju, B. B.; Hiller, R. G.; Sharples, F. P.; Gosztola, D.; Wasielewski, M. R.; Frank, H. A. Excited State Properties of Peridinin: Observation of a Solvent Dependence of the Lowest Excited Singlet State Lifetime and Spectral Behavior Unique Among Carotenoids. *J. Phys. Chem. B* 1999, *103*, 8751-8758.

[P4.18] Frank, H.A.; Bautista, J.A.; Josue, J.; Pendon, Z.; Hiller, R.G.; Sharples, F.P.; Gosztola, D.; Wasielewski, M.R. Effect of the Solvent Environment on the

Spectroscopic Properties and Dynamics of the Lowest Excited States of Carotenoids. *J. Phys. Chem. B* 2000, *104*, 4569–4577.

[P4.19] Zigmantas, D.; Hiller, R.G.; Sharples, F.P.; Frank, H.A.; Sundström, V.; Polívka, T. Effect of a Conjugated Carbonyl Group on the Photophysical Properties of Carotenoids. *Phys. Chem. Chem. Phys.* 2004, *6*, 3009–3016.

[P4.20] Kopczynski, M.; Ehlers, F.; Lenzer, T.; Oum, K. Evidence for an Intramolecular Charge Transfer State in 12'-apo-□-caroten-12'-al and 8'-apo-β-caroten-8'-al: Influence of Solvent Polarity and Temperature. *J. Phys. Chem. A* 2007, *111*, 5370–5381.

[P4.21] Kosumi, D.; Kusumoto, T.; Fujii, R.; Sugisaki, M.; Iinuma, Y.; Oka, N.; Takaesu, Y.; Taira, T.; Iha, M.; Frank, H. a; et al. Ultrafast Excited State Dynamics of Fucoxanthin: Excitation Energy Dependent Intramolecular Charge Transfer Dynamics. *Phys. Chem. Chem. Phys.* 2011, *13*, 10762–10770.

[P4.22] Di Donato, M.; Ragnoni, E.; Lapini, A. Foggi, P.; Hiller, R. G.; Righini, R. Femtosecond Transient Infrared and Stimulated Raman Spectroscopy Shed Light on the Relaxation Mechanism of Photoexcited Peridinin. *J. Chem. Phys.* 2015, *142*, 212409.

[P4.23] Stalke, S.; Wild, D. A.; Lenzer, T.; Kopczynski, M.; Lohse, P. W.; Oum, K. Solvent-Dependent Ultrafast Internal Conversion Dynamics of n'-apo-□-carotenoic-n'-acids (n=8, 10, 12). *Phys. Chem. Chem. Phys.* 2008, *10*, 2180-2188.

[P4.24] Chábera, P.; Fuciman, M.; Hříbek, P.; Polívka, T. Effect of Carotenoid Structure on Excited State Dynamics of Carbonyl Carotenoids. *Phys. Chem. Chem. Phys.* 2009, *11*, 8795-8803.

[P4.25] Enriquez, M. M.; Fuciman, M.; LaFountain, A. M.; Wagner, N. L.; Birge, R. R.; Frank, H. A. The Intramolecular Charge Transfer State in Carbonyl-Containing Polyenes and Carotenoids. *J. Phys. Chem. B* 2010, *114*, 12416-12426.

[P4.26] Ilagan, R. P.; Christensen, R. L.; Chapp, T. W.; Gibson, G. N.; Pascher, T.; Polivka, T.; Frank, H. A. Femtosecond Time-Resolved Absorption Spectroscopy of Astaxanthin in Solution and in □-crustacyanin. *J. Phys. Chem. A* 2004, *109*, 3120-3127.

[P4.27] Polívka, T.; Frank, H. A.; Enriquez, M. M.; Niedzwiedzki, D. M.; Liaaen-Jensen, S.; Hemming, J.; Helliwell, J. R.; Helliwell, M. X-ray Crystal Structure and Time-Resolved Spectroscopy of the Blue Carotenoid Violerythrin. *J. Phys. Chem. B* 2010, *114*, 8760-8769.

[P4.28] Kosumi, D.; Kajikawa, T.; Okumura, S.; Sugisaki, M.; Sakaguchi, K.; Katsumura, S.; Hashimoto, H. Elucidation and Control of an Intramolecular Charge Transfer Property of Fucoxanthin by a Modification of Its Polyene Chain Length. *J. Phys. Chem. Lett.* 2014, *5*, 792-797.

[P4.29] Niedzwiedzki, D. M.; Chatterjee, N.; Enriquez, M. M.; Kajikawa, T.; Hasegawa, S.; Katsumura, S.; Frank, H. A. Spectroscopic Investigation of

Peridinin Analogues Having Different □-Electron Conjugated Chain Lengths: Exploring the Nature of the Intramolecular Charge Transfer State. *J. Phys. Chem. B* 2009, *113*, 13604-13612.

[P4.30] Niedzwiedzki, D. M.; Kajikawa, T.; Aoki, K.; Katsumura, S.; Frank, H. A. Excited States Energies and Dynamics of Peridinin Analogues and the Nature of the Intramolecular Charge Transfer State in Carbonyl-Containing Carotenoids. *J. Phys. Chem. B* 2013, *117*, 6874-6887.

[P4.31] Macpherson, A. N.; Hiller, R. G. Light-Harvesting Systems in Chlorophyll-c Containing Algae. In *Light-harvesting antennas in photosynthesis*; Green, B. R; Parson, W. W; Eds. Kluwer Academic Publishers, Dordrecht 2004, p. 323-352.

[P4.32] Kosumi, D.; Kusumoto, T.; Fujii, R.; Sugisaki, M.; Iinuma, Y.; Oka, N.; Takaesu, Y.; Taira, T.; Iha, M.; Frank, H. A.; Hashimoto, H. One- and Two-Photon Pump-Probe Optical Spectroscopic Measurements Reveal the S_1 and Intramolecular Charge Transfer States are Distinct in Fucoxanthin. *Chem. Phys. Lett.* 2009, *483*, 95-100.

[P4.33] Kosumi, D.; Fujii, R.; Sugisaki, M.; Oka, N.; Iha, M.; Hashimoto, H. Characterization of the Intramolecular Transfer State of Marine Carotenoid Fucoxanthin by Femtosecond Pump-Probe Spectroscopy. *Photosynth. Res.* 2014, *121,* 61-68.

[P4.34] Kosumi, D.; Kajikawa, T.; Yano, K.; Okumura, S.; Sugisaki, M.; Sakaguchi, K.; Katsumura, S.; Hashimoto, H. Roles of Allene Group in an Intramolecular Charge Transfer Character of a Short Fucoxanthin Homolog as Revealed by Femtosecond Pump-Probe Spectroscopy. *Chem. Phys. Lett.* **2014**, *602*, 75–79.

[P4.35] Haugan, J. A.; Englert, G.; Liaaen-Jensen, S. Alkali Lability of Fucoxanthin – Reactions and Products. *Acta Chem. Scand.* 1992, *46*, 614-624.

[P4.36] Bonnett, R.; Mallams, A. K.; Spark, A. A.; Tee, J. L.; Weedon, B. C. L., McCormick, A. Carotenoids and Related Compounds. 20. Structure and Reactions of Fucoxanthin. *J. Chem. Soc. C* 1969, *3*, 429-454.

[P4.37] Jensen, A. Effect of Seaweed Carotenoids on Egg Yolk Coloration. *Poultry Sci.* 1963, *42*, 912.

[P4.38] Strand, A.; Herstad, O.; Liaaen-Jensen, S. Fucoxanthin Metabolites in Egg Yolks of Laying Hens. *Comp. Biochem. Physiol. A* 1998, *119*, 963-974.

[P4.39] Moore, R. B.; Oborník, M.; Janouškovec, J.; Chrudimský, T.; Vancová, M.; Green, D. H.; Wright, S. W.; Davies, N. W.; Bolch, C. J. S.; Heimann, K.; et al. A Photosynthetic Alveolate Closely Related to Apicomplexan Parasites. *Nature* **2008**, *451*, 959–963.

[P4.40] Durchan, M.; Keşan, G.; Šlouf, V.; Fuciman, M.; Staleva, H.; Tichý, J.; Litvín, R.; Bína, D.; Vácha, F.; Polívka, T. Highly Efficient Energy Transfer from a Carbonyl Carotenoid to Chlorophyll a in the Main Light Harvesting Complex of *Chromera Velia*. *Biochim. Biophys. Acta* **2014**, *1837*, 1748–1755.
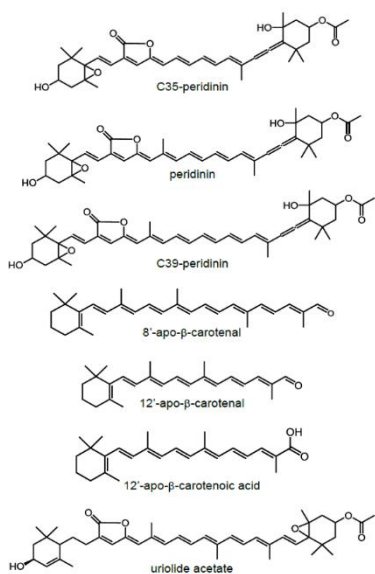
[P4.41] Tichý, J.; Gardian, Z.; Bína, D.v Koník, P.; Litvín, R.; Herbstová, M.; Pain, A.; Vácha, F. Light Harvesting Complexes of *Chromera velia*, Photosynthetic Relative of Apicomplexan Parasites. *Biochim. Biophys. Acta* **2013**, *1827*, 723–729.

[P4.42] Kohn, W.; Sham, L. J. Self-Consistent Equations Including Exchange and Correlation Effects. *Phys. Rev.* 1965, *140*, A1133-A1138.

[P4.43] Becke, A. D. Density-Functional Thermochemistry. III. The Role of Exact Exchange. *J. Chem. Phys.* 1993, *98*, 5648−5652.

[P4.44] Hirata, S.; Head-Gordon, M. Time-Dependent Density Functional Theory within the Tamm-Dancoff Approximation. *Chem. Phys. Lett.* 1999, *314*, 291−299.

[P4.45] Yanai, T.; Tew, D. P.; Handy, N. C. A New Hybrid Exchange-Correlation Functional Using the Coulomb-Attenuating Method (CAM-B3LYP). *Chem. Phys. Lett.* 2004, *393*,51−57.

[P4.46] Schaefer, A.; Huber, C.; Ahlrichs, R. Fully Optimized Contracted Gaussian Basis Sets of Triple Zeta Valence Quality for Atoms Li to Kr. *J. Chem. Phys.* 1994, *100*, 5829−5853.

[P4.47] Frisch, M. J.; Trucks, G. W.; Schlegel, H. B.; Scuseria, G. E.; Robb, M. A.; Cheeseman, J. R.; Scalmani, G.; Barone, V.; Mennucci, B.; Petersson, G. A.; et al. Gaussian, 09W; Gaussian Inc.: Wallingford,CT, 2009.

[P4.48] Wang, J.; Wolf, R. M.; Caldwell, J. W.; Kollman, P. A.; Case, D. A. Development and Testing of a General AMBER Force Field. *J. Comput. Chem.* 2004, *25*, 1157-1174.

[P4.49] Hess, B.; Kutzner, C.; van der Spoel, D.; Lindahl, E. GROMACS 4: Algorithms for Highly Efficient, Load-Balanced, and Scalable Molecular Simulation. *J. Chem. Theory Comput.* 2008, *4*, 435-447.

[P4.50] Wagner, N. L.; Greco, J. A.; Enriquez, M. M.; Frank, H. A.; Birge, R. R. The Nature of the Intramolecular Charge Transfer State in Peridinin. *Biophys. J.* 2013, *104*, 1314-1325.

[P4.51] Durchan, M.; Fuciman, M., Šlouf, V.; Keşan, G.; Polívka, T. Effect of Polarity and Aggregation on Excited-State Dynamics of 8'-apo-β-carotenal. *J. Phys. Chem. A.* 2012, *116*, 12330−12338.

[P4.52] Billsten, H. H.; Zigmantas, D.; Sundström, V.; Polívka, T. Dynamics of Vibrational Relaxation in the S_1 State of Carotenoids Having 11 Conjugated C=C bonds. *Chem. Phys. Lett.* 2002, *355*, 465-470.

[P4.53] Niedzwiedzki, D.; Koscielecki, J. F.; Cong, H.; Sullivan, J. O.; Gibson, G. N.; Birge, R. R.; Frank, H. A. Ultrafast Dynamics and Excited State Spectra of Open-Chain Carotenoids at Room and Low Temperatures. *J. Phys. Chem. B* 2007, *111*, 5984- 5998.

[P4.54] Fuciman, M.; Keşan, G.; LaFountain, A.; Frank, H. A., Polívka, T. Tuning the Spectroscopic Properties of Aryl Carotenoids by Slight Changes in Structure. *J. Phys. Chem. B*. 2015, *119*, 1457–1467.
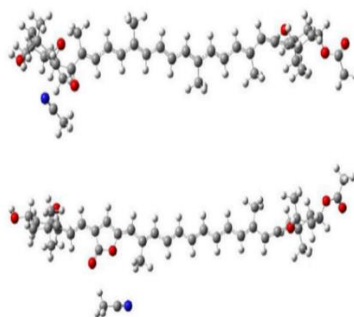
[P4.55] Mendes-Pinto, M. M.; Sansiaume, E.; Hashimoto, H.; Pascal, A. A.; Gall, A.; Robert, B. Electronic Absorption and Ground State Structure of Carotenoid Molecules. *J. Phys. Chem. B* 2013, *117*, 11015–11021.

[P4.56] Kajikawa, T.; Hasegawa, S.; Iwashita, T.; Kusumoto, T.; Hashimoto, H.; Niedzwiedzki, D. M.; Frank, H. A.; Katsumura, S. Syntheses of C33-, C35-, and C39-Peridinin and their Spectral Characteristics. *Org. Lett.* 2009, *11*, 5006-5009.

[P4.57] Zierkiewicz, W.; Michalska, D.; Havlas, Z.; Hobza, P. Study of the Nature of Improper Blue-Shifting Hydrogen Bonding and Standard Hydrogen Bonding in the X_3CH-OH_2 and $XH-OH_2$ Complexes (X = F, Cl, Br, I): A Correlated *ab initio* Study. *Chem. Phys. Chem.* 2002, *3*, 511–518.

[P4.58] Stolov, A. A.; Kamalova, D. I.; Borisover, M. D.; Solomonov, B. N. Hydrogen Bonds Formed by Methyl Groups of Acetonitrile – Infrared and Calorimetric Study. *Spectrochim. Acta A* 1994, *50*, 145-150.

[P4.59] Šlouf, V.; Fuciman, M.; Dulebo, A.; Kaftan, D.; Koblížek, M.; Frank, H.;A.; Polívka, T. Carotenoid Charge Transfer States and Their Role in Energy Transfer Processes in LH1-RC Complexes from Aerobic Anoxygenic Phototrophs. *J. Phys. Chem. B.* 2013, *117*, 10987−10999.

3.4.8 Supporting Information

Figure 3.4.8 Molecular structures of Fx-acetonitrile (top) and C39P-acetonitrile (bottom) complexes. Only the acetonitrile molecule closest to the keto group forming the complex is shown.

Figure 3.4.9 Molecular structures of carbonyl carotenoids discussed in the main text.

3.5 PAPER 5

Spectroscopic Properties of the Triple Bond Carotenoid Alloxanthin

Robert West, **Gürkan Keşan**, Eliška Trsková, Roman Sobotka, Radek Kaňa, Marcel Fuciman,

3.5.1 Abstract

Alloxanthin, which has two triple bonds within its backbone, was studied by steady-state and femtosecond transient absorption spectroscopies. Alloxanthin demonstrates an S_2 energy comparable to its non- triple bond homolog, zeaxanthin, while the S_1 lifetime of 19 ps is markedly longer than that of zeaxanthin (9 ps). Along with corroborating quantum chemistry calculations, the results show that the long-lived S_1 state of alloxanthin, which typically corresponds to the dynamic of a shorter carotenoid backbone, implies the triple bond isolates the conjugation of the backbone, increasing the S_1 state energy and diminishing the S_1–S_2 energy gap.

3.5.2 Introduction

There are no sources in the current document.Carotenoids are known for their rich excited-state dynamics, the elucidation of which is key to understanding the various functions the molecules perform in many biological systems [P5.1], [P5.2], [P5.3]. Basic spectroscopic properties of carotenoids can be explained using a three-state model consisting of the ground state (S_0), and two excited states denoted S_1 and S_2 [P5.4]. Assuming carotenoids belong to the idealized C_{2h} symmetry group, the S_0–S_1 transition is symmetry-forbidden for one-photon processes, while the characteristic visible coloration of carotenoids is due the S_0–S_2 transition that gives rise to strong absorption in the blue–green spectral region. Therefore, the symmetry of the carotenoid conjugated backbone is the key property determining the spectroscopic properties.
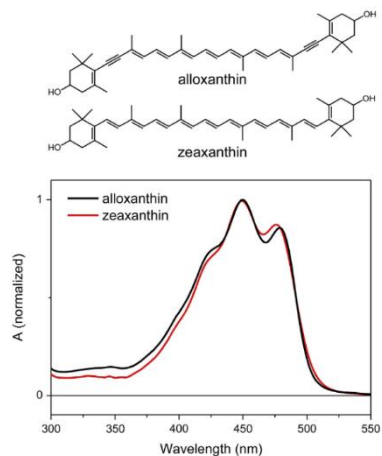
Another key parameter determining the spectroscopic properties is the conjugation length, N, defined as a number of conjugated C=C bonds in the carotenoid structure. For carotenoids with conjugation extended to various functional groups the effective conjugation length, N_{eff}, is often used. It makes use of the fact that some spectroscopic parameters, such as S_1 lifetime, have a well-defined dependence on 1/N [P5.5], [P5.6], [P5.7]. Therefore, knowing the value of e.g. S_1 lifetime of any carotenoid, and comparing the value to that of a linear carotenoid, allows one to obtain an effective value of N_{eff} [P5.7]. For example, it has been demonstrated that the extension of conjugation to various types of terminal rings decreases N_{eff}, but it also provides opportunity for tuning the spectroscopic properties as the torsional angle of a terminal ring in respect to the main conjugation allows for fine tuning of N_{eff} [P5.7]. Thus, in contrast to linear carotenoids whose properties can be only slightly altered

by environment, carotenoids with conjugated terminal rings may have a wide range of spectroscopic properties, depending on their protein binding sites [P5.8], [P5.9].

While there exist many carotenoids with conjugated terminal rings or keto groups, carotenoids having conjugated triple bonds are quite rare. Out of the nearly thousand carotenoids identified so far, only about 50 contain triple bonds [P5.10] and only three triple bond carotenoids are commonly found in nature. Alloxanthin (Figure 3.5.1) is a common carotenoid of cryptophytes [P5.11], and diadinoxanthin and diatoxanthin (Supporting Information, Figure 3.5.6) are found in diatoms and some marine algae [P5.12]. Diadinoxanthin and diatoxanthin have one triple bond in their structure and due to their well-documented role in photoprotection in diatoms [P5.12] -[P5.14], their excited-state properties were studied in detail.

Figure 3.5.1 Molecular structures (top) and absorption spectra (bottom) of alloxanthin and zeaxanthin in methanol.

Alloxanthin is the only carotenoid with two triple bonds found in photosynthetic organisms. The role of carotenoid triple bonds in proper functioning of carotenoids in light-harvesting systems remains unknown. As demonstrated earlier for diadinoxanthin and diatoxanthin, their specific molecular structure with a triple bond may help in tuning the spectroscopic properties when bound to protein [P5.17]. Alloxanthin, whose excited-state properties have not been reported so far, is the major antenna carotenoid in the cryptophyte *Rhodomonas salina* [P5.18]. This organism, despite lack of any xanthophyll cycle, has developed a flexible and effective photoprotective quenching [P5.18], in which alloxanthin may play a role.

Here we present ultrafast transient absorption study of alloxanthin complemented by quantum chemical calculations. We compare these results with those of zeaxanthin (Figure 3.5.1) which has comparable structure but lacks the triple bonds. We show that the presence of triple bonds in the carotenoid structure has important consequences for excited-state dynamics of alloxanthin.

3.5.3   Materials and methods

Alloxanthin was purified by an adapted method described previously for violaxanthin [P5.19]. Rhodomonas salina cells (strain CCAP 978/27) were grown in an artificial seawater medium supplemented with f/2 nutrient. Irradiation was provided by fluorescence tubes (40 µmol m^{-2} s^{-1}, day-night cycle 12/12 h) and cells were continuously bubbled by air. Harvested cells were re-suspended in 25mM Hepes buffer, pH 7.8 and broken by glass beads using Mini-Bead-Beater (BioSpec, USA). Thylakoid membrane fraction was separated by centrifugation, resuspended in 1ml of distilled water, mixed with 9ml of methanol and incubated for one hour in dark at room temperature. The extract was clarified by centrifugation and the remaining pellet was extracted again by 10 ml of 90% methanol. Both supernatants were pooled and completely evaporated by a vacuum evaporator. Pigments were dissolved in methanol and separated by HPLC (Agilent 1200) on a semi preparative reverse phase column (Reprosil 250 x 10mm C8 5 µm, Watrex, Czech Republic) with 35% methanol and 15% acetonitrile in 0.25M pyridine (solvent A) and 20% methanol and 20% acetone in acetonitrile as solvent B. Pigments were eluted with a linear gradient of solvent B (30–95% in 25 min) followed by 95% of solvent B at a flow rate of 0.8 mL min^{-1} at 40 °C.

The sample was maintained at room temperature during transient absorption measurements, constantly stirred with a magnetic stir bar within a 2mm quartz cuvette. The pump and probe pulses were generated by the Spitfire Ace regenerative amplifier system (Spectra Physics), producing 4.2 mJ pulses about 800 nm wavelength at 1 kHz by chirped pulse amplification of a mode-locked Ti:Sapphire laser (MaiTai, Spectra Physics) pumped by a Nd:YLF pump laser (Empower, Spectra Physics). The excitation wavelength of 490 nm was achieved through parametric amplification (TOPAS, Light Conversion) and reduced to ~18 nJ per pulse at the sample location (4×10^{13} photons/pulse cm^{-2}) for an excitation spot size of approximately 400 lm. The probe pulse super continuum was generated in a 2-mm sapphire plate and focused to an area smaller than the spot size of the pump beam by a spherical mirror. The resulting probe absorbance was observed using a double-diode array detection system (Pascher Instruments) with a 300-groove grating spectrometer calibrated by the absorption bands of holmium oxide. Data were fitted globally using Glotaran global fitting analysis software (VU Amsterdam) under a sequential exponential decay scheme [P5.20].

Optimized ground state geometries of carotenoids were created using standard ground-state density functional theory (DFT). All ground state conformers for each carotenoids were optimized with the B3LYP level of theory using the 6-31G (d,p) basis set in order to find stable conformers. This level of theory is suitable for calculations of structure geometry having C=C bonds [P5.21]. Stable con- formers were re-optimized by means of Becke–Lee–Yang–Parr (BLYP) with the triple-f-quality (TZVP) basis set. These optimized structures were used as an initial guess to determine the equilibrium geometries of the excited states by means of time-dependent density functional theory within the Tamm-Dancoff approximation (TD-DFT/TDA) using either the BLYP functional, which provides the correct energy ordering for the two lowest excited states of carotenoids [P5.7], [P5.22], [P5.23], or the hybrid exchange-correlation functional (Cam-B3LYP) with the TZVP basis set, which gives more reasonable data for the S_2 state energy [P5.7]. All calculations were completed in the gas phase and performed with the Gaussian09 package.

3.5.4 Results and discussion

The absorption spectra of zeaxanthin and alloxanthin displayed in Figure 3.5.1 show that adding two triple bonds to the carotenoid structure only marginally affects the S_0–S_2 transition. The absorption spectra are very similar, although alloxanthin has the lowest vibrational band slightly red-shifted, peaking at 479 nm while zeaxanthin's is at 477 nm. The resolution of vibrational bands, reflecting the conformational disorder in the ground state, is also comparable for both carotenoids. These observations imply that properties of the S_2 state are not much affected by the presence of triple bonds in alloxanthin.

Transient absorption spectra and dynamics monitoring spectroscopic properties of the S_1 state, however, demonstrate a more divergent spectral response among alloxanthin and zeaxanthin. The spectra in Figure 3.5.2a represent the transient absorption profiles measured at 4 ps after excitation, corresponding to the S_1–S_n transition after all S_1 vibrational dynamics, which usually takes place at subpicosecond time scales [P5.24], have subsided. In contrast to the S_0–S_2 transition shown in Figure 3.5.1, the spectral profiles of the S_1–S_n transitions are clearly different for alloxanthin and zeaxanthin. Again, the peak wavelength is comparable, yielding 548 nm for alloxanthin and 550 nm for zeaxanthin, but it must be noted that while for the S_0–S_2 transition (Figure 3.5.1) zeaxanthin has the slightly higher energy, it is opposite for the S_1–S_n transition. Further, the S_1–S_n profile of alloxanthin is
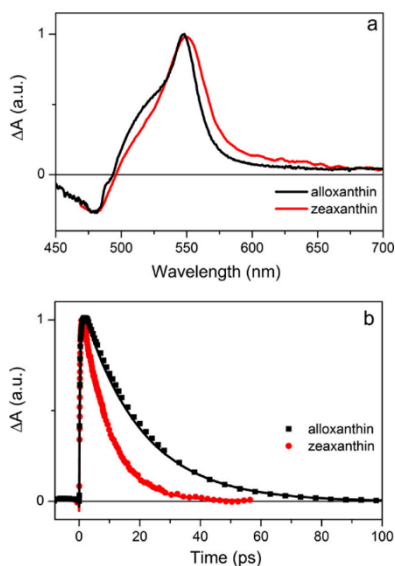
Figure 3.5.2 (a) Transient absorption spectra of alloxanthin and zeaxanthin in methanol measured at 4 ps after excitation at 490 nm. (b) Kinetics measured at the maximum of the S_1-S_n transition at 548 nm (alloxanthin) and 550 nm (zeaxanthin).
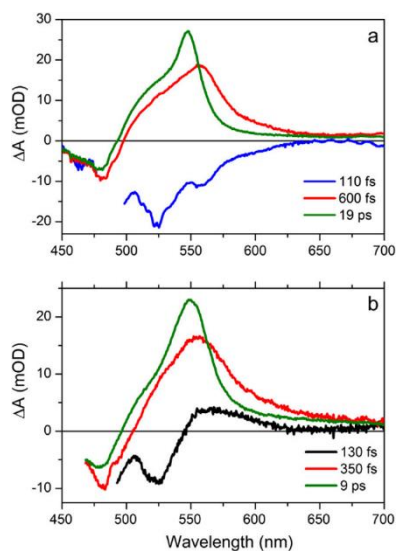
Figure 3.5.3 EADS obtained from global fitting the data measured for (a) alloxanthin and (b) zeaxanthin in methanol excited at 490 nm.

narrower with a pronounced, blue shoulder, found to decay at the same rate as the peak's maximum (see below). In contrast, the blue shoulder is much less pronounced in zeaxanthin, but its main peak is broader than alloxanthin and extends more to longer wavelengths (Figure 3.5.2a). Further, the kinetics measured at the peak S_1–S_n transition wavelengths in both carotenoids, monitoring the S_1 lifetime, are shown in Figure 3.5.2b, demonstrating markedly longer S_1 lifetime of alloxanthin compared to zeaxanthin.

Three sequentially decaying evolution associated difference spectra (EADS), shown in Figure 3.5.3, satisfactorily fit the total decay profiles of alloxanthin and zeaxanthin. The bleaching EADS, the fastest and most immediate profile, expresses the 110 fs (alloxanthin) and 130 fs (zeaxanthin) decay of the S_2 state stimulated emission combined with ground state bleaching. The second, broad spectrum, recognized as hot S_1 state [P5.24], [P5.25], decays to the slightly narrower, bluer S_1 signal within 600 fs in alloxanthin. For zeaxanthin, this component is faster, yielding 350 fs. The final EADS, effectively representing the spectrum of the S_1 state, decays by 19

ps in alloxanthin, confirming the difference in the S_1 lifetimes of alloxanthin and zeaxanthin shown in Figure 3.5.2b; the S_1 lifetime of zeaxanthin is 9 ps in agreement with a number of previous studies [P5.26], [P5.27].

Considering the spectroscopic findings described above, namely the nearly identical absorption spectra and the markedly longer S_1 lifetime of alloxanthin as compared to zeaxanthin, as well as the different spectral profiles of their S_1–S_n transitions, we must conclude that adding a triple bond into conjugation markedly affects the S_1 state while leaving the S_2 state nearly untouched. The alloxanthin S_1 lifetime of 19 ps is actually comparable to the S_1 lifetimes of carotenoids with N_{eff} = 9 such as neurosporene or violaxanthin whose S_1 lifetimes were reported in the 21–24 ps range [P5.6], [P5.24], [P5.26]. In contrast,
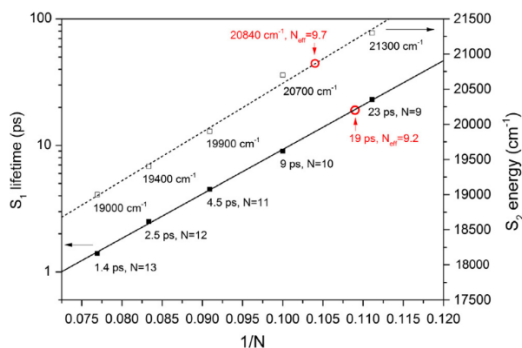
Figure 3.5.4 Dependence of the S_1 lifetime and S_2 energy on conjugation length. The S_1 lifetimes (full symbols) and S_2 energies (open symbols) of linear carotenoids in n-hexane (data taken from Ref. [6]) are plotted against 1/N. The lines represent linear fits to both dependencies. Red circles show the corresponding values for alloxanthin. Placing these values on the line allows a determination of the effective conjugation length, N_{eff}, of alloxanthin. Each point is labeled by a corresponding S_1 lifetime, S_2 energy and N (or N_{eff}). (For interpretation of the references to color in this figure legend, the reader is referred to the web version of this article.)

alloxanthin S_2 energy is rather in the range expected for carotenoids with N_{eff} = 10. This split effect of the triple bonds of alloxanthin can be visualized by comparing its S_1 lifetime and S_2 energy with those of linear carotenoids. For linear carotenoids with well-defined conjugation length N, these parameters depend linearly on 1/N and allow estimation of N_{eff}. As shown in Figure 3.5.4, the interpolation based on the S_1 lifetime yields for alloxanthin N_{eff} = 9.2, while the interpolation using the S_2 energy gives estimation of N_{eff} = 9.7, confirming the different effect of the triple bonds on the S_2 and S_1 states.

It is instructive to compare our results obtained for alloxanthin with those of diatoxanthin, a carotenoid having only one triple bond thus representing an intermediate structure between zeaxanthin and alloxanthin (Supporting Information, Figure 3.5.7). A previous study of diatoxanthin reported a 13 ps S_1 lifetime, thus markedly shorter than for alloxanthin, yet the S_2 energy of diatoxanthin remains the

same as for alloxanthin [P5.16]. Therefore, it is obvious that the number of triple bonds in the carotenoid backbone correlates monotonically to the S_1 lifetime, but the S_2 energy is insensitive to the presence or number of triple bonds in the carotenoid structure.

Interestingly, the intensity of the blue shoulder of the S_1–S_n transition also correlates with the number of triple bonds: it is weakest for zeaxanthin, increases slightly in diatoxanthin [P5.16], and it is strongest in the two triple bond carotenoid alloxanthin. This shoulder is known as the S^* signal whose origin is still a matter of considerable debate [P5.28], [P5.29], [P5.30]. Yet, it is generally agreed that whatever is the precise origin of the S^* signal, it is most likely related to specific conformations [P5.31], [P5.32], [P5.33], and extension of conjugation to the terminal rings allows for larger conformational space thereby enhancing the S^* signal [P5.32]. This hypothesis matches our observation and shows that connection of the terminal ring via a triple bond enhances the S^* signal, which in alloxanthin decays with the same lifetime as the S_1 state (Figure 3.5.3).

Table 3.5.1. Calculated ground state Gibbs free energies and dihedral angles of zeaxanthin and alloxanthin.
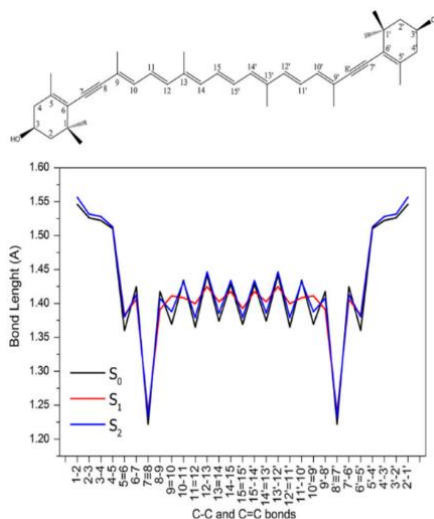
	conformers	Dihedral Angle (Degrees)	Gibbs free energy (Hartree)	Relative ΔG (kcal/mol)
zeaxanthin	*s-cis-s'-cis*	47.9/47.9	-1707.538685	0.0
	s-cis-s'-trans s-trans-s'-cis	46.2/-167.9	-1707.535694	1.88
	s-trans-s'-trans	169.05/169.05	-1707.532556	3.85
alloxanthin	s-cis-s'-cis	3.8/3.8	-1705.111494	0.51
	s-cis-s'-trans s-trans-s'-cis	0.9/175.9	-1705.107567	2.97
	s-trans-s'-trans	175.5/175.5	-1705.112307	0.0

Our observations show that the effect of triple bonds is different for the S_1 and S_2 states. To corroborate this finding, we carried out quantum chemical calculations to obtain equilibrium structures of zeaxanthin and alloxanthin in various energy states and to estimate vertical excited-state energies of the S_1 and S_2 states. Relative energies of the ground state optimized geometries for s-cis and s-trans configurations in gas phase of zeaxanthin and alloxanthin calculated with the B3LYP/6-31g(d,p) method are given in Table 3.5.1. For zeaxanthin, the lowest energy configuration is that with s-cis position of both terminal rings that are twisted by ~48° from the plane of the central conjugated chain, matching values reported earlier for zeaxanthin and β-carotene [P5.7], [P5.34]. The torsional twist of the terminal

ring is caused by repulsion between the methyl group at the ring and the hydrogen atoms near the ends of the conjugated chain [P5.35].

In alloxanthin, the terminal rings have the same structure as in zeaxanthin but since they are connected via triple bonds, the steric constraints which twist the terminal ring of zeaxanthin are relaxed. This results in terminal rings of alloxanthin being essentially the in plane of the main conjugation for both s-cis and s-trans configurations (Table 3.5.1). The s-trans configuration has slightly lower energy compared to zeaxanthin, whereby the lowest energy ground state structure of alloxanthin is s-trans with terminal rings nearly ideally aligned with the plane of the central conjugated backbone (Supporting Information, Figure 3.5.7). This configuration is likely the reason for the slightly lower S_2 energy of alloxanthin compared to zeaxanthin (Figure 3.5.1), because torsion of the ring critically determines how much the double bonds at the ring will be involved in conjugation [P5.7].

But this cannot explain why alloxanthin in the S_1 state behaves as a carotenoid with effective conjugation length clearly shorter than zeaxanthin. Thus, we calculated relaxed geometries in the S_1 and S_2 excited states, and bond lengths, corresponding to each excited state, as depicted in Figure 3.5.5. It is evident the S_0 and S_2 states are more congruent in bond length than the S_1 state. While in the S_0 and S_2 states the single and double bond character is retained, partial equilibration of the bond length is characteristic for the S_1 state [P5.7], [P5.34]. However, all states nearly coincide for the length of triple bonds, preventing the extension of the bond length equilibration in the S_1 state beyond the triple bonds.

Figure 3.5.5 Calculated bond lengths in the S_0 state (black), S_1 state (red), and S_2 state (blue) of alloxanthin in relaxed s-*trans*-s'-*trans* configuration.

Thus, the typical bond length alternation pattern of the S_1 state is disturbed by the triple bonds though it is obvious that the conjugation must extend beyond the triple bonds since N_{eff} >9 (Figure 3.5.4). The role of the conjugated triple bonds can be

visualized by calculating electron densities of the involved orbitals (Supporting Information, Figure 3.5.8): the triple bonds of alloxanthin significantly decrease p-electron densities at the end of the conjugated chain.

Finally, we calculated the S_0–S_2 and S_0–S_1 vertical transition energies for the optimized ground state geometry that are summarized in Table 3.5.2. Here, different levels of theory were used because, while the Cam-B3LYP and B3LYP functionals reasonably reproduce the S_2 energies, it gives the wrong excited state ordering resulting in the forbidden S_1 state being placed above the S_2 state [P5.22], [P5.23], [P5.36]. Thus, the TDA Cam-B3LYP/TZVP approach was used to calculate the S_2 energies, but the BLYP functional, which is known to give the proper state ordering, was used to calculate S_1 energies. It is obvious that regardless the method used to calculate S_2 energies, calculations reproduce qualitatively the experimental results.

Table 3.5.2 Dihedral angles and vertical excitation energies in various excited states.[a]

	Dihedral angle (degrees)			Transition energy (cm^{-1})	
	S_0	S_1	S_2	S_0-S_2	S_0-S_1
zeaxanthin	47.9	32.4	38.2	23 775 (4.796)	15 402 (0.000)
			44.7	*22 422 (5.222)*	
alloxanthin	175.5	176.6	176.5	21 551 (5.679)	16 077 (0.000)
				22 071 (5.325)	

a) Calculations were carried out using either the BLYP/TZVP (ground state) or TDA BLYP/TZVP (excited states) level of theory. Calculations involving the S_2 state were also carried out by TDA Cam-B3LYP/TZVP (results shown in italics). Oscillator strengths of the transitions are shown in parentheses.

While the calculated S_2 energy of alloxanthin is lower than that of zeaxanthin, the trend is opposite for the S_1 state, which is higher for alloxanthin than for zeaxanthin (Table 3.5.2). The S_1 energy correlates with the S_1 lifetime according to the energy gap law in non- carbonyl carotenoids [P5.37]. Thus, the measured alloxanthin S_1 lifetime of 19 ps implies the S_1 energy higher than that of zeaxanthin whose S_1 lifetime is 9 ps, precisely as predicted by calculations. The calculated difference of ~650 cm^{-1} matches reasonably the difference between S_1 energies of carotenoids with N = 9 and N =10 observed experimentally [P5.4]. For the S_2 state, the energy difference between alloxanthin and zeaxanthin calculated with the BLYP functional is far too large to match the experimental value, but using TDA Cam-B3LYP/TZVP approach gives the energy difference of ~150 cm^{-1} which is much closer to the observed value (Figure 3.5.1).

3.5.5 Conclusions

Comparison of spectroscopic properties of the triple bond carotenoid alloxanthin and its non-triple bond counterpart zeaxanthin revealed that the effect of a triple bond on carotenoid spectroscopic properties differ for the S_2 and S_1 excited states. While the S_2 energy is slightly lowered by introduction of two triple bonds into the carotenoid structure, the S_1 energy of alloxanthin is higher than that of zeaxanthin. This is evidenced by significantly longer S_1 lifetime of alloxanthin (19 ps) compared to zeaxanthin (9 ps). The different effect on the S_1 state is explained by the triple bonds preventing the extension of the typical S_1 state bond length equilibration to the terminal rings. Thus, the triple bonds in alloxanthin shrinks the S_1–S_2 energy gap by decreasing the S_2 energy and increasing the S_1 energy compared to zeaxanthin, which may have significant consequences for alloxanthin function in photosynthetic light-harvesting complexes. This effect, reminiscent of carbonyl carotenoids [P5.38], allows to extend the light-harvesting capacity to longer wavelengths, while keeping the S_1 energy high enough to transfer energy to Chl-a. Thus, it is likely that alloxanthin is a light-harvesting carotenoid transferring energy efficiently to Chl-a.

3.5.6 Acknowledgments

3.5.7 References

[P5.1] T. Polívka and H. A. Frank, Acc. Chem. Res. 46 (2010) 1125-1134.
[P5.2] H. A. Frank and R. J. Cogdell, Photochem. Photobiol. 63 (1996) 257-264.
[P5.3] H. Hashimoto, Y. Sugai, C. Uragami, A. T. Gardiner, R. J. Cogdell, J. Photochem. Photobiol. C 25 (2015) 46-70.
[P5.4] T. Polívka, V. Sundström, Chem. Rev. 104 (2004) 2021-2071.
[P5.5] R. L. Christensen, M. M. Enriquez, N. L. Wagner, A. Y. Peacock-Villada, C. Scriban, R. R. Schrock, T. Polívka, H. A. Frank, R. R. Birge, J. Phys. Chem. A 117 (2013) 1449-1465.
[P5.6] R. Fujii, T. Inaba, Y. Watanabe, Y. Koyama, J.-P. Zhang, Chem. Phys. Lett.

369 (2003) 165-172.

[P5.7] M. Fuciman, G. Keşan, A. M. LaFountain, H. A. Frank, T. Polívka, J. Phys. Chem. B 119 (2015) 1457-1467.

[P5.8] R. L. Leverenz, M. Sutter, A. Wilson, S. Gupta, A. Thurotte, C. Bourcier de Carbon, C. J. Petzold, C. Ralston, F. Perreau, D. Kirilovsky, C. A. Kerfeld, *Science* 348 (2015) 1463-1466.

[P5.9] V. Šlouf, P. Chábera, J. D. Olsen, E. C. Martin, P. Qian, C. N. Hunter, T. Polívka, Proc. Natl. Acad. Sci. 109 (2012) 8570-8575.

[P5.10] G. Britton, S. Liaaen-Jensen, H. Pfander, Eds., Carotenoids, Handbook, Birkäuser Verlag, 2004.

[P5.11] F. C. Pennington, F. T. Haxo, G. Borch, S. Liaaen-Jensen, Biochem. Syst. Ecol. 13 (2015) 215-219.

[P5.12] A. N. Macpherson, R. G. Hiller, in Light-Harvesting Antennas in Photosynthesis, Dordrecht 2003, pp. 323-352.

[P5.13] P. Horton, A. V. Ruban, J. Exp. Bot. 56 (2005) 365-373.

[P5.14] M. Olaizola, J. La Roche, Z. Kolber, P. G. Falkowski, Photosynth. Res. 41 (1994) 357-370.

[P5.15] H. A. Frank, A. Cua, V. Chynwat, A. Young, D. Gosztola, M. R. Wasielewski, Biochim. Biophys. Acta 1277 (1996) 243-252.

[P5.16] M. M. Enriquez, A. M. LaFountain, J. Budarz, M. Fuciman, G. N. Gibson, H. A. Frank, Chem. Phys. Lett. 493 (2010) 353-357.

[P5.17] M. Durchan, J. Tichý, V. Šlouf, Z. Gardian, P. Hříbek, F. Vácha, T. Polívka, J. Phys. Chem. B 116 (2012) 8880-8889.

[P5.18] R. Kaňa, E. Kotabová, R. Sobotka, O. Prášil, PLoS One 7 (2012) e29700.

[P5.19] R. Kaňa, E. Kotabová, J. Kopečná, E. Trsková, E. Belgio, R. Sobotka, A. V Ruban, *FEBS Lett.* (2016), in press. doi:10.1002/1873-3468.12130.

[P5.20] I. H. M. van Stokkum, D. S. Larsen, R. van Grondelle, Biochim. Biophys. Acta 1657 (2004) 82-104.

[P5.21] M. N. Ramos, K. C. Lopes, A. M. Tavares, E. Ventura, S. A. do Monte, R. Araujo, J. Mol. Struct. 758 (2006) 253-258.

[P5.22] C.-P. Hsu, S. Hirata, M. Head-Gordon, J. Phys. Chem. A 105 (2001) 451-458.

[P5.23] J. H. Starcke, M. Wormit, J. Schirmer, A. Dreuw, Chem. Phys. 329 (2006) 39-49.

[P5.24] D. Niedzwiedzki, J. F. Koscielecki, H. Cong, J. O. Sullivan, G. N. Gibson, R. R. Birge, H. A. Frank, J. Phys. Chem. B 111 (2007) 5984-5998.

[P5.25] H. H. Billsten, D. Zigmantas, V. Sundström, T. Polívka, Chem. Phys. Lett. 355 (2002) 465-470.

[P5.26] T. Polívka, J. L. Herek, D. Zigmantas, H. E. Åkerlund, V. Sundström, Proc. Natl. Acad. Sci. U. S. A. 96 (1999) 4914-4917.

[P5.27] H. H. Billsten, J. Pan, S. Sinha, T. Pascher, V. Sundström, T. Polívka, J. Phys. Chem. A 109 (2005) 6852-6859.

[P5.28] T. Polívka, V. Sundström, Chem. Phys. Lett. 477 (2009) 1-11.

[P5.29] F. Ehlers, M. Scholz, J. Schimpfhauser, J. Bienert, K. Oum, T. Lenzer, Phys. Chem. Chem. Phys. 17 (2015) 10478-10488.

[P5.30] V. Balevičius, A. G. Pour, J. Savolainen, C. N. Lincoln, V. Lukeš, E. Riedle, L. Valkunas, D. Abramavicius, J. Hauer, Phys. Chem. Chem. Phys. 17 (2015) 19491-19499.

[P5.31] P. Chábera, M. Fuciman, P. Hříbek, T. Polívka, Phys. Chem. Chem. Phys. 11 (2009) 8795-8803.

[P5.32] D. M. Niedzwiedzki, J. O. Sullivan, T. Polívka, R. R. Birge, H. A. Frank, J. Phys. Chem. B 110, (2006) 22872-22885.

[P5.33] V. Lukeš, N. Christensson, F. Milota, H. F. Kauffmann, J. Hauer, Chem. Phys. Lett. 506 (2011) 122-127.

[P5.34] A. Dreuw, J. Phys. Chem. A 110 (2006) 4592-4599.

[P5.35] R. L. Christensen, M. Goyette, L. Gallagher, J. Duncan, B. DeCoster, J. Lugtenburg, F. J. Jansen, I. van der Hoef, J. Phys. Chem. A 103 (1999) 2399-2407.

[P5.36] A. E. Masunov, I. A. Mikhailov, Eur. J. Chem. 1 (2010) 142-161.

[P5.37] V. Chynwat, H. A. Frank, Chem. Phys. 194 (1995) 237-244.

[P5.38] D. Zigmantas, R. G. Hiller, F. P. Sharples, H. A. Frank, V. Sundström, T. Polívka, Phys. Chem. Chem. Phys. 6 (2004) 3009-3016.
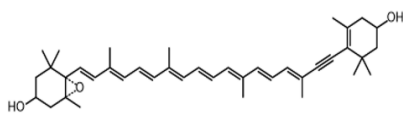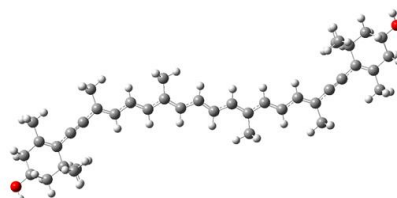
3.5.8 Supporting Information
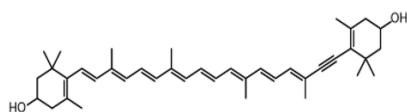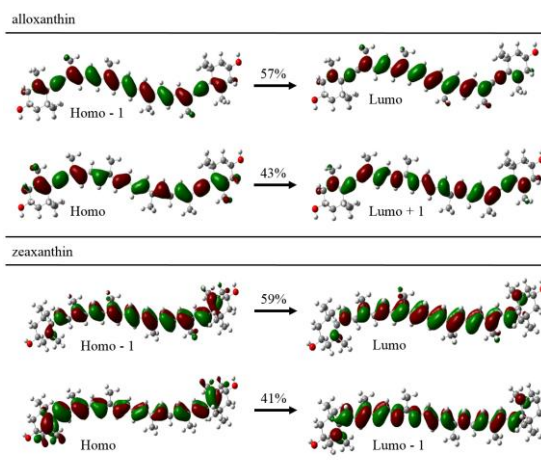

diatoxanthin
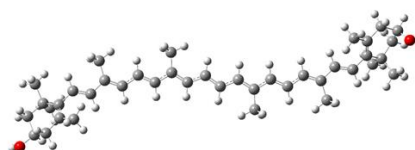
zeaxanthin

diadinoxanthin

alloxanthin

Figure 3.5.6 Molecular structures of diatoxanthin and diadinoxanthin.

Figure 3.5.7 Relaxed ground state geometries of zeaxanthin and alloxanthin.

Figure 3.5.8 The S_1 state transition densities of alloxanthin and zeaxanthin calculated by using TDDFT/TDA with BLYP method including TZVP basis set. In this level of theory, the S_1 state, which has the A_g^- symmetry, is a doubly-excited state represented as a linear combination of two singly-excited determinants corresponding to HOMO-1 →LUMO and HOMO → LUMO + 1 transitions [1]. Contribution of each transition to this linear combination is indicated in the figure. The calculations of electron densities show that electron density at the terminal parts of alloxanthin (triple bond and the C=C bond at the terminal ring) is less than the corresponding density in zeaxanthin. This difference implies that the presence of the triple bonds affects the overall electron densities and, consequently, the effective conjugation length.

 [1] J. H. Starcke, M. Wormit, J. Schirmer, A. Dreuw, Chem. Phys. 329 (2006) 39-49.

3.6 PAPER 6

Highly Efficient Energy Transfer Form a Carbonyl Carotenoid to Chlorophyll *a* in the Main Light Harvesting Complex of Chromera velia

Milan Durchan, **Gürkan Keşan**, Václav Šlouf, Marcel Fuciman, Hristina Staleva, Josef Tichý, Radek Litvín, David Bína, František Vácha, Tomáš Polívka,

3.6.1 Abstract

We report on energy transfer pathways in the main light-harvesting complex of photosynthetic relative of apicomplexan parasites, *Chromera velia*. This complex, denoted CLH belongs to the family of FCP proteins and contains chlorophyll (Chl) *a*, violaxanthin, and the so far unidentified carbonyl carotenoid related to isofucoxanthin. The overall carotenoid-to-Chl-*a* energy transfer exhibits efficiency over 90% which is the largest among the FCP-like proteins studied so far. Three spectroscopically different isofucoxanthin-like molecules were identified in CLH, each having slightly different energy transfer efficiency that increases from isofucoxanthin-like molecules absorbing in the blue part of the spectrum to those absorbing in the reddest part of spectrum. Part of the energy transfer from carotenoids proceeds via the ultrafast S_2 channel of both the violaxanthin and isofucoxanthin-like carotenoid, but major energy transfer pathway proceeds via the S_1/ICT state of the isofucoxanthin-like carotenoid. Two S_1/ICT-mediated channels characterized by time constants of ~0.5 and ~4 ps were found. For the isofucoxanthin-like carotenoid excited at 480 nm the slower channel dominates, while those excited at 540 nm employs predominantly the fast 0.5 ps channel. Comparing these data with the excited-state properties of the isofucoxanthin-like carotenoid in solution we conclude that, contrary to other members of the FCP family employing carbonyl carotenoids, CLH complex suppresses the charge-transfer character of the S_1/ICT state of the isofucoxanthin-like carotenoid to achieve the high carotenoid-to-Chl-*a* energy transfer efficiency.

3.6.2 Introduction

The primary function of light-harvesting complexes of photosynthetic organisms is to collect light and transfer the absorbed energy to the reaction centers [P6.1]. The key light-harvesting pigments are chlorophylls (Chl) or bacteriochlorophylls (BChl), but especially in photosynthetic microorganisms, the importance of the accessory pigments, carotenoids, as the light-harvesting agents increases [P6.2]. Carotenoids effectively cover the spectral region that is not accessible to (B)Chl, and due to the large structural variability of carotenoids found in nature, they are able to tune their spectral properties to a much larger extent than (B)Chl [P6.3]. This, in combination with their ability to transfer energy very efficiently to (B)Chl, makes carotenoids crucial components of light-harvesting proteins of many photosynthetic

microorganisms, which utilize carotenoids to develop various light-harvesting strategies that are optimized to the light conditions of their ecological niches [P6.2].

Chromera (*C*.) *velia* is a photosynthetic unicellular alveolate, a supposed symbiont of stony corals, and together with the recently described *Vitrella brassicaformis*, they are the closest known photosynthetic relatives of apicomplexan parasites such as *Plasmodium* which causes malaria [P6.4]. Ancestors of apicomplexan parasites have acquired their plastid bounded by a four-membrane envelop through secondary endosymbiosis of free-living photosynthetic red alga [P6.5]. The photosynthetic apparatus of *C. velia* is interesting as it utilizes three different and evolutionary distant types of light harvesting antenna complexes: one bound to PS I reaction center that it is related to the PS I light harvesting complex of red algae [P6.6], a second which is a far-red antenna complex absorbing above 700 nm [P6.7], [P6.8], and a third complex which shows sequential similarity to fucoxanthin chlorophyll *a/c* – binding light harvesting complex (FCP) [P6.9].

The FCP-like antenna complex of *C. velia*, which is a subject of this study, belongs to the family of FCP proteins that may be found in diatoms or kelps [P6.10]. Although FCPs are related to the well-known *Cab* protein family from higher plants [P6.11], the structures of FCPs remain unknown. No atomic structure of a member of the FCP family was resolved so far, and our knowledge relies solely on comparing the spectroscopic data taken for the FCP family proteins with those recorded for LHCII whose structure is known to a great detail [P6.12]. It is therefore expected that the central luteins known from the LHCII structure are likely replaced by two fucoxanthins in FCP from diatoms [P6.13].

The FCP-like light harvesting complex of *C. velia*, denoted as Chromera Light Harvesting (CLH) complex, was studied by electron microscopy and circular dichroism, suggesting its close relation to the XLH antenna from xanthophytes [P6.6]. Yet, while the XLH complex contains only non-carbonyl carotenoids, diatoxanthin and diadinoxanthin [P6.14], [P6.15], the CLH complex also accommodates a carbonyl carotenoid (carotenoid containing the conjugated C=O group). Thus it is spectroscopically and functionally closer to FCP proteins. Besides the Chl *a* and carotenoid violaxanthin, the CLH complex contains a carbonyl carotenoid yet to be identified. Based on HPLC, UV-VIS, electrospray mass spectroscopy, and chemical analysis, this unknown carotenoid must be related to isofucoxanthin. It contains all the functional groups of isofucoxanthin, and it is characterized by $C_{42}H_{58}O_6$ composition [P6.16]. The absorption spectrum of this carotenoid in methanol is,

however, red-shifted by about 13 nm compared to isofucoxanthin, indicating that conjugation length of the unknown carotenoid is longer than that of isofucoxanthin. We therefore denote this carotenoids as isofucoxanthin-like (Ifx-l). The pigment composition of CLH exhibits a Chl a : Vio : Ifx-l ratio of approximately 10:1:4 [P6.6]. A later report, using both gel filtration and anion exchange for purification of CLH, demonstrated that while the Chl a : Ifx-l ratio of 5:2 is constant, violaxanthin content may vary from 5-20% of Chl a depending on purification method, suggesting that violaxanthin is likely loosely bound in CLH and may be partially removed during purification [P6.8].

Even though the molecular structure of Ifx-l remains unknown, it clearly belongs to the family of carbonyl carotenoids whose spectroscopic properties are largely affected by environment [P6.17], [P6.18]. When embedded in a polar environment, these carotenoids often have an intramolecular charge transfer (ICT) state in their excited-state manifold. The ICT state is readily identified in transient absorption spectra due to its characteristic excited state absorption (denoted as an ICT-like band) in the 600-700 nm spectral region as well as the stimulated emission in the near infrared [P6.19], [P6.20]. The ICT state is believed to be coupled to the S_1 state, which is usually denoted S_1/ICT state [P6.20]. Depending on polarity, the degree of the charge transfer character of the S_1/ICT state varies, and this variation can be monitored by the magnitude of the ICT-like band. Importantly, for some carbonyl carotenoids the S_1/ICT state exhibits lifetime dependence on solvent polarity [P6.17], [P6.18]. Then, because the intrinsic carotenoid lifetime is a crucial parameter in determining the energy transfer efficiency [P6.2], if a carbonyl carotenoid is bound to a light-harvesting protein, the local polarity of the binding protein may tune the energy transfer efficiency as it was demonstrated for synthetic systems containing carbonyl carotenoids [P6.21].

Besides the possibility of tuning the energy transfer efficiency by polarity of the protein environment, there are two other properties that make the carbonyl carotenoids vital constituents of light-harvesting proteins. First, the symmetry breaking caused by the conjugated carbonyl group increases the dipole moment of the S_1/ICT state, which enhances the donor-acceptor coupling. Second, the conjugated carbonyl group decreases the energy of the S_2 state while keeping the S_1/ICT energy sufficiently high to enable transfer to the Q_y state of Chl a [P6.18]. This allows extension of absorption into the green-yellow region (520-580 nm) even for oxygen-evolving photosynthetic organisms utilizing Chl a.

The importance of the ICT state for maintaining a high light-harvesting capacity has been demonstrated in a number of antenna containing carbonyl carotenoids. Peridinin-chlorophyll-*a* protein (PCP) has been widely used as a model system, because its structure is known to atomic resolution [P6.22], [P6.23]. A number of studies [P6.24], [P6.31] provided a basic understanding of light-harvesting strategies utilizing carbonyl carotenoids. The S_1/ICT state of peridinin in PCP gains significant CT character, and the pathway through the S_1/ICT becomes dominant. This behavior is mirrored in light-harvesting complexes from the FCP family utilizing carbonyl carotenoids. The dominant S_1/ICT pathway in one carbonyl carotenoid having a substantial CT character of its S_1/ICT state was also reported for both FCP [P6.32]-[P6.35] and a chlorophyll-*a*–chlorophyll-*c₂*–peridinin protein complex (acpPC) of *Amphidinium carterae* [P6.36]-[P6.38]. Yet, it was found that in the complexes from the FCP family there are also peridinins or fucoxanthins with less CT character of the S_1/ICT state and that these carotenoids are only marginally (if at all) involved in energy transfer via the S_1/ICT state [P6.34], [P6.37], [P6.38]. The importance of the S_1/ICT state is also manifested by comparison of FCP and acpPC with XLH, another complex from the FCP family. XLH does not bind any carbonyl carotenoid; the overall efficiency of carotenoid-to-Chl-*a* transfer is markedly diminished compared to FCP and acpPC [P6.15].

Here we show the first time-resolved study of yet another light-harvesting complex from the FCP family, CLH, which comes from an evolutionarily old organism. Even though the exact molecular structure of the carotenoid in CLH remains unknown, the aim of this study was to compare spectroscopic properties of CLH with those reported earlier for other complexes from the FCP family and to test whether the light-harvesting strategy of utilizing the S_1/ICT state with enhanced CT character is employed also by *C. velia*, a photosynthetic relative of apicomplexan parasites.

3.6.3   Materials and Methods

The cells of *Chromera velia* were grown in 5 l Erlenmeyer flasks at 28 °C in modified f2 medium and bubbled with filtered air. The irradiance was 100 μmol photons $m^{-2} s^{-1}$, provided by a metal halide lamp (Osram Powerstar HQI 250W/D PRO, Osram GmbH, Germany). The light regime was 15 hour light – 9 hour dark. The antenna complex isolation was performed as described earlier [P6.6], [P6.8]. Briefly, thylakoid membranes solubilised by ☐-dodecyl maltoside were pre-purified on

sucrose gradient, the zone containing antenna complexes was collected and further purified by anion exchange chromatography on DEAE Sepharose CL-6B (Sigma-Aldrich, St. Louis, MO, USA) using a linear NaCl gradient, to eliminate minor antenna components [P6.8]. Fractions with highest Ifx-l: Chl *a* ratio (estimated as A_{540}/A_{674}) were pooled, desalted and stored at -80 C. As described earlier [P6.8], certain amount of violaxanthin was eluted in the protein-free fraction during the chromatographic step, indicating its loose binding to protein complexes.

Absorption spectra were measured on UV-300 (Spectronic Unicam, Cambridge, UK) spectrophotometer; fluorescence spectra were recorded on Fluorolog 2 (Spex) spectrofluorometer. A 1 cm path length cuvette was used for steady-state absorption and room-temperature fluorescence measurements. Optical density ∼0.6/mm at 677 nm for femtosecond transient absorption experiments, and 0.07/cm at 677 nm for fluorescence measurements were used.

Transient absorption spectra were measured at room temperature using a femtosecond spectrometer employing Ti:sapphire amplifier (Integra-i, Quantronix) as a primary source of femtosecond pulses. Excitation pulses were generated in an optical parametric amplifier (TOPAS, Light Conversion), while a white-light single filament continuum generated in a 2 mm sapphire plate was used as a probe. The mutual orientation of the excitation and probe beams polarization was set to the magic angle (54.7°). A 1 mm path length rotating quartz cuvette spinning at a rate to ensure that each excitation pulse hits a fresh sample was used for transient absorption measurements. Time-resolved absorption changes were measured in a broad spectral range from 470 to 720 nm by detecting the dispersed white light by double-diode array after excitation with ∼130 fs laser pulses centered at the desired excitation wavelength. Using neutral-density filters, the intensity of excitation in all experiments was kept at ∼5.0×10^{13} photons pulse^{-1} cm^{-2}.

Femtosecond transient absorption data collected by diode array detectors were fitted globally using either DAFit software (Pascher Instruments) or Glotaran package (glotaran.org). Both software packages fits the data to a sum of exponentials, including numerical deconvolution of the response function, and a polynomial describing the chirp. The fitting procedure used either general linear regression (DAFit) or single-value decomposition (Glotaran) to fit the data. To visualize the excited-state dynamics, we assumed that the excited CLH complex evolves according to a sequential, irreversible scheme A → B, B → C, C → D … The arrows represent increasingly slower monoexponential processes and the time constants of these

processes correspond to lifetimes of the individual excited-state species A, B, C, D … in the sequential scheme. The spectral profile of each species is called evolution-associated difference spectrum (EADS). Although EADS obtained from the sequential model do not correspond to individual excited states in a complex system such as the CLH complex studied here, they help to visualize excited-state processes and carry important information about excited-state dynamics [P6.39].

3.6.4   Results

Steady state spectroscopy. Absorption, fluorescence, and fluorescence excitation spectra of CLH complex are shown in Figure 3.6.1. The absorption spectrum has a shape typical for an antenna from the FCP family, consisting of sharp Soret and Chl *a* bands of Chl *a* and broad carotenoid absorption in the 450-570 nm spectral region. Closer inspection of the CLH absorption spectrum, however, reveals certain differences from other complexes. While there are no significant differences between the antenna complexes in the Soret region, the Q_y band of Chl *a* in the CLH complex peaks at 677 nm, which is red-shifted from other members of the FCP family: 670 nm for the FCP complex from *Cyclotella meneghiniana* [P6.32]-[P6.34], 672 nm for the acpPC complex from *Amphidinium carterae* [P6.36], and 675 nm for the XLH complex from *Xanthonema debile* [P6.15]. Carotenoid absorption in the CLH complex is rather featureless and extending even beyond 550 nm, which is

Figure 3.6.1. Absorption (black), fluorescence (red) and fluorescence excitation (blue) spectra of CLH complex. The absorption spectrum is shown as 1-T (T is transmission) spectrum to allow direct comparison with fluorescence excitation spectrum. Absorption spectrum of Ifx-l in acetonitrile is also shown (orange). All spectra are normalized to maximum of Q_y band of Chl-a. Fluorescence spectrum was obtained after excitation at 435 nm, detection wavelength for fluorescence excitation spectrum was 685 nm.

often observed for the light-harvesting complexes containing carbonyl carotenoids [P6.24]-[P6.28].

The CLH complex, when excited at 435 nm, exhibits characteristic Chl *a* fluorescence band with maximum at 683 nm. This again is red-shifted from the Chl *a* emission reported for other complexes from the FCP family, reflecting the red-shift observed in the absorption spectra. The fluorescence excitation spectrum, detected at

the emission maximum, shows that carotenoids contribute significantly to the emission and represents clear evidence of energy transfer from carotenoids to Chl *a*. Based on the comparison of absorption (1-T) and fluorescence excitation spectra, the overall efficiency of carotenoid – Chl *a* energy transfer is close to 100% in the 500-550 nm region, and it drops slightly to values 82-85 % in the 450-480 nm range. The decrease of the efficiency in the blue part of the carotenoid absorption band is likely due to violaxanthin, which is expected to absorb in this region. Comparing the carotenoid – Chl a energy transfer efficiency with other antenna complexes from the FCP family, the CLH complex is clearly the most efficient.

The spectral dependence of the energy transfer efficiency provided a basis for our choice of excitation wavelengths in transient absorption experiment. We have excited the CLH complex into the red edge of the absorption spectrum, at 540 nm, where the efficiency is largest, and we should selectively excite the lowest vibrational band of the S_0-S_2 transition of the Ifx-l that was identified by circular dichroism spectroscopy [P6.6]. For the second excitation wavelength we have chosen 480 nm where the absorption ratio of violaxanthin/Ifx-l molecules should be most favorable for violaxanthin. Thus, after 480 nm excitation we should be able to track excited-state dynamics of violaxanthin.

Transient absorption spectra. Transient absorption spectra measured after excitation at 540 nm are shown in Figure 3.6.2a. Already, 100 fs after excitation, the transient absorption spectrum contains a clear signal from the Chl *a* bleaching centered at 677 nm. Since there is essentially no Chl *a* absorption at 540 nm, the population of Chl *a* must be achieved via energy transfer from carotenoid. Also, excited state absorption around 600 nm indicates that the S_1/ICT state of the carotenoid is already partly populated for such a short delay after excitation. This observation implies that the S_2 state of the carotenoid excited at 540 nm is swiftly depopulated, both via energy transfer to Chl *a* and internal conversion to the S_1/ICT state. At 0.5 ps, the Chl *a* bleaching further increases. At longer delays, both the carotenoid ground state bleaching and S_1/ICT excited state absorption decreases with a concomitant rise of the Chl *a* signal, a process associated with another energy transfer channel from the S_1/ICT state to the Q_y state of Chl *a*. The spectrum measured at 20 ps delay has no carotenoid signal and is purely due to Chl *a* that is populated via energy transfer from carotenoid.

In order to quantitatively describe the dynamics of CLH after excitation at 540 nm, Figure 3.6.2b shows the EADS extracted from global fitting the data. To

obtain reasonable fits, three time components were needed. The first EADS is due to the excited S_2 state of Ifx-l and decays in less than 100 fs to the second EADS whose shape is characteristic of the S_1/ICT state of the carotenoid. In addition, a clear Chl a bleaching signal indicates a fast S_2-mediated energy transfer pathway. The second EADS decays in 530 fs. It is characterized by decay of the S_1/ICT excited state absorption, which peaks at 595 nm, decay of the carotenoid ground state bleaching, and rise of the Chl *a* bleaching at 677 nm. The third EADS, decaying in 4.2 ps, is almost identical in shape to the second EADS, but has smaller amplitude. This EADS is therefore associated with another energy transfer channel via the S_1/ICT state. However, the vibrational structure of the carotenoid bleaching is markedly less resolved in the 4.2 ps EADS which is likely due to a different carotenoid pool associated with this energy transfer pathway. The final EADS that does not decay within the time window of the experiment is due to Chl *a*.
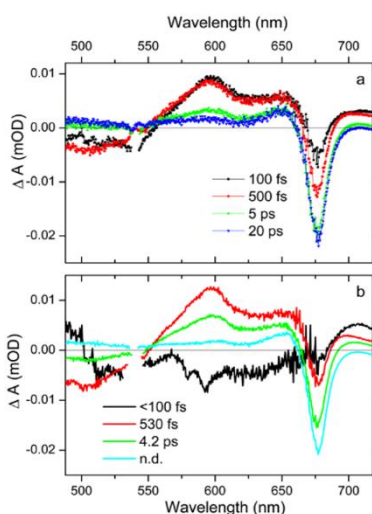
Figure 3.6.2 (a) Transient absorption spectra of CLH complex measured after different time delay after excitation at 540 nm. (b) EADS extracted from global fitting. n.d. – non decaying component.
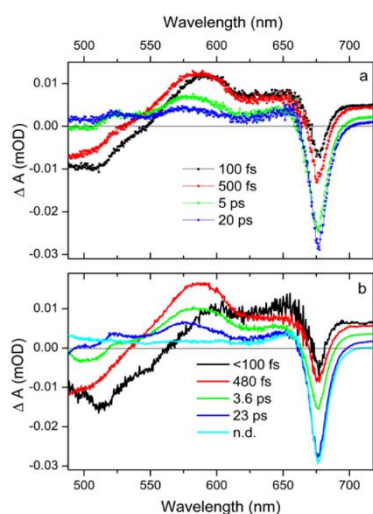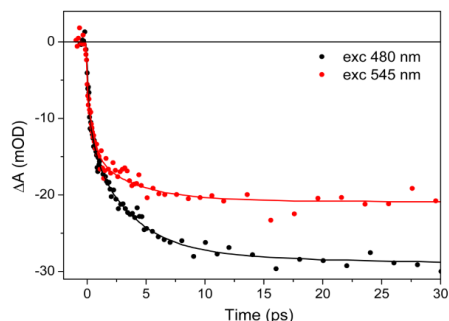
Figure 3.6.3 (a) Transient absorption spectra of CLH complex measured after different time delay after excitation at 480 nm. (b) EADS extracted from global fitting. n.d. – non decaying component.

Transient absorption spectra measured after excitation at 480 nm are depicted in Figure 3.6.3a As for the 540 nm excitation, already at 100 fs after excitation, at 480 nm we see significant Chl a bleaching and S_1/ICT excited state absorption, thus the fast S_2 channel is active also after excitation of the carotenoids absorbing in the blue part of the carotenoid absorption in CLH. Further dynamics is comparable to that after 540 nm excitation with exception to longer delays. Energy transfer is evidenced by comparison of transient absorption spectra measured at 0.5 and 5 ps. The part of the signal associated with carotenoid (ground state bleaching below 540 nm and excited state absorption in the 550-650 nm region) decays while the Chl a signal at 677 nm gains amplitude. Major differences between 540 and 480 nm excitations occurs at longer delays; the transient absorption spectrum taken at 20 ps after excitation at 480 nm contains weak positive bands at 520 and 575 nm that are not detected in the experiment using the 540 nm excitation. These two bands are most likely associated with 'slow' Ifx-l (575 nm) and violaxanthin (520 nm).

The results of fitting the data globally for excitation at 480 nm are shown in Figure 3.6.3b. Due to the differences at longer delays, one extra component is needed to fit the data measured after 480 nm excitation. In contrast to 540 nm excitation, the first EADS contains some Chl a bleaching indicating that the S_2 pathway is faster than for the 540 nm excitation as energy transfer from the S_2 state of carotenoids excited at 480 nm occurs essentially within the excitation pulse. We again extract two energy transfer channels via the S_1/ICT state. These two channels are associated with the second and third EADS which have very similar shape and time constants of 480 fs and 3.6 ps, respectively. These two energy transfer pathways are comparable to those found after 540 nm excitation. It must be noted, however, that the maximum of the S_1/ICT signal in the second and third EADS is at 585 nm and is thus blue-shifted by about 10 nm as compared to the S_1/ICT signal observed after 540 nm excitation (Figure 3.6.2b). This clearly shows that even though the dynamics of the two energy transfer channels are similar for both excitations, different carotenoids associated with these two channels are excited at 480 and 540 nm. The fourth EADS has a lifetime of 23 ps and is obviously unrelated to any dynamics in the Chl a region. Instead, this EADS is associated with decay of the two bands located at 520 and 575 nm that should be therefore associated with S_1 bands of carotenoids in CLH that do not transfer energy to Chl a. The non-decaying component is due to Chl a which does not exhibit any decay within the time window of the experiment.

Figure 3.6.4 compares kinetics measured at the maximum of Chl *a* bleaching after excitation at 480 and 540 nm. It is obvious that energy transfer dynamics, monitored as arrival of excitations to Chl *a* molecule in CLH, do not differ much for the two excitation wavelengths. The fast and slow channels are clearly distinguished in the kinetics and the major difference between 480 and 540 nm is the ratio between the fast and slow channel. The slow channel dominates after 480 nm excitation while the fast channel

Figure 3.6.4 Comparison of rise of the Chl-a signal after excitation of carotenoid at 480 nm (black) and 545 nm (red). Detection wavelength is 680 nm.

becomes more important when CLH is excited into the red edge of the carotenoid absorption at 540 nm.

For proper assessment of energy transfer dynamics we need to know the excited-state properties of the isolated carotenoids that are bound to CLH. While the spectroscopic properties of violaxanthin is well-known from previous reports [P6.40], [P6.41], Ifx-l has never been studied by time-resolved spectroscopy, and the only spectroscopic property known for Ifx-l is the absorption spectrum [P6.16]. Since Ifx-l has a conjugated carbonyl group and its molecular structure is related to that of fucoxanthin [P6.16], some dependence of its excited-state properties on polarity can be expected. To test whether Ifx-l exhibits polarity-dependent behavior we measured the transient absorption spectra and kinetics in the non-polar n-hexane and polar acetonitrile. The results are shown in Figure 3.6.5.
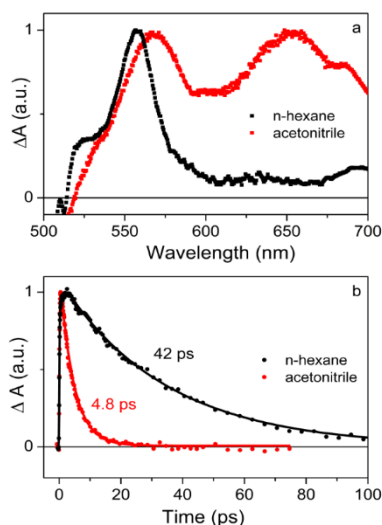
Figure 3.6.5 (a) Transient absorption spectra of Ifx-l measured at 1 ps delay in n-hexane (black) and acetonitrile (red). Kinetics (symbols) and fits (lines) of Ifx-l in n-hexane (black) and acetonitrile (red). Probing wavelengths were 555 nm (n-hexane) and 565 nm (acetonitrile). All data are normalized to maximum. Excitation at 510 nm.

The transient absorption spectrum in n-hexane taken at 1 ps after excitation at 510 nm is dominated by a single S_1-S_n band peaking at 555 nm with a distinct shoulder at 520 nm that is reminiscent of the S* state [P6.42], [P6.43]. When dissolved in polar acetonitrile, the transient absorption spectrum at 1 ps exhibits significant changes. The S_1-S_n band shifts to 565 nm and the S*-like shoulder disappears. A new spectral band centered at 650 nm appears exclusively in acetonitrile. This band, whose magnitude is comparable to that of the S_1-S_n transition, is known from previous reports on other carbonyl carotenoids [P6.17], [P6.18]. It is due to ICT-S_N transition, and it is a marker of significant charge transfer character of the S_1/ICT state. The intensity ratio of the ICT-like and S_1-like transitions is often taken as the measure of the CT character [P6.20]. For Ifx-l this ratio is ~1, larger than for fucoxanthin, for which this ratio is ~0.78 in acetonitrile [P6.18]. Because Ifx-l must have a longer conjugation than fucoxanthin (Figure 3.6.9), this is a surprising observation as it is known that the charge transfer character of the S_1/ICT state usually decreases with increasing conjugation length [P6.17], [P6.18], [P6.44].

The considerable polarity-dependent behavior of Ifx-l is further evidenced by the markedly different lifetimes of the S_1/ICT state in n-hexane and acetonitrile (Figure 3.6.5b). The lifetime decreases by an order of magnitude from 42 ps in n-hexane to 4.8 ps in acetonitrile. This is again a much larger change than for shorter fucoxanthin whose S_1/ICT lifetimes are 60 ps in n-hexane and 30 ps in acetonitrile [18]. Thus, although the exact molecular structure of Ifx-l remains unknown, its polarity dependent behavior is unexpectedly strong. This fact has important consequences for the light-harvesting function of Ifx-l in CLH.

3.6.5 Discussion

The overall energy transfer efficiency between carotenoids and Chl a in CLH is very high as evidenced by the fluorescence excitation spectrum shown in Figure 3.6.1. It reaches nearly 100% in the 500-560 nm spectral region, and it exceeds efficiencies reported for other light-harvesting complexes from the family of FCP-like proteins [P6.10], [P6.15], [P6.32]-[P6.35]. Yet, all FCP-like proteins do better than LHCII from higher plants, an antenna protein exhibiting close homology with FCP-like antenna proteins [P6.9], [P6.11]. Thus, it is obvious that diatoms, dinoflagellates, and other photosynthetic microorganisms utilize specific light-harvesting strategies to maximize the light-harvesting capacity of carotenoids. This is clearly achieved by employing carbonyl carotenoids, because XLH, an antenna protein from the FCP family that does not utilize carbonyl carotenoids, has the lowest efficiency of carotenoid-to-Chl a energy transfer from the FCP-like antenna complexes studied so far [P6.15]. This underscores the advantage of carbonyl carotenoids whose excited-state properties may be tuned by environment [P6.17], [P6.18], [P6.45], which in turn can tune efficiency of energy transfer as demonstrated in synthetic peridinin- and fucoxanthin-pyropheophorbide dyads [P6.21], [P6.46]. Since there is still some variability between complexes utilizing peridinin (acpPC, [P6.36]-[P6.38]), fucoxanthin (FCP, [P6.32]-[P6.35], Ifx-l (CLH) or siphonaxanthin (SPC, [P6.47]), it means that each of these organisms employ slightly different tools to achieve large efficiency of carotenoid-to-Chl a energy transfer.

In CLH, the spectral region with highest energy transfer efficiency is covered by Ifx-l, a carotenoid with unknown molecular structure, which must be related to isofucoxanthin (Figure 3.6.9). The other carotenoid in CLH, violaxanthin, has a relatively short conjugation (N=9) and lacks the conjugated carbonyl group (Figure 3.6.9). This molecular structure prevents violaxanthin from extending its S_0-S_2 transition beyond 520 nm. Moreover, violaxanthin is loosely bound to CLH as some violaxanthin can be removed during purification [P6.8]. The violaxanthin content in CLH also varies with growing conditions, and a recent report indicates that it has likely a photoprotective role in CLH [P6.8]. Thus, the key light-harvesting carotenoid in CLH is Ifx-l.

As for other light-harvesting complexes from the FCP family, also in CLH there are three distinct channels that are utilized to transfer energy from carotenoid to Chl *a*. First, there is the ultrafast S_2-mediated pathway that is observed in essentially all photosynthetic antenna studied so far by means of ultrafast methods [P6.2]. The rate constant cannot be resolved in our experiment due to limited time-resolution (~100 fs). The first EADS corresponding to the initially excited species in CLH contains significant Chl *a* signal. This initial Chl a bleaching constitutes ~50% and ~30% of total Chl *a* signal after 540 and 480 nm excitations, respectively (Figure 3.6.2a and Figure 3.6.2b). Such a large signal cannot be explained by direct excitation of Chl a, because, especially at 540 nm, Chl *a* has virtually zero absorption [P6.48]. Thus, regardless of the excitation wavelength, a significant fraction of Chl *a* is populated via energy transfer from Ifx-l within the time duration of our excitation pulse, most likely on a time scale significantly shorter than 100 fs. For the 480 nm excitation, involvement of violaxanthin in this ultrafast S_2-mediated

Figure 3.6.6 EADS corresponding to the fast (a) and slow (b) energy transfer channel. EADS were obtained from fitting the data measured after excitation at 480 nm (black) and 540 nm (red). All EADS are normalized to maximum.

channel cannot be excluded; thus, both carotenoids can in principle serve as energy donors in this channel. The other two energy transfer channels proceed via the S_1/ICT state. For both excitation wavelengths we observe nearly identical time constants of ~0.5 ps for the fast channel and ~4 ps for the slow channel, but the ratio between the two channels depends on excitation wavelength. While for the 540 nm excitation both channels contribute nearly equally, when carotenoids are excited at 480 nm the slow channel dominates. Even though the energy transfer rates are essentially the same for both excitation wavelengths, different excitation wavelengths must excite different Ifx-l molecules in CLH. Comparison of EADS corresponding to the fast and slow channels (Figure 3.6.6) reveals the spectral inhomogeneity in the Ifx-l pool. As for FCP [P6.33] or acpPC [P6.36]-[P6.38], there are at least two spectrally-distinct Ifx-l molecules having S_1/ICT-S_n peaks at 585 and 595 nm, respectively. These two Ifx-l pools are selectively excited at 480 and 540 nm. Whereas different Ifx-l molecules can be readily assigned to different excitation wavelengths, the Ifx-l molecules involved in
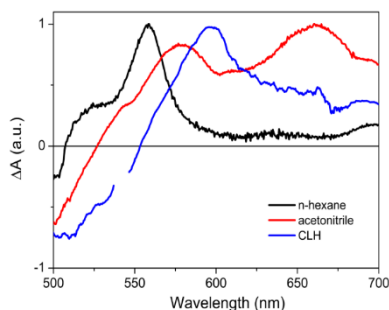
the fast and slow channel after the same excitation are spectrally very similar; the EADS corresponding to the fast and slow channels for each excitation wavelength have the same maxima (Figure 3.6.2b and Figure 3.6.3b).

The data recorded after excitation at 480 nm also revealed spectral bands associated with carotenoids that do not transfer energy to Chl *a*. The fourth EADS in Figure 3.6.3b has a lifetime of 23 ps and contains distinct excited state absorption bands centered at 520 nm and 575 nm. The weak band at 520 nm can be assigned to violaxanthin. Comparable S_1-S_n maxima were observed for either reconstituted or mutated LHCII containing predominantly violaxanthin [P6.49], [P6.50], and even the lifetime of 23 ps matches the lifetime of violaxanthin in solution [P6.40]. The other band at 575 nm is too red shifted to be associated with violaxanthin and must therefore be due to another spectral form of Ifx-l that does not transfer energy to Chl *a*. Thus, there must be at least three spectral forms of Ifx-l that have their S_1/ICT maxima at 575, 585 and 595 nm. The first one is exclusively excited at 480 nm and does not transfer energy to Chl a, the second one is also excited only at 480 nm but transfer energy from the S_1/ICT state via both fast and slow channel, and the third one is exclusively excited at 540 nm and again is active in both fast and slow energy transfer via the S_1/ICT state. Such spectral inhomogeneity is also known from another member of the FCP family, the FCP complex from diatom *C. meneghiniana*, for which also three distinct fucoxanthin pools were identified [P6.51]. Simplified scheme of major energy transfer pathways between carotenoids and Chl *a* in the CLH complex is depicted in Figure 3.6.8.

The presence of a non-transferring Ifx-l in CLH provides information about intrinsic S_1/ICT lifetime of Ifx-l. Assuming that all Ifx-l molecules in CLH have approximately the same intrinsic lifetime, the S_1/ICT lifetime of the non-transferring Ifx-l (23 ps), can serve as a basis for calculation of energy transfer efficiency. Taking into account the 0.5 and 4 ps lifetimes of the S_1/ICT state that transfers energy to Chl *a* via a fast and a slow channel, the estimated energy transfer efficiency is 98% and 83% for the fast and slow channels, respectively. For the 540 nm excitation, where fast and slow channels are about equally weighted, this gives the average efficiency of the S_1/ICT pathway over 90%, which together with a significant fraction (~50%) going via the S_2 route, is the reason for the highly-efficient energy transfer in the 500-560 nm spectral region evidenced by fluorescence excitation spectra (Figure 3.6.1). In the blue spectral region the overall efficiency is lower due to a few reasons. First, the S_2 route is less efficient as evidenced by the smaller fraction of the Chl *a* signal in the

first EADS that may account only for up to ~30% of total energy transfer (Figure 3.6.3b). Second, the slow S_1/ICT channel dominates after 480 nm excitation (Figure 3.6.4), decreasing the average efficiency of this pathway compared to the 540 nm excitation. Finally, in the blue part of the carotenoid absorption in CLH there are at least two carotenoids that do not transfer energy via the S_1/ICT route, violaxanthin having the S_1-S_n transition at 520 nm and Ifx-l with S_1/ICT maximum at 575 nm (Figure 3.6.3b).

The question is how the Ifx-l molecules in CLH achieve such efficiency. It is assumed that the charge transfer character of the S_1/ICT state increases the dipole moment of the S_1/ICT state thereby facilitating the coupling to Chl *a* resulting in enhanced efficiency of the S_1/ICT route [P6.24]. Indeed, a number of experiments exploring the excited-state dynamics of peridinin and fucoxanthin in PCP, acpPC, and FCP supports this hypothesis as in all these complexes, both peridinin and fucoxanthin exhibit behavior similar to that in polar solvents. The ICT-like band in transient absorption spectra, whose magnitude scales with increasing degree of charge transfer character of the S_1/ICT state, is observed in all these complexes [P6.24], [P6.32]-[P6.36]. One may thus expect to see the same behavior for Ifx-l too. To test this, Figure 3.6.7 compares EADS associated with the S_1/ICT lifetime of Ifx-l in n-hexane, acetonitrile and CLH. For Ifx-l in CLH, the EADS of the slow

Figure 3.6.7 Comparison of EADS corresponding to the S_1/ICT lifetime of Ifx-l in n-hexane (black), acetonitrile (red) and in CLH (blue). For Ifx-l in CLH, the EADS is the one associated with the fast energy transfer channel (0.53 ps) after 540 nm excitation. The Chl a contribution was removed by subtracting the scaled non-decaying EADS that corresponds solely to Chl a.

S_1/ICT channel is chosen, and, to allow for direct comparison with spectral properties in solution, the Chl *a* contribution in CLH is subtracted. It is apparent that EADS of Ifx-l in CLH do not contain any significant ICT bands, suggesting that the S_1/ICT state of Ifx-l in CLH has only weak charge-transfer character and its spectroscopic properties are close to those in non-polar solvent. This is in sharp contrast with other complexes containing carbonyl carotenoids, such as PCP [P6.24], FCP [P6.34], [P6.35] or acpPC [P6.36].

The reason for this behavior can be traced to the specific excited-state properties of Ifx-l. While fucoxanthin always has even in the most polar environment

the S_1/ICT lifetime always longer than 15 ps [P6.17], [P6.18], [P6.52], if the S_1/ICT state of Ifx-l possesses a significant charge transfer character (as in acetonitrile, see Figure 3.6.5) its lifetime can be as short as 4.2 ps. With such short intrinsic S_1/ICT lifetime the energy transfer channel could hardly compete with the S_1/ICT-S_0 relaxation. It seems that the intrinsic S_1/ICT lifetime in the range of 15-20 ps is ideal for proper balancing of the energy transfer rate and S_1/ICT-S_0 relaxation. In PCP for example, the intrinsic S_1/ICT lifetime of peridinin was estimated to be 16 ps [P6.24], and that is also the limit that could be theoretically achieved for fucoxanthin if it resides in polar environment. Thus, to maintain high efficiency, the CLH complex prevents the S_1/ICT state of Ifx-l from gaining a significant charge transfer character. Comparing the 23 ps S_1/ICT lifetime of the non-transferring Ifx-l in CLH with that in n-hexane (42 ps), we may conclude that Ifx-l resides in CLH in a weakly polar environment. This is consistent with the EADS shown in Fig. 7 as the Ifx-l in CLH clearly has more signal in the 630-700 nm region than Ifx-l in n-hexane, indicating weak charge transfer character of the S_1/ICT state of Ifx-l in CLH.

We conclude that the CLH complex is a light-harvesting system utilizing yet another light-harvesting strategy to achieve high efficiency of carotenoid-to-Chl *a* energy transfer. Since *C. velia* is a symbiont of corals thriving in shallow waters, harvesting the photons in the 500-560 nm spectral region is of high importance [P6.53]. To extend the absorption into the green-yellow region, CLH complex binds predominantly the carbonyl carotenoid Ifx-l, because, regardless of polarity, the conjugated carbonyl group shrinks the S_2-S_1/ICT gap, resulting in shifting the S_2 state to the 500-560 nm region while keeping the S_1/ICT state high enough to transfer energy to Q_y of Chl *a* [P6.18]. However, contrary to other light-harvesting complexes utilizing carbonyl carotenoids, CLH suppresses the charge transfer character of the S_1/ICT state to keep the high efficiency of energy transfer.

It is interesting to compare the light-harvesting properties of CLH with other complexes from the FCP family and also with PCP, the most studied antenna complex utilizing carbonyl carotenoid. First of all, the fast and slow S_1/ICT channels are present in all complexes, yet the contribution of these two channels varies significantly among the complexes. In CLH, the fast and slow channels contribute nearly equally to the S_1/ICT route, and a comparable contribution of the fast channel was reported for acpPC complex [P6.36]. It should be noted, though, that the fast channel in acpPC was attributed to a transfer from hot S_1/ICT state which is not the case for CLH. In FCP the contribution of the fast channel is less [P6.32]-[P6.35], and in PCP the

fast channel is negligible, and essentially all transfer via the S_1/ICT route in PCP proceeds with ~3 ps time constant [P6.24], [P6.28], [P6.30]. All complexes also contains non-transferring carotenoids with the S_1/ICT lifetime in the 15-30 ps range [P6.28], [P6.32]-[P6.36].
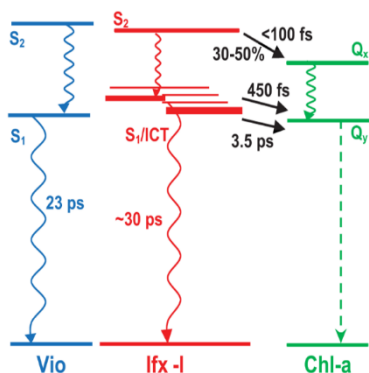
Figure 3.6.8. Scheme of energy transfer pathways between carotenoids and Chl a in CLH complex. The pathways are denoted as black solid arrows labelled by corresponding time constants. Wavy arrows correspond to internal conversion processes, dashed arrow denotes Chl a fluorescence. See text for details.

The most intriguing observation is the ubiquitous presence of the energy transfer channel characterized by the 2.5-4 ps time constant. This channel is present (and in most cases it is also dominant) in all complexes with Chl a acceptors even though they have completely different carotenoid composition and a completely different structure as in the case of PCP. A 3.5 ps energy transfer component was also found in the siphonaxanthin chlorophyll protein (SCP) from *Codium fragile* [P6.47]. In this complex, the final assignment of the 3.5 ps component is complicated by the fact that this complex contains also Chl *b,* and it was studied only by time-resolved fluorescence spectroscopy. Thus, the 3.5 ps component could also be due to Chl *b*-to-Chl *a* transfer as suggested by Akimoto et al. [P6.47]. Moreover, even the XLH complex belongs to the FCP family but has no carbonyl carotenoids, yet it has the S_1 route active and characterized by a 3.5 ps time constant [P6.15]. These observations suggest that despite different structures and different carotenoid composition, time constants of the major energy transfer channel via the S_1/ICT route converge to a 2.5-4 ps value, providing the Q_y band of Chl *a* is the acceptor. The role of the acceptor is likely crucial in this convergence as changing the acceptor molecule by reconstitution of PCP complex with different chlorophylls significantly alters this rate constant [P6.30].

3.6.6 Acknowledgment

3.6.7   References

[P6.1]   G.D. Scholes, G.R. Fleming, A. Olaya-Castro, R. van Grondelle, Lessons from nature about solar light harvesting, Nature Chemistry 3 (2011) 763-774.

[P6.2]   T. Polívka, H.A. Frank, Molecular factors controlling photosynthetic light harvesting by carotenoids, Acc. Chem. Res. 43 (2010) 1125-1134.

[P6.3]   T. Polívka, V. Sundström, Ultrafast dynamics of carotenoid excited states - From solution to natural and artificial systems, Chemical Reviews 104 (2004) 2021-2071.

[P6.4]   M. Oborník, D. Modrý, M. Lukeš, E. Černotíková-Stříbrná, J. Cihlář, M. Tesařová, E. Kotabová, M. Vancová, O. Prášil, J. Lukeš, Morphology, ultrastructure and life cycle of *Vitrella brassicaformis* n. sp., n. gen., a novel Chromerid from the Great Barrier Reef, Protist 163 (2012) 306–323.

[P6.5]   M. Oborník, J. Lukeš, Cell biology of chromerids, the autotrophic relatives to apicomplexan parasites. International Review of Cell and Molecular Biology 306 (2013) 333-369.

[P6.6]   J. Tichý, Z. Gardian, D. Bína, P. Koník, R. Litvín, M. Herbstová, A. Pain, F. Vácha, Light harvesting complexes of *Chromera velia*, photosynthetic relative of apicomplexan parasites, Biochim. Biophys. Acta 1827 (2013) 723–729.

[P6.7]   E. Kotabová, J. Jarešová, R. Kaňa, R. Sobotka, D. Bína, O. Prášil, Novel type of red-shifted chlorophyll a antenna complex from *Chromera velia*. I. Physiological relevance and functional connection to photosystems, Biochim. Biophys. Acta 1837 (2014) 734-743.

[P6.8]   D. Bína, Z. Gardian, M. Herbstová, E. Kotabová, P. Koník, R. Litvín, O. Prášil, J. Tichý, F. Vácha, Novel type of red-shifted chlorophyll a antenna complex from *Chromera velia*: II. Biochemistry and spectroscopy, Biochim. Biophys. Acta 1837 (2014) 802-810.

[P6.9]   H. Pan, J. Šlapeta, D. Carter, M. Chen, Phylogenetic analysis of the light-harvesting system in *Chromera velia*, Photosynth. Res. 111 (2012) 19-28.

[P6.10] R. Fujii, M. Kita, Y. Iinuma, N. Oka, Y. Takaesu, T. Taira, M. Iha, R.J. Cogdell, H. Hashimoto, Isolation and purification of the major photosynthetic antenna, fucoxanthin-Chl a/c protein, from cultured discoid germilings of the brown alga, *Cladosiphon okamuranus* TOKIDA (Okinawa Mozuku), Photosynth. Res. 111 (2012) 157-163.

[P6.11] J.A.D. Neilson, D.G. Durnford, Structural and functional diversification of the light-harvesting complexes in photosynthetic eukaryotes, Photosynth. Res. 106 (2010) 57-71.

[P6.12] Z. Liu, H. Yan, K. Wang, T. Kuang, J. Zhang, L. Gui, X. An, W. Chang, Crystal structure of spinach major light-harvesting complex at 2.72 Å resolution, Nature 428 (2004) 287-292.

[P6.13] M. Di Valentin, E. Meneghin, L. Orian, A. Polimeno, C. Büchel, E. Salvadori, C.W.M. Kay, D. Carbonera, Triplet-triplet energy transfer in fucoxanthin-chlorophyll protein from diatom *Cyclotella meneghiniana*:

Insights into the structure of the complex, Biochim. Biophys. Acta 1827 (2013) 1226-1234.

[P6.14] Z. Gardian, J. Tichý, F. Vácha, Structure of PSI, PSII and antennae complexes from yellow-green alga *Xanthonema debile*, Photosynth. Res. 108 (2011) 25–31.

[P6.15] M. Durchan, J. Tichý, R. Litvín, V. Šlouf, Z. Gardian, P. Hříbek, F. Vácha, T. Polívka, Role of carotenoids in light-harvesting processes in an antenna protein from the chromophyte *Xanthonema debile*, J. Phys. Chem. B 116 (2012) 8880–8889.

[P6.16] R.B. Moore, M. Oborník, J. Janouškovec, T. Chrudimský, M. Vancová, D.H. Green, S.W. Wright, N.W. Davies, C.J.S. Bolch, K. Heimann, J. Šlapeta, O. Hoegh-Guldberg, J.M. Logsdon Jr., D.A. Carter, A photosynthetic alveolate closely related to apicomplexan parasites, Nature 451 (2008) 959–963.

[P6.17] H.A. Frank, J.A. Bautista, J. Josue, Z. Pendon, R.G. Hiller, F.P. Sharples, D. Gosztola, M.R. Wasielewski, Effect of the solvent environment on the spectroscopic properties and dynamics of the lowest excited states of carotenoids, J. Phys. Chem. B 104 (2000) 4569-4577.

[P6.18] D. Zigmantas, R.G. Hiller, F.P. Sharples, H.A. Frank, V. Sundström, T. Polívka, Effect of a conjugated carbonyl group on the photophysical properties of carotenoids, Phys. Chem. Chem. Phys. 6 (2004) 3009-3016.

[P6.19] D. Zigmantas, T. Polívka, R.G. Hiller, A. Yartsev, V. Sundström, Spectroscopic and dynamic properties of the peridinin lowest singlet excited states, J. Phys. Chem. A 105 (2001) 10296-10306.

[P6.20] D. Zigmantas, R.G. Hiller, A. Yartsev, V. Sundström, T. Polívka, Dynamics of excited states of the carotenoid peridinin in polar solvents: Dependence on excitation wavelength, viscosity, and temperature, J. Phys. Chem. B 107 (2003) 5339-5348.

[P6.21] T. Polívka, M. Pellnor, E. Melo, T. Pascher, V. Sundström, A. Osuka, K.R. Naqvi, Polarity-tuned energy transfer efficiency in artificial light-harvesting antennae containing carbonyl carotenoids peridinin and fucoxanthin, J. Phys. Chem. C 111 (2007) 467-476.

[P6.22] E. Hofmann, P.M. Wrench, F.P. Sharples, R.G. Hiller, W. Welte, K. Diederichs, Structural basis of light harvesting by carotenoids: Peridinin-chlorophyll-protein from *Amphidinium carterae*, Science 272 (1996) 1788-1791.

[P6.23] T. Schulte, D.M. Niedzwiedzki, R.R. Birge, R.G. Hiller, T. Polívka, E. Hofmann, H.A. Frank, Identification of a single peridinin sensing Chl-a excitation in reconstituted PCP by crystallography and spectroscopy, Proc. Natl. Acad. Sci. U.S.A. 106 (2009) 20764-20769.

[P6.24] D. Zigmantas, R.G. Hiller, V. Sundström, T. Polívka, Carotenoid to chlorophyll energy transfer in the peridinin-chlorophyll-a-protein complex involves an intramolecular charge transfer state, Proc. Natl. Acad. Sci. U.S.A. 99 (2002) 16760-16765.

[P6.25] F.J. Kleima, M. Wendling, E. Hofmann, E.J.G. Peterman, R. van Grondelle, H. van Amerongen, Peridinin chlorophyll a protein: Relating structure and steady-state spectroscopy, Biochemistry 39 (2000) 5184-5195.

[P6.26] J.A. Bautista, R.G. Hiller, F.P. Sharples, D. Gosztola, M.R. Wasielewski, H.A. Frank, Singlet and triplet energy transfer in the peridinin-chlorophyll a protein from *Amphidinium carterae*, J. Phys. Chem. A 103 (1999) 2267-2273.

[P6.27] Damjanovic, T. Ritz, K. Schulten, Excitation transfer in the peridinin-chlorophyll-protein of *Amphidinium carterae*, Biophys. J. 79 (2000) 1695-1705.

[P6.28] B.P. Krueger, S.S. Lampoura, I.H. van Stokkum, E. Papagiannakis, J.M. Salverda, C.C. Gradinaru, D. Rutkauskas, R.G. Hiller, R. van Grondelle, Energy transfer in the peridinin chlorophyll-a protein of *Amphidinium carterae* studied by polarized transient absorption and target analysis, Biophys. J. 80 (2001) 2843-2855.

[P6.29] R.P. Ilagan, S. Shima, A. Melkozernov, S. Lin, R.E. Blankenship, F.P. Sharples, R.G. Hiller, R.R. Birge, H.A. Frank, Spectroscopic properties of the main-form and high-salt peridinin-chlorophyll a proteins from Amphidinium carterae, Biochemistry 43 (2004) 1478-1487.

[P6.30] T. Polívka, T. Pascher, V. Sundström, R.G. Hiller, Tuning energy transfer in the peridinin-chlorophyll complex by reconstitution with different chlorophylls, Photosynth. Res. 86 (2005) 217-227.

[P6.31] C. Bonetti, M.T.A. Alexandre, I.H.M. van Stokkum, R.G. Hiller, M.L. Groot, R. van Grondelle, J.T.M. Kennis, Identification of excited-state energy transfer and relaxation pathways in the peridinin-chlorophyll complex: an ultrafast mid-infrared study, Phys. Chem. Chem. Phys. 12 (2010) 9256-9266.

[P6.32] E. Papagiannakis, I.H.M. van Stokkum, H. Fey, C. Büchel, R. van Grondelle, Spectroscopic characterization of the excitation energy transfer in the fucoxanthin-chlorophyll protein of diatoms, Photosynth. Res. 86 (2005) 241-250.

[P6.33] N. Gildenhoff, J. Herz, K. Gundermann, C. Büchel, J. Wachtveitl, The excitation energy transfer in the trimeric fucoxanthin-chlorophyll protein from *Cyclotella meneghiniana* analyzed by polarized transient absorption spectroscopy, Chem. Phys. 373 (2010) 104-109.

[P6.34] N. Gildenhoff, S. Amarie, K. Gundermann, A. Beer, C. Büchel, J. Wachtveitl, Oligomerization and pigmentation dependent excitation energy transfer in fucoxanthin-chlorophyll proteins, Biochim. Biophys. Acta 1797 (2010) 543-549.

[P6.35] D. Kosumi, M. Kita, R. Fujii, M. Sugisaki, N. Oka, Y. Takaesu, T. Taira, M. Iha, H. Hashimoto, Excitation energy-transfer dynamics of brown algal photosynthetic antennas, J. Phys. Chem. Lett. 3 (2012) 2659-2664.

[P6.36] T. Polívka, I.H.M. van Stokkum, D. Zigmantas, R. van Grondelle, V. Sundström, R.G. Hiller, Energy transfer in the major intrinsic light-harvesting complex from *Amphidinium carterae*, Biochemistry 45 (2006) 8516-8526.

[P6.37] V. Šlouf, M. Fuciman, S. Johanning, E. Hofmann, H.A. Frank, T. Polívka, Low-temperature time-resolved spectroscopic study of the major light-harvesting complex of *Amphidinium carterae*, Photosynth. Res. 117 (2013) 257-265.

[P6.38] D. Niedzwiedzki, J. Jiang, C.S. Lo, R.E. Blankenship, Spectroscopic properties of the chlorophyll a – chlorophyll c_2 – peridinin – protein – complex (acpPC) from the coral symbiotic dinoflagellate *Symbiodinium*, Photosynth. Res. 120 (2014) 125-139.

[P6.39] I.H.M. van Stokkum, D.S. Larsen, R. van Grondelle, Global and target analysis of time-resolved spectra, Biochim. Biophys. Acta 1657 (2004) 82-104.

[P6.40] H.A. Frank, A. Cua, V. Chynwat, A. Young, D. Gosztola, M.R. Wasielewski, Photophysics of the carotenoids associated with the xanthophyll cycle in photosynthesis, Photosynth. Res. 41 (1994) 389-395.

[P6.41] D.M. Niedzwiedzki, J.O. Sullivan, T. Polívka, R.R. Birge, H.A. Frank, Femtosecond time-resolved transient absorption spectroscopy of xanthophylls, J. Phys. Chem. B 110 (2006) 22872-22885.

[P6.42] C.C. Gradinaru, J.T.M. Kennis, E. Papagiannakis, I.H.M. van Stokkum, R.J. Cogdell, G.R. Fleming, R.A. Niederman, R. van Grondelle, An unusual pathway of excitation energy deactivation in carotenoids: Singlet-to-triplet conversion on an ultrafast timescale in a photosynthetic antenna, Proc. Natl. Acad. Sci. U.S.A. 98 (2001) 2364-2369.

[P6.43] D. Kosumi, S. Maruta, T. Horibe, Y. Nagaoka, R. Fujii, M. Sugisaki, R.J. Cogdell, H. Hashimoto, Ultrafast excited state dynamics of spirilloxanthin in solution and bound to core antenna complexes: Identification of the S* and T-1 states, J. Chem. Phys. 137 (2012) 064505.

[P6.44] P. Chábera, M. Fuciman, P. Hříbek, T. Polívka, Effect of carotenoid structure on excited-state dynamics of carbonyl carotenoids, Phys. Chem. Chem. Phys. 11 (2009) 8795-8803.

[P6.45] P. Chábera, M. Fuciman, K.R. Naqvi, T. Polívka, Ultrafast dynamics of hydrophilic carbonyl carotenoids – Relation between structure and excited-state properties in polar solvents, Chem. Phys. 373 (2010) 56-64.

[P6.46] M.P. Debreczeny, M.R. Wasielewski, S. Shinoda, A. Osuka, Singlet-singlet energy transfer mechanisms in covalently-linked fucoxanthin- and zeaxanthin-pyropheophorbide molecules, J. Am. Chem. Soc. 119 (1997) 6407-6414.

[P6.47] S. Akimoto, T. Tomo, Y. Naitoh, A. Otomo, A. Murakami, M. Mimuro, Identification of a new excited state responsible for the in vivo unique absorption band of siphonaxanthin in the green alga *Codium fragile*, J. Phys. Chem. B 111 (2007) 9179-9181.

[P6.48] L.P. Vernon, Spectrophotometric determination of chlorophylls and pheophytins in plant extracts, Anal. Chem. 32 (1960) 1144-1150.

[P6.49] T. Polívka, D. Zigmantas, V. Sundström, E. Formaggio, G. Cinque, R. Bassi, Carotenoid S-1 state in a recombinant light-harvesting complex of photosystem II, Biochemistry 41 (2002) 439-450.

[P6.50] M. Fuciman, M.M. Enriquez, T. Polívka, L. Dall'Osto, R. Bassi, H.A. Frank, Role of xanthophylls in light harvesting in green plants: A spectroscopic investigation of mutant LHCII and lhcb pigment-protein complexes, J. Phys. Chem. B 116 (2012) 3834-3849.

[P6.51] L. Premvardhan, L. Bordes, A. Beer, C. Büchel, B. Robert, Carotenoid structures and environments in trimeric and oligomeric fucoxanthin chlorophyll a/c₂ proteins from resonance raman spectroscopy, J. Phys. Chem. B 113 (2009) 12565-12574.

[P6.52] D. Kosumi, T. Kusumoto, R. Fujii, M. Sugisaki, Y. Iinuma, N. Oka, Y. Takaesu, T. Taira, M. Iha, H.A. Frank, H. Hashimoto, One- and two-photon pump-probe optical spectroscopic measurements reveal the S-1 and intramolecular charge transfer states are distinct in fucoxanthin, Chem. Phys. Lett. 483 (2009) 95-100.

[P6.53] M. Stomp, J. Huisman, L.J. Stal, H.C.P. Matthijs, Colorful niches of phototrophic microorganisms shaped by vibrations of the water molecule, ISME 1 (2007) 271-282.

3.6.8 Supporting Information
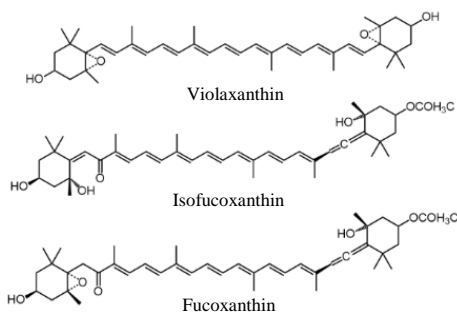
Figure 3.6.9 Molecular structures of violaxanthin, fucoxanthin and isofucoxanthin. While violaxanthin is bound to the CLH complex, fucoxanthin and violaxanthin are shown as reference molecules. Based on spectroscopic data, the unknown carotenoid bound to CLH, Ifx-l, is a derivative of isofucoxanthin. While the absorption maximum of isofucoxanthin in methanol was reported at 454 nm [1], the Ifx-l has its absorption maximum shifted to 465 nm (Fig. 1 shows absorption spectrum in acetonitrile, spectrum in methanol is nearly identical – data not shown). Because Isx-l exhibits behavior typical of carbonyl carotenoids (see Fig. 5), the conjugated carbonyl group must be conserved, yet the conjugation length of Isx-l must be longer than that of isofucoxanthin.

[1] R.B. Moore, M. Oborník, J. Janouškovec, T. Chrudimský, M. Vancová, D.H. Green, S.W. Wright, N.W. Davies, C.J.S. Bolch, K. Heimann, J. Šlapeta, O. Hoegh-Guldberg, J.M. Logsdon Jr., D.A. Carter, A photosynthetic alveolate closely related to apicomplexan parasites, Nature 451 (2008) 959–963.

3.7 PAPER 7

Efficient Light-Harvesting Using non-Carbonyl Carotenoids: Energy Transfer Dynamics in the VCP Complex from Nannochloropsis oceanica

Gürkan Keşan, Radek Litvín, David Bína, Milan Durchan, Václav Šlouf, Tomáš Polívka,

3.7.1 Abstract

Violaxanthin–chlorophyll a protein (VCP) from Nannochloropsis oceanica is a Chl a-only member of the LHC family of light-harvesting proteins. VCP binds carotenoids violaxanthin (Vio), vaucheriaxanthin (Vau), and vaucheriaxanthin-ester (Vau-ester).Here we report on energy transfer pathways in the VCP complex. The overall carotenoid-to-Chl a energy transfer has efficiency over 90%. Based on their energy transfer properties, the carotenoids in VCP can be divided into two groups; blue carotenoids with the lowest energy absorption band around 480 nm and red carotenoids with absorption extended up to 530 nm. Both carotenoid groups transfer energy efficiently from their S_2 states, reaching efficiencies of ~70% (blue) and ~60% (red). The S_1 pathway, however, is efficient only for the red carotenoid pool for which two S_1 routes characterized by 0.33 and 2.4 ps time constants were identified. For the blue carotenoids the S_1-mediated pathway is represented only by a minor route likely involving a hot S_1 state. The relaxed S_1 state of blue carotenoids decays to the ground state within 21 ps. Presence of a fraction of non-transferring red carotenoids with the S_1 lifetime of 13 ps indicates some specific carotenoid-protein interaction that must shorten the intrinsic S_1 lifetime of Vio and/or Vau whose S_1 lifetimes in methanol are 26 and 29 ps, respectively. The VCP complex from N. oceanica is the first example of a light-harvesting complex binding only non-carbonyl carotenoids with carotenoid-to-chlorophyll energy transfer efficiency over 90%.

3.7.2 Introduction

Photosynthetic organisms are vitally dependent on their light-harvesting systems to absorb light and transfer the excitation energy to the reaction centers [P7.1], [P7.2]. Photosynthetic eukaryotes predominantly utilize membrane light-harvesting proteins which belong to the LHC family. The LHC family, whose most explored member is the LHCII antenna protein of plants [P7.3], consists of different subgroups that share the same evolutionary origin and structural motifs [P7.4], [P7.5] but often accommodate different pigments. Besides the LHCII-type antenna of plants that binds Chl a and Chl b, other well-known members are, for example, Chl a/Chl c binding proteins such as fucoxanthin–chlorophyll protein (FCP) of diatoms and peridinin-binding acpPC antenna of dinoflagellates, or LHCSR/Lhcx proteins [P7.6], [P7.7]. The light harvesting capacity of LHC proteins reflects different ecological niches occupied by different photosynthetic eukaryotes and depends crucially on carotenoid-to-Chl energy transfer efficiency which varies from 40 to nearly 100% depending on
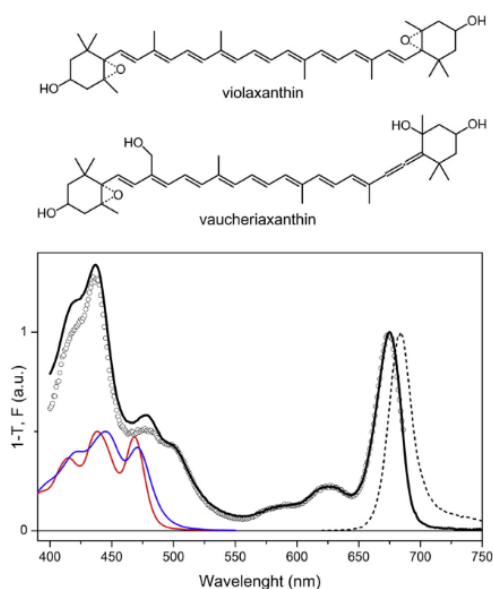
carotenoid composition [P7.8]. The proteins from the LHC family are also involved in photoprotection as bound carotenoids effectively quench both triplet [P7.9]-[P7.11] and singlet [P7.12]-[P7.14] excited states of Chl a.

The diversity of chlorophylls in the LHC family is limited to Chl a, Chl b and Chl c, but much larger diversity is found among carotenoids bound to various LHC members. Plant light-harvesting systems from the LHC family bind lutein, violaxanthin, neoxanthin and zeaxanthin [P7.3], [P7.5], [P7.16], while carbonyl carotenoids fucoxanthin and peridinin are typically found in diatoms and dinoflagellates [P7.17]. A number of other carotenoids were reported in other members of the LHC family [P7.18], [P7.19]. All LHC antennas bind Chl a as the main pigment and in most cases accessory chlorophylls, either Chl b or Chl c, are present. Recently, however, a few Chl a-only members of the LHC family lacking the accessory chlorophylls Chl b or Chl c were reported and spectroscopically characterized. A light harvesting complex from the soil chromophytic alga Xanthonema debile, XLH, contains only Chl a and four carotenoids diadinoxanthin, diatoxanthin, heteroxanthin and vaucheriaxanthin [P7.20] that transfer energy to Chl a with efficiency about 60% [P7.21]. Even higher carotenoid-to-Chl energy transfer efficiency, >90% was reported in Chl a only antenna from a photosynthetic unicellular alveolate Chromera velia, CLH, which binds violaxanthin and an unidentified carbonyl carotenoid [P7.22]-[P7.24]. Recently, stress-related light-harvesting complex LHCSR1 froma moss *Physcomitrella* patens was also shown to bind only Chl a [P7.25].

Another interesting Chl a-only member of the LHC family, violaxanthin–chlorophyll a protein (VCP) from a microalga *Nannochloropsis (N.) gaditana* from the *Eustigmatophyceae* class, has been recently described [P7.26]-[P7.28]. The Nannochloropsis genus gained interest due to its possible utilization of some species in biotechnology because of their high growth rate and accumulation of lipids [P7.29]. The high growth rate is indicative of effective light harvesting and photoprotection; thus, detailed investigation of the VCP complex is of interest. The VCP complex of *N. gaditana* binds mostly violaxanthin (Vio) and vaucheriaxanthin (Vau) in a Vio/Vau ratio of 1.5 as major carotenoids with minor appearance of zeaxanthin and antheraxanthin (b5% of total carotenoid content) [28]. Recently, Carbonera et al. reported optically-detected magnetic resonance (ODMR) and time resolved electron paramagnetic resonance (EPR) studies of the VCP complex from *N. gaditana* [P7.30].They identified efficient triplet-triplet energy transfer between Chl a and carotenoid, constituting an effective photoprotective pathway. Moreover, comparing

the data obtained from VCP, FCP and LHCII, these authors concluded that these complexes exhibit large structural similarity with a protein core binding two central carotenoids (at the L1 and L2 sites of the LHCII structure [P7.3]) surrounded by five Chl a molecules [P7.30].

While the efficient photoprotective actions of carotenoids in VCP have been reported [P7.30], nothing is known so far about their light-harvesting ability. In carotenoids, two excited states, denoted as S_1 and S_2, are common energy donors in light-harvesting proteins [P7.8]. While the S_2 state is the absorbing state responsible for the strong absorption of carotenoids in the 400–550 nm spectral region (the S_0–S_2 transition), the lowest-lying excited state S_1 is a dark state as the S_0–S_1 transition is forbidden for one-photon transitions [P7.31], [P7.32]. When the S_2 state is excited, it relaxes to the S_1 state in less than 300 fs; the S_1 state decays to the ground state on a picosecond time scale. Both energies and lifetimes of S_1 and S_2 states are mainly determined by the carotenoid conjugation length, N, which is defined as number of conjugated C=C groups in carotenoid structure [P7.32]. Thus, as the energy of the donor state must be higher than the acceptor state to achieve energy transfer, and as such energy transfer must compete with the state's intrinsic lifetime, the carotenoid structure crucially determines the energy transfer efficiency [P7.8].

Figure 3.7.1 (top) Molecular structures of violaxanthin and vaucheriaxanthin. (bottom) Absorption (solid line), fluorescence (dashed line) and fluorescence excitation (symbols) of VCP complex. To allow direct comparison with fluorescence excitation spectrum and estimate energy transfer efficiencies, absorption spectrum of VCP is presented as 1-T (T, transmittance). Absorption spectra of Vio (red) and Vau (blue) in methanol are also shown. Fluorescence spectra were obtained after excitation of the Soret band at 437 nm. Detection wavelength for the fluorescence excitation spectra was 695 nm.

From this point of view, Vio (see Figure 3.7.1 for structure) is a potentially efficient energy donor. It has conjugation length N=9, which places its S_2 and S_1 energies in solution at ~21,300 cm−1 (470 nm) and ~15,000 cm−1 (666 nm) [P7.32],

respectively, thus above the Q_x (energy acceptor for the S_2 state) and Q_y (energy acceptor for the S_1 state) states of Chl a. Moreover, carotenoids with N=9 have the longest S_2 lifetime reported so far [P7.33] and the S_1 lifetime of Vio is in the 21–26 ps range [P7.34], [P7.35]. This is fairly long in comparison with other carotenoids commonly found in LHC antenna proteins such as lutein or zeaxanthin. No spectroscopic data are available for Vau (Figure 3.7.1), but since its structure is very close to that of neoxanthin (see Supporting information, Figure 3.7.10 for comparison of Vau and Neo structures), which has an even shorter conjugation than Vio, the excited-state properties of Vau should also be favorable for energy transfer in a light-harvesting system with Chl a as the energy acceptor.

Energy transfer efficiency of Vio within the LHC family was determined for LHCII and CP29 antenna proteins. In LHCII Vio is bound to the peripheral V1 site and its involvement in energy transfer is negligible [P7.36]-[P7.38]. In CP29 Vio occupies the internal L2 carotenoid site [P7.15], resulting in opening an efficient energy transfer channel from the S_2 state of Vio, but involvement of the S_1 state of Vio in energy transfer is still unclear [P7.36], [P7.39]. Absence of S_1-mediated energy transfer of Vio was also reported for both Vio reconstituted [P7.40] and genetically modified [P7.41] LHCII complexes.

Although Vio has spectroscopic parameters favorable for efficient energy transfer to Chl, data reported so far for a few Vio-binding members of the LHC family show that Vio-Chl energy transfer efficiency does not exceed 60% and proceeds predominantly via the S_2 state. This could imply that Car-Chl energy transfer in the VCP complex, which binds Vio and Vau, will also be limited. Here we study energy transfer pathways between carotenoids and Chl a in the VCP complex from Nannochloropsis oceanica [P7.42] using femtosecond transient absorption spectroscopy. In contrast to reports on other members of the LHC family our data provide evidence of total carotenoid-to-Chl a energy transfer efficiency exceeding 90%.

3.7.3   Metarials and methods

Cultivation and VCP purification

Cells of N. oceanica CCALA 978 (CRIAR 2012/1) were grown in 5 L Erlenmeyer flasks in artificial seawater f/2-Si medium [P7.43] at 20 °C under irradiance of 20 μmol photons $m^{-2}s^{-1}$ provided by a metal- halide lamp (OSRAM POWERSTAR HQI-E 70W/NDL). The cultures were bubbled with filtered air and stirred.

The isolation of the VCP antenna complex was modified from [P7.44]. Briefly, thylakoid membranes were solubilized by 2% n-dodecyl β-D-malto side and pre-purified on a linear sucrose gradient. The antenna zone from the gradient was collected and further purified using the anion exchange chromatography on a 2 mL column packed with DEAE Sepharose CL-6B (Sigma-Aldrich, St. Louis, MO, USA) using a linear NaCl gradient of 5–300 mM (elution buffer: 50 mM Tris–HCl pH 7.5, 2 mM KCl, and 0.03% n-dodecyl β-D-maltoside). The fractions eluted at 80–120 mM NaCl were selected for spectroscopic measurements based on the simultaneous criteria of lowest protein:Chl a (A270/ A674 b 0.45) and highest carotenoid:Chl a (A480/A674 ~ 0.5) ratios. The chosen fractions were desaltedandstoredat−80°C. Prior to experiments, the isolated VCP complexes were dissolved in a buffer (50mM Tris–HCl pH 7.5, 2 mM KCl, and 0.03% n-dodecyl β-D-maltoside) to yield optical density ~ 0.6/mm at 675 nm for femtosecond transient absorption experiments, and 0.07/cm at 675 nm for fluorescence measurements.

Pigment analysis and purification were carried out as described in [P7.45] using high-performance liquid chromatography (Pump Controller Delta 600, Auto sampler 2707 injection system, PDA 2996 detector, Waters, USA) on a reverse-phase Zorbax SB-C18 column (Agilent, USA) using a linear gradient elution with a ternary solvent system with solvent A (80:20 methanol:0.5Mammoniumacetate (aq., pH 7.2 v/v)), solvent B (90:10 acetonitrile: water), and solvent C (100% ethyl acetate) adopted from[46]. Pigment samples were dried under vacuum in the dark and stored at−20 °C. For transient absorption experiments, isolated and purified carotenoids were dissolved in a spectroscopic grade methanol (Sigma Aldrich) to yield optical density of 0.5/mmat the absorption maximum. Protein content was characterized using CN-PAGE and SDS-PAGE electrophoresis as described in [45] and found to consist of a ~26 kDa protein [P7.28].

Spectroscopy

Steady-state absorption spectra were measured on Agilent 8453 UV–VIS spectrophotometer; fluorescence and fluorescence excitation spectra were recorded on a Fluorolog 2 (Spex, Horiba, USA) spectrofluorometer. A 1-cmpath length cuvette was used for steady-state absorption and room-temperature fluorescence measurements. By varying the sample concentration, we have tested that the concentration of samples for fluorescence spectroscopy was always low enough to prevent reabsorption.

The femtosecond spectrometer used for collecting transient absorption spectra is based on an amplified Ti:Sapphire laser system. The femto second pulses were generated by a modular laser system consisting of an ultrafast Ti:sapphire regenerative amplifier (Spitfire Ace-100F, Spectra-Physics, USA) seeded with a Ti:sapphire oscillator (MaiTai SP, Spectra-Physics, USA), and pumped by Nd:YLF laser (Empower 30, Spectra-Physics, USA). The laser system produces ~100 fs pulses centered at 800 nm with a 1-kHz repetition rate. The produced pulses were divided into excitation and probe beams by a beam splitter. Tunable excitation pulses were generated by an optical parametric amplifier (TOPAS, Light Conversion, Lithuania). The probe pulses were generated by focusing a fraction of the 800 nm beam to a 2-mm sapphire plate to generate a broadband (450–750 nm) white light pulse. In order to minimize chirp, the white light beam was collimated by an off-axis parabolic mirror and split by a broadband 50/50 beam splitter to a reference and probe beam. The probe beam was focused by a 150mmspherical mirror to a sample where it overlaps with the excitation beam. Probe and reference beams were then focused to the entrance slit of a spectrograph where the beams were dispersed onto a double CCD array allowing measurements of transient spectra in a spectral window of ~250 nm. The time delay between the excitation and probe pulses was introduced by a computer-controlled delay line. The mutual polarization of the excitation and probe beams was set to the magic angle (54.7°) by placing a polarization rotator in the excitation beam. For all measurements, a 2-mm path length quartz cuvette was used. To avoid sample degradation, we employed a micro stirrer that continuously mixed the sample during the measurements. For all excitation wavelengths, neutral density filters were used to keep the ex- citation intensity at ∼1014 photons pulse−1 cm−2. All measurements were realized at room temperature.

Data analysis

The spectrotemporal data matrices collected by the detection system were fitted globally using DAFit software package (Pascher Instruments, Lund, Sweden). This approach allows more precise determination of the time constants of the excited state processes and, more importantly, assignment of spectral profiles of the intermediate excited state species [P7.47]. The data were fitted to a sum of exponentials, including numerical deconvolution of the FWHM of the response function, and a fourth degree polynomial describing the chirp. The fitting procedure used general linear regression for the amplitudes of the exponentials and the Nelder–Mead simplex method for the rate constants, the FWHM and the chirp polynomial. To visualize the

excited state dynamics, we assumed sequential, irreversible scheme A→B, B→C, C→D…The arrows represent increasingly slower mono exponential processes and the time constants of these processes correspond to lifetimes of the species A, B, C, D…The spectral profiles of these species are called evolution-associated difference spectra (EADS), and although for complex systems such as VCP studied here they do not correspond to pure spectra of individual excited states, they pro- vide valuable information about the time evolution of the whole system [P7.47].

3.7.4 Results

Pigment composition

The pigment composition of the VCP complex from *N. oceanica* was determined by HPLC analysis. The chromatogram detected at 436 nm shown in
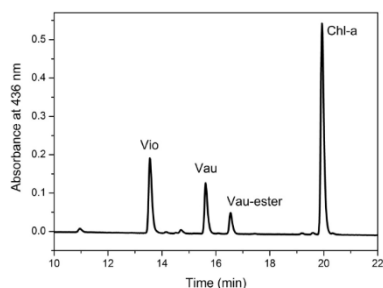
Figure 3.7.2 HPLC chromatogram of pigments extracted from VCP, detected at 436 nm. The pigment composition of the purified VCP antenna consists (by the order of elution) of violaxanthin (Vio), vaucheriaxanhin (Vau), esterified vaucheriaxanthin (Vau-ester) and chlorophyll a (Chl a).

Figure 3.7.2 consists of three carotenoid peaks corresponding to Vio, Vau and Vau-ester. Vau-ester accounts for about 30% of total Vau in VCP complex. Vau and Vau-ester differ only in esterification of the CH_2OH group at the carbon C9; thus, they have the same conjugation length. Consequently, they are spectroscopically identical as evidenced by their almost identical transient absorption spectra and kinetics (Fig. S_2, Supporting information). Therefore, hereafter we will treat Vau and Vau-ester as identical molecules for our analyses and the abbreviation Vau will be used for both Vau and Vau-ester. The final peak in the HPLC chromatogramis due to Chl a. No other peaks were detected confirming that *Nannochloropsis* lacks any accessory chlorophylls and contains only Chl a.

By integrating the peaks of Vio and Vau in the HPLC chromatogram shown in Figure 3.7.2 and correcting the result for different extinction coefficients of Vio and Vau [P7.46] we obtain Vio/Vau ratio of ~1.35 in the VCP complex of *N. oceanica*. This is slightly less than for VCP from *N. gaditana* for which the reported Vio/Vau ratio is in the 1.5–1.6 range depending on the oligomeric state of VCP [P7.28]. The same

procedure yields Chl a / Car ratio of ~2.2 for our VCP from *N. oceanica*, slightly larger than 1.8 reported for *N. gaditana* [P7.28].

Steady state spectroscopy

Absorption, fluorescence, and fluorescence excitation spectra of VCP complex are shown in Figure 3.7.1. The major absorption features of VCP complex are due to Chl a; a sharp Soret band peaks at 437 nm, while the low energy Q_y band has a maximum at 675nm. In addition, weaker bands at 585 and 625 nm correspond to the Q_x band and a higher vibrational band of the Q_y state of Chl a, respectively. The 450–550 nm spectral region is dominated by carotenoid absorption with two distinct peaks at 478 and 498 nm. Although it is tempting to assign these peaks to 0–0 and 0–1 vibrational bands of the S_2 state, their energy difference, ~900 cm^{-1}, is too small to allow for such assignment. Instead, as we will show later, the two carotenoid bands at 478 and 498 nm are due to 0–0 bands of two spectrally distinct carotenoids. A typical Chl a fluorescence band peaking at 684 nm is observed when the VCP complex is excited to the Soret band at 437nm. The comparison of absorbance and fluorescence excitation spectra of VCP complex indicates that carotenoids contribute substantially to the observed Chl a emission signal, which represents a clear evidence of energy transfer between carotenoids and Chl a. The overall efficiency of carotenoid-Chl a energy transfer is <90% in the spectral region (450–550 nm) of carotenoid absorption.

The absorption spectra of Vio and Vau in methanol are also shown in Figure 3.7.1.Three notable peaks at 417, 439 and 468 nm are associated with the 0–2, 0–1, and 0–0 vibrational bands of the $S_0 - S_2$ transition of Vio. Vau, having replaced one conjugated CC group by an allene group (see Figure 3.7.1.for structures), has the corresponding peaks at 422, 445 and 470 nm thus slightly red-shifted from that of Vio. Also, the resolution of vibrational bands is lower for Vau, indicating larger conformational disorder induced by the conjugated allene group of Vau.

Transient absorption spectroscopy

Because excited-state properties of Vau have not been studied so far, prior to examining the VCP complex by transient absorption spectroscopy we first compared excited-state properties of Vio and Vau in methanol. Transient absorption data shown
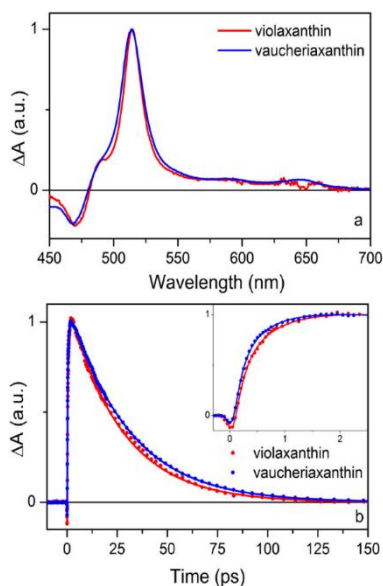
Figure 3.7.3 (a) Transient absorption spectra of Vio (red) and Vau (blue) in methanol measured 8 ps after excitation. (b) Kinetics of Vio (red) and Vau (blue) measured at the maximum of the S_1-S_n transition at 514 nm. Inset shows the rise of the S_1-S_n signal within the first 2.5 ps. The carotenoids were excited at 472 nm. All data are normalized to maximum.
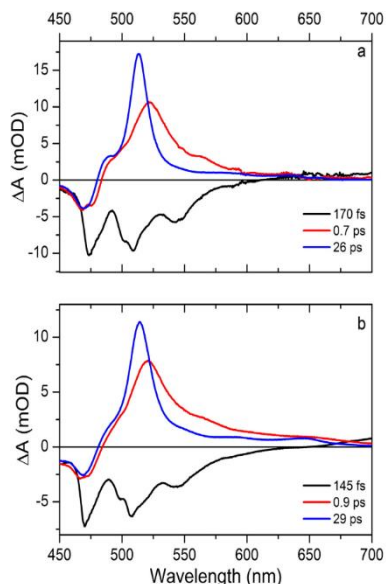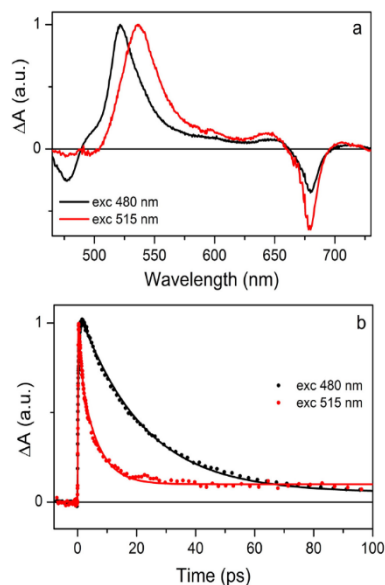
Figure 3.7.4 EADS extracted from global fitting of data measured for Vio (a) and Vau (b) in methanol.

in Figure 3.7.3 demonstrate that these two carotenoids are spectroscopically very smiler. The transient ab- sorption spectra recorded at 10 ps after excitation at 472 nm exhibit typical carotenoid band due to S_1–S_n excited-state absorption that peaks for both carotenoids at 514 nm. The S_1–S_n band of Vau is slightly broader than that of Vio, reflecting the larger conformational disorder of Vau. Kinetics recorded at the S_1–S_n maximum are also comparable for both carotenoids; the S_1 decay is slightly shorter for Vio, while the rise of the S_1–S_n signal, monitoring the S_2–S_1 relaxation, appears to be faster for Vau. These observations are confirmed by global fitting results shown in Figure 3.7.4. The results obtained for Vio agree with earlier reports on excited-state dynamics of this carotenoid [P7.35]. The first EADS (the S_2 state) decays in 170 fs to form a hot S_1 state (red EADS) which cools down within 0.7 ps to generate a relaxed S_1 state. The S_1 state of Vio has a 26 ps lifetime, in agreement with previous values of 24– 26 ps obtained for Vio in various solvents [P7.34], [P7.35]. Very similar results were obtained for Vau, except the lifetimes of S_2, hot S_1 and S_1 state are 145 fs, 0.9 ps and

178

29 ps, confirming faster S_2 depopulation and longer S_1 lifetime of Vau comparing to Vio.

In order to distinguish the carotenoids in VCP complex and their involvement in energy transfer to Chl a, 480 and 515 nm wavelengths were chosen to excite the VCP complex. Transient absorption spectra of VCP complex measured 1 ps after excitation at 480 and 515 nm are shown in Figure 3.7.5a. The significant difference between the two excitation wavelengths shows clearly that the two carotenoid peaks in the VCP steady-state absorption spectrum are not vibrational bands of the same carotenoid. Instead, they must correspond to spectroscopically distinct carotenoids. When the VCP is excited at 480 nm, the S_1–S_n peaks at 521 nm, while for the 515 nm excitation the S_1–S_n maximum is red-shifted to 536 nm. Because of essentially no Chl a absorption at either 480 or 515 nm, the presence of a bleaching at 679 nm is clearly due to the excited Chl a being populated by energy transfer from carotenoids. The distinction between the carotenoids in VCP excited at 480 and 515 nm is further underscored by comparing kinetics measured at probing wavelengths corresponding to S_1–S_n maxima (Figure 3.7.5b). The carotenoid predominantly excited at 480 nm has an S_1 lifetime comparable to that obtained for Vio and Vau in solution

Figure 3.7.5. (a) Transient absorption spectra of the VCP complex excited at 480 nm (black) and at 515 nm (red) in methanol. Spectra are measured at 1 ps after excitation and data are normalized to maximum of the S_1-S_n band. (b) Kinetics at the maximum of the S_1-S_n band after excitation of the VCP complex at 480 nm (black) and 515 nm (red). Probing wavelength were 520 nm (excitation at 480 nm) and 536 nm (excitation at 515 nm). Kinetics are normalized to maximum, solid lines are fits.

(Figure 3.7.3b). On the other hand, exciting the VCP complex at 515 nm populates a carotenoid with much shorter S_1 lifetime, presumably due to effective energy transfer route via the S_1 state.
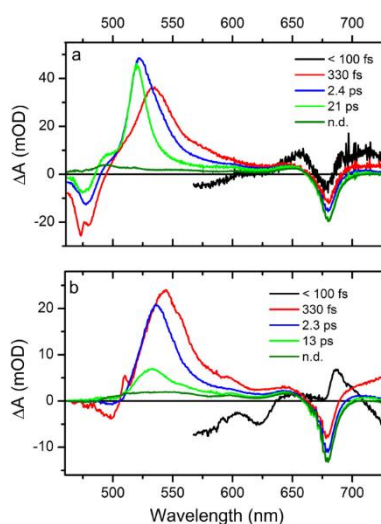
Figure 3.7.6 EADS obtained from global fitting of the data measured for the VCP complex excited at 480 nm (a) and 515 nm (b). The spectral region 460-555 nm is omitted in the first EADS due to strong scattering from the excitation light. n.d. – non decaying component.
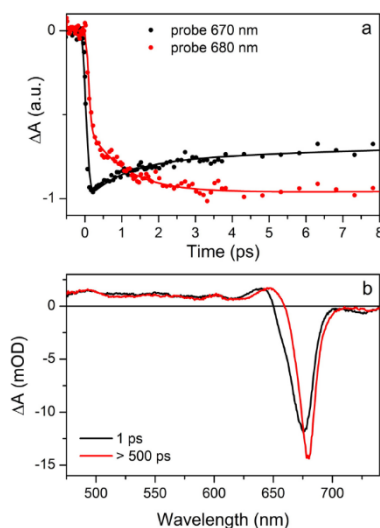
In order to describe the excited state pathways of VCP in more detail, we fitted whole datasets globally. EADS extracted from data corresponding to excitation of VCP at 480 and 515 nm are shown in Figure 3.7.6. While three components are sufficient to fit Vio and Vau in solution (Figure 3.7.4), at least four components are necessary to obtain a good fit for the VCP complex. The first EADS (black in Figure 3.7.6) is due to the initially excited state of the VCP complex. For both excitations this EADS should correspond to the S_2 state of the carotenoid excited at either 480 or 515 nm. For both excitations, the first EADS decays in less than 100 fs as we can obtain good fits with time constants in the 80–100 fs range. Since such times represent the limit of the time-resolution of our setup, we cannot resolve the decay of the first EADS precisely. However, when VCP is excited at 480 nm, even the first EADS contains significant contribution from the Chl a bleaching, while no such Chl a signal occurs in the first EADS excited at 515 nm. This implies that Chl a signal is impossible to separate from the first EADS after 480 nm excitation, indicating that energy transfer from the S_2 state of a carotenoid ex- cited at 480 nm is faster than 80 fs, which is the limit achievable with proper deconvolution of the instrument response function for our experimental setup. Thus, although we cannot determine the life- time of the first EADS precisely, we can conclude that the first EADS obtained after 480 nm decays faster than the one obtained after 515 nm excitation.

The next EADS (red in Figure 3.7.6) decays with 0.33 ps time constant for both excitations and bear a resemblance to a spectrum characteristic of a hot S_1 state identified for both carotenoids in solution (Figure 3.7.4). How- ever, for carotenoids in solution there is essentially no change in the carotenoid bleaching region associated with the decay of a hot S_1 state, indicating it is a purely excited-state process; in VCP there is a clear loss of ground state bleaching during the decay of the red EADS. Moreover, the loss of ground state bleaching is accompanied by increase of Chl a

signal, clearly signaling that the 0.33 ps process is associated with energy transfer from carotenoid to Chl a. This energy transfer channel is more pronounced after 515 nm excitation.

The next EADS (blue in Figure 3.7.6) has again nearly the same time constant for both excitation wavelengths, yielding 2.4 ps (480 nm excitation) and 2.3 ps (515 nm excitation). The process described by this EADS is again associated with energy transfer from carotenoid to Chl a as evidenced by a slight increase of the Chl a bleaching signal during this process. While the dynamics are only mildly dependent on excitation wavelength for the first three EADS, further time evolution is distinct for 480 and 515 nm excitations. When the VCP complex is excited at 480 nm, decay of the 2.4 ps EADS generates a spectrum (green EADS in Figure 3.7.6a) with a narrow S_1–S_n peak at 520 nm and carotenoid ground state bleaching with a maximum at 475 nm. This EADS decays in 21 ps, and since no further rise of Chl a signal is observed, it must correspond to a carotenoid

Figure 3.7.7 Direct excitation of Chl *a* at 665 nm. (a) Kinetics measured at blue (probe 670 nm) and red (probe 680 nm) of the Chl *a* bleaching band. (b) EADS obtained from global fitting the data measured for the VCP complex excited at 665 nm.

with a 21 ps S_1 lifetime which does not transfer energy to Chl a. For 515 nm excitation, the corresponding EADS is much weaker in magnitude and exhibits an S_1–S_n band that is broader and red-shifted to 532 nm. The lifetime of the green EADS after 515 nm excitation is 13 ps. Again, no energy transfer to Chl a is associated with this process. The final EADS which does not decay within the time window of our experiment corresponds to excited Chl a which decays at a time scale longer than 1 ns.

We have also excited Chl a directly at 665 nm to explore excited state dynamics within Chl a molecules bound to VCP. The results are shown in Figure 3.7.7. Energy flow among the Chl a pool in VCP is readily identified by comparison of kinetics probed at a blue (670 nm) and red (680 nm) side of the Chl a bleaching band. The rise of the bleaching signal associated with red-absorbing Chl a matches nicely the decay of signal probed at 670 nm which is due to Chl a molecules absorbing

at this wavelength and, thus, directly excited by the 665 nm excitation. The energy equilibration, which is characterized by a 5 nm red-shift of the Chl a bleaching maximum, is achieved within 1 ps (Figure 3.7.7b).

3.7.5 Discussion

Fluorescence excitation spectra and transient absorption data described in the previous section demonstrate very efficient energy flow from carotenoids to Chl a in the VCP complex from *N. oceanica.* In fact, energy transfer efficiencies over 90% in antenna systems having Chl a as the energy acceptor have so far been reported only for light-harvesting proteins that bind carbonyl carotenoids such as peridinin or fucoxanthin [P7.48]-[P7.51]. Even though VCP is a close relative of FCP [P7.28], observation of such efficient energy transfer in VCP suggests that the specific spectroscopic properties of carbonyl carotenoids do not represent a necessary condition to achieve energy transfer efficiencies approaching 100%. Most likely, the important parameter is the conjugation length of carotenoids bound to VCP from *N. oceanica*, Vio and Vau, which both have N ~ 9; thus, their S_1 energy in solution should be high enough to transfer energy to Chl a. Yet, in some proteins from the LHC family, e.g. LHCII, carotenoids having the same conjugation length (Vio or neoxanthin) do not transfer energy via the S_1 state [P7.36], [P7.37]. Thus, specific carotenoid-protein interactions must be the key factor determining the high energy transfer efficiency in VCP. Our data show that at least two spectroscopically different carotenoid pools exist in VCP; one absorbing at the red edge of carotenoid absorption in VCP and transferring energy with essentially 100 % efficiency, while the second one exhibits lower energy transfer efficiency and absorbs predominantly in the 450–480 nm spectral region.

Excited state properties of Vio and Vau in solution

To find out which carotenoids are associated with these two pools, we first analyze the spectroscopic properties of both VCP carotenoids, Vio and Vau, in solution. While excited-state properties of Vio were explored and reported in detail earlier [P7.34], [P7.35], no data exists so far for Vau. Comparing structures of Vio and Vau, one conjugated C=C bond of Vio is replaced by an allene group in Vau (Figure 3.7.1). This replacement leads to a slight red-shift of absorption maximum. The allene group also promotes conformational disorder in the ground state as evidenced by diminished resolution of the vibrational bands of the S_2 state of Vau. In fact, with exception of the hydroxyl group attached to one of the methyls (Figure 3.7.1), Vau has identical

structure to neoxanthin (Neo, comparison of Vau and Neo structures is shown in
Supporting Information, Figure 3.7.10). Based on this similarity we could expect also
spectroscopic properties of Vau to be identical to those of Neo because the extra OH
group of Vau should not affect N_{eff}, making Vau and Neo spectroscopically identical.
The 0-0 band of the S_2 state of Vau peaks at 470 nm (Figure 3.7.1), which is indeed
the same as for all-trans Neo [P7.52]. It must be noted that reported absorption spectra
of Neo clearly exhibit better resolution of vibrational bands than observed in Vau
absorption spectrum in Figure 3.7.1. This is an indication that extra hydroxyl group
of Vau makes the molecule more prone to conformational disorder. The same was
recently reported for C19-methyl and C19-dimethyl substituted β-carotene [P7.53]; both
molecules exhibit increased conformational disorder compared to β-carotene.

The transient absorption spectra of Vio and Vau are nearly identical except
slightly broader S_1–S_n band of Vau (Figure 3.7.3), and similarity of spectroscopic
properties of Vio and Vau is further underlined by their comparable S_1 lifetimes, 26
ps (Vio) and 29 ps (Vau). The S_1 lifetime of Vau is, however, shorter than for Neo
whose S_1 lifetime was reported to be 35 ps in methanol [P7.54] and 37 ps in pyridine
[P7.35]. Thus, it is possible that the OH group of Vau (or the esterifying chain in Vau-
ester) somehow perturbs the conjugation in the S_1 state, making the effective
conjugation of Vau slightly longer than that of Neo. Comparison of Vio and Vau
excited-state properties suggests that replacement of a conjugated C=C group by a
conjugated allene group has different effect on S_2 and S_1 states. While the S_2 state of
Vau (0–0 peak at 472 nm) has slightly lower energy than Vio (470 nm), suggesting
effective conjugation is longer for Vau, the effect on S_1 lifetime is opposite. Vau has
longer S_1 lifetime than Vio which would imply shorter effective conjugation of Vau.
Yet, the differences in both parameters, the S_2 energy and the S_1 lifetime, are small,
allowing the conclusion that despite differences in molecular structure Vio and Vau
have very similar spectroscopic properties in solution.

Energy transfer pathways in the VCP complex

Despite comparable excited-state properties of both carotenoids in solution,
the data measured for VCP identify two spectroscopically distinct carotenoids in
VCP, which is a conclusion reported earlier also for VCP from *N. gaditana* [P7.28]. The
first, denoted hereafter as a red carotenoid, is responsible for the red tail of carotenoid
absorption in VCP (N500 nm) and its carotenoid-to-Chl a energy transfer efficiency
is close to unity. The other carotenoid will be further denoted as a blue carotenoid in
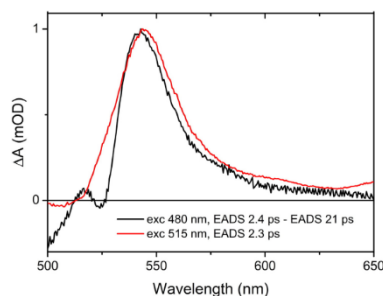
VCP; it does not absorb above 500 nm, and its 0–0 band causes the 480 nm carotenoid band in the absorption spectrum (Figure 3.7.1). Energy transfer from the blue carotenoid to Chl a is less efficient than from the red one as evidenced by the fluorescence excitation spectra (Figure 3.7.1). The decrease in energy transfer efficiency of blue carotenoids is caused by the diminished S_1 pathway (Figure 3.7.6a).

Both red and blue carotenoids in VCP transfer energy from their S_2 states. Depopulation of the S_2 state of both carotenoids in VCP is shorter than 100 fs, too fast to be precisely determined with our experimental setup. Given the S_2 lifetimes of Vio and Vau in solution, 170 and 145 fs (Figure 3.7.4), we can conclude that efficiency of the S_2 pathway must be at least 40%. For the blue carotenoid the efficiency should be larger as the Chl a bleaching signal reaching about half the total magnitude appears already in the first EADS. This is a clear indication that the S_2 lifetime of the blue carotenoid should be shorter than ~80 fs. Moreover, we can estimate the efficiency of the S_2 transfer pathway by comparing the area of the Chl a bleaching band in the red EADS in Figure 3.7.6 (the spectrum formed after decay of the S_2 state) with the area of the full Chl a bleaching in the final EADS. Such comparison gives estimation of energy transfer efficiencies of the S_2 pathway of ~60% for the red carotenoid and ~70% for the blue carotenoid.

The other energy transfer channels characterized by 0.33 and 2.3 ps (2.4 ps for the 480 nm excitation) time constants are associated with the S_1 state. The 0.33 ps process is reminiscent of energy transfer from a hot S_1 state, especially for the 480 nm excitation for which the 0.33 ps EADS shown in Figure 3.7.6a exhibits typical hot S_1 behavior, a spectrum broader and red-shifted compared to the relaxed S_1–S_n EADS (see Figure 3.7.4 for hot S_1 EADS of both carotenoids in solution). Also, shortening of the hot S_1 lifetime from 0.7 to 0.9 ps in solution to 0.33 ps in VCP indicates that some fraction of energy is indeed transferred from the hot S_1 state. Inspection of the change of Chl a bleaching magnitude during the 0.33 ps process, however, shows that this energy transfer channel is only minor. When VCP is excited at 515 nm (Figure 3.7.6b), the EADS associated with the 0.33 ps lifetime has the largest magnitude of the S_1–S_n band which is not usual for a hot S_1 state [P7.35]. Also, this channel contributes to overall energy transfer more than after 480 nm excitation. In fact, the EADS in Figure 3.7.6b show that for the 515 nm excitation this is the dominant pathway associated with the S_1 state. Thus, it is likely that while for the 480 nm excitation the 0.33 ps process corresponds to energy transfer from a hot S_1 state of the blue

carotenoid in VCP, for 515 nm excitation it may represent an efficient energy transfer from a relaxed S_1 state of the red carotenoid.

The 2.4 ps energy transfer channel is again observed after both 480 and 515 nm excitations. Here we argue that this energy transfer process is associated solely with the red carotenoid which is also partly excited at 480nm. If we subtract the 21 ps EADS from the 2.4 ps EADS (480nm excitation, Figure 3.7.6a) the resulting spectrum is nearly the same as the 2.3 ps EADS obtained after 515 nm excitation (Figure 3.7.8). This suggests that the extra amplitude at the low energy side of the S_1–S_n band of the blue carotenoid with the 21 ps S_1 lifetime corresponds to the S_1–S_n signal of the red carotenoid. Apparently, the red carotenoid is also partially excited at 480 nm resulting in intrusion of its features into the signal from the

Figure 3.7.8 The 2.3 ps EADS obtained from fitting the data excited at 515 nm (red). The difference between 2.4 and 21 ps EADS extracted from data excited at 480 nm (black).

blue carotenoid. The 2.4 ps energy transfer channel is thus associated only with the red carotenoid, implying that the red carotenoid in VCP represents at least two distinct carotenoids, each transferring energy from the S_1 state with different time constant, 0.33 and 2.4 ps. Even after 515 nm excitation there is still a fraction of a non-transferring carotenoid decaying with a 13 ps time constant.

The analysis of energy transfer pathways presented above shows that while the blue carotenoid transfers predominantly from the S_2 state with only minor additional pathway via a hot S_1 state, the red carotenoid efficiently utilizes efficiently the S_1 route as well. Since the S_1 lifetimes of Vio and Vau in solution are longer than 25 ps (Figure 3.7.4), the carotenoid S_1 lifetimes of 0.33 and 2.4 ps in VCP show that the efficiency of the S_1 transfer must exceed 90% for the red carotenoid. The spectral dependence of the energy transfer efficiency (see fluorescence excitation spectrum in Figure 3.7.1) is thus caused by different energy transfer path- ways associated with the blue and red carotenoids in VCP. The lack of S_1-mediated pathway in the blue carotenoid is partially compensated by a more efficient S_2 route than for the red carotenoid, but since excitations reaching the S_1 state of the blue carotenoid will inevitably convert a significant fraction of their energy to heat, the weakness of the

S_1 energy transfer route is the reason for a decrease of the overall energy transfer efficiency in the 450–480 nm spectral region.
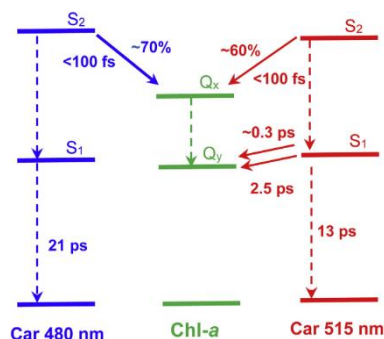
Figure 3.7.9 Scheme of energy transfer pathways between carotenoids and Chl *a* in VCP. The pathways are denoted by solid arrows labelled by corresponding time constants. Thickness of the arrow is proportional to efficiency of energy transfer. Dashed arrows correspond to internal conversion processes.

It is also interesting to note that all carotenoids in VCP transfer energy preferentially to the low energy Chl a, which have their Q_y bleaching band centered at 680 nm. Except for the first EADS obtained after 480 nm excitation, which has the Chl a bleaching peak at 678 nm (black EADS in Figure 3.7.6a), Chl a bleaching centered at 680 nm is observed in all EADS. This means that Chl a molecules excited directly at 665 nm with Chl a bleaching maximum at 676 nm (Figure 3.7.7) are not acceptors of energy from carotenoids. A scheme of energy transfer pathways in VCP is shown in Figure 3.7.9.

Identification of carotenoids involved in energy transfer in VCP

We now turn to the question whether we can determine which of the two carotenoids from VCP, Vio and Vau, are associated with the red and blue carotenoids described above. In contrast to VCP complex from *N. gaditana,* in which also a low, yet detectable, amount of antheraxanthin and zeaxanthin was reported [P7.28], we have found only Vio and Vau in the VCP complex from *N. oceanica* (Figure 3.7.2). Since Vio and Vau have very similar spectroscopic properties (Figure 3.7.3), identification of these two carotenoids based on spectroscopic markers is essentially impossible. Recent ODMR and EPR study of *N. gaditana* [P7.30] indicated structural similarity of VCP with other members of the LHC family which apparently share the protein core where carotenoids bind to the L1 and L2 sites. Then, based on previous data collected for CP29 and LHCII whose structures are known [P7.3], [P7.15] it is expected that the red-shifted carotenoids excited in VCP at 515 nm will be those bound to the inner L1/L2 sites while those bound at the VCP periphery will be the blue carotenoids excited at 480 nm [P7.16], [P7.38], [P7.55].

It is known that Vio can bind to the internal sites either naturally in CP29 [P7.15] or by reconstitution in other LHC proteins [P7.40], [P7.41]. We may thus expect the same in VCP. Moreover, about 30% of Vau in VCP is esterified (Figure 3.7.2), and presence of the extra aliphatic chain will likely prevent binding of Vau-ester to the internal carotenoid sites, as was also pro- posed by Basso et al for *N. gaditana* [P7.28]. We can therefore suggest that the red carotenoids may be Vio bound to the internal L1/L2 sites. These Vio molecules would transfer energy with nearly 100% efficiency, more efficiently than Vio in CP29 [P7.36], [P7.39]. The enhancement of Vio-Chl energy transfer in VCP must then be achieved by opening the S_1 channel that is nearly silent in CP29 [P7.36], [P7.39].

Within this hypothesis, the blue carotenoids in VCP should be Vau. The 21 ps EADS observed after 480 nm excitation (Figure 3.7.6a) then corresponds to a non-transferring Vau bound to the periphery of the VCP complex. However, it must be noted that FCP, another member of the LHC family, binds fucoxanthin which contains an allene group. Since fucoxanthin is the dominant carotenoid in FCP [P7.50], it must be bound to the internal carotenoid sites implying that the presence of allene group does not rule out such binding. Vau can thus be also bound to the internal sites. Moreover, the Vau structure containing the allene group is more prone to a conformational disorder as evidenced by ab- sorption spectrum in solution (Figure 3.7.1). This could invoke assignment of Vau to the red carotenoids as they clearly have broader S_1–S_n band indicating larger conformational disorder than the blue carotenoids (Figure 3.7.6). On the other hand, Vio-only LHCII complex exhibits an S_1–S_n spectrum very similar to that of the red carotenoid here [P7.41], suggesting that the increased conformational disorder has its origin in the binding site rather than in the carotenoid structure. It is therefore obvious that based on the presented data we cannot unequivocally assign Vau or Vio to the blue and red carotenoids in VCP.

In an attempt to facilitate the assignment of the spectral species to the pigment pools we tried to manipulate the pigment composition of VCP by treating the complex with higher detergent concentration (Supplementary Information). Analysis of pigment composition of the treated complex showed preferential removal of Vio, leading to a decrease of Vio/Vau ratio to ~1 (Figure 3.7.12b). This change was manifested as a loss of carotenoid absorption in VCP, especially around 480 nm (Figure 3.7.12a). This suggests that the blue carotenoid exhibiting negligible efficiency of the S_1 route is Vio. It must be noted though that the Chl a/car ratio of the washed complex dropped to ~1.4, indicating a major loss of Chl a accompanied by a

red shift of the Chl a Qy band (Figure 3.7.12a). Given the Vio/Vau ratio of ~1, it is likely that the pool of tightly bound carotenoids in VCP, the red carotenoid pool accompanying the red-shifted Chl a forms, comprises of both Vio and Vau.

Regardless whether the red carotenoids in VCP are Vau or Vio, the question remains: what is the carotenoid excited at 515 nm that does not transfer energy (the 13 ps EADS in Figure 3.7.6b)? Even though fluorescence excitation spectra (Figure 3.7.1) suggest nearly 100% energy transfer efficiency in that spectral region, transient absorption data revealed a small amplitude of a non-transferring carotenoid. However, the S_1 lifetime of this carotenoid is 13 ps, much shorter than the S_1 lifetimes of Vio and Vau in solution, 26 and 29 ps, respectively (Figure 3.7.4). The shorter S_1 lifetime could be explained by prolonged effective conjugation length upon binding, which is possible for carotenoids with conjugation length extended to the terminal rings [P7.56], but for Vio or Vau there is no such option as their conjugation chain is linear (Figure 3.7.1). A similar, yet smaller, effect occurs also for the blue carotenoid in VCP which has the intrinsic S_1 lifetime 21 ps (Figure 3.7.6a), again shorter than in solution.

This shortening of the S_1 lifetime is thus likely induced by some specific interaction between Vio/Vau and protein. It should be noted that similar effect was observed also for Vio-reconstituted or genetically modified Vio-only LHCII, for which the bound Vio did not transfer energy to Chl, but had S_1 lifetimes of 11 and 12.5 ps [P7.40], [P7.41]. Our data thus confirm that certain, so-far-unknown interaction between Vio/Vau and protein shortens the intrinsic S_1 lifetime and downshifts the S_2 energy of Vio/Vau in LHC proteins.

Ultrafast transient absorption spectroscopy revealed energy transfer network between carotenoids and Chl a in VCP complex from *N. oceanica*. In contrast to other light-harvesting complexes containing non-carbonyl carotenoids, VCP exhibits very high carotenoid-to-Chl a energy transfer efficiency exceeding 90%. In the 500–530 nm spectral region, where most likely Vio absorbs in VCP, the efficiency is close to 100%, thus achieving efficiencies reported so far only for light-harvesting systems containing carbonyl carotenoids. Such a high energy transfer efficiency in VCP shows that specific Vio–protein interactions can mimic typical properties of carbonyl carotenoids, i.e. absorption extending far beyond 500 nm and shrinking the S_2–S_1 energy gap. These properties make the VCP the first light- harvesting system from the LHC family that exhibits <90% carotenoid-Chl a efficiency with non-carbonyl carotenoids.

3.7.6 Acknowledgments

The authors thank Marcel Fuciman and Valentyna Kuznetsova for their help with transient absorption measurements. The research was funded from the Czech Science Foundation grants P205/11/1164 (G.K., M.D., T.P), 14-01377P (R.L. and D.B.) and P501/12/G055 (T.P., V.Š.), and by institutional support RVO:60077344.

3.7.7 References

[P7.1] G.D. Scholes, G.R. Fleming, A. Olaya-Castro, R. van Grondelle, Lessons from nature about solar light harvesting., Nat. Chem. 3 (2011) 763–74.

[P7.2] R. Croce, H. van Amerongen, Natural strategies for photosynthetic light harvesting., Nat. Chem. Biol. 10 (2014) 492–501.

[P7.3] Z. Liu, H. Yan, K. Wang, T. Kuang, J. Zhang, L. Gui, et al., Crystal structure of spinach major light-harvesting complex at 2.72 Å resolution, Nature. 428 (2004) 287–292.

[P7.4] J. Engelken, H. Brinkmann, I. Adamska, Taxonomic distribution and origins of the extended LHC (light-harvesting complex) antenna protein superfamily., BMC Evol. Biol. 10 (2010) 233

[P7.5] J.A. Neilson, D.G. Durnford, Structural and functional diversification of the light-harvesting complexes in photosynthetic eukaryotes, Photosynth. Res. 106 (2010) 57–71.

[P7.6] G. Peers, T.B. Truong, E. Ostendorf, A. Busch, D. Elrad, A.R. Grossman, M. Hippler, K.K. Niyogi, An ancient light-harvesting protein is critical for the regulation of algal photosynthesis, Nature 462 (2009) 518-521.

[P7.7] B. Bailleul, A. Rogato, A. de Martino, S. Coesel, P. Cardol, C. Bowler, A. Falciatore, G. Finazzi, An atypical member of the light-harvesting complex stress-related protein family modulates diatom responses to light, Proc. Natl. Acad. Sci. U.S.A. 107 (2010) 18214-18219.

[P7.8] T. Polívka, H. A. Frank, Molecular factors controlling photosynthetic light harvesting by carotenoids, Acc. Chem. Res. 43 (2010) 1125–1134.

[P7.9] J.G. Peterman, F.M. Dukker, R. van Grondelle, H. van Amerongen, Chlorophyll a and carotenoid triplet states in light-harvesting complex II of higher plants, Biophys. J. 69 (1995) 2670-2678.

[P7.10] M. Mozzo, L. Dall'Osto, R. Hienerwadel, R. Bassi, R. Croce, Photoprotection in the antenna complexes of photosystem II - Role of individual xanthophylls in chlorophyll triplet quenching, J. Biol. Chem. 283 (2008) 6184-6192.

[P7.11] M. Di Valentin, E. Salvadori, G. Agostini, F. Biasibetti, S. Ceola, R. Hiller, G.M. Giacometti, D. Carbonera, Triplet-triplet energy transfer in the major intrinsic light-harvesting complex of Amphidinium carterae as revealed by ODMR and EPR spectroscopies, BBA-Bioenergetics 1797 (2010) 1759-1767.

[P7.12] N.E. Holt, D. Zigmantas, L. Valkunas, X.P. Li, K.K. Niyogi, G.R. Fleming, Carotenoid cation formation and the regulation of photosynthetic light harvesting, Science 307 (2005) 433–436.

[P7.13] A. V. Ruban, R. Berera, C. Ilioaia, I.H.M. van Stokkum, J.T.M. Kennis, A.A. Pascal, H. van Amerongen, B. Robert, P. Horton, R. van Grondelle, Identification of a mechanism of photoprotective energy dissipation in higher plants, Nature 450 (2007) 575–578.

[P7.14] H. Staleva, J. Komenda, M.K. Shukla, V. Šlouf, R. Kaňa, T. Polívka, R. Sobotka, Mechanism of photoprotection in the cyanobacterial ancestor of plant antenna proteins, Nat. Chem. Biol. 11 (2015) 287–291.

[P7.15] X. W. Pan, M. Li, T. Wan, L.F. Wang, C.J. Jia, Z.Q. Hou, X.L. Zhao, J.P. Zhang, W.R. Chang, Structural insights into energy regulation of light-harvesting complex CP29 from spinach, Nat. Struct. Mol. Biol. 18 (2011) 309-315.

[P7.16] R. Croce, S. Weiss, R. Bassi, Carotenoid-binding sites of the major light-harvesting complex II of higher plants, J. Biol. Chem. 274 (1999) 29613-29623.

[P7.17] D.G. Durnford, J.A. Deane, S. Tan, G.I. McFadden, E. Gantt, B.R. Green, A phylogenetic assessment of the eukaryotic light-harvesting antenna proteins, with implications for plastid evolution, J. Mol. Evol. 48 (1999) 59-68.

[P7.18] K. Mikami, M. Hosokawa, Biosynthetic pathway and health benefits of fucoxanthin, an algae-specific xanthophyll in brown seaweeds, Int. J. Mol. Sci. 14 (2013) 13763-13781.

[P7.19] S. Takaichi, Carotenoids in algae: Distributions, biosyntheses and functions, Marine Drugs 9 (2011) 1101-1118.

[P7.20] Z. Gardian, J. Tichý, F. Vácha, Structure of PSI, PSII and antennae complexes from yellow-green alga *Xanthonema debile*, Photosynth. Res. 108 (2011) 25–32.

[P7.21] M. Durchan, J. Tichý, R. Litvín, V. Šlouf, Z. Gardian, P. Hříbek, F. Vácha, T. Polívka, Role of carotenoids in light-harvesting processes in an antenna protein from the chromophyte *Xanthonema debile*, J. Phys. Chem. B. 116 (2012) 8880–8889.

[P7.22] J. Tichý, Z. Gardian, D. Bína, P. Koník, R. Litvín, M. Herbstová, A. Pain, F. Vácha, Light harvesting complexes of *Chromera velia*, photosynthetic relative of apicomplexan parasites, Biochim. Biophys. Acta 1827 (2013) 723–729.

[P7.23] M. Durchan, G. Keşan, V. Šlouf, M. Fuciman, H. Staleva, J. Tichý, R. Litvín, D. Bína, F. Vácha, T. Polívka, T. Highly efficient energy transfer from a carbonyl carotenoid to chlorophyll a in the main light harvesting complex of *Chromera velia*, Biochim. Biophys. Acta. 1837 (2014) 1748–1755.

[P7.24] G. Keşan, M. Durchan, J. Tichý, B. Minofar, V. Kuznetsova, M. Fuciman, V. Šlouf, C. Parlak, T. Polívka, Different response of carbonyl carotenoids to

solvent proticity helps to estimate structure of the unknown carotenoid from *Chromera velia*, J. Phys. Chem. B. 119 (2015) 12653–12663.

[P7.25] A. Pinnola, L. Ghin, E. Gecchele, M. Merlin, A. Alboresi, L. Avesani, M. Pezzotti, S. Capaldi, S. Cazzanina, R. Bassi, Heterologous Expression of Moss Light-harvesting Complex Stress-related 1 (LHCSR1), the Chlorophyll a-Xanthophyll Pigment-protein Complex Catalyzing Non-photochemical Quenching, in Nicotiana sp., J. Biol. Chem. 290 (2015) 24340-24354.

[P7.26] A. Sukenik, A. Livne, A. Neori, Y.Z. Yacobi, D. Katcoff, Purification and characterization of a light-harvesting chlorophyll protein complex from the marine Eustigmatophyte *Nannochloropsis* sp., Plant Cell Physiol. 33 (1992) 1041-1048.

[P7.27] A. Sukenik, A. Livne, K.E. Apt, A.R. Grossman, Characterization of a gene encoding the light-harvesting violaxanthin-chlorophyll protein of *Nannochloropsis* sp. (Eustigmatophyceae), J. Phycol. 36 (2000) 563–570.

[P7.28] S. Basso, D. Simionato, C. Gerotto, A. Segalla, G.M. Giacometti, T. Morosinotto, Characterization of the photosynthetic apparatus of the Eustigmatophycean *Nannochloropsis gaditana*: evidence of convergent evolution in the supramolecular organization of photosystem I, Biochim. Biophys. Acta. 1837 (2014) 306–314.

[P7.29] D. Simionato, E. Sforza, E. Corteggiani Carpinelli, A. Bertucco, G.M. Giacometti, T. Morosinotto, Acclimation of Nannochloropsis gaditana to different illumination regimes: Effects on lipids accumulation, Bioresour. Technol. 102 (2011) 6026–6032.

[P7.30] D. Carbonera, A. Agostini, M. Di Valentin, C. Gerotto, S. Basso, G.M. Giacometti, et al., Photoprotective sites in the violaxanthin-chlorophyll a binding Protein (VCP) from *Nannochloropsis gaditana*, Biochim. Biophys. Acta. 1837 (2014) 1235–1246.

[P7.31] P. Tavan, K. Schulten, Electronic excitations in finite and infinite polyenes, Phys. Rev. B 36 (1987) 4337-4358.

[P7.32] T. Polívka, V. Sundström, Ultrafast dynamics of carotenoid excited states. From solution to natural and artificial systems, Chem. Rev. 104 (2004) 2021-2072.

[P7.33] D. Kosumi, M. Fujiwara, R. Fujii, R.J. Cogdell, H. Hashimoto, M. Yoshizawa, The dependence of the ultrafast relaxation kinetics of the S_2 and S_1 states in β-carotene homologs and lycopene on conjugation length studied by femtosecond time-resolved absorption and Kerr-gate fluorescence spectroscopies, J. Chem. Phys. 130 (2009) 214506.

[P7.34] T. Polívka, J.L. Herek, D. Zigmantas, H.-E. Åkerlund, V. Sundström, Direct observation of the (forbidden) S_1 state in carotenoids, Proc. Natl. Acad. Sci. 96 (1999) 4914–4917.

[P7.35] D.M. Niedzwiedzki, J.O. Sullivan, T. Polívka, R.R. Birge, H.A. Frank, Femtosecond time-resolved transient absorption spectroscopy of xanthophylls, J. Phys. Chem. B. 110 (2006) 22872–22885.

[P7.36] C.C. Gradinaru, I.H.M. van Stokkum, A.A. Pascal, R. van Grondelle, H. van Amerongen, Identifying the pathways of energy transfer between carotenoids and chlorophylls in LHCII and CP29. A multicolor, femtosecond pump-probe study, J. Phys. Chem. B. 104 (2000) 9330–9342.

[P7.37] R. Croce, M.G. Müller, R. Bassi, A.R. Holzwarth, Carotenoid-to-chlorophyll energy transfer in recombinant major light-harvesting complex (LHCII) of higher plants. I. Femtosecond transient absorption measurements, Biophys. J. 80 (2001) 901-915.

[P7.38] S. Caffarri, R. Croce, J. Breton, R. Bassi, The major antenna complex of photosystem II has a xanthophyll binding site not involved in light harvesting, J. Biol. Chem. 276 (2001) 35924- 35933.

[P7.39] R. Croce, M.G. Müller, S. Caffarri, R. Bassi, A.R. Holzwarth, Energy transfer pathways in the minor antenna complex CP29 of photosystem II: A femtosecond study of carotenoid to chlorophyll transfer on mutant and WT complexes, Biophys. J. 84 (2003) 2517-2532.

[P7.40] T. Polívka, D. Zigmantas, V. Sundström, E. Formaggio, G. Cinque, R. Bassi, Carotenoid S_1 state in a recombinant light-harvesting complex of Photosystem II, Biochemistry 41 (2002) 439–450.

[P7.41] M. Fuciman, M.M. Enriquez, T. Polívka, L. Dall'Osto, R. Bassi, H.A. Frank, The role of xanthophylls in light-harvesting in green plants: A spectroscopic investigation of mutant LHCII and Lhcb pigment-protein complexes, J. Phys. Chem. B 116 (20120 3834−3849.

[P7.42] A. Vieler, G. Wu, C.-H. Tsai, B. Bullard, A.J. Cornish, C. Harvey, et al., Genome, functional gene annotation, and nuclear transformation of the heterokont oleaginous alga Nannochloropsis oceanica CCMP1779., PLoS Genet. 8 (2012) e1003064.

[P7.43] R.R. Guillard, J.H. Ryther, Studies of marine planktonic diatoms I. *Cyclotella nana* Hustedt and *Detonula confervacea* (Cleve) Gran, Can. J. Microbiol. 8 (1962) 229–239.

[P7.44] D. Bína, Z. Gardian, M. Herbstová, E. Kotabová, P. Koník, R. Litvín, O. Prášil, J. Tichý, F. Vácha, Novel type of red-shifted chlorophyll a antenna complex from Chromera velia: II. Biochemistry and spectroscopy, Biochim. Biophys. Acta 1837 (2014) 802-810.

[P7.45] M. Herbstová, D. Bína, P. Koník, Z. Gardian, F. Vácha, R. Litvín, Molecular basis of chromatic adaptation in pennate diatom *Phaeodactylum tricornutum*, Biochim. Biophys. Acta 1847 (2015) 534–543.

[P7.46] S.W. Jeffrey, R.F.C. Mantoura, S.W. Wright, Phytoplankton pigments in oceanography: Guidelines to modern methods, 2nd edition, Monographs on Oceanographic Methodology, 10, UNESCO Publishing, Paris, 2005.

[P7.47] I.H.M. van Stokkum, D.S. Larsen, R. van Grondelle, Global and target analysis of time-resolved spectra, Biochim. Biophys. Acta 1657 (2004) 82- 104.

[P7.48] T. Polívka, R.G. Hiller, H.A. Frank, Spectroscopy of the Peridinin – Chlorophyll-a Protein: Insight into light-harvesting strategy of marine algae. Arch. Biochem. Biophys. 458 (2007) 111-120.

[P7.49] R. P. Ilagan, T.W. Chapp, R,G. Hiller, F.P. Sharples, T. Polivka, H.A. Frank, Optical spectroscopic studies of light-harvesting by pigment-reconstituted peridinin-chlorophyll-proteins at cryogenic temperatures, Photosynth. Res. 90 (2006) 5-15.

[P7.50] N. Gildenhoff, S. Amarie, K. Gundermann, A. Beer, C. Büchel, J. Wachtveitl, Oligomerization and pigmentation dependent excitation energy transfer in fucoxanthin-chlorophyll proteins. Biochim. Biophys. Acta 1797 (2010) 543-549.

[P7.51] T. Polívka, I.H.M. van Stokkum, D. Zigmantas, R. van Grondelle, V. Sundström, R.G. Hiller, Energy transfer in the major intrinsic light-harvesting complex from *Amphidinium carterae*. Biochemistry 45 (2006) 8516-8526.

[P7.52] G. Britton, S. Liaaen-Jensen, H.P. Pfander, Carotenoids Handbook, Birkhäuser Basel, 2004.

[P7.53] M. Quick, M. Kasper, C. Richter, R. Mahrwald, A. L. Dobryakov, S. A. Kovalenko, N. P. Ernsting, $\square$-Carotene revisited by transient absorption and stimulated Raman spectroscopy, Chem. Phys. Chem. In press. DOI: 10.1002/cphc.201500586.

[P7.54] H.A. Frank, J.A. Bautista, J. Josue, Z. Pendon, R.G. Hiller, F.P. Sharples, D. Gosztola, M.R. Wasielewski, Effect of the solvent environment on the spectroscopic properties and dynamics of the lowest excited states of carotenoids, J. Phys. Chem. B. 104 (2000) 4569-4577.

[P7.55] S. Caffarri, F. Passarini, R. Bassi, R. Croce, A specific binding site for neoxanthin in the monomeric antenna proteins CP26 and CP29 of Photosystem II, FEBS Lett. 581 (2007) 4704-4710.

[P7.56] M. Fuciman, G. Keşan, A.M. LaFountain, H.A. Frank, T. Polivka, Tuning the spectroscopic properties of aryl carotenoids by slight changes in structure., J. Phys. Chem. B. 119 (2015) 1457-1467.

3.7.8 Supplementary Material
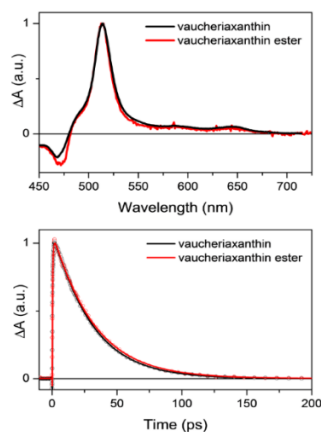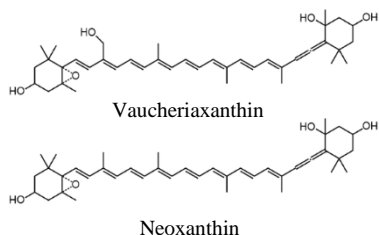
Figure 3.7.10 Molecular structures of vaucheriaxanthin and neoxanthin.

Figure 3.7.11 Transient spectra (top) and kinetics (bottom) of vaucheriaxanthin and vaucheriaxanthin ester. Transient spectra were measured at 10 ps after excitation into the 0-0 band of the S_0-S_2 transition at 472 nm. Kinetics were recorded at wavelength corresponding to the maximum of the S_1-S_n band at 514 nm.
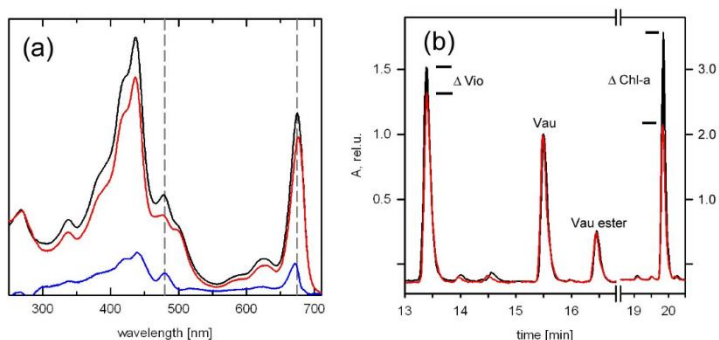
Figure 3.7.12 (a) Comparison of the absorption spectra of VCP before (black) and after (red) treatment with increased detergent concentration. The procedure consisted of extended washing of the purified VCP bound on a chromatographic column with a gradient of n-Dodecyl β-D-maltoside from 0.03 % to 3 % over 100 column volumes, followed by thorough washing with 0.03 % detergent and elution of the protein with 100 mM NaCl. Difference between the two spectra is shown in blue. The 'washed VCP' spectrum (red) was taken immediately after elution of the complex from column with NaCl. Absorption spectra were scaled to absorption at 270 nm; (b) HPLC analysis of the sample before (black) and after (red) washing. Data are shown relative to Vau elution peak, note the decrease of Vio and major loss of Chl *a*. The right Y-axis corresponds to the Chl *a* peak.

Chapter 4. SUMMARY AND CONCLUSIONS

In this section, the most importing findings which are presented in the Research Section will be highlighted. In Chapter 3, paper 1 to 5PAPER 5 discuss spectroscopic properties of carotenoids while the remaining papers, paper 6 and paper 7, describe carotenoid-to-chlorophyll energy transfer pathways and efficiency in two light-harvesting systems with unknown structure.

Photophysical properties of carotenoids are mostly determined by effective conjugation length that is directly related to the number of conjugated carbon-carbon double bonds. However, the actual effective conjugation length further depends on type of the functional groups attached to the carbon backbone. These features were discussed in the Paper 3 and Paper 5. In the Paper 3, influence of various terminal rings on effective conjugation was experimentally and theoretically explored for two carotenoids containing aryl group, isorenieratene and renierapurpurin. These two aryl carotenoids have the same number of double bonds, but conjugation is extended to different terminal rings, ϕ-ring and χ-ring, respectively. The results were compared with a non-aryl carotenoid, β-carotene. It was shown that renierapurpurin has a shorter S_1 lifetime. Thus, its effective conjugation length, estimated from the S_1 lifetime, is longer than that of isorenieratene and β-carotene. This observation was explained by ground state conformational analysis of all three carotenoids using DFT. These analyses showed that dihedral angles between the conjugation chain and χ-rings are smaller than for the ϕ-rings, implying that the double bonds in χ-ring contribute more to the effective conjugation. Also, it was argued that a small dihedral angle makes energy of the S_0-S_2 transition lower for renierapurpurin compared to isorenieratene. Similarly, the effect of a triple bond to the conjugation length was discussed in the Paper 5. It is observed that the triple bond carotenoid alloxanthin has a longer S_1 lifetime than its non-triple bond homolog, zeaxanthin, resulting in shorter effective conjugation of the triple-bond carotenoid. It was concluded that the triple bond isolates the conjugation of the central part of the conjugated system. This isolation increases the S_1 state energy of alloxanthin and diminishes the S_1–S_2 energy gap. These findings were supported by computational methods.

The spectroscopic properties of carbonyl carotenoids were presented in Paper 1 and Paper 4. The conjugated carbonyl group makes the S_1 lifetime shorter in polar solvents due to interaction between solvent and carbonyl group, resulting in stabilization of an intramolecular charge transfer (ICT) state. Even though different hypotheses for the role of the ICT state in affecting the excited-state dynamics of carbonyl carotenoids were suggested by various research groups as specified in the introduction of this thesis, a general acceptance is that the ICT state couples to the S_1

state. However, it was argued by us in the Paper 1 that the ICT state is rather the S_1 state itself, gaining different charge transfer character depending on solvent polarity. This hypothesis, based on matching the S_1-S_3 transition of 8'-apo-β-carotenal in the non-polar solvent hexane (where no ICT state should be observed) with the ICT-S_N transition, has been however proven wrong in later studies using multipulse spectroscopy.

Paper 4 aims for elucidation of molecular structure of an unknown carotenoid related to isofucoxanthin, denoted as isofucoxanthin-like (Ifx-l) carotenoid. The spectroscopic properties of Ifx-l in various environments were presented and compared to those of fucoxanthin (Fx) and Ifx, and DFT calculations on a few possible structures were used to estimate a possible structure of Ifx-l. The experimental results showed that Ifx-l is red shifted in comparison with Fx and Ifx, and the polarity-dependent behavior is observed. As for other carbonyl carotenoids with known structure, the magnitude of the ICT band increases with polarity also for Ifx-l as well as the characteristic shortening of the S_1 lifetime in polar solvents. Therefore, it is clear that Ifx-l must have longer effective conjugation length than Fx and Ifx, and it must contain a conjugated carbonyl group. Because of the larger magnitude of the polarity-induced effects, we expected a conjugated carbonyl group positioned asymmetrically to the main conjugation. The key observation was that the S_1/ICT lifetime of Ifx-l in the aprotic solvent acetonitrile is shorter than in the protic solvent methanol. This behavior has been so far reported only for peridinin and its analogues. This observation led us to a proposal that Ifx-l contains a lactone ring. Using DFT calculations, we suggested a possible structure for Ifx-l based on our spectroscopic observations and on the mass spectroscopy data provided by Moore et al.[P4.39]. Our DFT calculations also proved the existence of nonstandard hydrogen bonds between acetonitrile and the lactone ring in peridinin, explaining the behavior in aprotic solvent. This nonstandard bond makes a shorter lifetime in acetonitrile.

Energy transfer pathways between carotenoids and chlorophylls were investigated in a light-harvesting complex from *Chromera velia* (CLH) and in violaxanthin-chlorophyll-a protein (VCP) from *Nannochloropsis oceanica*, and results are described in Paper 6 and Paper 7. CLH from *C. velia* is a member of the FCP family, binding Chl-a, violaxanthin, and Ifx-l carotenoid which was discussed in detail in Paper 4. In Paper 6, it is argued that only Ifx-l is involved in the energy transfer between carotenoids and Chl-a in CLH. As for other carbonyl carotenoids bound in light-harvesting systems, the efficiency of energy transfers from Ifx-l to Chl-a is high. This high efficiency is achieved by decreasing the charge-transfer character

of the S_1/ICT state of Ifx-l, which is a strategy different from other highly-efficient antenna systems containing carbonyl carotenoids, such as FCP or PCP.

VCP from *Nannochloropsis oceanica*, described in Paper 7, binds two carotenoids: violaxanthin and vaucheriaxanthin. The spectroscopic data showed that there are two absorption bands in the carotenoid spectral region, at ~480 and ~500 nm, which are denoted as blue and red carotenoids. The blue carotenoids transfer energy efficiently from their S_2 states alone, while both S_2 and S_1 states of red carotenoids are involved in energy transfer pathways in VCP. In Paper 7, it was reported that the total carotenoid-Chl energy transfer efficiency in VCP exceeds 90%, making VCP the first Chl-a based light-harvesting system with such a high efficiency utilizing non-carbonyl carotenoids. It was concluded that there must be a specific interaction between carotenoids and protein in VCP enabling such a high efficiency of energy transfer. The origin of this interaction, however, was not possible to extract from our spectroscopic data.

Although not a main topic of this thesis, we note here that carotenoids form aggregates in hydrated polar solvents. Studies of aggregation and its effect on excited-state properties of carotenoids 8'-apo-β-carotenal and astaxanthin were presented in Paper 1 and Paper 2. Two types of aggregates, called H- and J-type, were identified for both carotenoids in water-methanol mixtures by UV-visible steady-state spectroscopy measurements. Two major effects on excited-state dynamics of aggregates were observed: formation of a triplet state within the first few picoseconds, most likely due to a singlet homofission, and shortening of the S_1 lifetimes due annihilation occurring within the carotenoid aggregate.

In conclusion, this thesis shows that many structural factors can modify the spectroscopic properties and, consequently, usability of carotenoids in light harvesting systems. Moreover, proteins enrich the versatility of the bound carotenoids by forcing them into configurations which would otherwise be unstable in solution.